SPATIAL AND TEMPORAL MAGNETIC CORRELATIONS IN TRANSITION METAL SOLID SOLUTIONS

by

Peter William Mitchell

Submitted for the degree of

Doctor of Philosophy

Imperial College of Science and Technology

University of London

October 1981

ABSTRACT

A framework is outlined in which various magnetic properties are discussed in terms of the spin-spin correlation function. This was developed in order to provide a unified description of experimentally observed magnetic properties without relying on any particular model of those properties.

The frequency dependence of the low temperature, low field, magnetic susceptibility of canonical metallic spin glass alloys copper-manganese and gold-iron was measured, and compared with the same quantity in a frozen, superparamagnetic, copper-cobalt alloy. An experimental criterion for distinguishing between the two types of system was deduced.

The chromium-iron alloy system was examined to establish whether it showed spin-glass-like bulk properties in the antiferromagnetic phase, with less than 7% iron. It did not. The sublattice magnetisation was measured by neutron diffraction and was found to decrease smoothly with temperature. At low temperatures, it was consistent with a decrease in proportion to the square of the temperature, in accordance with simple spin wave theory.

The nature of the isolated iron site moment in the spin density wave and commensurate antiferromagnetic phases of dilute solid solutions of iron in chromium was investigated by diffuse neutron scattering, and by bulk measurements. Neither the weak coupling hypothesis nor the strong coupling hypothesis was found to be adequate to explain the results. An alternative approach is suggested.

Alloys of chromium and iron which are ferromagnetic, but with transition temperatures below room temperature, were examined by low temperature, high field, magnetisation measurements. Analysis in terms of simple spin wave theory gave qualitative agreement with published neutron inelastic scattering results, and the spin wave stiffness became very small at low temperatures, in contrast to the usual monotonic increase as the temperature is reduced. Quantitative differences have not been explained.

CONTENTS

ACKNOWLEDGEMENTS AND DEDICATION

It is a pleasure for me to be able to acknowledge the assistance and co-operation of many people during the course of the work described in this thesis. I would like to thank all of the members of the Metal Physics, Solid State Theory and Theoretical Magnetism groups at Imperial College who have made the time spent on this work enjoyable, and who have provided a stimulating environment for learning.

In particular, I would like to thank Professor Bryan Coles, who has been a judicious adviser, a willing teacher, an unfathomable source of knowledge and a valued friend. Dr. Chris Guy, in addition to having built the magnetometers used in the bulk of the experiments described herein, has been a constant source of encouragement, enthusiasm, practical advice and assistance, and has far exceeded the call of duty in his readiness to consider and discuss all of the experiments and ideas which form this thesis, and many more besides.

Particular thanks are also extended to Dr. Steve Burke, who first brought to my attention the delights of chromium-iron alloys, and whose extensive investigations have made an indellible mark on our understanding of them. The very numerous references I make to his doctoral thesis and published papers pay tribute to the contribution he has made, not only to the knowledge of alloy magnetism, but also to my own "Postgraduate's Progress". He it was who introduced me to neutron scattering in practice, and he was responsible to a large degree for initiating and co-ordinating the neutron experiments described in chapters 3 and 4. The single crystal experiment described in chapter 4 was also conceived by Dr. Burke. It is also a pleasure to thank Dr. John Davis, whose expertise and untiring dedication made these neutron experiments possible. To be explicit, the D2 experiment described in chapter 3 was done jointly by Dr. Burke, Dr. Davis and

myself, although I prepared the samples and did most of the data analysis. The D5 experiment described in chapter 4 was a joint effort by myself, Dr. Burke, Dr. Davis, and also Dr. Graham Booth. In this case, Dr. Burke prepared the samples, and I processed the data. I would also like to thank Dr. Brian Rainford for helpful discussions and advice on the interpretation of neutron scattering experiments, and also for making possible, and assisting with, the small angle scattering measurement described in chapter 4.

I thank Dr. Evan Gray, who suggested the experiments described in chapter 2, and also supervised the sample preparation and took part in the measurements. Also Dr. David Sherrington, who suggested the experiments described in chapter 5, and Mr. Malcolm Dunlop, who discussed these experiments and their interpretation at great length. I would also like to thank Dr. Nick Rivier and Professor Peter Wohlfarth for helpful discussions and theoretical assistance. Thanks are due too to Dr. Arun Grover, whose able assistance with the long process of thermometer calibration described in appendix A is gratefully acknowledged.

It is a very great pleasure to thank Dr. Howard Stone for valuable metallurgical advice on the science and witch-craft of sample preparation, and for preparing the samples used in the experiments described in chapters 2 and 5. Perhaps more than anyone else, Dr. Stone has enlivened the routine of research with knowledgeable and wide-ranging discussions, and his own blend of metallurgical expertise, common sense, and insight have often provided a welcome counter-weight to the purity of pure physics.

Concerning the preparation of this thesis manuscript, I thank Dr. Guy for scientific corrections and suggestions, Dr. Stone and my wife Jean for a careful reading of the text, and also my sister Ruth for the typing. These valuable contributions notwithstanding, I accept

complete responsibility for any errors which remain.

The neutron scattering work was supported by the Neutron Beam Committee of the Science Research Council. I also acknowledge the financial support of the S.R.C. while this thesis work was in progress.

Finally, I would like to thank all those who have been my teachers in the physical sciences, and especially Mr. Michael Connolly and Mr. Malcolm Todd, whose unstinting efforts and enthusiasm first directed my steps to the study of this subject. To them I dedicate this thesis.

NOTE ON NOMENCLATURE AND UNITS

The author acknowledges the benefits of a unified, standard, system of units, in particular the Système Internationale. Unfortunately, this system has gained very little popularity, and especially in magnetism the c.g.s. e.m.u. system is still used almost universally. For ease of comparison with other work in the field, therefore, the units used in this thesis are substantially of the latter system. But even that does not describe the extent of the shabby compromise here adopted. Neutron scattering in particular is still beset with many completely unsystematic units, and these too have been used where they offer the path of least resistance.

The interested reader is referred to the discussion by Bennett, Page and Swartzendruber (1976), while for the benefit of those to whom S.I. is the only intelligible system, the table below indicates the S.I. equivalent of non-S.I. units used in this thesis.

The indications of alloy composition always refer to atomic %, rather than weight %.

The notation ^{n}X is used for the isotope of element X and mass number n.

TABLE OF NON-S.I. UNITS AND S.I. EQUIVALENTS

QUANTITY	NON-S.I. UNIT	S.I. EQUIVALENT
Time	hour	3.6 ks
	week	0.6048 Ms
Length	cm	10 mm
	Å	0.1 nm
Area	b (barn)	10^{-28} m^2
Pressure	atmosphere	101325 Pa
Energy	eV *	$\simeq 1.60219 \times 10^{-19}$ J
Temperature	^oC	K - 273.150
Magnetic field (H)	Oe	$10^3/4\pi$ Am^{-1}
Magnetic flux density (B)	G	10^{-4} T
Magnetic moment	μ_B *	$\simeq 9.27410 \times 10^{-24}$ JT^{-1}
	e.m.u.	10^{-3} JT^{-1}
(per unit mass)	e.m.u. g^{-1}	1 JT^{-1} kg^{-1}
Magnetic susceptibility	e.m.u. g^{-1}	10^4 JT^{-2} kg^{-1}

* These are not, strictly speaking, units at all. They are physical quantities. Their values depend not on defined quantities, but on measured quantities (electronic charge, electronic mass, etc.).

CHAPTER 1

MAGNETIC CORRELATIONS

A Perspective on the Magnetism of Transition Metals

Magnetism is one of the most ancient of the branches of physical science. Naturally occurring magnetic materials, especially magnetite, Fe_3O_4, have fascinated men for millenia. A crude science slowly emerged, and the interaction with technology has been strong ever since the demand for magnetic needles for use as navigational aids.

The connection with electricity, established experimentally by Ampère and others in the early nineteenth century, was consolidated in the theoretical unification of Maxwell. This carried, in embryo, both the theory of relativity and, more importantly perhaps, the quantum theory. It is a result of classical physics that there can be no magnetic response (Feynman 1964).

The motion of electrons in a material can give rise to a magnetic effect in two ways. The first is the purely quantum mechanical property of spin angular momentum and the second is the "classical" notion of orbital angular momentum. The latter corresponds on an atomic scale to the magnetic effect of a flow of charge, or electric current. In the first row transition elements which are considered here, the orbital contributions to the magnetic properties are found to be small. This is due to quenching, a lifting of the orbital degeneracy, while leaving each component of the orbital angular momentum with an expectation value of zero. This quenching is an effect of the environment of the magnetic atom. In what follows, only spin angular momentum will be considered, although, in many cases, the generalisation to include orbital effects involves computational, but not conceptual, difficulty.

An exact solution of the relativistic Schrödinger equation for any

solid system with a large number of atoms is not yet possible. Progress is made by successive approximation and refinement. A great deal of progress can be made along the lines of elementary solid state theory (e.g. Ashcroft and Mermin 1976). Since there is a periodic potential provided in a crystalline material by the ion cores (nuclei plus core electron states, up to 3 p, treated as atomic states) some simplifications may be made. In the Hartree approximation, exchange and correlation effects are ignored, and the solution gives single-particle equations. Corrections due to exchange and correlation may then be added. The Hartree-Fock approximation incorporates exchange effects, and correlation effects may then be added ad hoc. Ideally, of course, it would be best to include the electron-electron interactions exactly from the start, and this is done in spin density functional theory. Computational complexity is not the only obstacle to the solution of the single-particle equations which result. There is also a non-local potential which is not known in detail.

All of these approximations which give rise to single-particle equations do not describe electrons as the solutions to these equations, but quasi-electrons or quasi-particles. At such high densities of electrons, the free electron picture is hopelessly inadequate, but Landau in his Fermi liquid theory justified the use of the idea of these nearly free quasi-particles (Landau 1957). It remains one of the most awesome results of twentieth century physics that from this conceptual mill, the solutions which emerge at the end actually resemble the electrons which were fed in at the beginning, although some of their properties may be modified (re-normalised) by the so-called many-body effects. Their mass may also be negative (holes).

In the Hartree approximation, the 3 d transition metals have a conduction band into which is fed the appropriate number of 4 s and 3 d

atomic electrons. These emerge as a mixture of a wide s-like band and a narrow (∿5-10 eV) d-like band. The Fermi surface has both s-like and d-like parts to it, and as all the 4 s and 3 d electrons are involved in the conduction band, any property arising from these electrons must be considered to be itinerant. However, there are some circumstances in which the effect of electron-electron interactions may be represented in an effective Hamiltonian by a term which resembles the interaction of local magnetic moments (moments due to electrons which are localised at a particular atomic site). It is then a good physical picture to consider such a system in terms of the effective moments which appear in the effective Hamiltonian.

The simpler aspects of some of the theories built on these ideas will be referred to in the course of this thesis, as they have been applied to the spin density wave antiferromagnetism of chromium, and the weak itinerant ferromagnetism of iron (chapters 3 and 5 respectively). A review of the theory of structural and magnetic properties of transition metals is given by Friedel (1969).

Alloys of iron, both solid solutions and intermetallic phases, and also of other magnetic elements alloyed with noble metals and other transition metals, have been studied extensively, both in their own right, and also as an aid to the understanding of the pure magnetic elements. In this thesis I report on various measurements made on solid solutions of iron, and also of manganese and cobalt. The primary aim is to document various forms of magnetic response in these materials, but the materials and experiments in question have been chosen to provide data in areas which are currently of theoretical interest too.

When a ferromagnetic material like iron is diluted with a non-magnetic species (or with chromium, which, while not being obviously non-magnetic, in many ways behaves as such in this case), the

ferromagnetic order is diminished both in its magnitude at zero temperature, and in the range of temperature over which order is established. The second order phase transition which exists in iron at the Curie temperature persists in dilute solid solutions.

At the other end of the concentration range, when small quantities of iron are dissolved in a non-magnetic host, various types of behaviour are observed. In a random alloy, however, the periodicity, which is at the heart of the simplifications of the Schrödinger equation described above, is lost. Roughly the same treatment can be applied, however, taking into account not only the dynamic fluctuations (zero-point and thermal) which are an important part even of uniform, pure systems, but also the static fluctuations of the random alloy.

It turns out that in many cases of interest, the spin density at the site of a "magnetic impurity" in a "non-magnetic host" resembles the spin density which would arise from a local magnetic moment. In some cases, the fluctuations of this effective moment are too fast to be important in many observable properties, while in other cases, the moment is not apparent because of a compensation of the spin density by other conduction electrons (Kondo systems). Theories of this type of phenomenon are hideously complicated, and in most cases merely enable one to be wise after the event. Prediction is rarely, if ever, possible. The experimental question as to whether there is an uncompensated spin density at any given site is simple by comparison. Whether that spin density is static or fluctuating, the spin-spin correlation function may be measured (see the next section), and the spin density deduced.

An extensive review of the experimental and theoretical approaches to the dilute magnetic alloy problem is given by Rado and Suhl (eds.) (1973). The discussion there is largely based on Hartree-Fock theory, while some is based on Hartree theory with ad hoc additions. The

latter allows many experimental properties to be discussed in a coherent framework (Wohlleben and Coles 1973), and is therefore of physical value. The short-comings even of the former, however, are rather severe, especially at non-zero temperature, as discussed by Blandin (1973). There are also problems in Hartree-Fock because the interaction used is an average, so that fluctuations are ignored even at zero temperature. More satisfying conceptually is the spin density functional approach outlined by Hamann and Schrieffer (1973), although actual progress is hampered by computational difficulties.

The problem to be tackled in this thesis, concerning the isolated iron atom dissolved in antiferromagnetic chromium has not been solved either experimentally or theoretically. One approach is to compare the behaviour of iron atoms dissolved in neighbouring 3 d and 4 d transition metals, but this evidence is ambiguous. In vanadium and niobium, with one electron less than chromium in the conduction band, there is no evidence for a moment on iron sites, while in molybdenum, chromium's 4 d equivalent, iron takes on its most favoured moment of about 2 μ_B. The success of the Hartree-Fock approximation in describing impurities dissolved in ferromagnetic hosts has not been repeated so far for antiferromagnets, and the glib extension of ideas from the non-magnetic host problem, like the Kondo effect, to a problem of this complexity is not helpful.

The questions at the centre of attention now concern the interactions of finite concentrations of magnetic species in a non-magnetic host, and the development of ferromagnetism from the non-ferromagnetic solid solution alloys when the concentration of magnetic species is increased still further.

There exists a large class of magnetic/non-magnetic solid solution systems which show curious behaviour between the very dilute, and the ordered magnetic regions, which are called "spin glasses". This

terminology has been in use for about a decade, but the materials have been under scrutiny for much longer. The central problem is the understanding of the rather sharp feature in the magnetic susceptibility measured at finite frequency (typically 1 kHz), see figure 1.1 for 1% to 8% iron in gold, taken from Cannella and Mydosh (1972). This sharp feature ("cusp") is not accompanied by similarly sharp features in other properties, such as the magnetic specific heat, which would be expected to show similar anomalies.

A great deal of experimental and theoretical effort has been expended since 1972. Experimental reviews are given by Mydosh (1975 and 1981), and a theoretical review by Blandin (1978). In chapter 2 below I describe a series of experiments designed to clarify some of the magnetic properties of metallic spin glasses in general, comparing and contrasting them with the properties of fine-particle ferromagnetic (superparamagnetic) materials, to which they have often been likened.

Chapter 3 is a report on several experiments designed to establish whether spin glass behaviour is observed in the chromium-iron alloy system, and chapter 4 is concerned with the problem mentioned above, of the isolated iron atom dissolved in (antiferromagnetic) chromium. These experiments were pursued with the intention of further documenting spin glass properties, but in the event, the system did not reveal spin glass behaviour. The question of the iron moment's nature, to which attention is given in chapter 4, is largely of particular, rather than general, interest, though an understanding of this problem within a given theoretical framework would inspire confidence in that framework.

Another class of systems of interest is made up of those alloys which have just a little more of the magnetic species than is necessary to establish ferromagnetism. There is some behaviour in these materials which is suggestive of the loss of long range order at

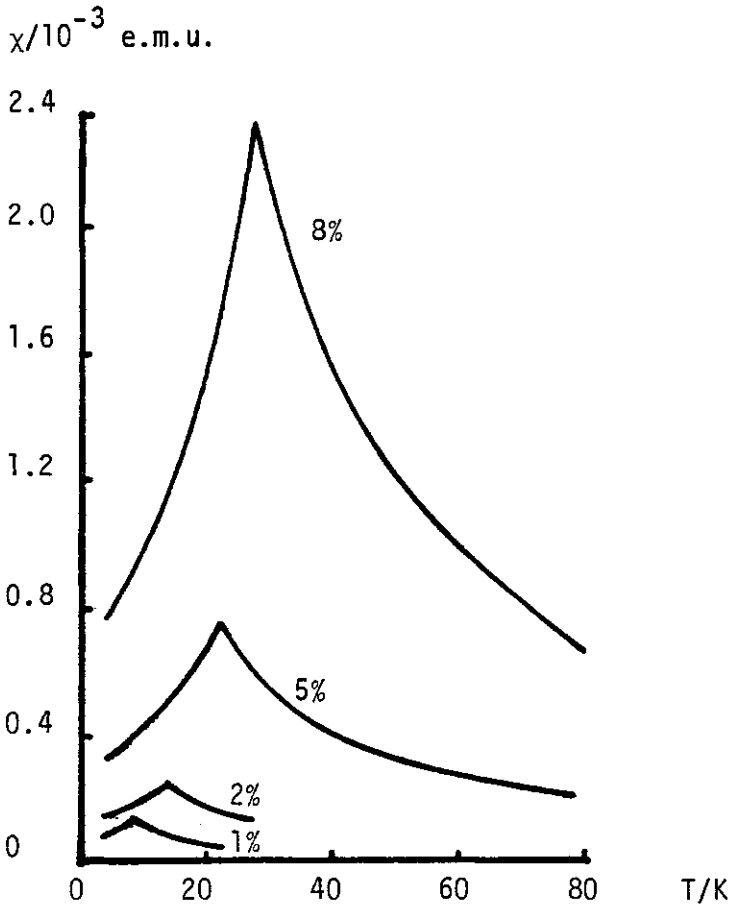

FIGURE 1.1 Low field susceptibility of gold-rich gold-iron alloys. From Cannella and Mydosh (1972).

temperatures well below the Curie temperature. It may be that this behaviour is related in some way to the behaviour of the spin glass found at lower concentrations. In chapter 5 some measurements are described on chromium-iron alloys which are just ferromagnetic. Some implications for the theory of this type of disordered system are discussed.

In the remainder of this chapter, a short discussion will be given of magnetic correlation functions (not to be confused with electron-electron correlations discussed above), and of their connections with experimental measurements and theories of magnetic systems. Consideration will also be given to the question of what constitutes a ferromagnet.

Magnetic Correlations and Experimental Measurements

The two-particle spin-spin correlation function between vector spin operators $\hat{\underline{S}}$ at sites i, j at times t_1, t_2 is defined as

$$C_{ij}^{\alpha\beta}(t_1,t_2) = \langle \hat{S}_i^{\alpha}(t_1)\hat{S}_j^{\beta}(t_2)\rangle,$$

where $\langle x \rangle$ denotes an ensemble average of x, and α, β denote Cartesian components x, y and z. For a system with a position and time dependent spin-density operator $\hat{\underline{\zeta}}(\underline{r},t)$, the equivalent correlation function is

$$C^{\alpha\beta}(\underline{r}_1,\underline{r}_2,t_1,t_2) = \langle \hat{\zeta}^{\alpha}(\underline{r}_1,t_1)\hat{\zeta}^{\beta}(\underline{r}_2,t_2)\rangle.$$

These functions are of great utility in describing the magnetic state of a system of local moments, or distributed spin density.

i. Neutron Scattering

By far the most powerful technique currently available for the study of magnetic systems is neutron scattering. A rigorous theory of this is developed by Marshall and Lovesey (1971), but here a summary is given of the steps essential for this discussion.

The partial differential scattering cross-section, which is what is measured in a neutron scattering experiment, $\frac{d^2\sigma}{d\Omega dE'}$, may be written

in terms of the interaction potential operator $\hat{V}$ (interaction between the neutrons and the target system) and in the Born approximation as

$$\frac{d^2\sigma}{d\Omega dE'} = \frac{k'}{k}\left(\frac{m}{2\pi\hbar^2}\right)^2 \sum_{\lambda,\sigma} p_\lambda p_\sigma \sum_{\lambda',\sigma'} |\langle \underline{k}'\sigma'\lambda'|\hat{V}|\underline{k}\sigma\lambda\rangle|^2 \delta(\hbar\omega + E_\lambda - E'_{\lambda'})$$

where $\underline{k}$ is the neutron wave-vector,

σ is the neutron spin,

m is the neutron mass,

λ characterises the target system,

p_λ is the probability that the target is in state λ,

p_σ is the probability that the neutron has spin σ,

ω is the change in neutron frequency, and is given by

$$\hbar\omega = \frac{\hbar^2}{2m}(k'^2 - k^2),$$

and primed quantities indicate the final values, while unprimed are the initial values, and the other notation is standard.

When the interaction potential is the interaction with electron spin angular momentum, the cross-section for unpolarised incident neutrons is

$$\frac{d^2\sigma}{d\Omega dE'} = \left(\frac{\gamma e^2}{m_e c^2}\right)^2 \frac{k'}{k} \sum_{\alpha,\beta} (\delta_{\alpha\beta} - \hat{\kappa}_\alpha \hat{\kappa}_\beta) \times$$

$$\times \sum_{\lambda,\lambda'} p_\lambda \langle\lambda|\hat{Q}_\alpha^+|\lambda'\rangle\langle\lambda'|\hat{Q}_\beta|\lambda\rangle \delta(\hbar\omega + E_\lambda - E_{\lambda'})$$

where $\underline{\kappa} = \underline{k}' - \underline{k}$,

γ is the neutron gyromagnetic ratio = -1.91,

m_e is the mass of an electron,

c is the velocity of light in vacuo,

and

$$\hat{\underline{Q}} = \sum_i \exp(i\underline{\kappa}.\underline{r}_i)\hat{\underline{S}}_i$$

for moments on sites i, or

$$\hat{\underline{Q}} = \int \underline{dr} \exp(i\underline{\kappa}.\underline{r})\hat{\underline{\zeta}}(\underline{r})$$

for a distributed spin density $\underline{\zeta}(\underline{r})$.

For a rigid lattice of moment sites, and a system in equilibrium, this reduces to

$$\frac{d^2\sigma}{d\Omega dE'} = \left(\frac{\gamma e^2}{m_e c^2}\right)^2 \frac{k'}{k}\{\tfrac{1}{2}gF(\underline{\kappa})\}^2 . \frac{1}{2\pi\hbar}\sum_{\alpha,\beta}(\delta_{\alpha\beta} - \hat{\kappa}_\alpha\hat{\kappa}_\beta) \times$$

$$\times \sum_m\sum_l \exp(i\underline{\kappa}.\underline{l})\int_{-\infty}^{\infty} dt \exp(-i\omega t)\langle \hat{S}_m^\alpha(0)\hat{S}_{m+l}^\beta(t)\rangle$$

for the local moment system, where

g is the Landé splitting factor, ≈2 for spin only,

$F(\underline{\kappa})$ is the normalised form factor for each ion

$$F(\underline{\kappa}) = \int \underline{dr} \exp(i\underline{\kappa}.\underline{r})\zeta(\underline{r})$$

$$\text{with } \int \underline{dr}\zeta(\underline{r}) = 1,$$

where both integrals are over the unit cell.

The transformed correlation function for local moments is defined as

$$C^{\alpha\beta}{}_m(\underline{\kappa},\omega) = \sum_l \exp(i\underline{\kappa}.\underline{l})\int_{-\infty}^{\infty} dt \exp(-i\omega t) C^{\alpha\beta}_{m\,m+l}(0,t).$$

The cross-section expression reduces in this case to

$$\frac{d^2\sigma}{d\Omega dE'} = \left(\frac{\gamma e^2}{m_e c^2}\right)^2 \frac{k'}{k}\{\tfrac{1}{2}gF(\underline{\kappa})\}^2 . \frac{N}{2\pi\hbar}\sum_{\alpha,\beta}(\delta_{\alpha\beta} - \hat{\kappa}_\alpha\hat{\kappa}_\beta)\{C_m^{\alpha\beta}(\underline{\kappa},\omega)\}_{av}$$

where $\{\ \}_{av}$ denotes an average over all target sites, m, and N is their number.

For the distributed spin density system in equilibrium,

$$\frac{d^2\sigma}{d\Omega dE'} = \left(\frac{\gamma e^2}{m_e c^2}\right)^2 \frac{k'}{k} \cdot \frac{1}{2\pi\hbar\alpha} \sum_{\alpha,\beta} (\delta_{\alpha\beta} - \hat{\kappa}_\alpha \hat{\kappa}_\beta) \times$$

$$\times \int \underline{dr}_1 \int \underline{d}(\underline{r}_1 - \underline{r}_2) \exp(-i\underline{\kappa}.(\underline{r}_1 - \underline{r}_2)) \int_{-\infty}^{\infty} dt \exp(-i\omega t) \langle \hat{\zeta}^\alpha(\underline{r}_1, 0) \hat{\zeta}^\beta(\underline{r}_2, t) \rangle .$$

The distributed spin-density transformed correlation function is also defined as

$$C^{\alpha\beta}(\underline{r}_1, \underline{\kappa}, \omega) = \int \underline{d}(\underline{r}_1 - \underline{r}_2) \exp(-i\underline{\kappa}.(\underline{r}_1 - \underline{r}_2)) \int_{-\infty}^{\infty} dt \exp(-i\omega t) C^{\alpha\beta}(\underline{r}_1, \underline{r}_2, 0, t)$$

and its average over the target volume V as

$$\int \underline{dr}_1 C^{\alpha\beta}(\underline{r}_1, \underline{\kappa}, \omega) = V C^{\alpha\beta}_{av}(\underline{\kappa}, \omega).$$

So finally

$$\frac{d^2\sigma}{d\Omega dE'} = \left(\frac{\gamma e^2}{m_e c^2}\right)^2 \frac{k'}{k} \cdot \frac{V}{2\pi\hbar\alpha} \sum_{\alpha,\beta} (\delta_{\alpha\beta} - \hat{\kappa}_\alpha \hat{\kappa}_\beta) C^{\alpha\beta}_{av}(\underline{\kappa}, \omega).$$

The neutron magnetic partial differential cross-section is thus a combination of some uninteresting constants and well-known parameters, an orientation factor, and most importantly, the space and time Fourier transformed spin-density correlation function, suitably averaged over the sample. For a system in equilibrium, the correlation function is a function of the time difference, and not of the absolute time values. By measuring the partial differential cross-section as a function of ω, the energy transfer, and $\underline{\kappa}$, the momentum transfer, the spin-spin correlation function can be mapped out in time and space. In practice, this is not always possible, partly because of resolution effects. If the resolution of the experiment is too demanding, the scattering intensity may be too small to be detected reliably, for reasons either of time or of background. Energy resolution may sometimes be purchased with a loss of momentum resolution, and vice versa.

The technique of neutron spin echo, developed by F. Mezei and others at the Institut Laue-Langevin in Grenoble (Mezei 1980), measures

a different function. Instead of the space and time Fourier transform of the spin-spin correlation function, the scattering maps out the so-called "intermediate scattering function", which is the spatial Fourier transform only of the space and time correlation function. The range of time which may be measured is from 5×10^{-11} s to 5×10^{-9} s with the current instrument, IN11.

ii. Bulk Measurements

The principal bulk magnetic measurements are the magnetisation and the susceptibility. A brief discussion of their definitions and relationships with the correlation function is given in an attempt to clarify what is often over-simplified.

The bulk isothermal susceptibility, χ_{is}, is defined in terms of the macroscopic variables magnetisation, M, and uniform applied field, H, at temperature T

$$\chi_{is} = \left(\frac{\partial M}{\partial H}\right)_T \Bigg|_{H = 0}$$

In general, in the formalism of linear response theory, we consider the change in the wave-vector, $\underline{q}$, and time, t, dependent magnetisation $\Delta M(\underline{q},t)$ when a small, arbitrary field $H(\underline{q},t)$ is turned on slowly (in amplitude), so that transients are avoided and we measure the adiabatic response.

$$\Delta M(\underline{q},t) = \int_{-\infty}^{t} dt' K(\underline{q},t - t')H(\underline{q},t')$$

where $K(\underline{q},t)$ is the response function at wave-vector $\underline{q}$ and time t. The upper limit of the integral is a manifestation of causality. The generalised susceptibility is then defined as

$$\chi(\underline{q},\omega) = \lim_{\varepsilon \to 0^+} \int_0^{\infty} dt K(\underline{q},t)\exp\{i\omega t - \varepsilon t\}.$$

In general, this susceptibility is complex, and we write

$$\chi(\underline{q},\omega) = \chi'(\underline{q},\omega) + i\chi''(\underline{q},\omega).$$

The real and imaginary parts are related by the Kramers-Kronig relations (Landau and Lifshitz 1969),

$$\chi'(\underline{q},\omega) = \frac{2}{\pi}P\int_0^\infty \frac{\zeta\chi''(\underline{q},\zeta)d\zeta}{\zeta^2 - \omega^2}$$

and

$$\chi''(\underline{q},\omega) = \frac{1}{\pi}P\int_{-\infty}^{\infty} \frac{\chi'(\underline{q},\zeta)d\zeta}{\zeta - \omega}.$$

Here, the P denotes the principal value of the integral. In general, χ'' may contain an additional term if χ has a pole at $\omega = 0$, but this will not concern us here.

The fluctuation-dissipation theorem relates the equilibrium fluctuations in a quantity, in this case the (wave-vector dependent) magnetisation, to the imaginary (dissipative) part of its associated susceptibility (Landau and Lifshitz 1969), at any frequency ω

$$\left(\Delta M(\underline{q},\omega)\right)^2 = \frac{\hbar}{2\pi}\chi''(\underline{q},\omega)\coth(\tfrac{1}{2}\hbar\beta\omega)$$

(where the Fourier transform is defined as

$$M(\omega) = \frac{1}{2\pi}\int_{-\infty}^{\infty} M(t)e^{i\omega t}dt).$$

It is generally true that the generalised susceptibility obeys this relation

$$\chi(\underline{q},-\omega) = \chi^*(\underline{q},\omega)$$

so that

$$\chi''(\underline{q},-\omega) = -\chi''(\underline{q},\omega)$$

and in most cases, the imaginary part of the susceptibility is zero at zero frequency. In many simple cases, it is true that, near zero

frequency,

$$\chi''(\underline{q},\omega) \propto \omega\chi'(\underline{q},\omega).$$

This relationship clearly breaks down at higher frequencies. For example, in the region of a spin-wave resonance, χ' goes to zero while χ'' has a maximum. The constant of proportionality may vary as the temperature changes.

In the limit of small ω,

$$\coth(\tfrac{1}{2}\hbar\beta\omega) = \frac{2}{\hbar\beta}\cdot\frac{1}{\omega}$$

so that for $\hbar\omega\beta << 1$ (i.e. classical fluctuations)

$$\left(\Delta M(\underline{q},\omega)\right)^2 \propto \omega\chi'(\underline{q},\omega) \times \frac{1}{\omega}$$

or

$$\left(\Delta M(\underline{q},\omega)\right)^2 \propto \chi'(\underline{q},\omega).$$

It is not clear that the adiabatic susceptibility defined above is simply related to the static isothermal susceptibility, χ_{is}. The condition that they be related is that

$$\lim_{t\to\infty} \langle \hat{M}(\underline{q},0)\hat{M}(\underline{q},t)\rangle = \langle \hat{M}(\underline{q})\rangle^2$$

(Marshall and Lovesey 1971). This is usually valid, but may be in question in some cases, like some spin glass experiments. If it is true, then

$$\chi_{is} = \chi'(\underline{q} = \underline{0},\ \omega = 0).$$

A measured bulk susceptibility is effectively at $\underline{q} = \underline{0}$ usually, but at non-zero frequency, ω

$$\chi'(0,\omega) = \chi_{is}(\omega) \propto \left(\Delta M(\underline{q} = \underline{0},\ \omega)\right)^2.$$

The magnetisation operator, $\hat{M}$, is given by

$$\hat{M}(t) = \frac{1}{V}\int d\underline{r}\hat{\zeta}^z(\underline{r},t)$$

where the integral is over the sample volume, V.

$$\hat{M}(\omega) = \frac{1}{2\pi}\int_{-\infty}^{\infty}\hat{M}(t)e^{i\omega t}dt = \frac{1}{V}\int d\underline{r}\hat{\zeta}^z(\underline{r},\omega)$$

and

$$\Delta\hat{M}(\omega) = \hat{M}(\omega) - <\hat{M}(\omega)>.$$

The observable magnetisation is the expectation value of the operator, so that

$$\left(\Delta M(\underline{0},\omega)\right)^2 = <\left(\Delta\hat{M}(\omega)\right)^2>,$$

$$M(\omega) = <\hat{M}(\omega)> = \left(<\hat{M}(\omega)>^2\right)^{\frac{1}{2}},$$

$$\chi_{is}(\omega) \propto <\left(\Delta\hat{M}(\omega)\right)^2>,$$

and

$$M^2(\omega) = <\left(\hat{M}(\omega)\right)^2> - <\left(\Delta\hat{M}(\omega)\right)^2>.$$

The magnetisation and susceptibility may be expressed in terms of the spin density correlation functions, $C_{av}^{\alpha\beta}(\underline{\kappa},\omega)$ and $\Delta C_{av}^{\alpha\beta}(\underline{\kappa},\omega)$, where

$$\Delta C^{\alpha\beta}(\underline{r}_1,\underline{r}_2,t_1,t_2) = <\Delta\hat{\zeta}^{\alpha}(\underline{r}_1,t_1)\Delta\hat{\zeta}^{\beta}(\underline{r}_2,t_2)>$$

and

$$\Delta\hat{\underline{\zeta}}(\underline{r},t) = \hat{\underline{\zeta}}(\underline{r},t) - <\hat{\underline{\zeta}}(\underline{r})>.$$

Consider a system in equilibrium, so that

$$<\hat{\zeta}^z(\underline{r}_1,t_1)\hat{\zeta}^z(\underline{r}_2,t_2)> = <\hat{\zeta}^z(\underline{r}_1,0)\hat{\zeta}^z(\underline{r}_2,t_2 - t_1)>.$$

$$\left|\hat{M}(\omega)\right|^2 = \frac{1}{(2\pi)^2}\cdot\frac{1}{V^2}\int\underline{dr}_1\int\underline{dr}_2\int_{-\infty}^{\infty}e^{i\omega t_1}dt_1\int_{-\infty}^{\infty}e^{i\omega t_2}dt_2 \times$$

$$\times\ \hat{\zeta}^z(\underline{r}_1,t_1)\hat{\zeta}^z(\underline{r}_2,t_2)$$

and

$$\left|\Delta\hat{M}(\omega)\right|^2 = \frac{1}{(2\pi)^2}\cdot\frac{1}{V^2}\int\underline{dr}_1\int\underline{dr}_2\int_{-\infty}^{\infty}e^{i\omega t_1}dt_1\int_{-\infty}^{\infty}e^{i\omega t_2}dt_2 \times$$

$$\times\ \Delta\hat{\zeta}^z(\underline{r}_1,t_1)\Delta\hat{\zeta}^z(\underline{r}_2,t_2)$$

which have expectation values of

$$<\left|\hat{M}(\omega)\right|^2> = \frac{1}{(2\pi)^2}\cdot\frac{1}{V^2}\int\underline{dr}_1\int\underline{dr}_2\ \overline{C^{zz}(\underline{r}_1,\underline{r}_2,\omega)}$$

$$<\left|\Delta\hat{M}(\omega)\right|^2> = \frac{1}{(2\pi)^2}\cdot\frac{1}{V^2}\int\underline{dr}_1\int\underline{dr}_2\ \overline{\Delta C^{zz}(\underline{r}_1,\underline{r}_2,\omega)}$$

where the bar denotes an equilibrium time average. Using the same notation as above for spatial averages over the sample,

$$<\left|\hat{M}(\omega)\right|^2> = \frac{1}{(2\pi)^2}\cdot\ \overline{C^{zz}_{av}(0,\omega)}$$

$$<\left|\Delta\hat{M}(\omega)\right|^2> = \frac{1}{(2\pi)^2}\cdot\ \overline{\Delta C^{zz}_{av}(0,\omega)},$$

so that the bulk magnetisation and susceptibility are

$$M^2(\omega) \propto \overline{C^{zz}_{av}(0,\omega)} - \overline{\Delta C^{zz}_{av}(0,\omega)}$$

and

$$\chi_{is}(\omega) \propto \overline{\Delta C^{zz}_{av}(0,\omega)}.$$

The assumptions which have gone into this result are the following.

1. The system is in equilibrium. This requires the time scale of any experiment to be much greater than the longest relaxation time of

the system.

2. $\lim_{t\to\infty} \langle \hat{\zeta}^z(0)\hat{\zeta}^z(t)\rangle = \langle \hat{\zeta}^z\rangle^2$.

This is usually satisfied if the system is in equilibrium.

3. $\chi''(\underline{q},\omega) \propto \omega\chi'(\underline{q},\omega)$.

When the system is not in equilibrium, it may be very difficult to define separate quantities like magnetisation and susceptibility. The problem stems from the time dependence of the ensemble average in non-equilibrium systems. We have assumed above that

$$\langle \hat{\underline{\zeta}}(\underline{r},t)\rangle = \langle \hat{\zeta}(\underline{r})\rangle,$$

that the ensemble average is not a function of time. When the system is not in equilibrium, the same experimental techniques may be used, and quantities may be measured which are called the magnetisation and susceptibility, but their connection with the theoretical constructs, and with the correlation function in particular, then becomes unclear.

iii. Mössbauer Effect

The Mössbauer effect provides a sensitive measurement of the hyperfine field, or the magnetic field experienced by the nucleus. Only certain nuclei may be used, and the most appropriate for our discussion is ^{57}Fe. There are many effects which contribute to the signals observed, but, through the spin density of the s-electrons, there is a contribution to the hyperfine field from the total spin centred on each atomic site. The γ-ray absorption spectrum shows two effects. Firstly, the absorption line may split, and secondly it may broaden. These effects are related to the time average of the spin density, and the time average of the spin density fluctuations respectively. The averages are over the decay time of the nuclear excited state, which is $\sim 10^{-7}$ s for ^{57}Fe (Hirst 1974).

If the nuclear decay time is τ, writing the average

$$\frac{1}{\tau}\int_0^{\tau} A dt = (A)_{\tau},$$

the hyperfine field splitting, H_{hf}, and width ΔH_{hf} are given by

$$H_{hf} \propto (S_i^{\alpha})_{\tau} = \{(S_i^{\alpha}(0)S_i^{\alpha}(t))_{\tau} - (\Delta S_i^{\alpha}(0)\Delta S_i^{\alpha}(t))_{\tau}\}^{\frac{1}{2}}$$

and

$$\Delta H_{hf} \propto \{(\Delta S_i^{\alpha}(0)\Delta S_i^{\alpha}(t))_{\tau} + (\Delta S_i^{\beta}(0)\Delta S_i^{\beta}(t))_{\tau} + (\Delta S_i^{\gamma}(0)\Delta S_i^{\gamma}(t))_{\tau}\}$$

where the cartesian axes α, β, γ are defined <u>at each Mössbauer nucleus</u> by

$$(S_i^{\beta})_{\tau} = 0$$

$$(S_i^{\gamma})_{\tau} = 0.$$

Thus the Mössbauer effect measures only single site, or auto-correlations. The absolute orientation of the α, β, γ axes with respect to any external axes is not investigated, and so no information is gained concerning spatial correlations. If the temporal correlations exist for longer than the decay time τ, then they are perceived as a splitting. This does not, however, imply an infinite time, or zero frequency, correlation.

<u>iv. Other Techniques</u>

In similar vein, many other measurements of magnetic effects could be discussed in terms of the spin-spin correlation function. Magnetic resonance experiments measure sharp features in the dynamic response, and usually these are uniform measurements (zero wave-vector), but they may extend to small wave-vectors in thin film resonance experiments. Various transport properties also depend upon magnetic correlations. In the case of electrical resistivity, the correlations are measured up

to a spatial range of about the electron mean free path, which may itself be a complicated function of many other variables.

The correlation function of any specified system under a given set of conditions (temperature, pressure, applied magnetic field, etc.) is unique. Differences between values measured by different techniques should be traceable to deficiencies in one, or more, of those techniques.

It should be stressed that most magnetic measurements, at least in principle, measure magnetic correlations. In some very restricted cases, like the de Haas-van Alphen experiments in good single crystals of pure (elementary or compound) magnetic metallic materials at low temperatures and high applied fields (Lonzarich 1980), it may be possible to measure magnetic interaction energies more directly.

Magnetic Correlations and Theoretical Models

The process of physical description of real systems involves relating the observed properties to the known laws of physics. Now the complete description of interacting systems of more than two bodies has so far eluded exact treatment. Such descriptions necessarily involve approximation, and so it is with all treatment of solid materials. However, it is the belief of the magnetician that the observed magnetic properties of solids may be "understood" in the physical sense of being traceable to specific features of the arrangement of the atomic nuclei and their associated electrons.

It is not within the scope of this work to review such models and their developments, although individual models and their implications will be discussed where applicable in the following chapters. What should be stressed here is that a particular model may be shown to imply a particular correlation function. However, if a measurement of only part of the correlation function is carried out, as is generally

the case, then there may be several quite different models which predict the same behaviour over the measured range. To decide which, if any, of the models gives the best description, the correlation function must be measured more thoroughly, and compared again. If the predicted correlation functions are the same, then a judgement may be made on the models using Occam's razor.

The interactions between various entities within a model, in particular, are not measurable directly, and any measurement of them relies on the interpretation of the predictions of the model.

What is a Ferromagnet?

i. Definition

Perhaps the simplest view of a ferromagnet is that it is a material which exhibits a spontaneous magnetisation (i.e. a magnetisation in zero applied field). This, however, must be tempered with all kinds of caveats. Firstly, a sample of, say, iron, the archetypal ferromagnet, which is larger than a few hundred Angstroms in linear dimension, may not exhibit a bulk magnetisation in zero field because, in order to minimise the magnetostatic energy, it spontaneously divides into domains, separated by domain walls whose width is determined by the competition between anisotropy and the exchange which produces the ordering. The observed, remanent magnetisation, which is usually very small, may depend entirely on the recent history of the sample, and bears little relation to the magnetisation seen on a scale of a few atoms. Secondly, there are materials, like Fe_3O_4, which show a spontaneous magnetisation in the same sense as does iron, which are usually called ferrimagnetic because, on an atomic scale, there is actually a fraction of the spin density which is aligned anti-parallel to the direction of bulk magnetisation. The limiting case of this, where the contributions from

the parallel and anti-parallel moments are equal, is antiferromagnetism. Antiferromagnets do not usually display a spontaneous magnetisation at all. There are also some materials which exhibit a helical magnetic structure, which may be quasi-ferrimagnetic, with a net moment, or quasi-antiferromagnetic, with none. This helix may be incommensurate with the lattice spacing in general. Such materials are sometimes called helimagnets. Thirdly, there are materials which display remanent magnetisation in zero field, after an external field has been applied and removed, but which are not usually considered to be ferromagnetic. Spin glasses fall into this category.

Our ferromagnet, then, is a material which displays a spontaneous magnetisation without a magnetic field ever having been applied, or which would do so if it did not break up into domains, and which is not a ferrimagnet nor a helimagnet.

If we bear in mind that in an itinerant magnetic system, such as the alloys of the first row transition metals considered here, the magnetic moment at, or near, any given atomic site is the result of conduction electron interactions, and is not a localised magnetic moment (in the sense that it is not due to localised electrons), we may write the definition above in terms of the correlation function of the site moments, $\underline{S}_i(t)$, where

$$\underline{S}_i(t) = \int_{\text{cell}} \underline{\varsigma}(t)dr.$$

The condition for long-ranged magnetic order is that the average instantaneous correlation function

$$\langle \underline{S}_i(t).\underline{S}_j(t) \rangle$$

should be non-zero for all values of $r_{ij} = |\underline{r}_{ij}|$, where

$$\underline{r}_{ij} = \underline{r}_i - \underline{r}_j.$$

To define ferromagnetism, then, we should want to say that this correlation function is a monotonic function of r_{ij} to exclude the ferrimagnets and helimagnets, that it should be non-zero even if no magnetic field is ever applied, to exclude spin glasses and similar materials, but that we may only consider $\underline{r}_{ij}$'s which do not cross or enter domain walls.

This question of the domains may be crucial in the end, particularly if the anisotropy, which limits the width of the domain walls, becomes very weak, as it does, for example, in chromium-iron alloys when the iron concentration is reduced (David and Heath 1971). The magnetic structure may then be dominated by the walls themselves, and our notion of the correlation function outside the walls may then be nonsense. What is often considered to be a technical property (and therefore uninteresting to the physicist), under these circumstances thrusts itself to the fore, and must be considered as physically important. It may be possible, theoretically, to consider needle-shaped or quasi-one-dimensional samples, in which the magnetostatic effects may be reduced arbitrarily, but in practice, this may not be feasible for reasons of sensitivity, nor desirable because of the shape anisotropy introduced by this procedure. This may have the effect of inducing metastable states in the sample, and catastrophic effects, such as the large Barkhausen discontinuities observed in iron wires (e.g. Sixtus and Tonks 1931).

ii. Experimental Decisions on Ferromagnetism

The methods employed experimentally to decide whether or not a given alloy is ferromagnetic are all stretched when it comes to alloys with very small ordered moments. Many of the possible techniques exploit the effects of the transition to ferromagnetism from the (high temperature) disordered phase.

The magnetic susceptibility is a much used, but difficult tool. A

discussion of some of the subtleties associated with it has been given above. Experimentally, even more care is required. The isothermal susceptibility, now assumed to be at zero frequency, but as a function of internal field, is defined as

$$\chi_{is}(H) = \left(\frac{\partial^2 F}{\partial H^2}\right)_T \Big|_H$$

where F is the Helmholtz free energy,

$$dF = MdH - SdT$$

with M, the magnetisation, assumed to be uniform, so that

$$\chi_{is}(H) = \left(\frac{\partial M}{\partial H}\right)_T \Big|_H.$$

If there is a spontaneous magnetisation, then the definition of the zero field susceptibility needs more care, (assuming T = constant)

$$\chi_{is}(H = 0) = \lim_{H \to 0^+} \left(\frac{\partial M}{\partial H}\Big|_H\right).$$

Note also that H is the field inside the sample, and is assumed to be uniform.

If the transition to ferromagnetism is a second order transition, then the zero-field susceptibility diverges at the transition temperature. If the transition is first order, this is not necessarily so.

Experimentally, what is measured is χ_e

$$\chi_e(H_a) = \frac{\delta M}{\delta H_a}\Big|_{\overline{H}_a} = H_a.$$

That is, with some mean or bias field $\overline{H}_a$, the applied field is varied by δH_a, and the response δM is measured. In general, the applied field, H_a is not equal to the internal field, H, but in simple cases,

$$H = H_a - NM$$

where N is the demagnetising factor, and M is the (uniform) magnetisation.

When there is no spontaneous magnetisation, and M is a continuous function of H, then

$$\lim_{\delta H \to 0} \chi_e(H_a = NM) = \chi_{is}(H = 0).$$

However, if there is a spontaneous magnetisation, and

$$M_S = \lim_{H \to 0^+} (M(H)) \neq \lim_{H \to 0^-} (M(H)) = -M_S$$

then the experimentally measured susceptibility bears little relation to the theoretical quantity. If we could measure

$$\lim_{\delta H_a \to 0} \{\chi_e(H_a = NM_S + \frac{\delta H_a}{2})\}$$

then this would correctly reproduce the theoretical value

$$\chi_{is}(H = 0) = \lim_{H \to 0^+} \left(\frac{\delta M}{\delta H}\bigg|_H\right)$$

to within a constant factor of

$$\lim_{\delta H_a \to 0} \frac{\delta H_a}{\delta H} = \frac{\delta H + N\delta M}{\delta H} = 1 + N\chi_{is}.$$

So that

$$\chi_{is}(H = 0) = (1 + N\chi_{is}) \lim_{\delta H_a \to 0} \{\chi_e(H_a = NM_S + \frac{\delta H_a}{2})\}$$

and finally

$$\chi_{is}(H = 0) = \frac{\lim_{\delta H_a \to 0} \{\chi_e(H_a = NM_S + \frac{\delta H_a}{2})\}}{1 - N \lim_{\delta H_a \to 0} \{\chi_e(H_a = NM_S + \frac{\delta H_a}{2})\}}.$$

But even this is far removed from reality, because for any real, ferromagnetic system, the behaviour of M for small values of H is dominated by the domain properties. When $H_a < NM_S$, then the system is

far from homogeneous because of the domain structure. The above analysis assumes that the domain walls move freely, which is nearer the truth in some cases than others. In a simple measurement of the experimental susceptibility near the Curie temperature of a ferromagnet, the measured value is the reciprocal of the demagnetising factor.

$$\chi_e(0) = \frac{\delta M}{\delta H_a} = \frac{1}{N}$$

for all $\delta H_a < NM_s$. As the temperature falls, anisotropy of various forms restricts the domain wall motion, and the susceptibility falls below the demagnetising limit, and continues to fall as the temperature falls. This effect was first observed by Rowland (1873) in nickel, but is generally referred to as the Hopkinson effect, after the latter's measurements on iron (Hopkinson 1889).

Thus the measured susceptibility never exceeds the demagnetising limit, even if the transition is second order. The critical fluctuations may be reflected above the transition temperature as a fast-falling susceptibility (as the temperature increases), but below the Curie temperature, the measured susceptibility is some complicated function of the demagnetising factor, the anisotropy, the spontaneous magnetisation and the measuring field amplitude δH. In general, it will show one maximum, or possibly two maxima, which may be in the vicinity of the Curie temperature, or at any lower temperature. If the transition is not second order, then there is no requirement that the susceptibility, as defined, need do anything unusual, although a step change or a break in slope as a function of temperature would be expected.

Susceptibility is, therefore, a fallible tool, and one furthermore which gives little information on the correlation function of interest. Measurements of the bulk magnetisation in principle give the

information required concerning the correlation function

$$\langle \underline{S}_i(t).\underline{S}_j(t) \rangle,$$

but again, the properties of real ferromagnets pose difficulties in elucidation. The complication of hysteresis will be ignored here, because the remanence and hysteresis are small effects in the alloys to be considered later. The magnetisation as a function of internal field might be expected to behave as in figure 1.2, with a sharp kink point when the average internal field ceases to be zero. For any real material this is not so, partly because of the effects of anisotropy (which may be partly eliminated in a single crystal by doing the measurement along an easy crystal axis, in an easy direction with respect to the sample's shape), and partly because of the effect of sample defects, which can never be eliminated completely.

In the absence of any such sharp feature, a method of extrapolation to zero applied field is required to give the spontaneous magnetisation. Such an extrapolation may be straightforward if there is an obvious straight line to extrapolate from. It is necessary to derive zero field values, even to look for the transition, since, for the case of a well-defined, but continuous (e.g. second order) transition in zero field, in any finite field there is no phase transition.

One method of extrapolation is to use an Arrott plot. This is a quite general extrapolation technique which should be valid in the limit of small magnetisation in homogeneous systems. Quite how small it needs to be will be discussed later. The Helmholtz free energy, F, of any magnetic system may be written, generally, as the sum of even powers of the magnetisation with suitable co-efficients, plus a term related to the magnetic inhomogeneity, and the term due to the interaction with an applied field. At constant temperature,

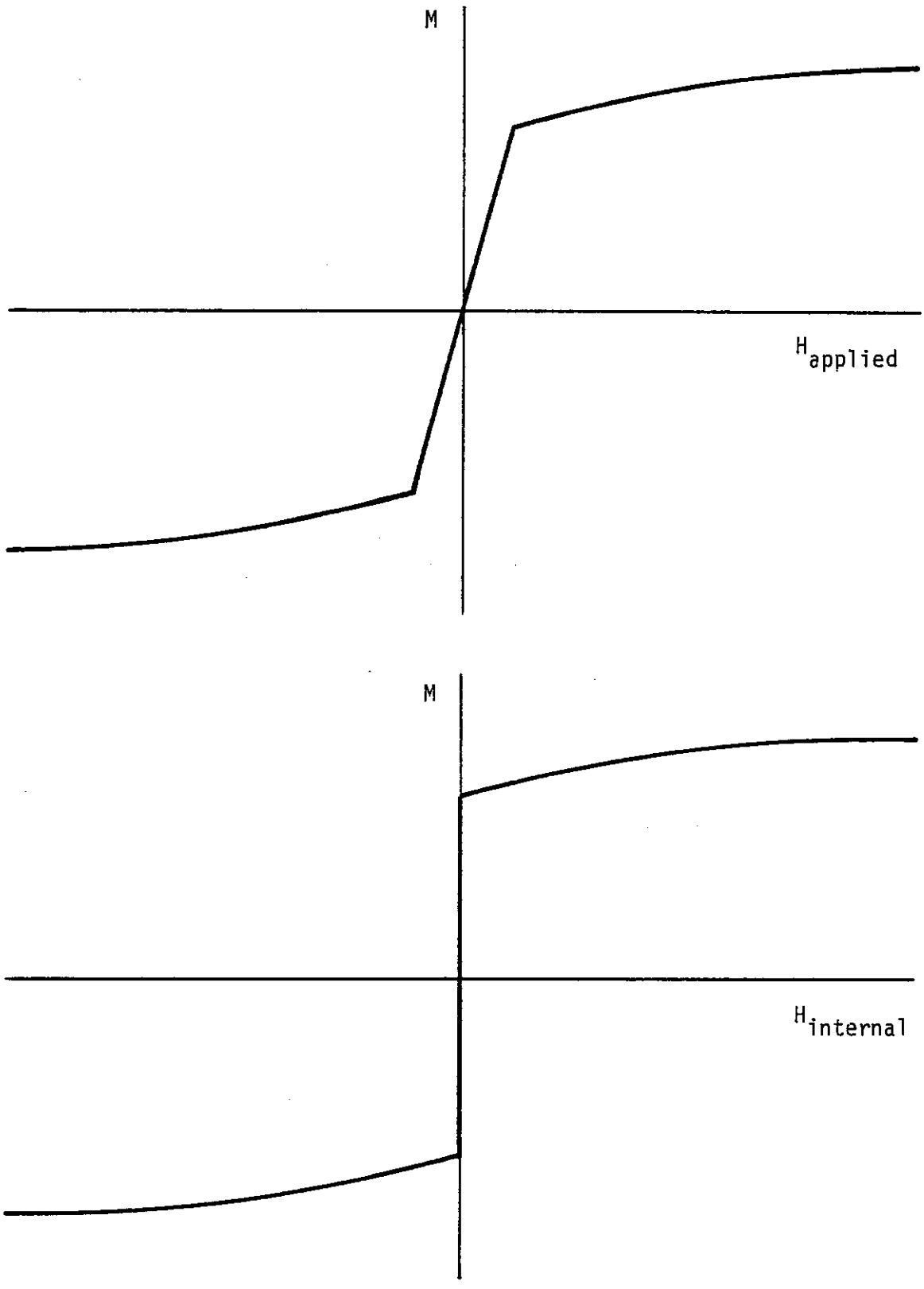

FIGURE 1.2 Idealised forms of the dependence of magnetisation, M, on applied and internal fields in a ferromagnet.

$$F = -(aM^2 + bM^4 + cM^6 + \ldots) + \alpha\int(\underline{\nabla}M)^2 d\tau + HM$$

or

$$dF = -(2aM + 4bM^3 + 6cM^5 + \ldots)dM + \alpha d\left[\int(\underline{\nabla}M)^2 d\tau\right] + HdM + MdH.$$

But $dF = MdH$.

$$\therefore \quad HdM = (2aM + 4bM^3 + 6cM^5 + \ldots)dM - \alpha d\left[\int(\underline{\nabla}M)^2 d\tau\right]$$

$$\therefore \quad H = 2aM + 4bM^3 + 6cM^5 + \ldots - \alpha\frac{d}{dM}\left[\int(\underline{\nabla}M)^2 d\tau\right].$$

At this point, it is usual to drop the inhomogeneity term, and to make the approximation of small magnetisation. This latter enables us to neglect the term in M^5 and higher powers, and we have

$$\frac{H}{M} = 2a + 4bM^2.$$

An Arrott plot is a graphical means of testing this, by plotting M^2 against H/M. The spontaneous magnetisation is given by

$$M_S = \left(\frac{-a}{2b}\right)^{\frac{1}{2}}$$

and exists only when $\frac{a}{b} < 0$.

The co-efficient "a" changes sign at a ferromagnetic transition, so that there is a spontaneous magnetisation below, but not above the transition temperature.

If the Arrott plot turns out to be curved, however, then one of the two approximations above must be inadequate. Either the terms in M^5 and higher powers are significant, or else there is a significant magnetic inhomogeneity contribution to the free energy, or both. In any case, extrapolation to zero internal field then becomes very difficult, and the method is of limited usefulness. For a brief review

and discussion of some applications to real, inhomogeneous systems, see Edwards, Mathon and Wohlfarth (1973).

Perhaps, then, a decision as to whether there is a ferromagnetic phase can be made as a result of a neutron scattering experiment. The correlation function we require would appear most directly in the zero-q scattering, which is the one part of the scattering function inaccessible to experiment, because of interference from the unscattered beam.

The response due to the ensemble average part of the correlation function appears in the scattering as a set of δ-functions in both energy and momentum transfer, since, if the average correlation is periodic in real space, we can represent it as a Fourier series. If

$$\langle \underline{\zeta}(\underline{r}).\underline{\zeta}(\underline{0}) \rangle = \sum_{n=0}^{\infty} a_n \exp\{i2\pi n \underline{r}.\underline{\kappa}\},$$

then the Fourier transform, which appears in the expression for the neutron cross-section, is a series of δ-functions (Bragg peaks) in reciprocal space at zero energy transfer (elastic scattering). The apparent width of these peaks in energy and momentum transfer is limited only by the instrumental resolution, however high it may be.

Unfortunately, these magnetic Bragg peaks occur at precisely the same places in reciprocal space as do the nuclear Bragg peaks. Separation of the intensities may usually be effected by extrapolation of the nuclear intensity from temperatures well above the magnetic transition temperature. Use can also be made of the different dependence of the nuclear and magnetic Bragg scattering on the spin state of the scattered neutron. The former is non-spin-flip, and the latter is spin-flip scattering. In some cases, the guide field which, in such a neutron polarisation analysis experiment needs to be applied at the sample to prevent depolarisation (by domain walls, for example), will make this method less than straightforward.

In a second order phase transition, the critical point is the focus of a series of critical phenomena related to the transition. In particular, the critical fluctuations in the magnetic spatial and temporal correlations, the range of which, both in space and in time, diverge at the critical temperature, give rise to a cross-section which is peaked at the magnetic Bragg peak positions with ranges in reciprocal space and energy which are related to the inverse of the real space and time ranges. The intensity of the critical scattering rises to a maximum at the transition temperature. Experiments directly measuring this critical scattering are probably the most direct experimental method of all to observe a transition to ferromagnetism, if it is second order.

Other, less direct methods have been employed to determine the existence of, or transition to, ferromagnetism, but their evidence is generally corroborative, rather than definitive. The heat capacity may be a useful tool, but it includes many contributions in an undiscriminating way. At a transition of first or second order, however, there should be a divergence in the magnetic contribution. This may, in some severe cases, be masked by other terms. Electron spin resonance, Mössbauer spectroscopy and electrical transport properties such as resistivity, and magnetoresistivity may also provide useful information. None of these, however, can measure the average correlation over infinite spatial range in zero field.

CHAPTER 2

SPIN GLASSES AND LOW FREQUENCY MEASUREMENTS

Introduction

Many of the problems posed experimentally by spin glass materials are due partly to the difficulty of relating the results of one type of measurement to another. This difficulty is related to the unusual low frequency behaviour of the correlation function. For example, the early Mössbauer data (Borg, Booth and Violet 1963) for gold-rich gold-iron alloys revealed resolved spectra similar (though not identical) to those characteristic of a ferromagnetic transition, in the composition region of 1-10% iron, where magnetisation studies (Crangle and Scott 1964) showed no such transition. There are many examples of apparent conflicts of this kind.

Tholence and Tournier (1974) showed that, because of the slow response of a spin glass to an applied magnetic field, the apparent susceptibility (or magnetisation change per field change) could depend on the frequency of the measurement.

This observation has several implications. Firstly, the normal connections between the results of different measuring techniques may be modified if the techniques employ different time scales, or equivalently, frequencies of measurement. Secondly, a good theory of spin glasses would predict the rôle of measuring frequency. And finally, since the "irreversible" effects associated with spin glasses may appear at a temperature just above the so-called "freezing temperature", T_f, defined as the maximum in the "a.c. susceptibility" (Guy 1979), it may be that the so-called transition is nothing but an artefact of the frequency of the measurement, and would cease to exist if a zero frequency measurement could be employed.

Thus there is scope both experimentally and theoretically to

investigate the frequency dependence of the properties of spin glasses, and this has indeed been pursued by a number of people since 1974.

Experimental Investigations of Frequency Dependence

Under this heading I shall include experiments designed to monitor the time evolution of spin glasses in certain states, as these are clearly related to experiments in the frequency domain. In either case, the idea is to change the time window or effective frequency of one measuring technique, in order to measure the frequency dependence directly.

It is appropriate at this juncture to consider the terminology used by Tholence and Tournier (1974) of a "total susceptibility" made up of a "reversible" and an "irreversible" part. Note that these terms are not used in the thermodynamic sense, but are used to indicate some response which is much faster than the experimental measuring time, and some response which is (or would be, isothermally) much slower than the measuring time. Thermodynamically, any property of a system which is not measured while the system is in equilibrium has no claim to be reversible, so if the system does have some long time response, any reversible procedure must be on an even longer time scale, to ensure that departures from thermodynamic equilibrium are infinitesimal. It is probably impractical to measure a truly reversible, isothermal susceptibility of a spin glass at temperatures well below T_f, and it should not be considered disturbing that any non-equilibrium quantity, such as Tholence and Tournier's "reversible susceptibility" does not have a vanishing first temperature derivative as the temperature tends to zero. This condition, imposed by the third law of thermodynamics, can only apply to equilibrium properties. It is probably not significant in this context, but should perhaps be mentioned, that none of the alloys considered as spin glass alloys is actually in

equilibrium at low temperatures in the random or quenched state. The diffusion rates at low temperatures are, however, very much slower even than the magnetic relaxation rates, and so the alloy appears to be in "metallurgical equilibrium" in so far as any magnetic properties (equilibrium or non-equilibrium) are concerned.

Mukhopadhyay, Shull and Beck (1975), using rather unconventional apparatus, measured a large change in the susceptibility of copper 16.7% manganese at the freezing temperature when they varied the frequency from 0.5 Hz to 2000 Hz. These experiments, however, are not now thought to be reliable (Gray 1979 (a)).

Sarkissian (1978) made measurements of susceptibility as a function of frequency of applied field on a number of rare-earth spin glass alloys. None of these shows the characteristic spin glass peak in susceptibility, with the possible exception of the scandium 13% gadolinium alloy, and in that case, the effect on the susceptibility of increasing the frequency from "d.c." to 80 Hz to 1000 Hz changes as a function of temperature such that it effects an increase at some temperatures, and a decrease at others. The observation of marked frequency dependence in the paramagnetic phase (well above the temperature of maximum susceptibility) must cast doubt on the reliability of these measurements also.

Zibold (1978) observed a small ($\sim$1% per decade) change in the freezing temperature of gold 8.5% iron and gold 12.3% iron, between 10 Hz and 10 kHz of applied field, but none in gold 4.5% iron. However, he did not observe sharp cusps in the susceptibility (as a function of temperature) in these alloys, which he attributed to the cold rolling used in preparation.

Von Löhneysen, Tholence and Tournier (1978) measured a large ($\sim$10% per decade) change in the freezing temperature of the pseudo-binary alloy (lanthanum 0.6% gadolinium) Al_2, when they varied the

frequency of applied field from 7 Hz to 1100 Hz. They also observed that the frequency dependence of the susceptibility became smaller at temperatures well below the freezing temperature.

Dahlberg, Hardiman, Orbach and Souletie (1979) measured the susceptibility of several silver-manganese alloys from 0.1% manganese to 0.5% manganese, over a frequency range of 16 Hz to 2.8 MHz using three different techniques, and found no dependence of T_f on the frequency at all (<0.5% per decade).

Holtzberg, Tholence, Godfrin and Tournier (1979) reproduced Zibold's result for gold 10% iron, and found that in the pseudo-binary insulator (strontium 10% europium) sulphide, there was a shift of the order of 7% per decade in T_f from 7 Hz to 1300 Hz.

Tholence (1980) measured the frequency dependence of T_f in copper-manganese spin glasses with 3.3, 4.6 and 8% manganese, and found a dependence of about 1% per decade from 10 Hz to 10 kHz in all three samples.

More recently, Mulder, van Duyneveldt and Mydosh (1981) made an extensive study of the frequency dependence of the susceptibility of quenched copper-manganese alloys from 0.57% to 6.3% manganese. They found that samples with less than 0.7% manganese showed no detectable frequency dependence either in T_f or in the susceptibility below T_f (<0.05% per decade), but that with 0.94% manganese, T_f was increased by 0.5% per decade and the susceptibility at fixed temperatures below T_f decreased by about 1% per decade of increase in frequency from 1 to 10 kHz just below T_f, and that this change in susceptibility was roughly linear in the temperature, so that at $T_f/2$, the decrease was about 0.5% per decade. The behaviour in higher concentrations was qualitatively similar, and quantitatively "essentially independent of the manganese concentration".

All of the above were measured using some mutual inductance

technique (except the low and high frequency measurements of Dahlberg et al., which used a SQUID magnetometer and a tank circuit resonance respectively) with all the accompanying problems of phase monitoring, skin effects, and, at lower frequencies, signal detection.

As early as 1977, Guy (1977) had measured the susceptibility of gold 4% iron using what is essentially a "d.c." technique (that is, it does not depend on a time derivative of the applied field to give the magnetisation) with the low field vibrating sample magnetometer described in appendix B. He made measurements at what he called "d.c.", with a time constant of about 2 minutes (10^{-2} Hz), and at 0.3 Hz modulation of the applied field ($\sim$10 Oe r.m.s.). He found no detectable frequency dependence at or near T_f, but a large ($\sim$30%, or 20% per decade) reduction in the low temperature ($T < 0.6\ T_f$) susceptibility at the higher frequency.

Gray (1979 (b)) performed similar measurements on copper 16.7% manganese and found no frequency dependence (<0.5% per decade) of the susceptibility at a constant temperature, 1 K below T_f, with a measuring field of 10 Oe r.m.s. from 3×10^{-4} Hz to 0.3 Hz.

Guy (1978) also investigated the time evolution of various remanent states in gold-iron alloys (up to 7% iron) and found a logarithmic decay in time, similar to the behaviour found in fine particle magnets (e.g. rock magnets) which are well described by the theory of Néel (1955). In principle, this could be related to the frequency dependence experiments by a suitable transformation.

More recent measurements (Guy 1981) made using a more sensitive and stable SQUID magnetometer on copper-manganese spin glass alloys indicate that the remanence decays as a power law of the time, the power being dependent on the initial remanence.

At the other end of the frequency spectrum, Mezei and Murani (1979), using the elegant and subtle techniques of neutron spin echo,

measured the time dependent spin correlation function $S(\kappa,t)$ in copper 5% manganese for times from 3×10^{-12} s to 5×10^{-9} s and $\kappa = 0.093$ $\mathring{A}^{-1}$ from low temperatures up to 50 K. The difference of the ratio $S(\kappa,t)/S(\kappa,0)$ from unity is related to the susceptibility at a frequency $f \sim 1/t$, and although the precise relation is not clear, it is clear that the experiments indicate at least two "relaxation mechanisms". One is the fast ($\sim 10^{-11}$ s) Korringa relaxation, and the other is strongly temperature dependent, and shifts rapidly to lower frequencies as the temperature is lowered below the freezing temperature.

Theoretical Approaches to Frequency Dependence

A vast theoretical onslaught on the spin glass problem, especially since 1972 (Cannella and Mydosh), has failed to produce a satisfactory theory to account quantitatively for all the observed properties of metallic spin glasses. However, certain aspects of the various theories have recurred in the discussion of the frequency dependent behaviour of spin glasses.

Néel's theory of monodomains, introduced to account for the properties of rock magnets, has been applied by many authors to spin glasses. Tholence and Tournier (1974) claimed, from the similarity of their gold-iron data to the known properties of monodomain materials, that the remanence effects in spin glasses were due to spontaneous division into regions because of anisotropy.

Smith (1975) devised a semi-empirical theory based on the idea of magnetic clusters whose size was assumed to vary with temperature. To account for the susceptibility cusp at T_f, some anisotropy was introduced.

Wohlfarth (1977) claimed that there was no essential difference between spin glasses and rock magnets and later (Wohlfarth 1979) made

quantitative the connection between an assumed distribution of anisotropy barrier energies and the temperature dependence of the susceptibility.

Tholence (1979) claimed to be able to explain the frequency dependent effects in all dilute metallic spin glasses in terms of the "magnetic cloud model" with the Arrhenius law (relating the relaxation time to the exponential of the barrier energy) to describe the low temperature properties, but with a linear connection between the measuring frequency and the freezing temperature. Later (Tholence 1980), he claimed that the frequency dependence of the freezing temperature could be fitted with a Fulcher law dependence, relating the measuring time, τ, the effective activation energy E_a, the freezing temperature T_f and some parameter T_o,

$$\tau = \tau_o \exp\left(\frac{E_a}{k(T_f - T_o)}\right).$$

Using this formula, he managed, using one unique value for the attempt time, τ_o ($= 10^{-13}$ s), to fit much of the available data for copper-manganese and gold-iron spin glasses, and for many others, with reasonable values of T_o and E_a. However, the underlying physics remains unclear, although implying that there is some unique (thermodynamic transition) temperature, T_o.

Gray and Cywinski (1979) took up the connection between (so-called) barrier height distribution (or alternatively, blocking temperature distribution) and the temperature dependence of the susceptibility (Wohlfarth 1979), and using several such "reasonable" distributions, failed to produce any behaviour at T_f as sharp as is observed.

Mulder, van Duyneveldt and Mydosh (1981) operated the same procedure in reverse and extracted from their susceptibility data (at different frequencies) distributions of blocking temperatures for each

frequency. They found that the distribution was slightly frequency dependent and also quite sharply peaked at the freezing temperature.

Purpose and Scope of the Present Measurements

The present experiments were undertaken with a view to making a direct comparison between the low frequency dependence (10^{-3} to 0.3 Hz) of the susceptibility of a well-known superparamagnetic material (annealed copper 2% cobalt) and the dilute spin glass alloys copper 1.5% manganese and gold 4% iron, at temperatures well below the temperature of the maximum in the susceptibility (i.e. at 4.2 K for all samples). These measurements supplement the measurements of Guy (1977) in gold 4% iron, using a number of intermediate frequencies, those of Gray (1979 (b)) on copper 16.7% manganese, probing the same alloy system at much lower concentrations, and also all of the higher frequency measurements referred to above, simply by extension to lower frequencies. It was hoped to distinguish between superparamagnetic blocking behaviour and spin glass behaviour, if indeed a distinction can be made.

Measurements performed in a vibrating sample magnetometer at these low frequencies avoid many of the problems associated with higher frequency measurements. In particular, skin depth problems are avoided, which can be very important even when the sample dimensions are of the order of one third of the skin depth (Dahlberg et al. 1978). The very careful study of Mulder et al. (1981) revealed big problems in a.c. measurements on bulk samples even at frequencies of the order of 10 Hz because of the large apparent quadrature response.

Samples

i. Copper 2% Cobalt

The solid solubility of cobalt in copper is very small (<0.1%) at 500^{o}C (Hansen 1958), so after melting the constituent elements

(Johnson Matthey Specpure) in an argon arc furnace, the alloy was sealed in a quartz capsule under vacuum and annealed at 500°C for a week to encourage the formation of dispersed ferromagnetic cobalt clusters which would behave superparamagnetically (Gray and Cywinski 1979). It was then cooled slowly to room temperature and made spherical by rolling it in an emery-paper-lined tin using a stream of compressed air. The final mass of the sample was 314 mg.

ii. Copper 1.5% Manganese

Johnson Matthey Specpure elements were melted together in an argon arc furnace, and the button was sealed in a quartz capsule under vacuum and annealed at 850°C for about a week, and then quenched into water. The solid solubility of manganese in copper is high (Hansen 1958), and the annealing procedure was chosen to give as near as possible a random solid solution. This sample weighed 1.059 g.

iii. Gold 4% Iron

Appropriate quantities of Johnson Matthey Specpure gold and iron were melted together in an argon arc furnace. The sample was made as large as could be measured with this equipment, for reasons of sensitivity, and weighed 1.750 g. As in the case of copper-manganese, the solid solubility presents little obstacle to the formation of a random solid solution (Hansen 1958), and the alloy was heat treated as before, under vacuum at 900°C for a week, and quenched into water.

Experiments and Data Reduction

The apparatus used for these experiments was the low field vibrating sample magnetometer described in appendix B.

Each of the samples was mounted in the cryostat in turn, and the low frequency, low field susceptibility was measured at 4.22 K as a function of frequency, and, in the case of the copper-manganese, as a function of applied field amplitude also.

The susceptibility was derived from an output trace on an X-t plotter, which displayed the sample moment as a function of time over one or more cycles of the applied field, while a trace on an X-Y plotter enabled the applied field amplitude to be estimated.

At very low frequencies, one cycle was sufficient, as the noise on the moment signal was averaged out by the low pass filter, but at higher frequencies, the filter was less effective, and so many cycles (up to 50) were recorded, and the noise eliminated by averaging the recorded amplitude of response manually. In this way, sensitivity was maintained over the range of frequency used.

The lower frequency limit was set by the signal source at about 10^{-3} Hz, which is the frequency at which analogue synthesis of undistorted sine waves becomes prohibitively difficult. The upper limit was just less than 1 Hz, which was determined by the band width of the measuring circuitry and the response of the plotter. This pole may be seen in some of the data, and the precise frequency of it depends on the configuration used (control loop gain and p.s.d. integration time constant).

Results

The results are shown in figures 2.1, 2.2 and 2.3 for the copper-cobalt, copper-manganese and gold-iron respectively.

The susceptibility of the copper-cobalt alloy varies linearly in the logarithm of the frequency, while all the other data shows no significant frequency dependence. Table 2.1 shows the least squares gradient of these data in % per decade, along with the r.m.s. value of applied field.

The copper-cobalt data is in agreement with previous measurements (Gray and Cywinski 1979) on an alloy of the same nominal composition, which showed behaviour qualitatively similar to that found in cobalt-

FIGURE 2.1 Alternating susceptibility, χ, of copper 2% cobalt as a function of frequency, f.

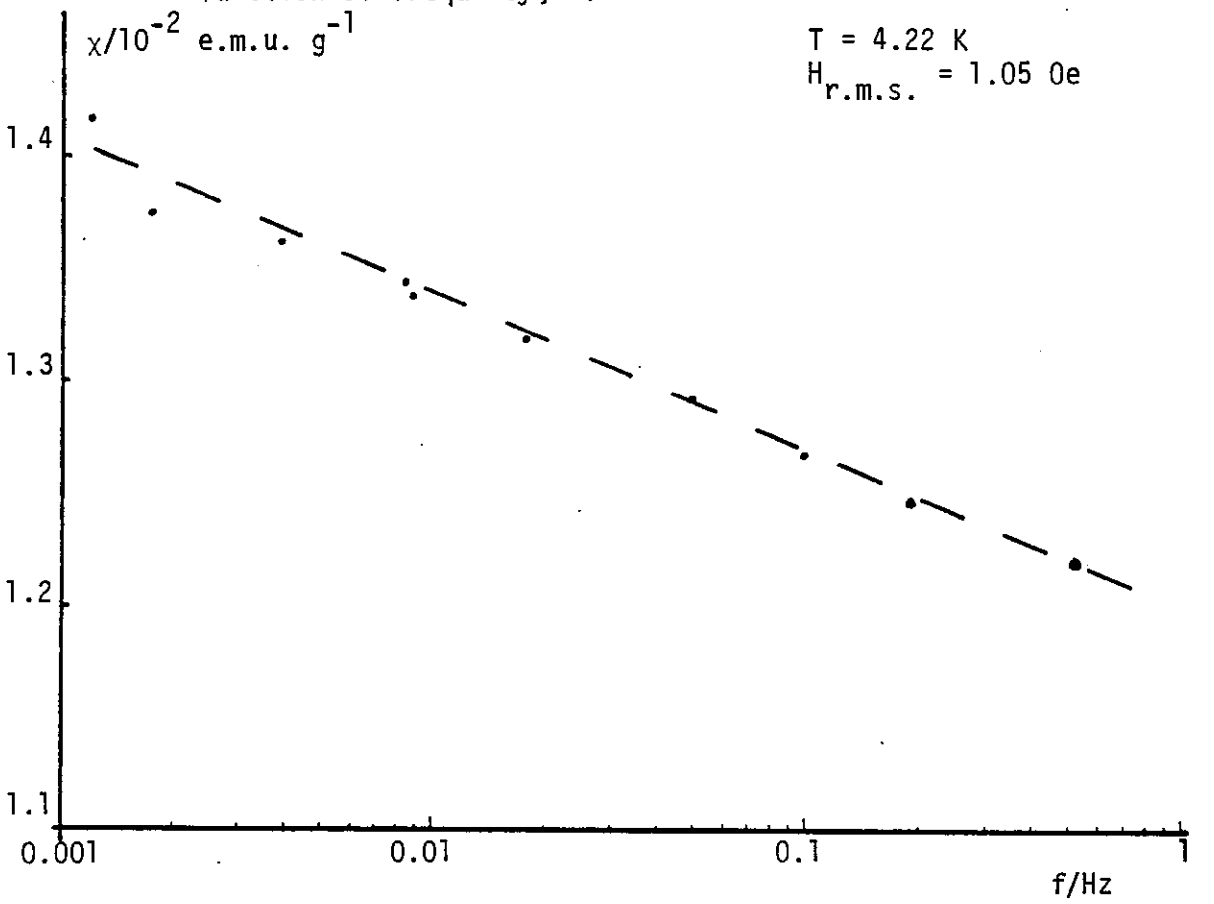

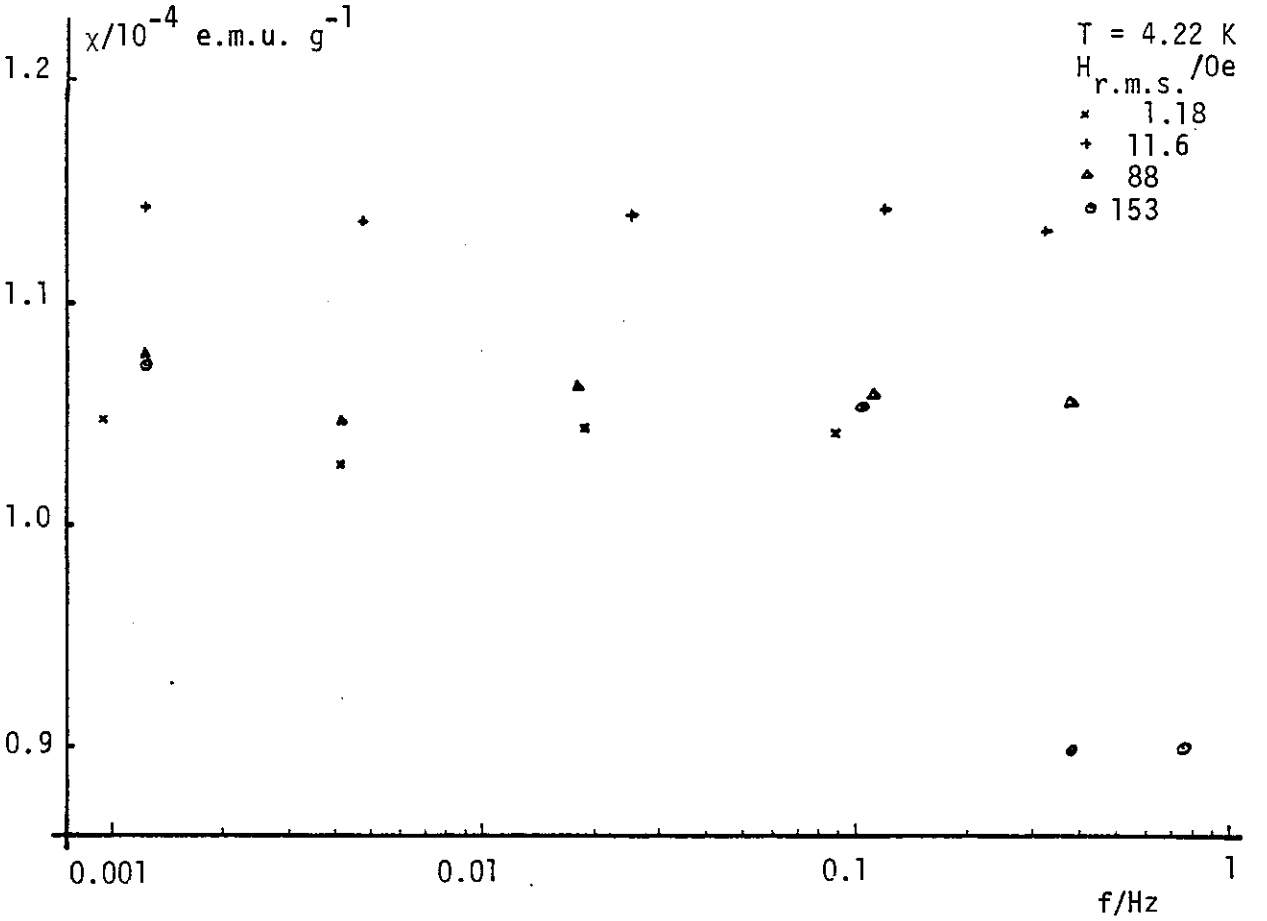

FIGURE 2.2 Alternating susceptibility, χ, of copper 1.5% manganese as a function of frequency, f.

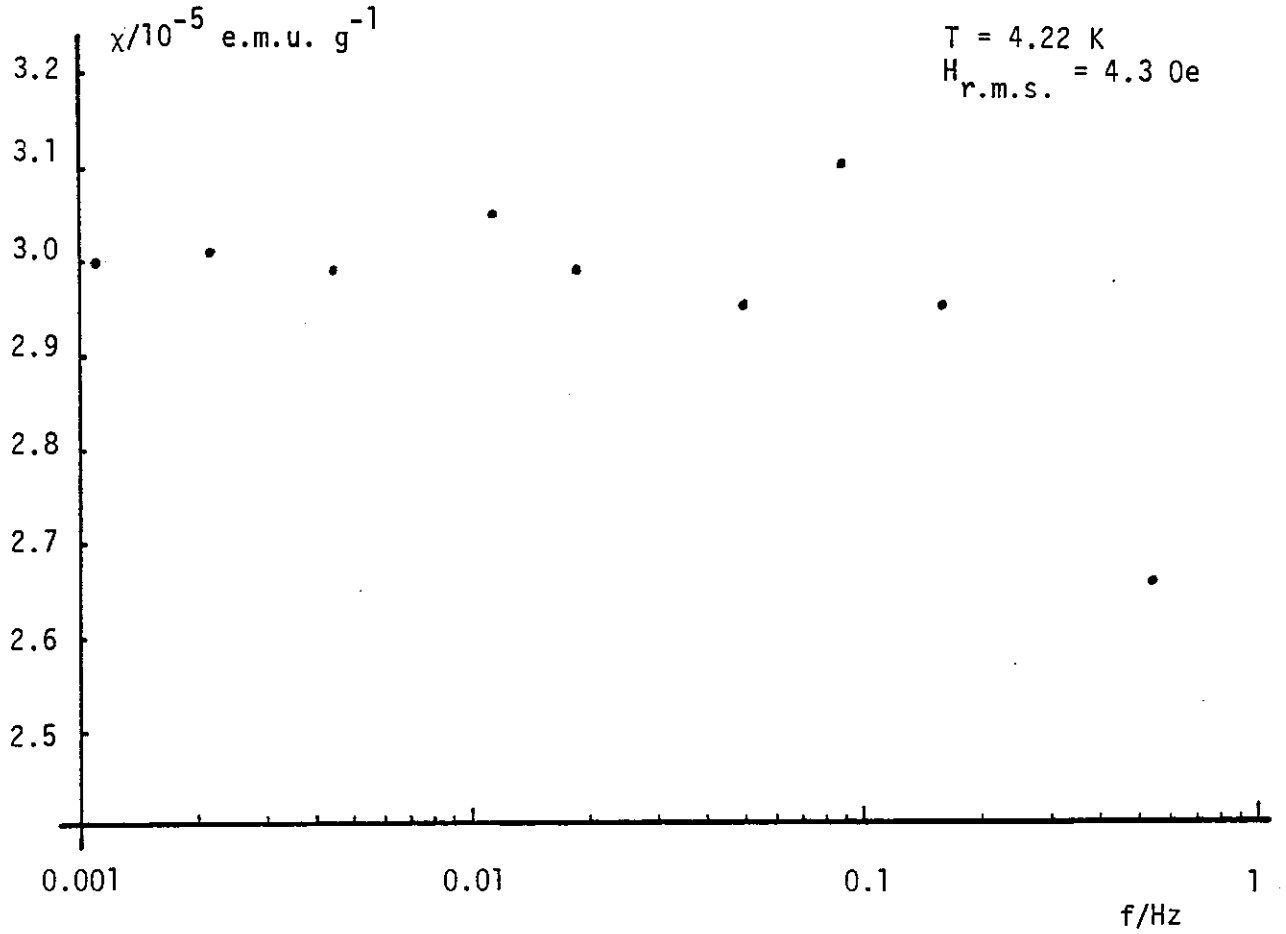

FIGURE 2.3 Alternating susceptibility, χ, of gold 4% iron as a function of frequency, f.

TABLE 2.1

FREQUENCY DEPENDENCE OF SUSCEPTIBILITIES

SAMPLE	R.M.S. APPLIED FIELD/Oe	R/% DECADE^{-1}
Copper 2% cobalt	1.05	-(5.8 ± 0.3)
Copper 1.5% manganese	1.18	(0.0 ± 0.7)
	11.6	-(0.1 ± 0.2)
	88	-(0.4 ± 0.6)
	153	-(0.5 ± 0.6)
Gold 4% iron	4.3	-(0.1 ± 0.9)

R is defined in terms of the susceptibility, χ, and the frequency, f, as

$$R = \frac{\Delta\chi}{\chi(f = 1\ \mathrm{Hz})\ \Delta \lg f}.$$

gallium alloys just to the gallium-rich side of "percolation" (Cywinski and Gray 1980), and with a broad susceptibility maximum at about 25 K.

The different absolute magnitudes of the copper-manganese data for different applied fields reflect the problems of cross-calibration of the X-Y plotter ranges. The last two points at 153 Oe reflect the measuring system response, and have been neglected in calculating the slope.

The increased scatter in the gold-iron data reflects a smaller signal and a consequential decrease in signal to noise ratio, especially at higher frequencies where the low pass filter can not be used so effectively.

Discussion of the Results

The most striking feature of these results is the large difference between the frequency dependence of the aged copper-cobalt alloy and the canonical spin glass alloys. In the former, the change of about 6% per decade at about one sixth of the temperature of the susceptibility maximum contrasts starkly with the changes of less than 1% per decade at $T_f/3$ in the copper-manganese, and $T_f/6$ in the gold-iron.

Thus it is clear that spin glass freezing is not just superparamagnetic blocking.

These results are consistent with the following picture. A superparamagnet begins to show a small frequency dependence in the susceptibility slightly above the temperature of the susceptibility maximum. As the temperature is lowered further, the frequency dependence continues to increase down to very low temperatures (Cywinski and Gray 1980). In a spin glass likewise, frequency dependent effects begin to be seen just above T_f, rapidly rising to a maximum, which may be large, as in the lanthanum-gadolinium-aluminium alloys (von Löhneysen et al. 1978) or small, as in copper-manganese,

and then, as the temperature is further reduced, these effects become smaller, possibly disappearing altogether as $T \to 0$ (Mulder et al. 1981). Both the susceptibility (as a function of frequency at constant temperature), and the value of T_f, vary, if at all, linearly in the logarithm of the frequency over a wide range of frequencies (10^{-3} Hz to 10^{4} Hz).

This may be expressed in terms of the correlation function. In both a superparamagnet and a spin glass the width in frequency of the transformed, zero-q correlation function $C^{zz}(0,\omega)$ is large at high temperatures and decreases as the temperature is lowered towards the freezing temperature. At any given fixed frequency, the response begins to decrease from a 1/T form (constant $C^{zz}(0,\omega)$) when the width in frequency becomes comparable to the measuring frequency.

The connection between the susceptibility and the correlation function becomes less certain at low temperatures for two reasons. Firstly, if the system is not in equilibrium (where the measuring time is less than the relaxation time) the connection between generalised (adiabatic) susceptibility and isothermal susceptibility is not maintained. That is

$$\lim_{t\to\infty} \langle \hat{\zeta}^z(0)\hat{\zeta}^z(t)\rangle \neq \langle \hat{\zeta}^z\rangle^2.$$

Secondly, and more significantly, even if the real part of the adiabatic susceptibility could be measured, the simple connection between the real and imaginary part,

$$\chi''(\omega) \propto \omega\chi'(\omega)$$

is not valid if there are low energy (frequency) magnetic excitations. The connection between real and imaginary parts must be derived using the full Kramers-Kronig relations, and it is only the imaginary part which is related to the (fluctuating part of the) correlation function.

The most that can be said is that a spin glass has a different form of correlation function from a frozen superparamagnet at low temperatures. One cause of this could be different types of low energy excitations or resonances (damped or undamped) in the correlation functions.

Although the present study did not involve variations of concentration of magnetic species at all, it seems clear that the frequency dependent effects are too small to measure, with current techniques, in very dilute spin glass alloys, but they increase as the concentration increases. This, however, does not imply that simple superparamagnetic blocking is becoming important, as this gives frequency dependence which varies very differently, with temperature, from that observed in spin glass materials.

These experiments could have been pursued further, but I decided not to do so because this technique is not the best one for this purpose. The changes in response with frequency are small compared with the total response in this frequency range, while experiments in the time domain, where the decay or growth of the magnetisation is observed over a long time interval, avoid this problem, and so are, in principle, more sensitive to the "low frequency" response. The reported logarithmic behaviour at intermediate times (Guy 1978) is consistent with the logarithmic behaviour in frequency at high frequencies in spin glasses (e.g. Mulder et al. 1981), but confirmation of preliminary results suggesting power law decay, using a very stable SQUID magnetometer system (Guy 1981, Dolezal and Guy 1981), is eagerly awaited.

CHAPTER 3

CHROMIUM-IRON ALLOYS - i. IS THERE A SPIN GLASS TRANSITION?

Introduction and Review

Chromium-iron binary alloys have been studied extensively in recent years from many points of view. The binary phase diagram (Hansen 1958, Elliott 1965 and references cited by them) is relatively simple, with an extended range of α (b.c.c.) solid solution. The only complications are the γ (f.c.c.) loop above 830°C and for less than 13.3% chromium, the appearance of a σ phase near the equi-atomic composition between 520°C and 820°C, and a low temperature miscibility gap extending between about 5% of either component at 450°C. With suitable preparation and heat treatment, therefore, a continuous series of b.c.c. solid solution alloys may be obtained, by quenching where necessary, at room temperature and below, from pure chromium to pure iron.

The magnetic possibilities of this system are intriguing, with the weak itinerant ferromagnetism of iron at one extreme (weak in the sense of having both up and down spin electrons at the Fermi level in the d-band), and the itinerant spin density wave (SDW) antiferromagnetism of chromium at the other. It is not surprising, therefore, that these alloys have attracted attention from many angles, both experimental and theoretical.

Much of this work has been reviewed by Burke (1980). The theory of the SDW ordering in chromium has now reached the stage of being able to account for the Néel temperature, the amplitude of the spin density wave, and the optical absorption peaks (the energy gaps at the Fermi level) (Fenton and Leavens 1980) in terms of an electron-hole k-state pairing model, which is thought to be equivalent to the virtual-bound-state model of Teraoka and Kanamori (1977) discussed by Burke.

However, the real behaviour even of pure chromium in undergoing a spin flip transition from a longitudinal to a transverse SDW requires yet more subtle theories. It is not surprising, therefore, that there are no adequate theories yet to explain the effect of alloying on the magnetic properties. A rigid band approach including the pair breaking effect of impurities is quite successful for "normal" solutes, which simply increase or decrease the effective number of electrons per atom in the band, but the effects of scattering by magnetic impurities in particular may be dominant, as in the case of iron as a solute.

The results of a large number of experiments, of many different kinds, for the magnetic structure of alloys of chromium with up to 35% iron are summarised in figure 3.1 (taken from Burke 1980). The antiferromagnetism is gradually destroyed by the addition of iron, and the Néel temperature goes to zero at about 16% iron. Ferromagnetism is established at 19% iron, and the behaviour in this concentration region resembles that of f.c.c. gold-iron alloys near 15% iron (figure 3.2, taken from Coles, Sarkissian and Taylor 1978). The obvious difference between the two systems is provided by the antiferromagnetic phase field in the chromium-iron system. But it is precisely in the corresponding region that the gold-iron alloys exhibit spin glass behaviour. The question to which this chapter is addressed is whether there exist in the chromium-iron alloys spin freezing phenomena similar to those in the dilute (<7% iron) gold-iron, canonical spin glass alloys.

On the face of it, it seems unlikely that the iron moments (if moments are indeed sustained on the iron sites) could ignore the magnetic ordering around them and behave as in a non-magnetic host like gold, but there are some suggestions that this is so. In the first place there is the magnetic susceptibility which was found to be given by a constant plus a Curie law (1/T) term in the early investigations

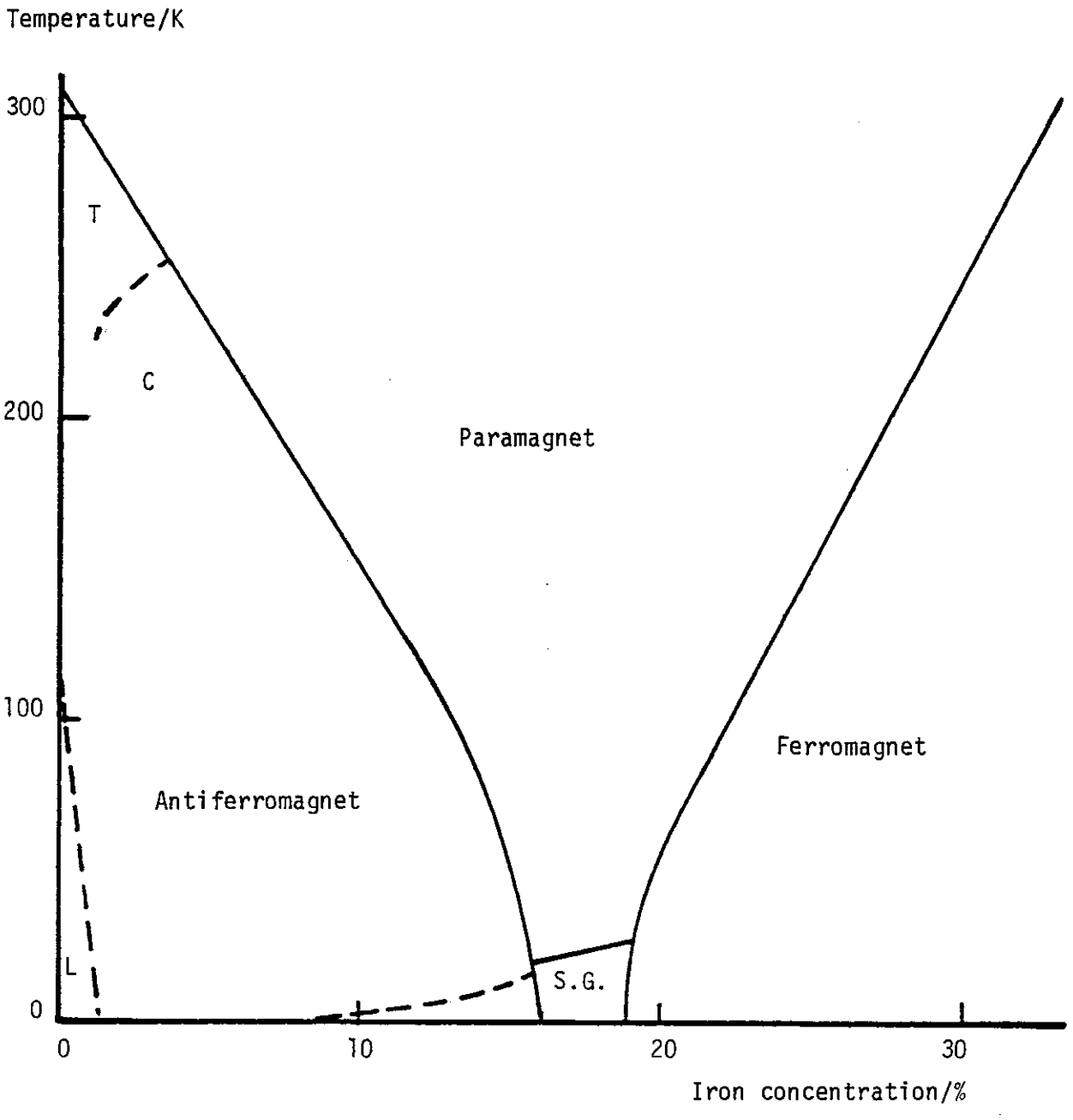

FIGURE 3.1 Magnetic phase diagram for chromium-rich chromium-iron alloys given by Burke (1980).

S.G. Spin Glass. The phase line is drawn as the locus of temperatures of susceptibility maxima.

C Commensurate antiferromagnet.

T Transverse Spin Density Wave (SDW).

L Longitudinal SDW.

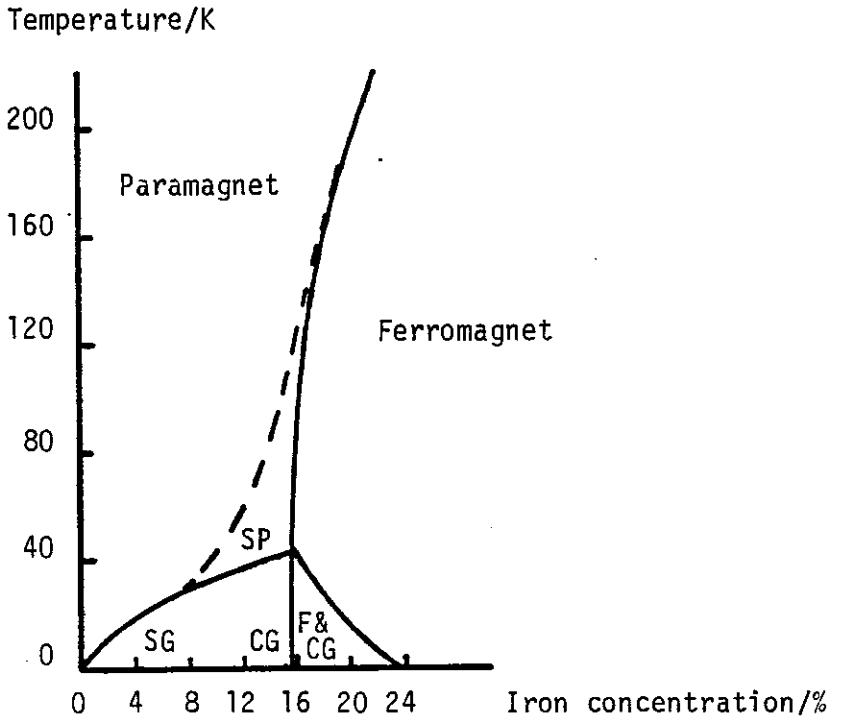

FIGURE 3.2 Magnetic phase diagram for gold-rich gold-iron alloys given by Coles et al. (1978).

SP Superparamagnet.

SG Spin Glass.

CG Cluster Glass.

F&CG Ferromagnet and Cluster Glass co-existence.

of the system by Newmann and Stevens (1959). They attributed this to the undisturbed chromium susceptibility (essentially independent of temperature) plus a term from very weakly interacting single iron moments, and they deduced an effective moment per iron atom of about 2.9 μ_B. Subsequent investigations have revealed that this latter term is linear in iron concentration (figure 3.3, taken from Hedgcock, Strom-Olsen and Wilford 1977) up to 5% iron and gives an effective moment of about 3.2 μ_B per iron atom. This should be compared with the effective moment of about 3.5 μ_B per iron atom found by Cannella and Mydosh (1972) in dilute iron in gold alloys (1 and 2%) at temperatures well above the freezing temperature. Note that this procedure for analysing the susceptibility, by subtracting some constant term to represent the undisturbed chromium susceptibility, is suspect in that it assumes a very weak coupling of the iron in the first place. However, for alloys with more than 2% iron, the contribution from the "constant term" is very small, and may be ignored at low temperatures ($T \lesssim 100$ K) in comparison with the Curie-like term.

Other interpretations of the susceptibility as a function of temperature have been suggested, and these will be discussed in chapter 4. The simple approach outlined above remains quite convincing, viewed in isolation.

The low field susceptibility of alloys with more than 10% iron shows a broad maximum at temperatures up to about 25 K (Burke 1980) and there are time-dependent remanence effects which persist down to 1.2 K (Ishikawa, Tournier and Filippi 1965, Burke 1980). These are the characteristics, as we have seen (chapter 2) of superparamagnetic freezing, and they seem to disappear at concentrations just less than 10% iron.

There is one reported measurement of "a.c. susceptibility" in chromium 1.5% iron (Katano and Mori 1979) which shows a sharp cusp at

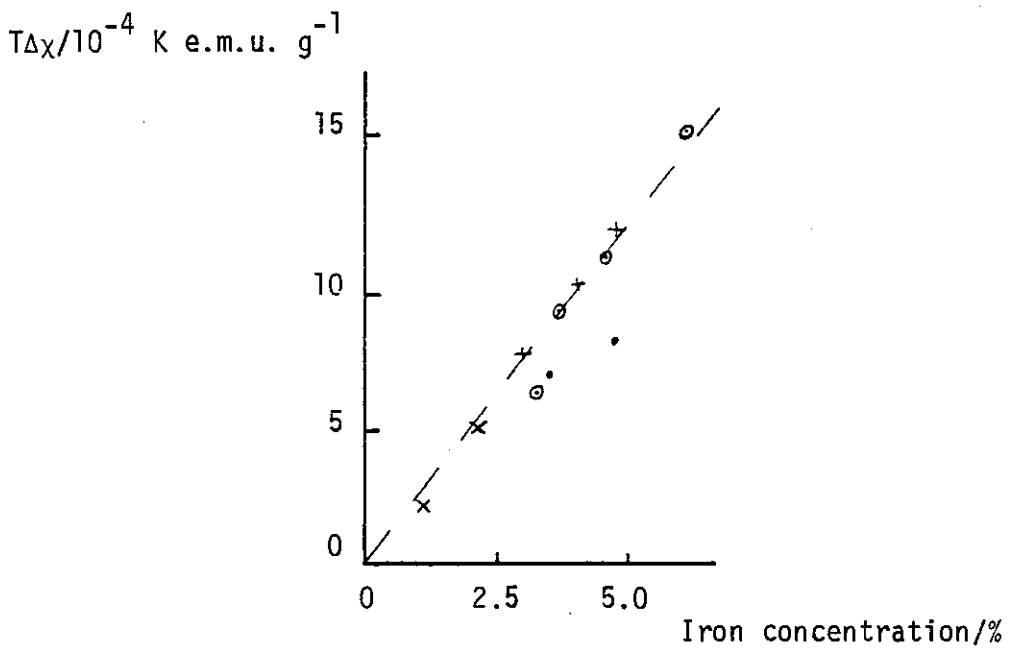

FIGURE 3.3 Effective low temperature Curie constant as a function of iron concentration, from Hedgcock et al. (1977).

⊙ Hedgcock et al. (1977).

· Ishikawa et al. (1965).

+ Suzuki (1966).

× Newmann and Stevens (1959).

2.8 K. Very little detail is revealed by these authors, and there may be reason to doubt this result. This will be further discussed in the conclusion of this chapter.

There are many other measurements which have been made which suggest that the isolated iron atoms behave very differently in chromium from the way they behave in gold, but the evidence above was considered sufficient to search for a "single-ion spin glass" in chromium-iron, as opposed to the superparamagnetic freezing seen at concentrations greater than 10% iron.

The possibility of such a spin glass is extremely attractive in that the properties will presumably be affected to some extent by the magnetically ordered environment, and there may be sufficient anisotropy imposed by the host to create an effectively Ising local moment system. That is, in the "paramagnetic" region, the moments will be constrained to lie in one of two (symmetrically opposed) directions in space, and in the "freezing" process, this choice is limited to just one of those directions. This direction may be defined by the local exchange field.

What, then, are the consequences of this picture? Firstly, that the magnetic susceptibility should exhibit a maximum at some non-zero temperature, which may be a sharp feature, as in the celebrated spin-glass "cusp" (Cannella and Mydosh 1972). Secondly, below this freezing temperature, there might appear small remanence effects, which may or may not be detected as being time dependent on the usual time scales. Thirdly, if there is some preference for an iron moment, on freezing, to choose one particular direction, either parallel to the chromium moment it replaces, or anti-parallel to it, then there would be an associated increase or decrease in the antiferromagnetic sublattice magnetisation over a limited temperature interval at the freezing temperature.

With the primary aim of finding this exotic spin glass, and thereby shedding light on the spin glass problem, a series of samples was prepared of chromium with up to 16% iron in solid solution.

Sample Preparation

Polycrystalline samples of about 15 g each were prepared of nominal compositions 0.0, 0.5, 1.0, 1.5, 2.0, 2.5, 3.5, 7.0, 10.0, 13.0 and 16.0% iron in chromium. The starting materials were Koch-Light chromium crystals prepared by reduction of the iodide (99.995% pure) and, for the samples up to 3.5%, Koch-Light iron wire (99.998% pure) and for the more concentrated alloys, Johnson Matthey Specpure iron bar (>99.998% pure). The ex-iodide chromium was used in preference to the (nominally higher spectrographic purity) Johnson Matthey chromium because of the high oxygen content of the latter (up to 1.14 atomic % according to Stone 1979). This causes a dispersion of oxide to form in the alloy on quite a fine scale, which may alter the properties both by changing the metallic composition of the alloy and by interfering with the magnetic properties directly (several of the oxides of chromium order magnetically). Small quantities of metallic impurity were considered to be less likely to affect the magnetic properties of these alloys.

The pure chromium was first melted in an argon arc furnace by standard techniques, re-weighed and then melted together with the appropriate quantity of iron. Repeated turning and re-melting of the ingot ensured large scale homogeneity. Typically, each ingot was melted eight to twelve times in this way. The ingot was then melted on a hearth with a semi-cylindrical depression to shape it into a roughly cylindrical form suitable for neutron diffraction measurements. The overall weight loss from this procedure varied from 0.4% to 2.3%. This is probably mostly due to the evaporation of the volatile chromium and

has an insignificant effect on the alloy composition.

Because of the large separation of the liquidus and solidus in this composition region (Hansen 1958), the solidification of the alloys in the arc furnace is likely to give rise to small scale inhomogeneities which may be large fractional composition fluctuations. To homogenise the samples, therefore, they were sealed under purified argon ($\sim$1/3 atmosphere) in a quartz capsule and kept at 1250^{o}C for 40 to 60 hours. To prevent de-vitrification of the quartz by the chromium, the samples were placed in a cleaned, re-crystallised alumina crucible inside the capsule. This, however, retained some nitrogen, and subsequently the samples were found to have needle-shaped inclusions characteristic of chromium nitride, Cr_2N (Hansen 1958 and references cited therein). The 1.0% and 2.0% samples were homogenised by wrapping them in tantalum foil, and sealing under argon in one quartz capsule which itself was encapsulated under argon in another, larger quartz capsule. This prevented nitride formation.

The samples were all quenched into water, breaking the capsule to ensure rapid cooling, directly from the furnace at 1250^{o}C. This should preserve the high temperature (single phase, almost random) structure of the alloys.

Sections of each ingot were taken from both ends and examined under the light microscope. Some of the samples, as noted above, showed small amounts of nitride inclusions, but they were all otherwise single phase. Electron microprobe analysis (Monk 1981 (a)) revealed good homogeneity on a scale of a few μm (±10% of nominal iron composition) with fluctuations of comparable magnitude on a scale of $\sim$100 μm in some, but not all, samples. The microprobe was also used to measure the average composition in each section. Some of the results are presented in table 3.1.

TABLE 3.1

RESULTS OF ELECTRON MICROPROBE ANALYSIS (MONK 1981 (a))

NOMINAL IRON COMPOSITION/%	COMPOSITION AS MEASURED BY ELECTRON MICROPROBE/%
1.0	1.0
2.5	2.6
3.5	3.5
7.0	7.3
16.0	16.1

Susceptibility Measurements

i. Samples

Samples for the susceptibility measurements were spark cut from the ingots to a suitable size (0.2 to 2.5 g). The shape is not important, as the relative permeability in the most concentrated sample measured (7% iron) does not exceed 1.002 even at helium temperatures. The samples were cleaned briefly in hydrochloric acid to remove both the thin surface coating of oxide which resulted from the quenching procedure and the thin layer damaged by spark machining.

ii. Apparatus and Measuring Procedure

The susceptibilities were measured in the low field vibrating sample magnetometer described by Howarth (1978) with the modifications described in appendix B. The (more or less) sharp features observed in metallic spin glasses in the susceptibility against temperature curves are not observed in applied magnetic fields larger than a few tens or hundreds of oersteds. Isothermal and thermal remanence are observed even in small fields down to $\sim$10 Oe (Guy 1977). As a compromise between high resolution and using a small applied field, a field of the order of 20 Oe was applied for about 20 s and then removed. This technique allowed the measurement of the (high frequency response) susceptibility, and also, observation of the (low frequency response) time dependent, or stable, remanence.

Measurements of the susceptibility in these alloys over the temperature range from 90 K to 500 K (Newmann and Stevens 1959) and from helium temperatures up to the Néel temperature (Hedgcock, Strom-Olsen and Wilford 1977 and references cited therein), have been performed many times, by many workers, with consistent results (figure 3.3), but this investigation concentrated on the temperature range from 1.8 K to 7 K, as this is the region where curious phenomena, from slight deviations from Curie-Weiss behaviour (Hedgcock et al.) to sharp

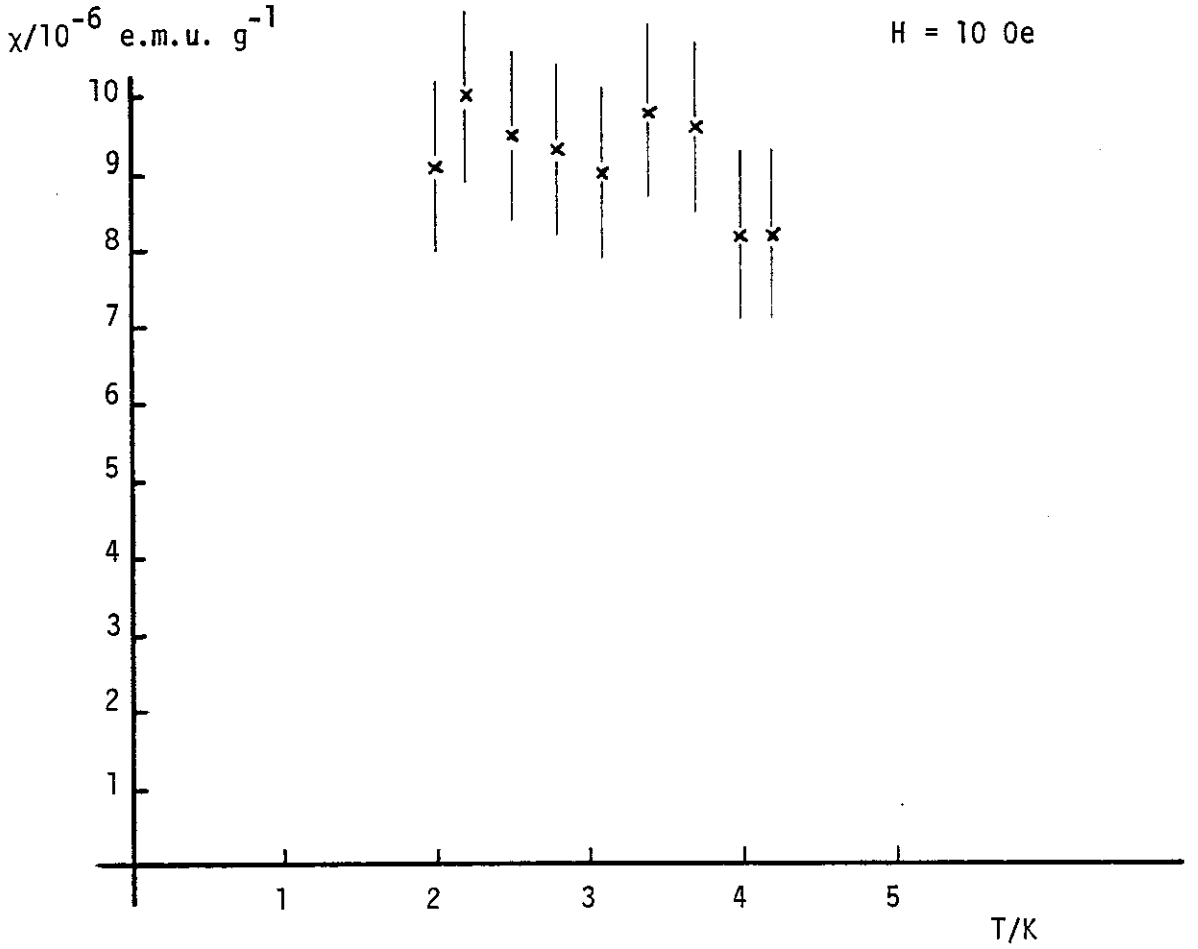

FIGURE 3.4 Low-field susceptibility of chromium 0.5% iron.

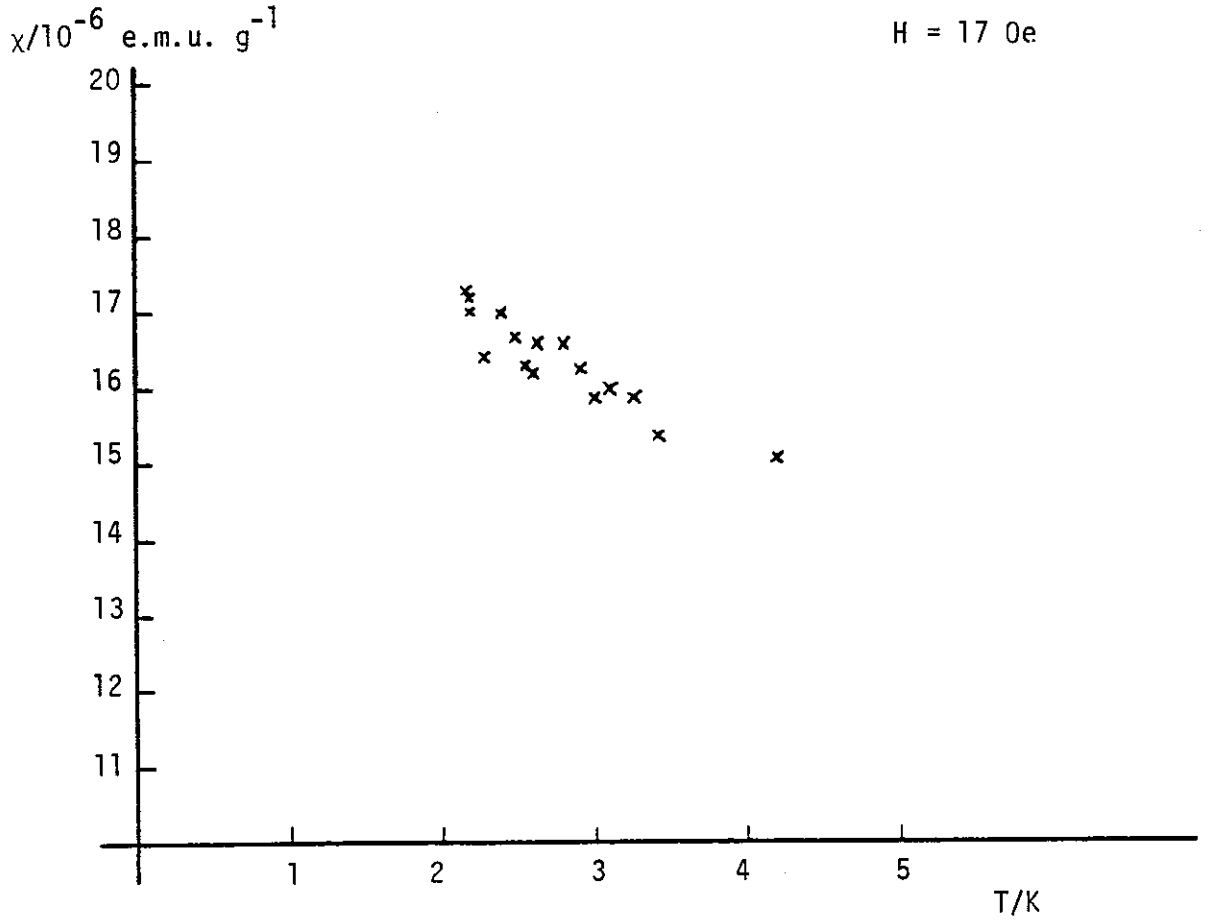

FIGURE 3.5 Low-field susceptibility of chromium 1.5% iron.

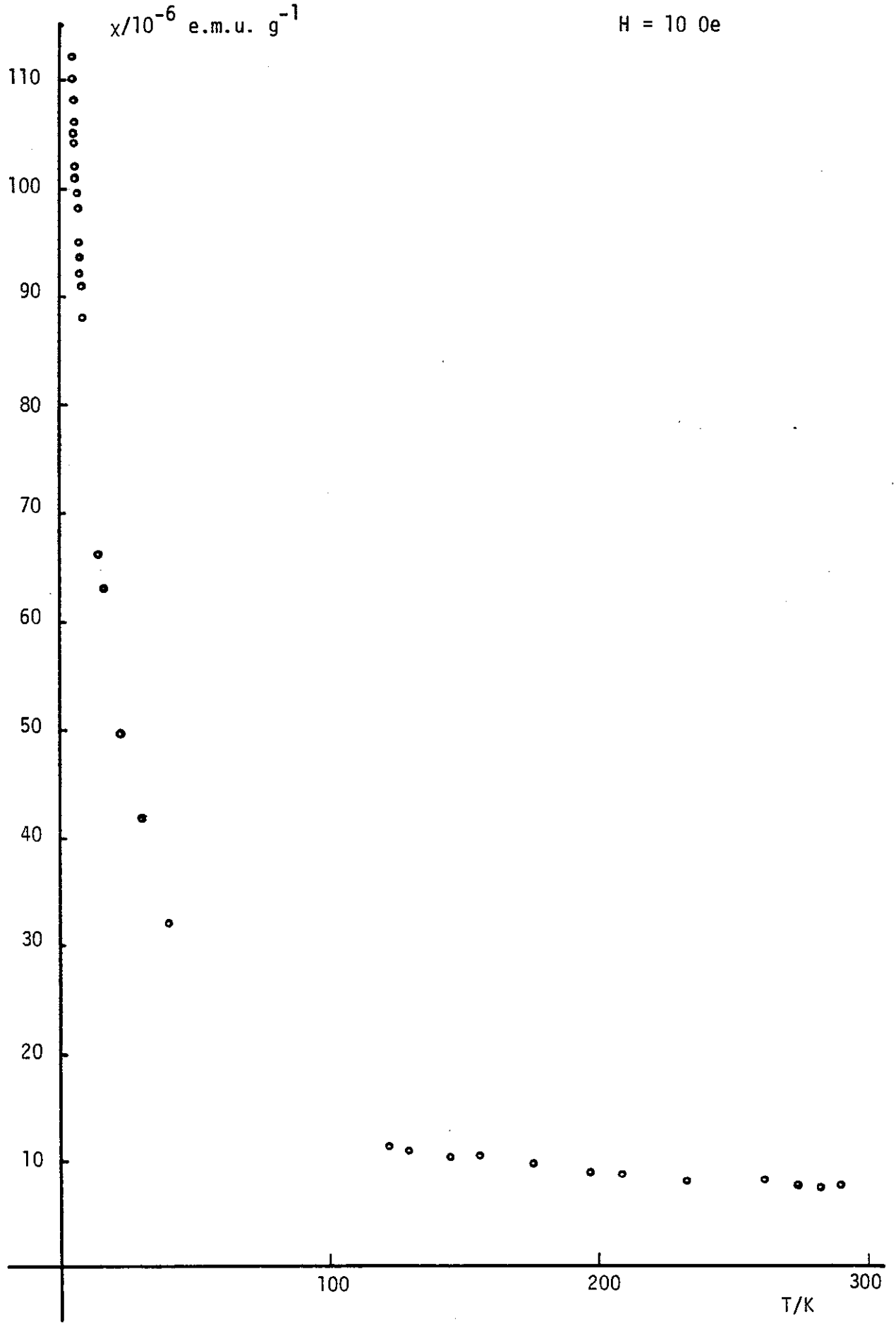

FIGURE 3.6 (a) Low field susceptibility of chromium 3.5% iron.

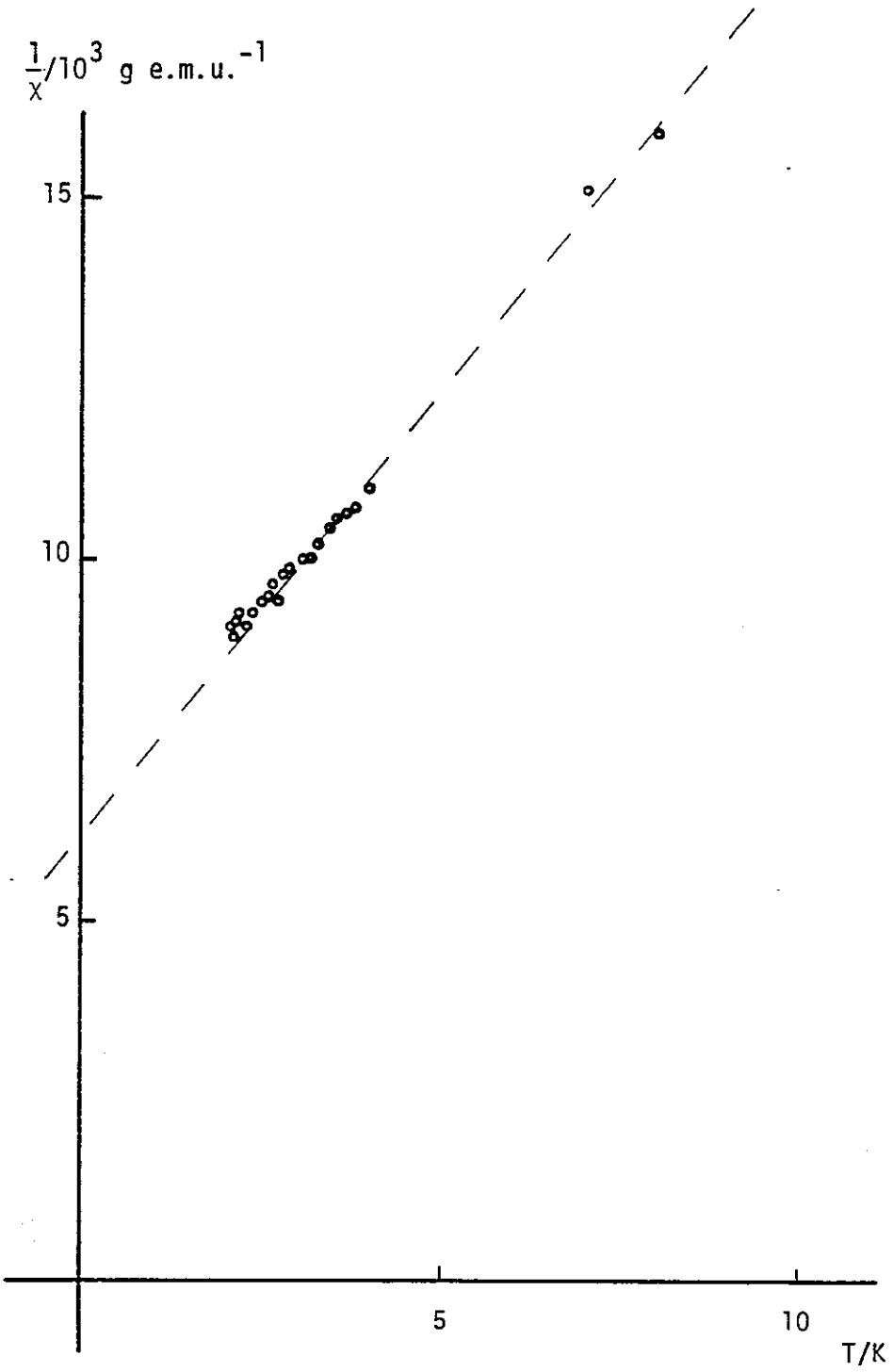

FIGURE 3.6 (b) Inverse susceptibility at low temperatures of chromium 3.5% iron.

The dashed line is a Curie-Weiss fit to the data in the range 7 K < T < 20 K.

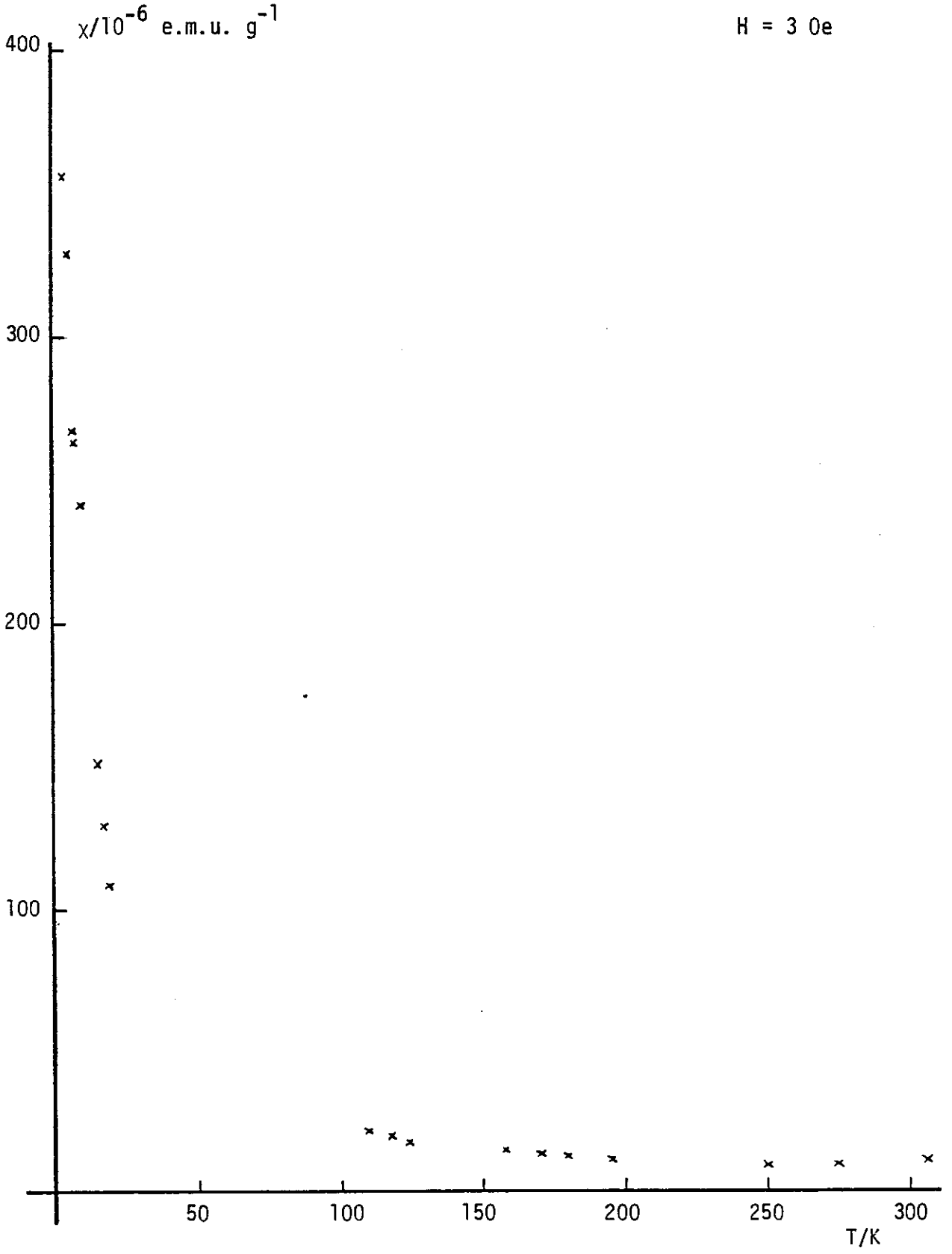

FIGURE 3.7 (a) Low field susceptibility of chromium 7% iron.

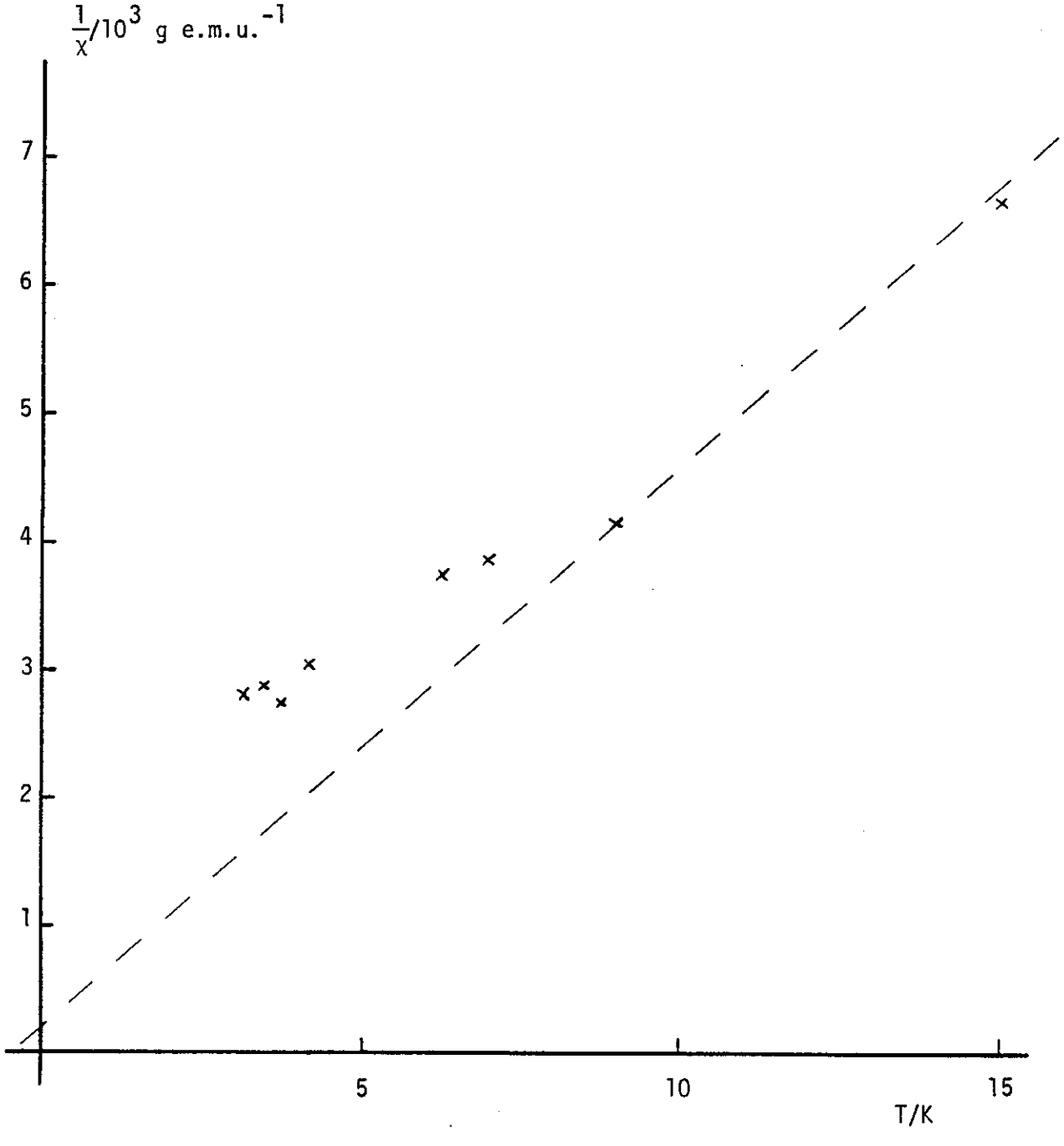

FIGURE 3.7 (b) Inverse susceptibility at low temperatures of chromium 7% iron.

The dashed line is a Curie-Weiss fit to the data in the range 10 K < T < 200 K.

maxima (Katano and Mori 1979) have been observed.

iii. Results

In these measurements, no remanence was detected at all within the experimental resolution, time dependent or time independent. This is in agreement with previous experiments (e.g. Ishikawa, Tournier and Filippi 1965). Furthermore, while some of the samples showed slight deviations at low temperatures from the Curie-Weiss-like behaviour seen at intermediate temperatures, none of the samples measured showed a maximum in susceptibility. The results for the chromium 0.5%, 1.5%, 3.5% and 7% iron samples are shown in figures 3.4 to 3.7 respectively.

iv. Discussion

The susceptibility, while deviating from the Curie-Weiss law at low temperatures, shows no maximum in alloys up to 7% iron between 1.8 K and 7 K. Thus while there may be some phenomenon in this range which might possibly be called "freezing", it is not characteristic spin glass freezing. This contradicts the result of Katano and Mori (1979) mentioned above.

The Search for Remanence

Remanent magnetisation, or the persistence of a magnetic moment in a material after the applied magnetic field is removed, has been known for millenia (in lodestones), and indeed has played a key rôle in the development of the science of magnetism. Most ferromagnetic materials exhibit remanence, but this is largely a "technical property" rather than a "physical" one, and it can be manipulated by changing the history of the material. This is largely due to the influence of impurities and imperfections which are said to pin the domain walls, or prevent them from moving. The shape and size of the sample may also affect the remanence, by stabilising a single domain state in a very small ($\sim$100 Å) particle, for example.

In a spin glass, however, the remanence, or the magnetic moment left after an applied field is removed "quickly", appears to be more of a fundamental physical property of the material. The dependence on sample thermal history is not so obviously large, although it may depend on the chemical short range order, or lack of it, in the alloy. But even when the chemical S.R.O. is made negligibly small, the remanence persists. It is also time dependent, and may depend in a very complicated way on the low temperature ($T \lesssim T_f$) magnetic history (e.g. copper manganese, Monod, Préjean and Tissier 1979).

i. Sample

A large sample (2.3 g) was cut in the form of a short cylinder from the chromium 3.5% iron ingot using the spark lathe. The surface was cleaned in hydrochloric acid to remove the oxide contamination and spark damage. This is as large a sample as may easily be measured in this apparatus.

ii. Apparatus and Procedure

The vibrating sample magnetometer used for these measurements is the high field apparatus built by Dr. C. N. Guy and modified by the author and described in appendix B. For this experiment, the magnet was the 40 kOe superconducting solenoid.

The remanence was measured isothermally by cooling to the temperature of the measurement in zero applied field (the earth's field was not eliminated) and then applying some field in one sense and removing it, then applying the same field in the other sense and removing that. The difference between the sample moments as measured five minutes after the removal of each sense of field was taken to be twice the remanence.

iii. Results

A very small remanent magnetisation was found in chromium 3.5% iron, and its dependence on applied field and temperature are shown in

figures 3.8 and 3.9. It was also time dependent, but the signal to noise was not sufficiently high to make a detailed analysis of its dependence on time. The slow decay seen could be fitted to a logarithmic dependence on time, or a (small) power law (figure 3.10).

It should be emphasised, however, that the magnitude of the observed remanence is extremely small. It was never observed to be greater than 4×10^{-4} e.m.u. g^{-1}, whereas the moment in a field of 20 kOe is about 1 e.m.u. g^{-1} (figure 3.11), in agreement with other measurements (Ishikawa et al. 1965, Babic et al. 1980).

iv. Discussion

The signals observed represent an upper limit to the isothermal remanence in chromium 3.5% iron. Other possible causes of the signal are trapped field in the magnet after the current leads are disconnected, or magnetic impurities either in the sample itself or, more probably, in the grease used to mount the sample to the holder. The former is possible, though unlikely, because of the observed dependence of the remanence on sample temperature (the magnet itself always being under liquid helium at 4.2 K). 8 Oe is, however, not a large value for the field trapped by such a solenoid, and would account for the "remanence" in terms of the sample susceptibility. The reproducibility of the results, after removing and remounting the sample, is not very good (figure 3.9), which suggests some contamination in the grease used for mounting as the cause of at least some of the observed remanence signal.

If the present result is compared to the results of Ishikawa et al. (1965) for the remanence in chromium 9% iron and 15% iron, where the remanence at 2 K is seen to scale roughly as the square of the concentration, it is smaller by a factor of 20 than the extrapolation to this concentration, assuming a continued quadratic dependence. In fact, if this upper limit is taken to be the true remanence at 2 K,

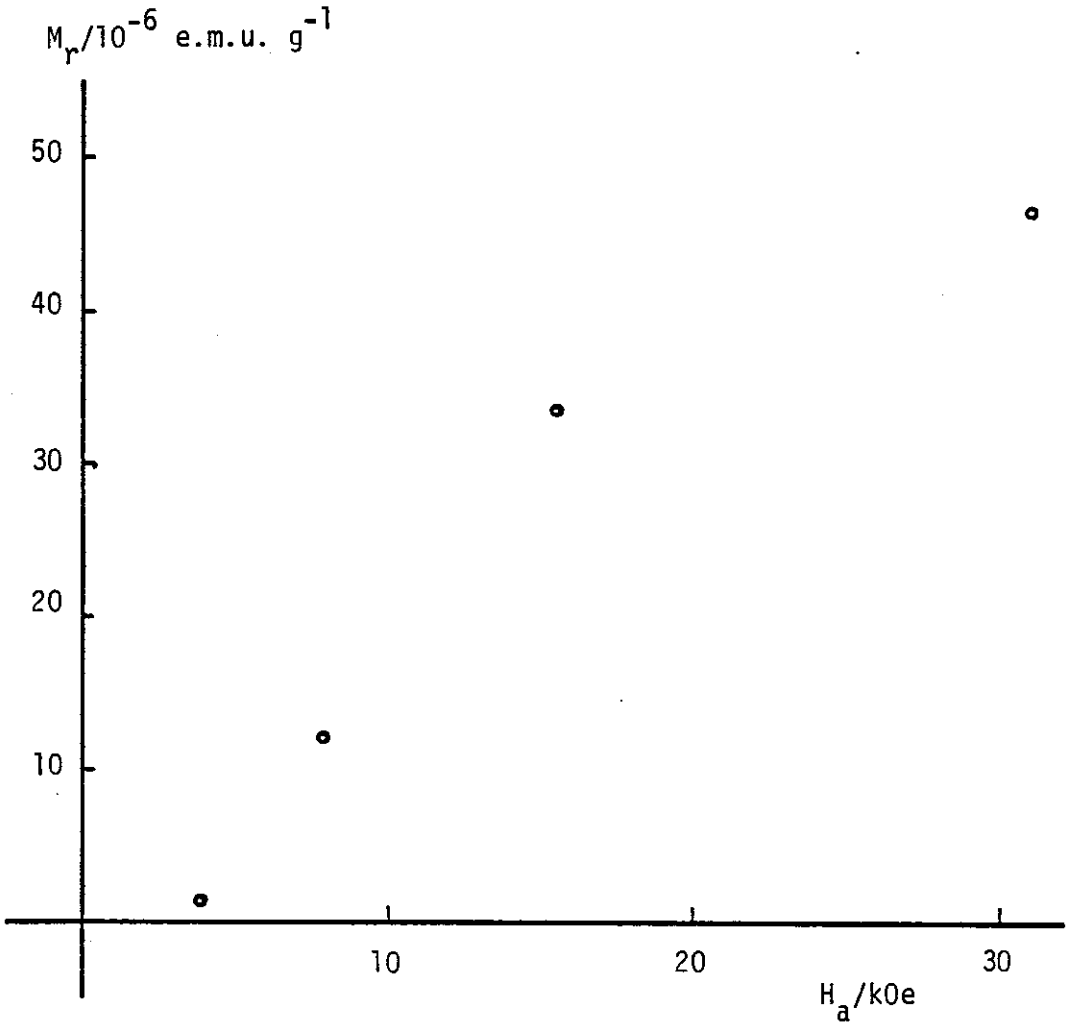

FIGURE 3.8 Remanent magnetisation, M_r, of chromium 3.5% iron at 4.2 K as a function of applied field, H_a.

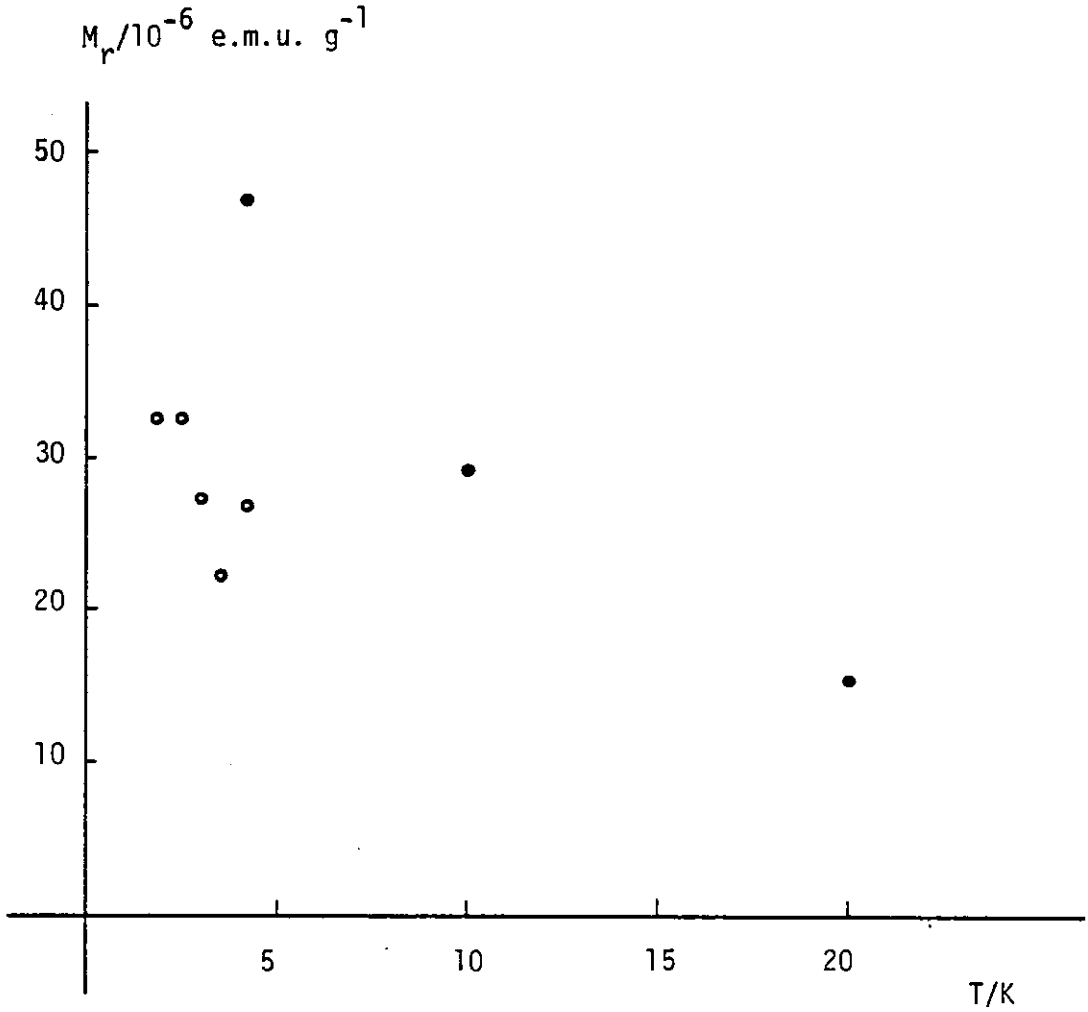

Measurements made

- ● 3.10.80
- ○ 15.10.80

FIGURE 3.9 Remanent magnetisation, M_r, of chromium 3.5% iron after 31 kOe applied, as a function of temperature, T.

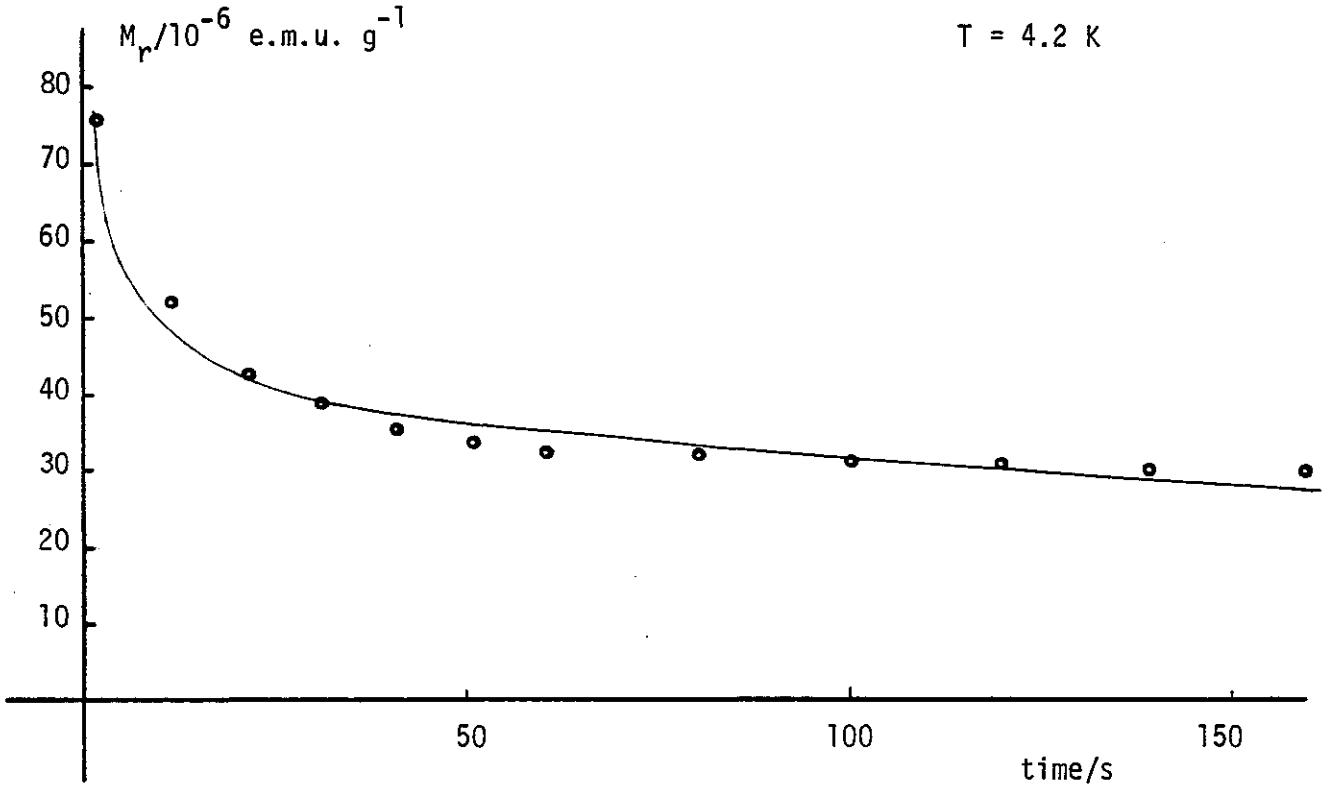

FIGURE 3.10 Remanent magnetisation, M_r, of chromium 3.5% iron as a function of time after the removal of 31 kOe applied field at 4.2 K.

The solid line represents

$$M_r(t) = M_r(0) - 7.31 \ln t$$

or

$$M_r(t) = 79.3\ t^{-0.20}.$$

On this scale, these two forms are almost indistinguishable.

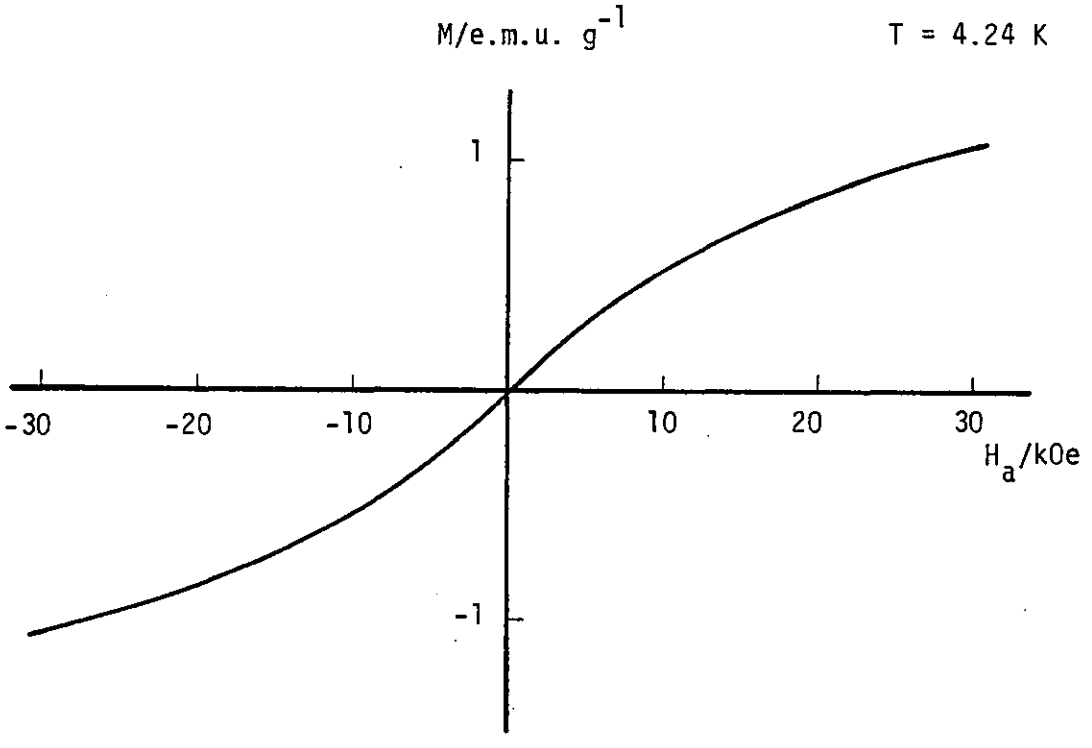

FIGURE 3.11 Magnetisation, M, of chromium 3.5% iron at 4.24 K as a function of applied field, H_a.
Time taken for 1 complete cycle of H_a is $\sim$500 s.
No hysteresis is observable on the scale of this figure.

then between 9% and 3.5%, it scales as the eighth power of the concentration.

If this remanence were a property of the sample, its temperature dependence (figure 3.9) reveals that it is unlikely to be associated with a transition around 4 K, as it has, if anything, a maximum in this temperature region.

The best explanation of these results is that they are to do with the magnetic impurities in the grease used to mount the sample. In any case, the remanence of the sample is very much smaller than that observed in the canonical spin glasses (e.g. gold 2% iron has a remanence of about 1 e.m.u. g^{-1} after field cooling to 10 K in 128 Oe, Guy 1978).

Sublattice Magnetisation Measurements

Measurements of the antiferromagnetic ordered moments as a function of temperature in polycrystalline alloys from pure chromium through to chromium 16% iron were made by neutron diffraction using the diffractometer D2 at the Institut Laue-Langevin in Grenoble. The intensity of the magnetic Bragg peak is proportional to the square of the ordered sublattice moment (e.g. Bacon 1975).

i. Powder Diffractometer D2

A detailed description and specification is given by Maier (1981). The main features are illustrated in figure 3.12. The neutrons come from the thermal beam tube H11 and are monochromated using a germanium 311 reflection with a wave length of 1.22 Å. This reflection has very low second order contamination because the 622 reflection, and all the even order reflections from these planes, are systematically extinct (i.e. they have zero structure factor).

The sample is mounted in a helium flow cryostat 53 IL HV 49 which has a wide aluminium tail with cadmium shields to prevent Bragg

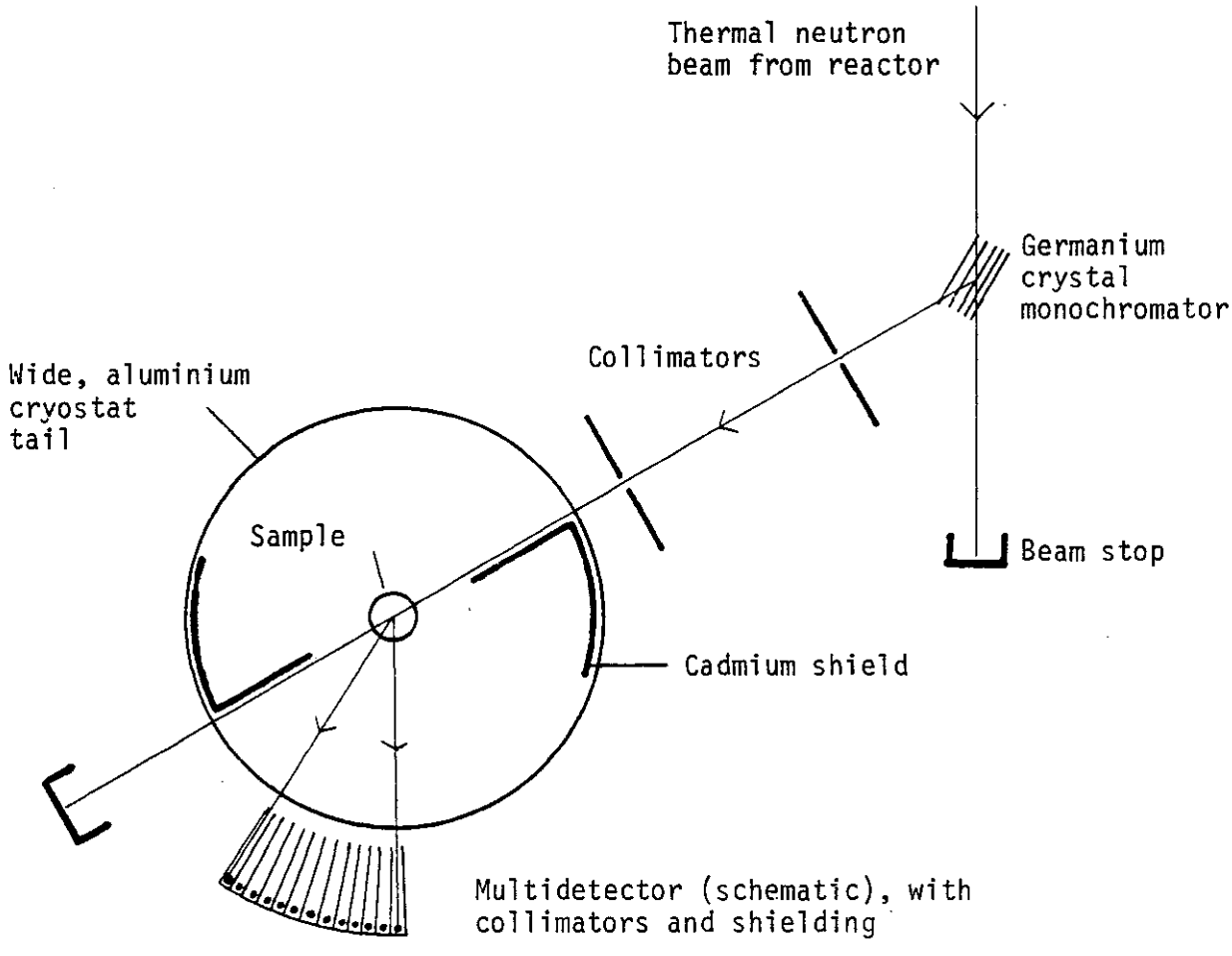

FIGURE 3.12 D2 diffractometer, plan in scattering plane. The cadmium shields prevent neutrons scattered by the aluminium tail from entering the detectors.

reflections from the aluminium from entering the counter.

The counter is a multidetector using ^{3}He gas and 64 detection cells which are 0.2^o apart, subtended at the sample position. The height of each detector is 80 mm, or $\pm 3^o$ from the horizontal.

The temperature of the sample is controlled from a calibrated silicon diode using a three term control heater in the block, and by adjusting the rate of helium flow. Temperatures below 4.2 K may be achieved by pumping on the helium bath.

ii. Measurements

The time available limited the number of samples measured to seven. They were the pure chromium, the 1.5%, 2%, 2.5%, 3.5%, 7% and 16% iron samples. The ingots were fastened to the sample rod of the top-loading cryostat using Kwikfill and with a small ring of boron carbide plastic at each end to facilitate the positioning of the sample in the neutron beam. This was achieved using a neutron sensitive polaroid camera. Typical photographs are shown in figure 3.13 for the 2.5% sample. The first picture shows the boron carbide rings, and the second was taken after finally setting the incident beam collimation.

The intensities of the magnetic (100) and nuclear (110) and (200) reflections were measured at a number of temperatures by positioning the multidetector to each reflection in turn. The magnetic and nuclear reflections are completely separated in a b.c.c. antiferromagnet with the simple two-sublattice structure of these (commensurate) alloys because of the conditions for non-zero structure factor, which are that $h + k + l$ is even for nuclear, and odd for magnetic Bragg peaks (hkl). It was planned to normalise the magnetic scattering with reference to the (110) peak, but problems with the samples prevented this in most cases. Normalisation to the (200) is in any case a safer procedure because preferred orientation has no effect on the (100) to (200) intensity ratio.

(a)

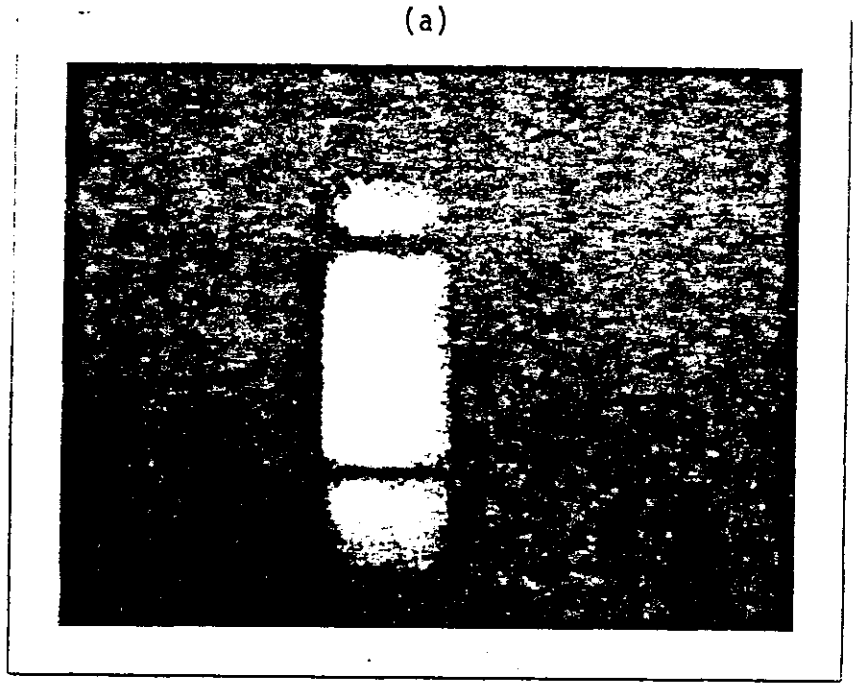

(b)

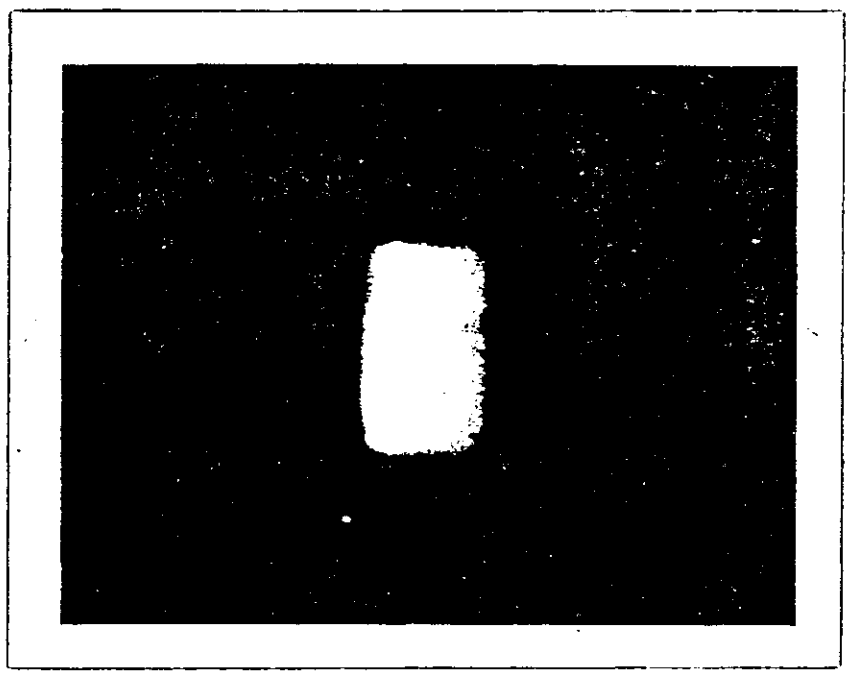

FIGURE 3.13 Neutron polaroid photographs of chromium 2.5% iron sample mounted in the cryostat on D2.

(a) Shadows of B_4C rings form dark bars.

(b) After final collimation of incident beam.

There have been several previous measurements of the temperature dependence of the magnetic reflections (Arrott, Werner and Kendrick 1967, Ishikawa, Hoshino and Endoh 1967, Burke and Rainford 1978, and Burke 1980) but these have tended to concentrate on the transition regions from paramagnetic to antiferromagnetic, and between the various antiferromagnetic phases. The purpose of this experiment was to concentrate on the low temperature region (2 K < T < 20 K), although some of the samples were also measured at higher temperatures.

iii. Problems Encountered

Very severe problems were encountered in this experiment. The prime cause was the very large grain size in some of the samples. Indeed, multicrystalline is a better description than polycrystalline for some of the samples, particularly the more dilute ones. This was suspected after observing some inconsistent and irreproducible results in the diffraction measurements, which were aggravated by small movements of the sample in the beam caused by the vibrations when the detector was moved from one position to another.

A neutron Weissenberg photograph (figure 3.14) taken on the pure chromium sample shows the scale of the problem. The Weissenberg picture is characteristic of two or three crystallites at most, through the thickness ($\sim$8 mm) of the sample.

The grain growth is thought to have taken place during the heat treatment of the samples. While this procedure was not very different from other preparation procedures of polycrystalline samples (e.g. Burke and Rainford 1978), the purer starting materials, particularly the reduction of the amount of oxide inclusions by using ex-iodide chromium, the strain induced by the fast cooling on the hearth of the arc furnace, and the higher annealing temperature combined to give "strain-anneal" crystal-growing conditions in the homogenisation treatment. The problem was not so severe in the more concentrated

FIGURE 3.14 Neutron Weissenberg photograph of pure chromium sample. Discrete spots are characteristic of large crystallites.

alloys, presumably because the oxygen dissolved in the iron precipitated out as oxide inclusions, and these helped to prevent the growth of the grains.

iv. Results

Many of the data taken during this experiment were worthless because of the problems outlined above. Normalisation to any nuclear peak other than one of the same symmetry as the magnetic (100) peak, like the (200), is meaningless, and the movement of the sample caused by moving the detector from the magnetic to nuclear peak and back again means that this procedure is also likely to be unreliable.

Nevertheless, some of the data are thought to be reliable. These are from the more concentrated alloys, where the grain size was small, or from the others when the detector was not moved, but left to track the (100) peak as a function of temperature at low temperatures. (Small movements due to thermal expansion make the higher temperature data suspect.) Only such data are here presented, in figures 3.16 to 3.19. A normalisation to the (200) intensity has been made only where the data permit. Otherwise the units for the cross-section are arbitrary.

The data were analysed both on-line on the PDP11 on D2 itself (detector efficiency corrections) and on the I.L.L. PDP10 after transfer of the data files. Standard programmes were used to normalise to the monitor counts and to create files of suitable format (D2MULT), and to fit each peak to a flat background and a gaussian peak (INTEGR) by an iterative least squares method. A permanent copy of each peak, with the fitting curve superimposed was obtained (e.g. figure 3.15), together with a listing of the background level and standard error, the peak centre, height, width and area, and their standard errors.

The most significant feature to note is that in none of the samples is there any significant change in the ordered moment between

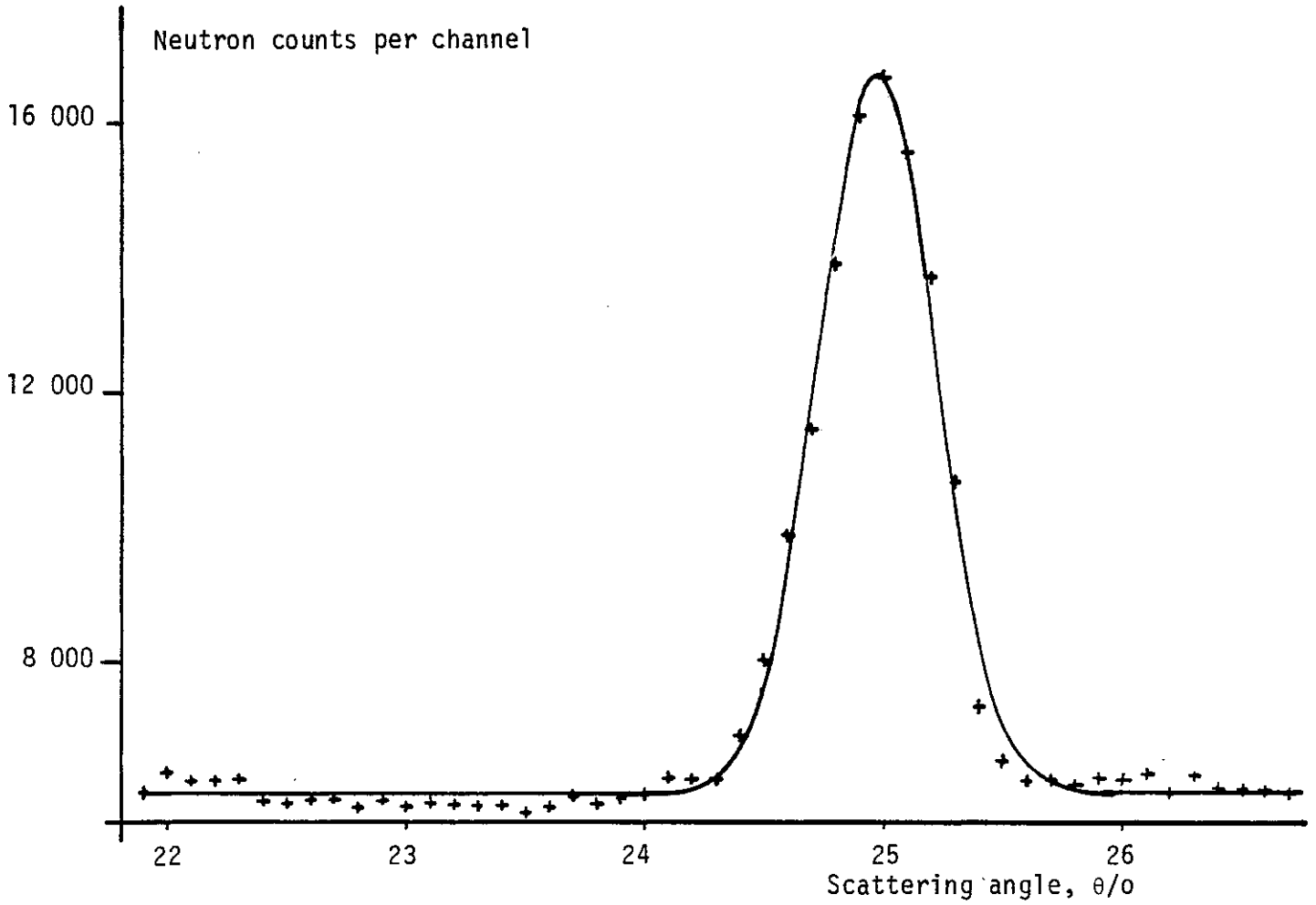

FIGURE 3.15 Computed fit of Gaussian peak and flat (isotropic) background. This is the (200) nuclear Bragg peak of chromium 1.5% iron.

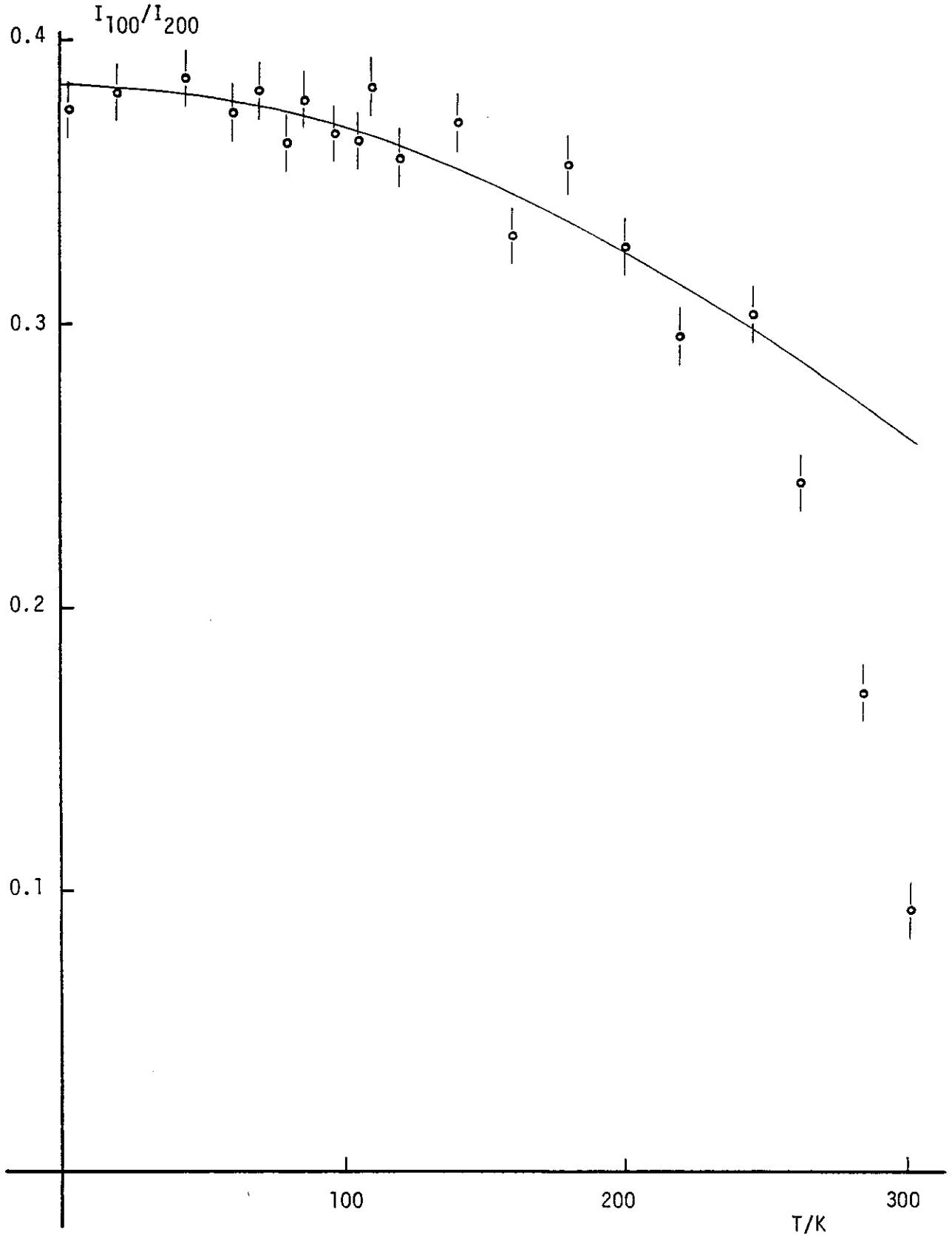

FIGURE 3.16 Ratio of magnetic (100) to nuclear (200) Bragg intensities in chromium 1.5% iron as a function of temperature, T. The line is a least squares fit to the spin-wave form

$$(I(T))^{\frac{1}{2}} = (I(0))^{\frac{1}{2}} - aT^2$$

for $T \leqslant 245$ K.

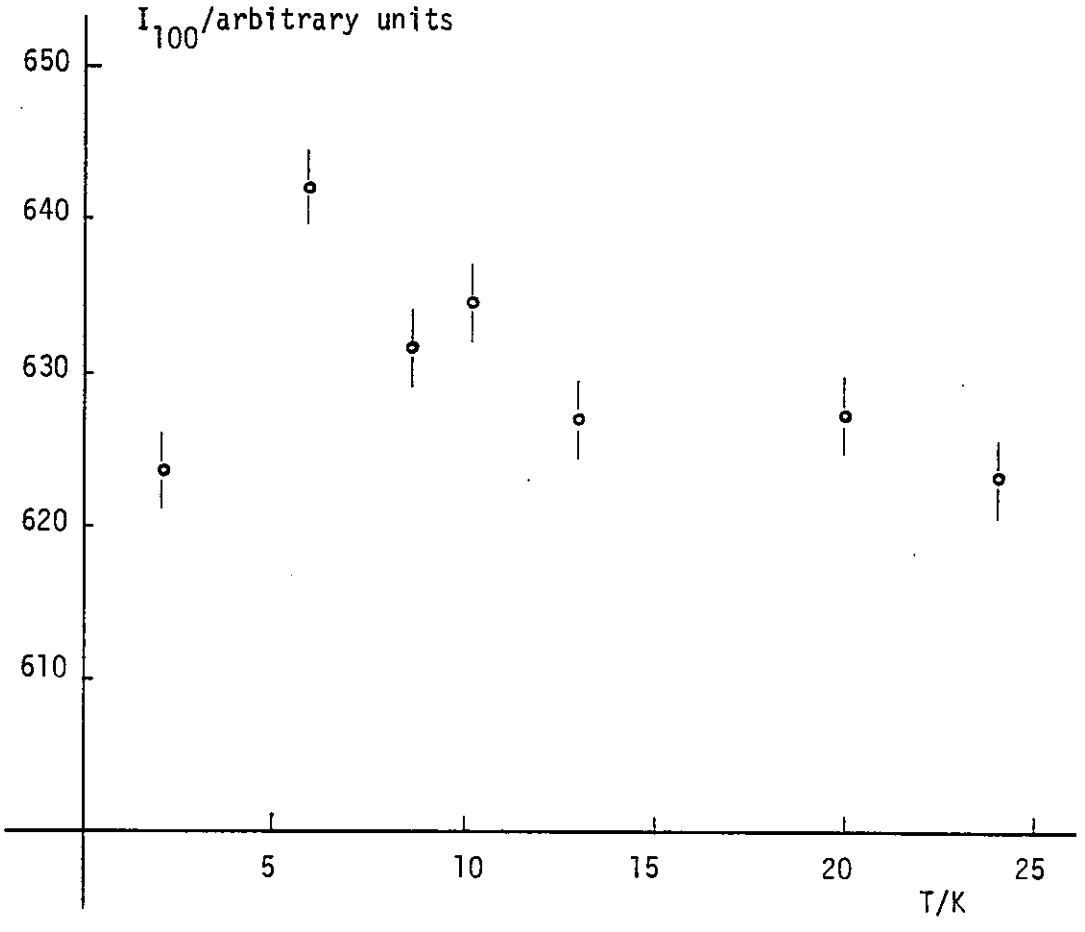

FIGURE 3.17 Intensity of (100) magnetic Bragg peak in chromium 2.5% iron at low temperatures. Error bars represent the statistical uncertainty.

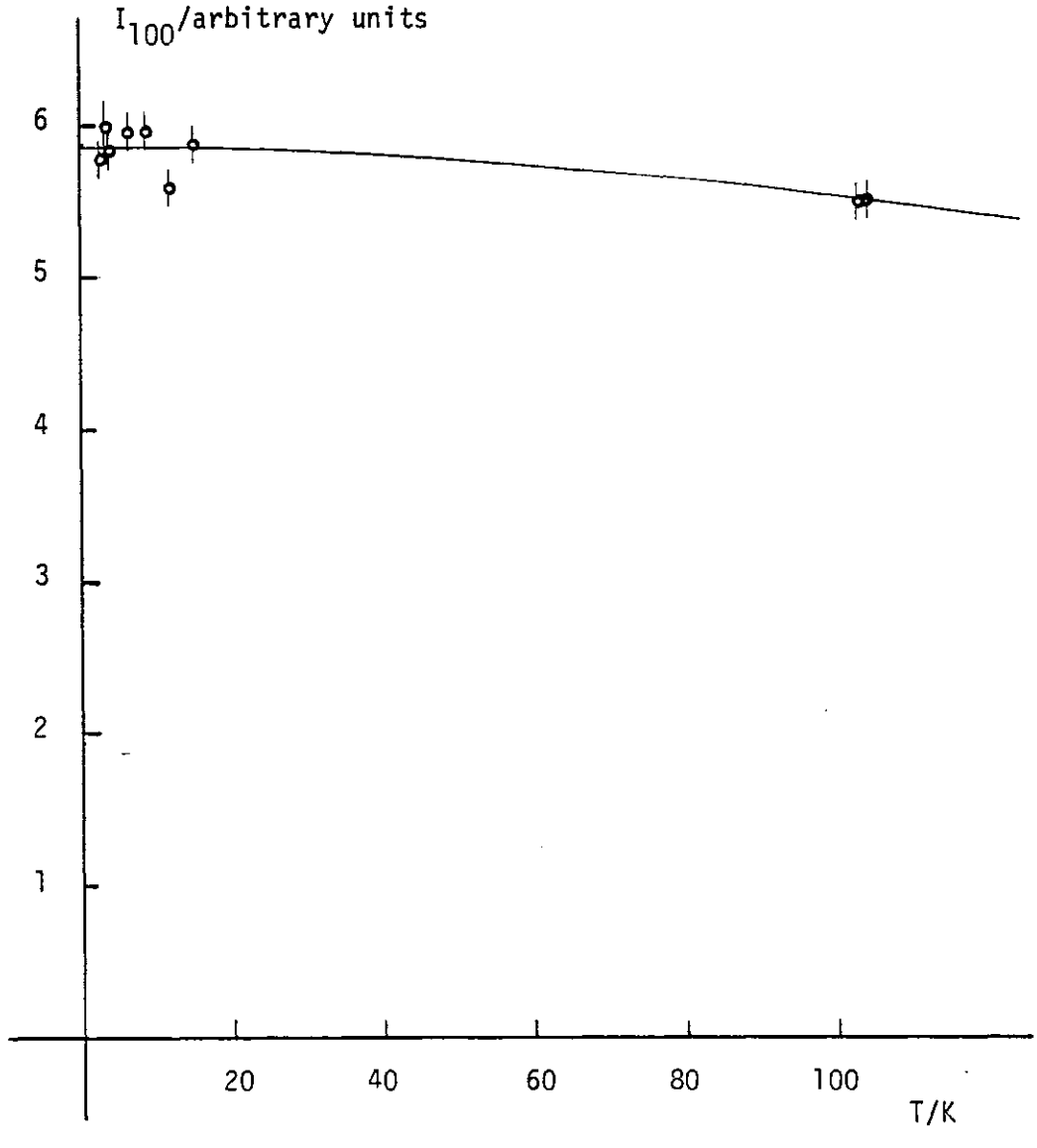

FIGURE 3.18 Intensity of (100) magnetic Bragg peak in chromium 7% iron at low temperatures. Error bars represent the uncertainty in fitting the raw data to a Gaussian peak.

The line represents a least squares fit to the spin-wave form

$$(I(T))^{\frac{1}{2}} = (I(0))^{\frac{1}{2}} - aT^2$$

for $T < 105$ K.

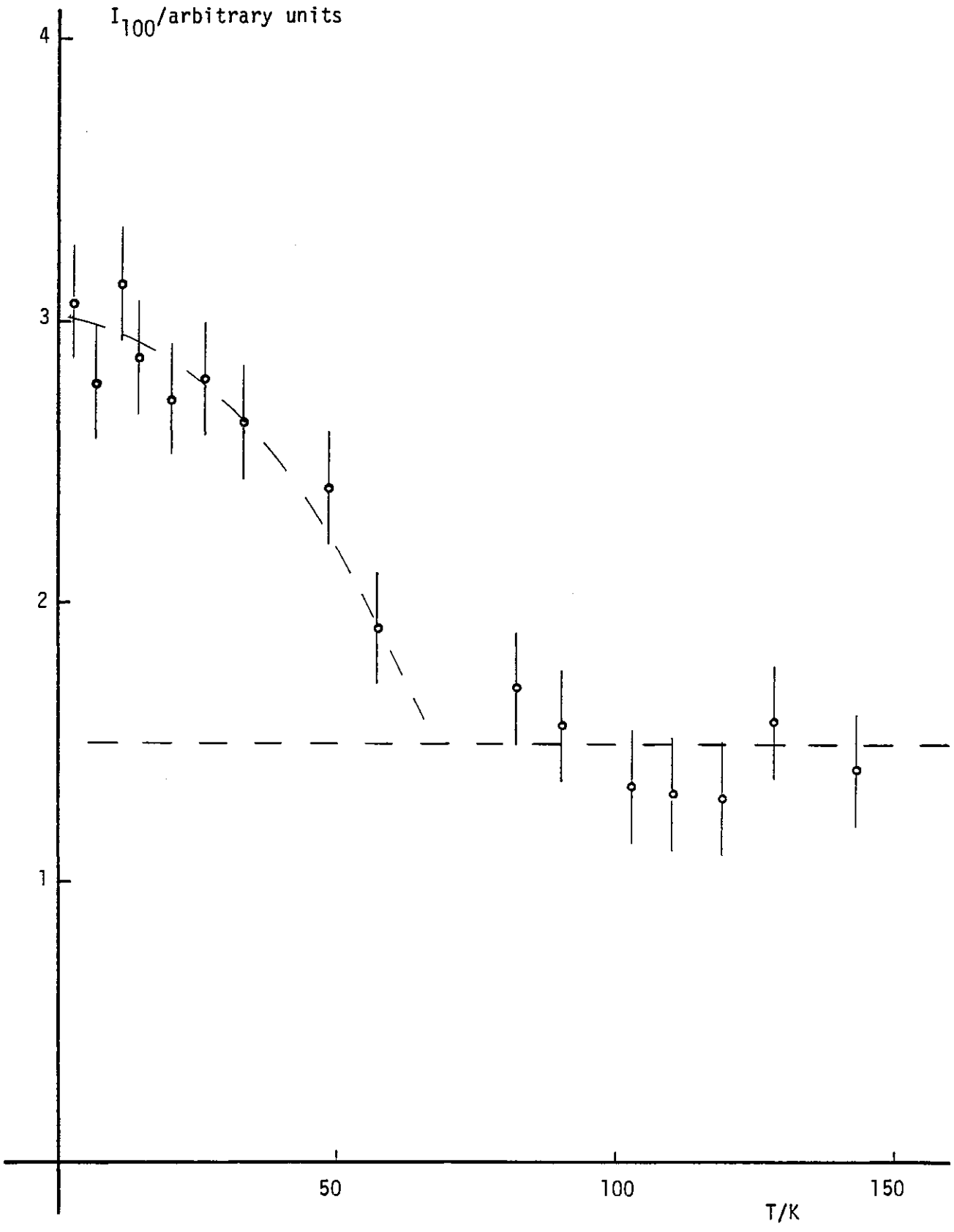

FIGURE 3.19 Intensity of (100) magnetic Bragg peak in chromium 16% iron. Error bars represent the uncertainty in fitting the raw data to a Gaussian peak.
The broken lines are guides to the eye.

2 K and 20 K, in which temperature region the "spin glass" transition is postulated to occur.

Perhaps the other feature worth noting is the existence of a temperature dependent (100) reflection in the 16% iron sample. The appearance of a temperature independent intensity, though extremely small, is surprising. It may be some higher order contamination effect, in view of the high flux at high energies in the thermal beam tube (measured in fact for H12, Maier 1981) although this is unlikely to be the cause as discussed above. The temperature dependent part, however, is certainly a magnetic contribution. The possibility that this is caused by inhomogeneities in the sample is ruled out by the electron microprobe analysis which shows an average composition of 16.1% and fluctuations corresponding to (16.1 ± 0.8)% on a scale of 5 μm. While these fluctuations could explain the apparent Néel temperature (70 ± 15 K), they do not explain the size of the ordered moment (0.09 ± 0.01 μ_B at^{-1}) c.f. Burke and Rainford (1978).

Although the data are not very good, some of the sublattice moment against temperature measurements have been fitted to the form

$$M_S(T) = M_S(0)(1 - aT^n)$$

The fitting parameters are shown in table 3.2 for the best (least squares) value of n, and the value of the parameter "a" when n = 2, corresponding to the spin wave theory prediction (Marshall and Lovesey 1971).

v. Discussion

The antiferromagnetic phase is seen to extend to slightly higher concentrations than was previously thought.

There is no sign in any of the samples measured of any low temperature anomaly in the ordered moment corresponding to a non-random freezing transition. The upper limit to the "ordered" iron moment in,

TABLE 3.2

LOW TEMPERATURE LEAST SQUARES FIT OF SUBLATTICE MAGNETISATION, M_S, TO THE FORM $M_S(T) = M_S(0)(1 - aT^n)$

NOMINAL SAMPLE COMPOSITION/%	BEST (LEAST SQUARES) VALUE OF n	$a/10^{-6}$ K^{-2} WHEN n = 2
1.5	2.4	2.01 ± 0.22
2.5	2.2	2.44 ± 0.30
7.0	0.4	2.96 ± 0.85

for example, the 7% sample is about 0.2 μ_B per iron atom.

In spite of the severe difficulties encountered in this experiment, the results are sufficient to show that the observed effect is very much smaller than that corresponding to an ordered iron moment of 2 μ_B, if such a moment were to "freeze into" the ordered structure at low temperatures.

Conclusion

The conclusion drawn from the experiments described here is that there is no spin glass freezing in alloys of chromium with less than 7% iron. The susceptibility result of Katano and Mori (1979) showing a sharp cusp is hard to reconcile with the data presented here. The magnitude of their result is larger than the magnitude I measured by a factor of 3×10^4. (This odd factor renders less likely the possibility of their omitting a power of 10 scale factor.)

The conclusion of the absence of a spin glass phase in chromium-iron alloys (though there is certainly evidence for superparamagnetic freezing in alloys with 10% iron and more) does not solve any of the problems associated with these alloys. The very nature of the moment sustained on the iron sites, if any, has not been conclusively decided, and it is to this quest that we turn in the next chapter.

CHAPTER 4

CHROMIUM-IRON ALLOYS - ii. NATURE OF THE IRON MOMENT

Introduction

The magnetic properties of dilute alloys of iron in chromium are not yet well understood. The essential problems are two. Firstly, do isolated iron atoms sustain a magnetic moment within the antiferromagnetic or spin density wave (SDW) structure of the chromium? Secondly, if so, what is the nature and strength of the interaction between the impurity and the host?

In this chapter, a brief review of some of the experimental and theoretical work done on these alloys will be followed by the description of some experiments designed to help answer these questions, and finally an ad hoc theory will be tentatively suggested to resolve some of the problems.

Review - a. Experimental Properties

Some of the experimental results for chromium-iron alloys were mentioned in chapter 3. They will be recalled here, with some others. For convenience, they will be divided into four groups: bulk properties, hyperfine field (Mössbauer) measurements, E.S.R., and neutron diffraction studies. It should be stressed that many of the alloys used for the measurements are only metastable at low temperatures because of the miscibility gap in the phase diagram. This means that the physical properties may depend on the method of preparation, and in particular, the thermal history after mixing. It will be assumed here that the alloys have been quenched rapidly to room temperature from 1000^{o}C or higher (but below the melting point) after some time at high temperature after solidification. I will indicate if the results are from samples prepared in a different way.

i. Bulk Properties

The magnetic susceptibility has been measured as a function of temperature by many workers, with broad agreement (Lingelbach 1958, Newmann and Stevens 1959, Ishikawa et al. 1965, Suzuki 1966, Booth 1966, Hedgcock et al. 1977, Hedman et al. 1978, Makarov et al. 1979, Burke 1980, this work (chapter 3 above); note that the samples of Suzuki were annealed but not quenched, and the samples of Makarov et al. were quenched from the melt), see figure 4.1, compiled from several sources. The data is rarely presented as susceptibility against temperature, as most authors wish to emphasize the Curie-Weiss-like nature of the change in susceptibility from pure chromium to the alloy, both above and below the Néel temperature, and so the usual plot is of inverse susceptibility change against temperature. By using the Curie constant, values are then extracted for the (local) moment per iron atom and the Curie-Weiss temperature (figure 4.2, taken from Ishikawa et al. 1965). More subtle fitting schemes have also been used (e.g. Hedman et al. 1978) with more fitting parameters. The susceptibility of the alloys generally shows a more emphatic change at the Néel temperature than does pure chromium, which shows a very small change in slope. This effect becomes smaller again for more concentrated alloys.

The low temperature, almost Curie-like, contribution to the susceptibility has been interpreted in many ways (see the theory review below), but is generally taken to indicate that some, or all of the iron atoms carry (local) moments which are free to behave paramagnetically to a greater or lesser degree, in spite of the antiferromagnetic order of the matrix in which they lie.

Several measurements have been made of the magnetisation as a function of applied field and temperature at low temperatures (Ishikawa et al. 1965, Babic, Kajzar and Parette 1980, who used pulsed fields up to 33 T at 4.2 K, Hedgcock et al. 1977, who also measured the

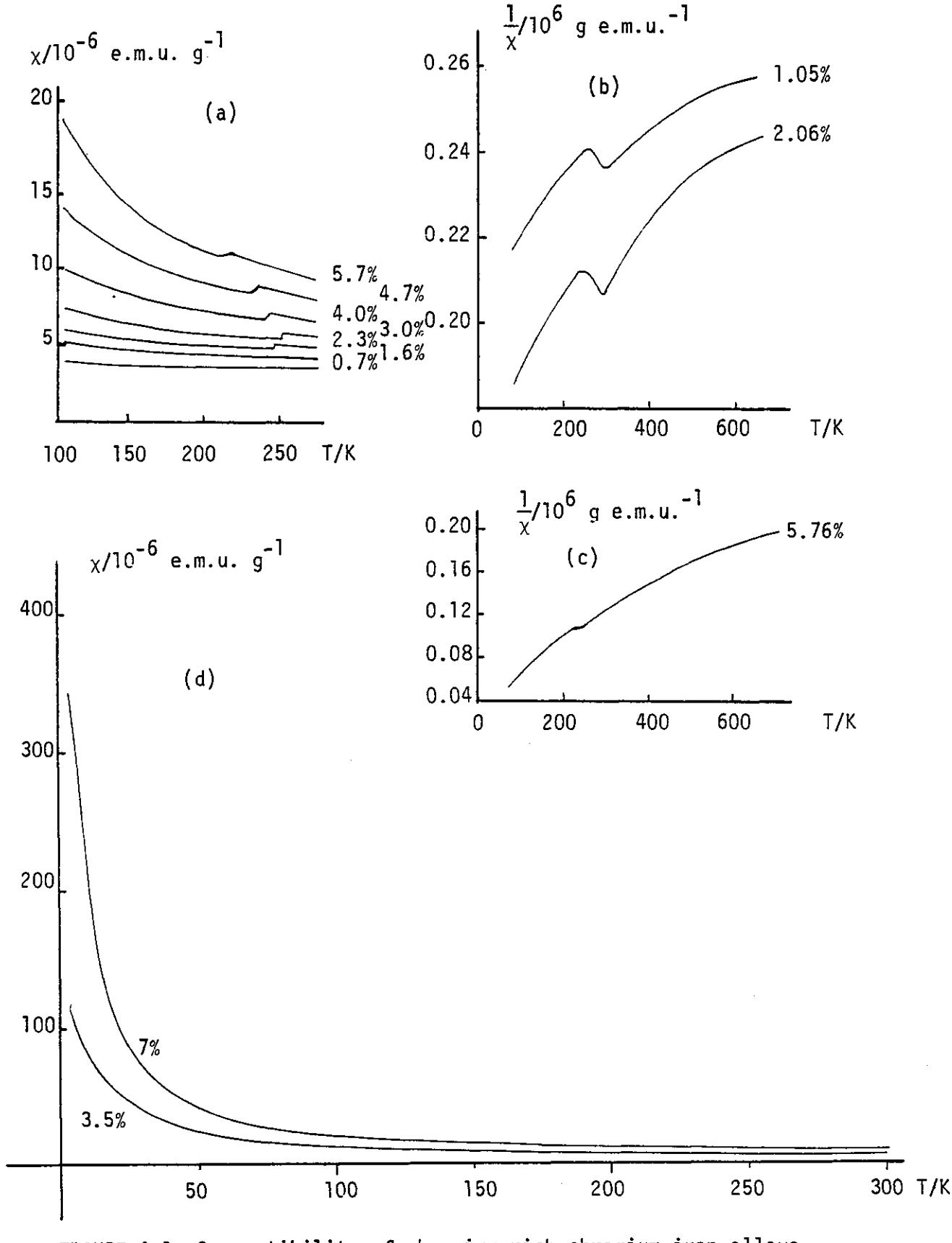

FIGURE 4.1 Susceptibility of chromium-rich chromium-iron alloys.

% figures indicate iron composition.

(a) Suzuki (1966).

(b) and (c) Newmann and Stevens (1959).

(d) This work, reduced from figures 3.6 and 3.7.

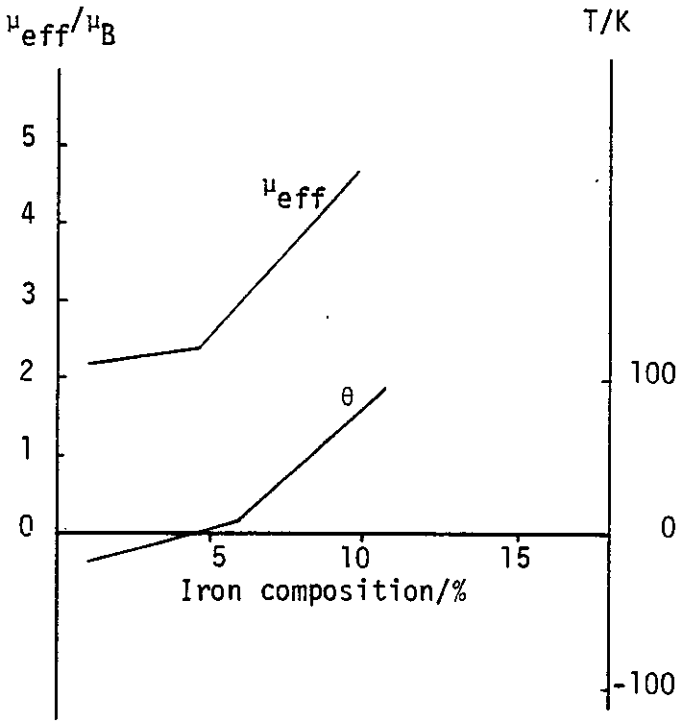

FIGURE 4.2 Iron atom effective moment, μ_{eff}, and Curie-Weiss temperature, θ, for chromium-rich chromium-iron alloys at low temperatures ($T < T_N$).
From Ishikawa et al. (1965).

magnetoresistance, and the present work, chapter 3; the samples of Babic et al. were quenched from the melt).

The difficulty in describing the magnetisation curves is well illustrated by the very high field results of Babic et al. (figure 4.3). At 4.2 K there is an obvious (notional) separation into two additive terms. One is linear in field, and it increases in magnitude as the concentration of iron increases. The other is a saturating, or "ferromagnetic", term which is curved up to fields of the order of 100 kOe or more. As the temperature is raised, the saturation of this latter term moves to higher fields and the curvature decreases in the accessible field range. At temperatures above 4.2 K, it becomes extremely difficult convincingly to separate these two terms, and so it is not clear whether the linear term is temperature dependent or not.

Thus the magnetisation against field plots are extremely difficult to describe in analytical terms, even at a fixed, low temperature. It appears, though, that there is general agreement as to the actual shape and scale of these plots, in spite of the different methods of sample preparation.

The electrical resistivities of chromium-iron alloys have been measured by Newmann and Stevens (1959), Rajan, Waterstrat and Beck (1960), Arajs and Dunmyre (1966), Suzuki (1966), Schröder, Yessik and Baum (1966), Syono and Ishikawa (1967), Mitchell and Goff (1972), Rice, Jayaraman and McWhan (1971), Hedgcock et al. (1977), Burke and Rainford (1978) and Katano and Mori (1979, 1980 (a) and 1980 (b)). There is little disagreement amongst all of these studies. The results are shown in figures 4.4, 4.5, 4.6 and 4.7 (taken from Arajs and Dunmyre 1966 and Katano and Mori 1979).

The effect of adding iron to chromium, in addition to raising the zero temperature resistivity as expected, is to enhance the anomaly at the Néel temperature (which corresponds to the minimum in the

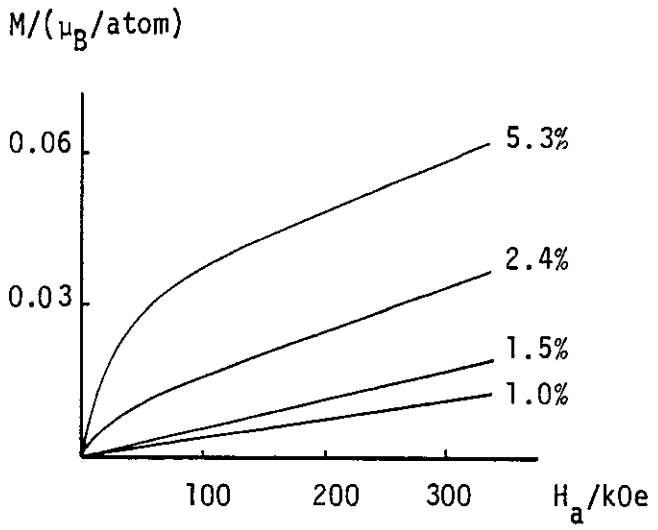

FIGURE 4.3 Magnetisation of chromium-rich chromium-iron alloys as a function of applied field at 4.2 K.
From Babic et al. (1980).

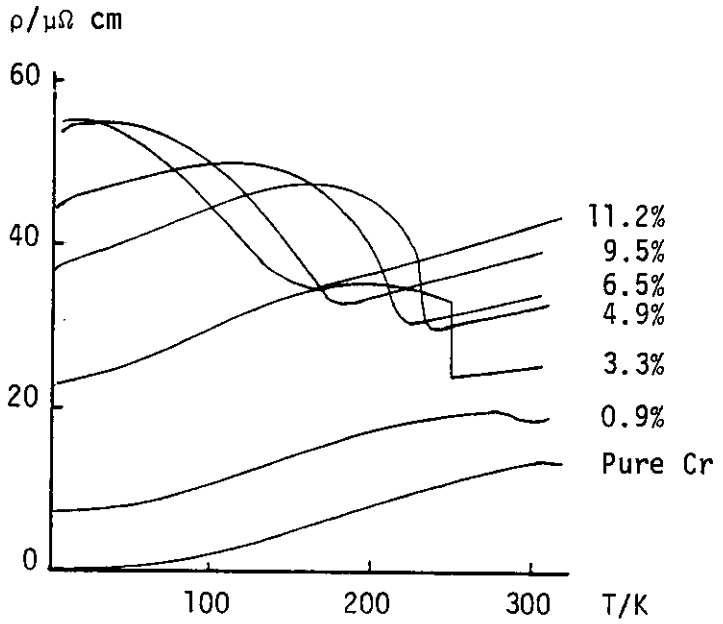

FIGURE 4.4 Electrical resistivity, ρ, of chromium-iron alloys. From Arajs and Dunmyre (1966).

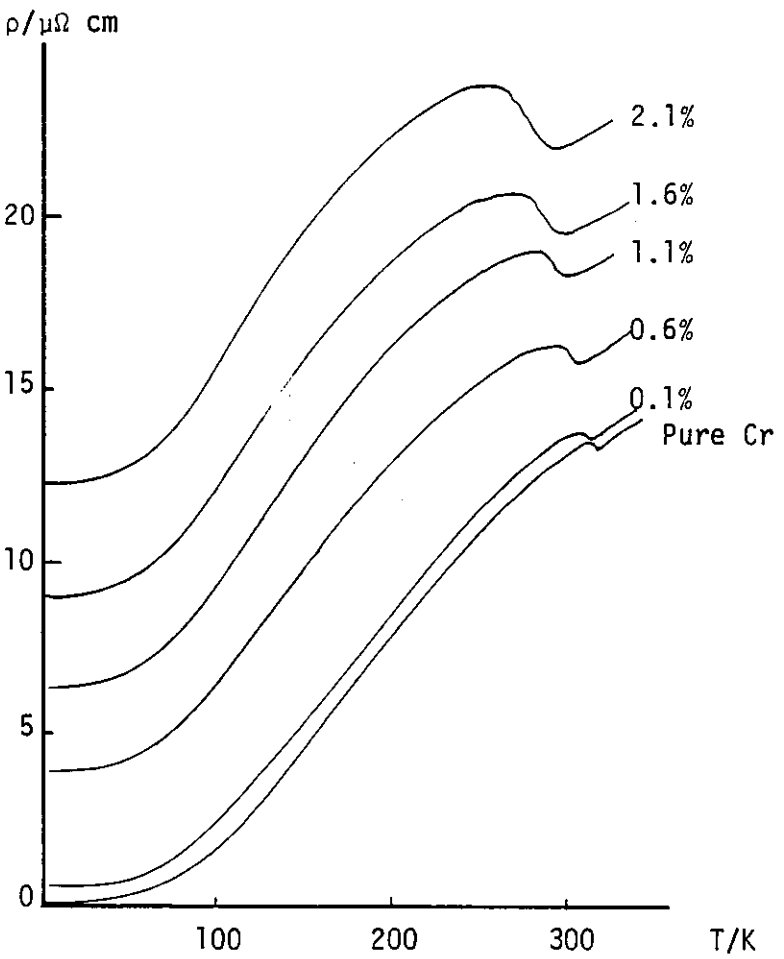

FIGURE 4.5 Electrical resistivity, ρ, of chromium-iron alloys. From Katano and Mori (1979).

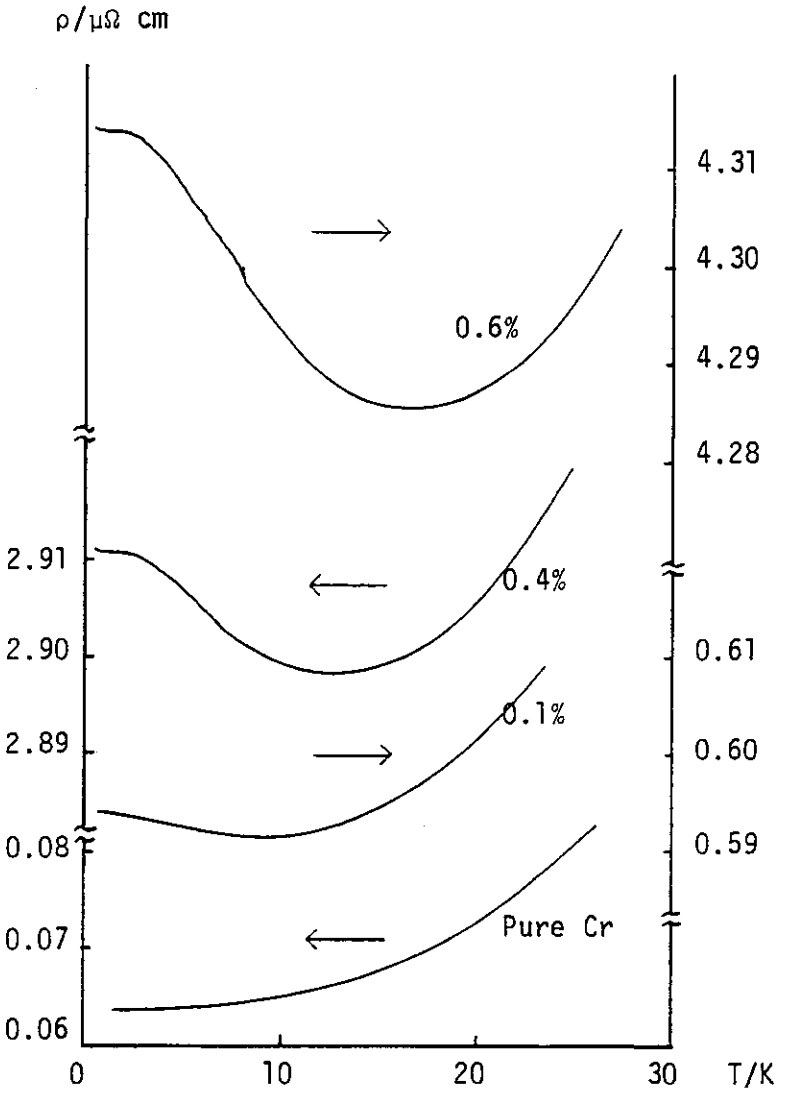

FIGURE 4.6 Electrical resistivity of chromium-iron alloys at low temperatures.

From Katano and Mori (1979).

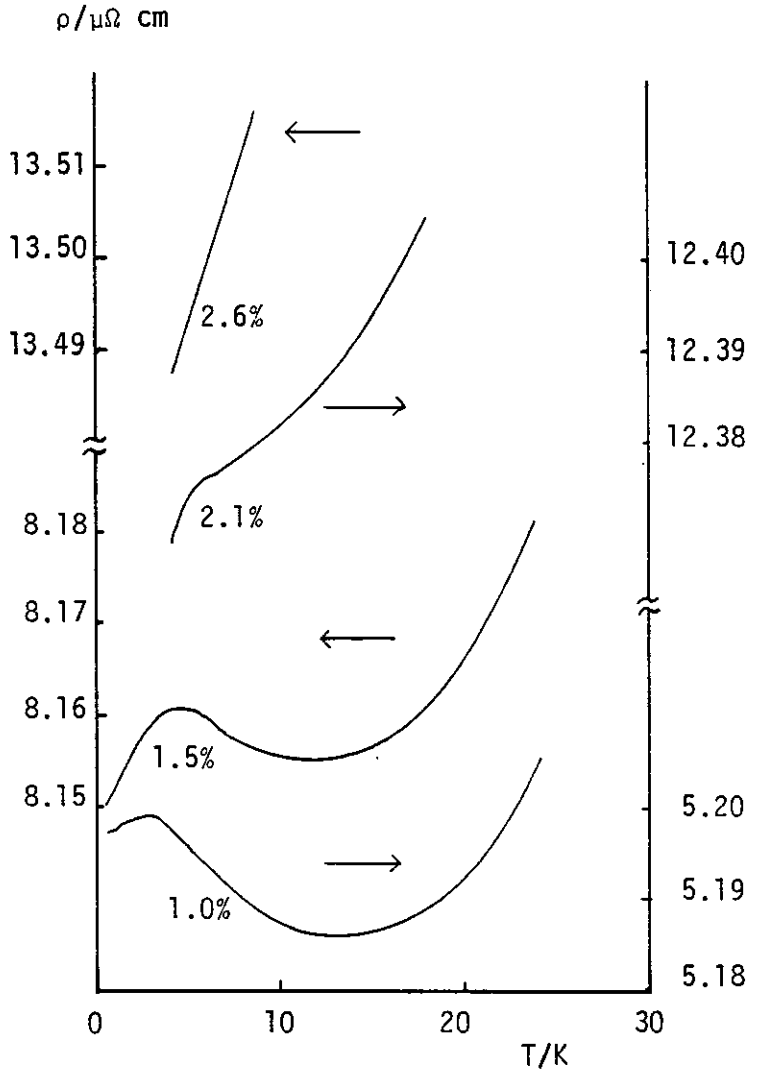

FIGURE 4.7 Electrical resistivity of chromium-iron alloys at low temperatures.
From Katano and Mori (1979).

temperature derivative of the resistivity, Burke and Rainford 1978), and also, for alloys up to about 2% iron, to introduce a low temperature minimum and maximum (figure 4.7).

The relative transverse magnetoresistivity at 4.2 K (figure 4.8, taken from Arajs and Dunmyre 1966) is rapidly reduced from the pure chromium value ($\Delta\rho/\rho_o$ = 1.77 in 12 kOe) to zero in alloys up to 2% iron, and then becomes negative and increases in magnitude linearly in composition.

The effect of applying hydrostatic pressure has been investigated by Syono and Ishikawa (1967), Rice et al. (1971) and by Katano and Mori (1980 (a) and (b)). Increasing the pressure reduces the sharpness of the Néel temperature anomaly, and increases the depth of the low temperature minimum by a factor of about 3 under 19 kbar.

Schröder et al. (1966) also measured the thermopower for alloys up to 4% iron, and found that the peak near T_N in pure chromium is accentuated, and the low temperature value is raised.

The thermal expansion of dilute chromium-iron alloys has been measured by Newmann and Stevens (1959) and Suzuki (1966). The small anomaly in pure chromium at the Néel temperature is accentuated by the addition of iron, up to 5.7% iron (figure 4.9).

The low temperature (1.4 K to 4.2 K) specific heat was measured by Cheng, Wei and Beck (1960). With the exception of the chromium 2%, 5% and 19% iron samples, the specific heats all fitted well to the expression

$$C = \gamma T + \beta T^3,$$

which represents the conduction electron term linear in T (γ may be related to the density of states at the Fermi surface) and the phonon term. These three exceptions all showed low temperature deviations with terms in C increasing with T, but not as fast as T. No analytical

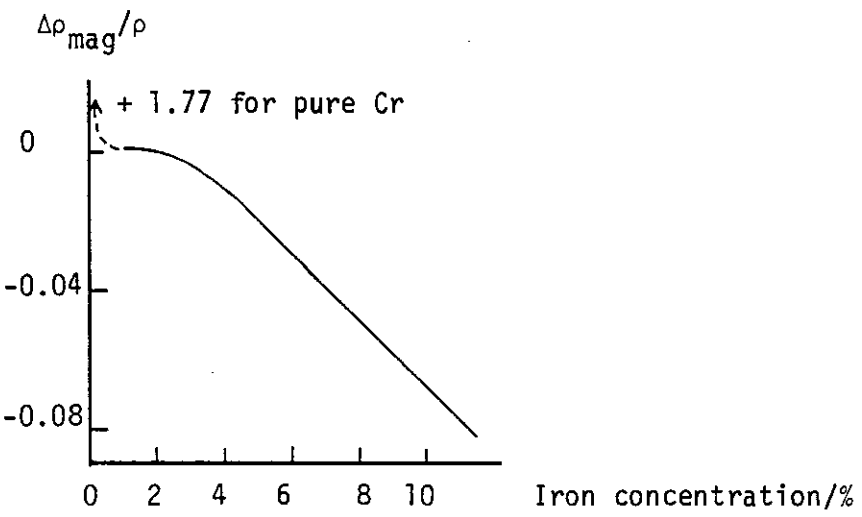

FIGURE 4.8 Transverse electrical magnetoresistivity of chromium-iron alloys at 4.2 K in H = 12 kOe.

From Arajs and Dunmyre (1966).

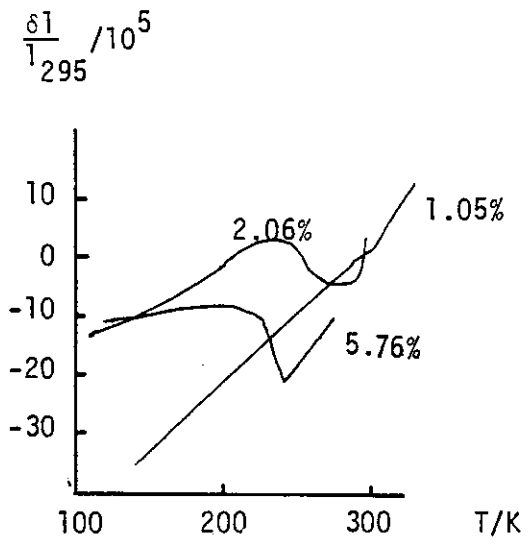

FIGURE 4.9 Thermal expansion of chromium-rich chromium-iron alloys, $\Delta l/l_{295}$.

From Newmann and Stevens (1959).

expression was found for these alloys.

The specific heat has been measured at higher temperatures by Suzuki (1976) from 160 K to 320 K in alloys up to 8% iron, and by Åstrom, Benediktsson and Rao (1978) (see figure 4.10, taken from Suzuki 1976). The transition to paramagnetism is marked by a divergent, hysteretic peak for 3.0 to 4.9% iron, which becomes broader for higher concentrations. Pure chromium shows a similar divergent peak in the specific heat at the Néel temperature, and also a decrease in the "level" of C(T) on going from $T<T_N$ to $T>T_N$. For iron concentrations up to 2%, both of these features remain, although with some degree of broadening and reduction respectively.

Some samples show more than one sharp peak, and this is variously attributed to multiple transitions of the same kind due to gross inhomogeneities, and to transitions of different kinds, from commensurate antiferromagnet to incommensurate SDW, and then to paramagnet.

ii. Mössbauer Measurements

Mössbauer studies of chromium-iron alloys have been undertaken by Wertheim (1961), Blum and Grodzins (1964), Herbert, Clark and Wilson (1972) and Makarov et al. (1979). The initial conclusion was that there was no hyperfine structure, but the measurements of Herbert et al. revealed a broad distribution of hyperfine fields in alloys up to 5% iron, with a maximum of the distribution at about 34 kOe at 4.2 K. If the spectra are resolved, they are not clearly so, and it is the computer fitting of the broadening of the line which gives the hyperfine field distribution. At higher temperatures, the spectra are not resolved at all, but the broadening (in excess of the width at a temperature well above the Néel temperature) has been used to deduce the most probable hyperfine field (figure 4.11, taken from Herbert et al.). The data of Makarov et al. are in broad agreement with those of

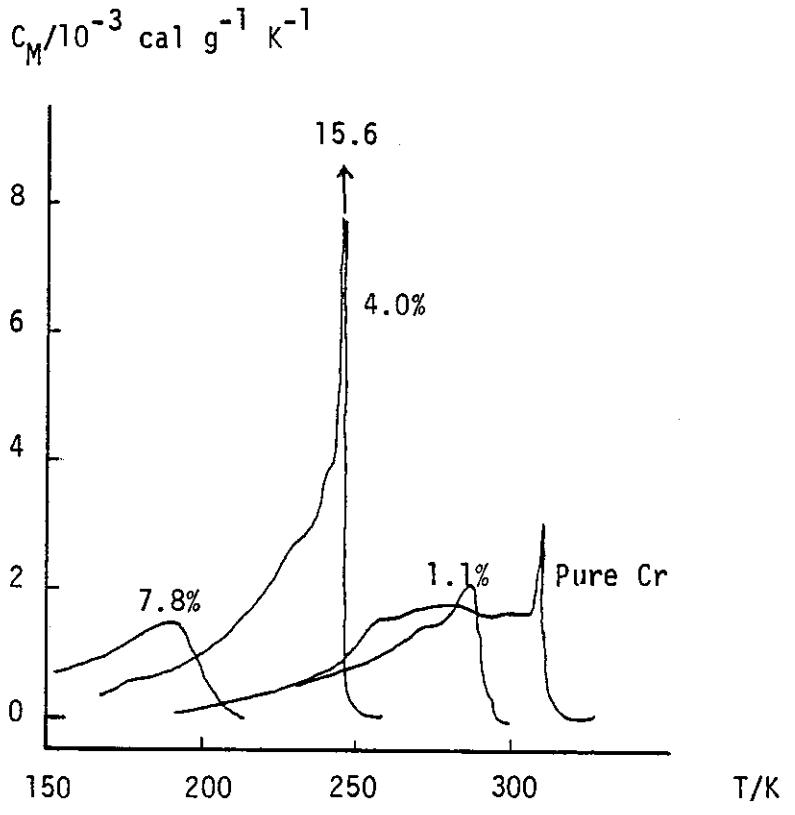

FIGURE 4.10 Magnetic specific heat, C_M, of chromium-rich chromium-iron alloys (1 cal = 4.184 J, by definition). From Suzuki (1976).

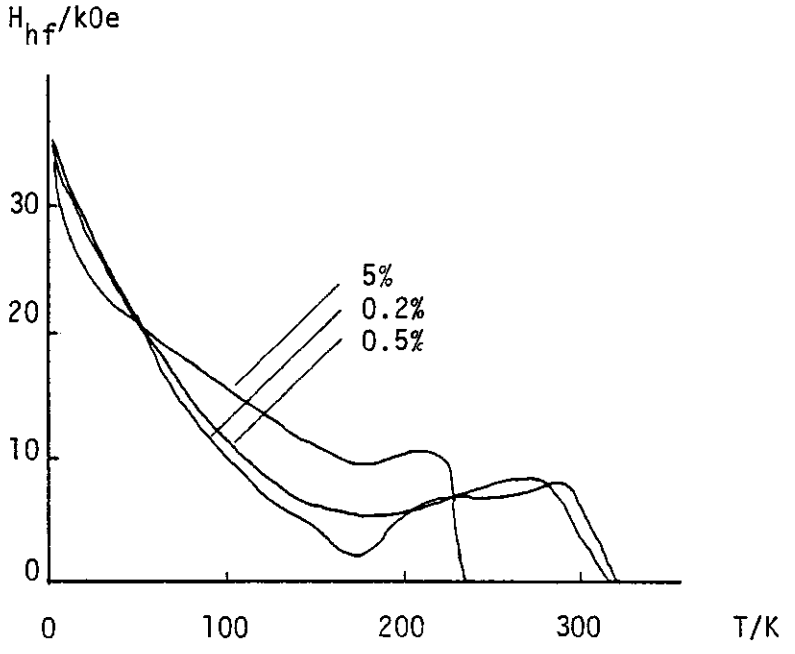

FIGURE 4.11 Hyperfine field, H_{hf}, at ^{57}Fe nuclei in chromium-rich chromium-iron alloys, as a function of temperature in zero applied field. From Herbert et al. (1972).

Herbert et al..

There is clearly an onset of hyperfine field at the Néel temperature, but as the temperature is decreased, the most probable value goes through a broad minimum, and then rises to its maximum value of about 34 kOe at 4.2 K in 0.2, 0.5 and 5% samples.

A chromium 10% iron sample at 4.2 K shows a similar maximum probability of hyperfine field at about 34 kOe, but also a new, very broad, second maximum at about 105 kOe. Again the spectra are not resolved. As the temperature is raised, the hyperfine field values fall, but there is no clear reduction to zero as there is at the Néel temperature in the more dilute alloys.

The sign of the hyperfine fields may in principle be determined by the Mössbauer spectra in an applied magnetic field, but the result appears to be model dependent. Blum and Grodzins find it to be positive, while Herbert et al. find it to be negative (i.e. parallel and antiparallel respectively to the field acting on the iron atom's electrons).

iii. Electron Spin Resonance

Salamon and Feigl (1968) observed electron paramagnetic resonance in chromium 3.6% iron above the Néel temperature, with a rapid g-shift (to higher g) below T_N, accompanied by a rapid broadening, soon becoming too broad to be observed. Larica (1981) found no detectable resonance at all in alloys with less than 7% iron. At higher concentrations he saw a narrowing of the line as the temperature was reduced, a minimum at $T_{E.S.R.}$ (about three times the freezing temperature, T_f, defined as the maximum in the low field susceptibility), and then a broadening again at lower temperatures. At the same time, the g-value shifts to lower fields as the temperature is reduced below $T_{E.S.R.}$.

From a comparison with E.S.R. results for gold-iron alloys, Larica

concludes that the signals are due to superparamagnetic pairs of iron atoms or larger clusters, and for concentrations below 7%, the resonance is too broad, or simply too weak to be detected.

iv. Neutron Diffraction

The classic neutron diffraction experiments which led to the elucidation of the structures of the SDW states in pure chromium, and the details of those structures, are described by Bacon (1975), and Burke (1980). Further studies of chromium-iron alloys by Arrott, Werner and Kendrick (1967) and by Ishikawa, Hoshino and Endoh (1967) on single crystal samples up to 4.9% iron, have formed the basis for the belief in the magnetic phase diagram in this region since then.

Diffraction experiments on polycrystalline samples by Burke and Rainford (1978) and by the author (see chapter 3 above) have established the behaviour of T_N, the Néel temperature, up to the iron concentration where T_N goes to zero, although there is still some doubt in detail as T_N approaches zero, largely because the ordered moment is becoming very small, and the magnetic Bragg peak intensity is masked by the large incoherent background.

It is worthy of note that the single crystal neutron experiments identify the "strongly first order" transition not with the Néel temperature but with the transition from the commensurate antiferromagnetic structure to the incommensurate.

There are problems with the interpretation of the single crystal data, due to sample inhomogeneity and extinction effects. The SDW amplitude in a 0.5% iron sample as measured by Arrott et al. changes by 46% on changing the wavelength from 1 Å to 2 Å. In particular, Arrott et al. report an increase in SDW amplitude on addition of iron, while Ishikawa et al. find that it is constant, then changes abruptly when the commensurate structure forms. There is little doubt about the ordered moment at higher concentrations of iron, and it scales with the

Néel temperature from 5% to 15%.

The spin-flip transition is smeared on alloying, and the transition temperature is reduced to zero with the addition of only 1.5% of iron.

All of this magnetic structure information is important, but not central to the search for the nature of the isolated iron atom in chromium. Diffuse neutron scattering is of more use in this regard, as it will show both paramagnetic scattering, thereby giving the dimensions of the entities involved, and also the magnetic defect scattering. That is, if an iron atom sustains a moment which is different from that of the chromium it replaces, there will be diffuse elastic scattering with a form factor dependence on momentum transfer, and if the impurity disturbs the host, there will be diffuse elastic scattering peaked at the magnetic reciprocal lattice vector. A theory of these effects is described by Marshall and Lovesey (1971) although it is developed only for defects which superpose linearly. There have been several attempts to examine the magnetic diffuse scattering from chromium-iron alloys, with conflicting results.

Holden and Fawcett (1978) used a single crystal of chromium 2.8% iron, and with an unpolarised neutron triple axis instrument, they measured the total elastic diffuse cross-section from 0.5 $\mathring{A}^{-1}$ to 7 $\mathring{A}^{-1}$ in momentum transfer. They found only a smoothly varying signal, with no sign of any scattering with a 3d magnetic form factor dependence, nor did they see any defect scattering peaked around the magnetic reciprocal lattice positions.

Cywinski and Hicks (1980) performed a neutron polarisation analysis scattering experiment at low temperature, which in principle allows an unambiguous separation of the magnetic diffuse scattering from the other diffuse contributions. Their sample, a polycrystalline ingot of nominal composition 5% iron, apparently lost more than 24 g of

chromium in the melting, and was analysed at 6.5 ± 0.5% iron. From a remarkably featureless total cross-section over a limited range in reciprocal space, not encompassing even the first magnetic Bragg reflection, the (100), they separated a falling non-spin-flip component, which they attributed to modulation of the Laue (alloy) scattering (the modulation coming from chemical clustering of the iron atoms), and a spin-flip cross section, which increased with momentum transfer. Even so, for most of the range, the magnetic contribution was found to be zero within the estimated error, increasing monotonically to about 20 mb sr^{-1} at^{-1} at 1.9 $\mathring{A}^{-1}$, with an estimated error of ±6 mb sr^{-1} at^{-1}.

Burke (1980) performed an unpolarised neutron diffuse scattering experiment on chromium 10% iron, with energy analysis by a time-of-flight technique. He found the energy width of the diffuse scattering decreased with temperature, but there was a slight broadening associated with cooling through the Néel temperature of the alloy. He then looked for the dependence on momentum transfer by looking at the intensity within ±0.5 meV of zero (the "elastic window") as a function of q, the momentum transfer. This shows an increase towards the forward direction with a half width in q of about 0.4 $\mathring{A}^{-1}$. This quantity is markedly temperature dependent, and this led Burke to conclude that the scattering is magnetic in origin. It should be noted, however, that the integrated (Lorentzian) scattering over an energy window much larger than the half-width in energy, is essentially temperature independent, which would support the conclusion that the scattering is either nuclear in origin, or derives from a non-interacting, or weakly-interacting, paramagnetic or superparamagnetic system. (The cross-section is proportional to the susceptibility multiplied by the temperature, which is constant for a Curie-law susceptibility.)

Burke also undertook a polarisation analysis study of a chromium 5% iron alloy over a wide range of momentum transfer (0.3 $\mathring{A}^{-1}$ to 5.5 $\mathring{A}^{-1}$) at three temperatures. However, the separated magnetic diffuse scattering was small ($\lesssim$10 mb sr^{-1} at^{-1}) for all values of momentum transfer, and not significantly different from zero. The results are in conflict with those of Cywinski and Hicks concerning the magnitude of the magnetic contribution to the scattering, especially near to the (100) position.

Kajzar, Parette and Babic (1981) performed an unconventional series of experiments using polarised neutrons with no polarisation analysis. They looked at samples of chromium with 1.5%, 2.4%, 12% and 14.2% iron, at several temperatures, and measured the sum and difference cross-sections with the incident neutron polarisation parallel and antiparallel to the applied magnetic field of 13 kOe at the sample. Note that these are the samples used by Babic et al. (1980), and were quenched from the melt.

The sum cross-section at 4.6 K shows a peak in the forward direction which develops from nothing in the 1.5% sample to more than 200 mb sr^{-1} at^{-1} in the 14.2% sample. The authors' analysis excludes the possibility that the magnetic diffuse scattering as such is significant, and they analyse this data solely in terms of nuclear short range order in the alloys. It is not obvious, particularly in the 2.4% sample, that this assumption is correct, and indeed it seems quite likely that in this alloy in particular, the signal is all magnetic in origin. In the other, more concentrated, alloys, the magnetic contribution is still significant, as seen in the change with temperature ($\sim$25%) of the short range order parameters.

The difference cross-section, presented for the 12% and 14.2% samples, shows a similar shape, but is observed to become much smaller in amplitude as the temperature is increased.

Costa, Booth, Ziebeck and Brown (1981) essentially repeated the polarisation analysis experiment of Burke (1980) but with a sample of chromium 12% iron. They measured the magnetic diffuse elastic scattering, and they found significant scattering which they identified as paramagnetic scattering from entities (assumed spherical) 2.7 $\mathring{A}$ in extent (i.e. the reciprocal space half-width is about 1 $\mathring{A}^{-1}$). This scattering appeared both at low temperature (10 K) and above the Néel temperature (at 290 K), and was attributed to superparamagnetic iron clusters. Note that the size of these objects is much less than that implied by the results of Burke on the 10% alloy.

Review - b. Theory

As outlined in chapter 3, first-principles theories are almost at the stage of describing pure chromium, but the theory of its alloys, especially with magnetic solutes, is far from complete. (For a fuller discussion see Burke (1980).)

However, there is clearly a place for a more ad hoc description of a system such as this, and several of these have been attempted. The problem essentially stems from the requirement that one theory describe the many different observations.

There have been two distinct approaches to the nature of the iron site moment. (The existence of such a moment is almost universally accepted.) The first is to assume that the coupling of the moment to the SDW is weak ($\sim 4\ k_B$, e.g. Ishikawa et al. 1965, Hedgcock et al. 1977). The second starts from the assumption of strong coupling ($\gtrsim k_B T_N$, e.g. Friedel and Hedman 1978).

The weak coupling theory is the obvious candidate to explain the nearly Curie-law susceptibility, the large resistivity below the Néel temperature and the negative magnetoresistance at low temperatures. However, it fails to describe the magnetisation data quantitatively,

and the expected paramagnetic scattering fails to appear in the neutron cross-section. It is also intuitively surprising to find a large impurity moment defying so ostentatiously the invitation of its host to join the ordered structure.

The strong coupling theory avoids this worry, but it demands a high degree of iron atom clustering to explain the susceptibility, and then falls foul of the linear concentration dependence of the Curie constant. By sophisticated subtraction methods and subtle physical arguments, Friedel and Hedman manage to find a good fit to the limited susceptibility data of Hedman et al. (1978).

All of the theories consider the possibility that two near-neighbour iron atoms might have a sufficiently strong ferromagnetic coupling to each other for their net interactions with the antiferromagnetic order, and with the incommensurate SDW, to be zero, and very small, respectively. However, if this were the cause of the 1/T-like susceptibility, the Curie constant would scale as the square of the concentration. It is, in fact, proportional to the concentration itself.

The interpretation of the Mössbauer data is difficult. The lines are undoubtedly broad, which supports the weak coupling picture, but the hyperfine field width would be expected to follow a similar Curie-law to the susceptibility. It does not. The behaviour is, however, remarkably similar in the 0.2%, 0.5% and 5% samples, and markedly different in the 10% sample, which may be attributed to the effect of nearest neighbour iron coupling.

The question of the influence of nearest neighbour pairs of iron atoms is central to the discussion, and much hinges on their behaviour and concentration at low iron concentrations. It is here, perhaps, more than anywhere, that the method of sample preparation is important. Quenching from the melt or slow cooling are both likely to produce

chemical inhomogeneities, because of the gap between liquidus and solidus, and the low temperature miscibility gap respectively.

The tendency of iton atoms to cluster is marked in more concentrated alloys. Aldred, Rainford, Kouvel and Hicks (1976) find, for a 27% iron alloy, a nearest neighbour Cowley short range order parameter of 0.14. This parameter is usually a function of concentration (even for similar preparation procedures), and is expected to vanish in the limit of small concentration. It is astonishing then to find Cywinski and Hicks (1980) reporting a value of 0.15 for their 6.5% alloy. This implies clustering of iron atoms on an enormous scale. Each iron atom would have 1.6 nearest neighbour iron atoms, or more than three times the number expected in a random alloy picture. Kajzar et al. (1981) report a value of zero for their 1.5% alloy, and 0.15 for their 2.4% alloy. Their values for 12% and 14.2% samples are temperature dependent, but are approximately 0.11. (Note that these are not strictly the same parameters, but averages of the first and second Cowley parameters.)

However, there are indications also that the chemical short range order is very small in carefully prepared, homogenised and quenched alloys with 5% iron or less. The low temperature E.S.R. signal, believed to come from nearest neighbour pairs of iron atoms, becomes undetectably weak for less than 7% iron samples. The belief that this is a correct identification of the signal is bolstered by the concentration-independent limit of the value of the temperature of the line-width minimum, T_{ESR}, for less than 10% iron (Larica 1981). It is only at these concentrations, and higher, that superparamagnetic iron clusters become significant. The non-spin-flip diffuse neutron cross-section of the 5% alloy of Burke (1980) also shows no signs of structure indicative of short range order. The magnetic diffuse scattering measured by Costa et al. in a 12% alloy indicates a size of

superparamagnetic entity of 2.7 Å in diameter which corresponds to a volume approximately equal to one atomic volume. Thus it seems unlikely that it represents clusters larger than two, or possibly three, nearest neighbours. The likelihood, therefore, of finding a significant contribution from clusters of two or more at half that concentration and less, seems to be very small.

Are the pairs dominant then, in, say, a 5% alloy? The best indication, in principle, is the neutron diffuse non-spin-flip cross-section, and here the only two results are contradictory. Burke says they are not significant, while Cywinski and Hicks say they are dominant. Perhaps it is worth comparing the results of Cywinski and Hicks (1980) for their chromium-iron alloy with their results for pure chromium (Cywinski and Hicks 1978). These data are reproduced in figure 4.12. The sloping non-spin-flip (and indeed total) cross-section, which in the alloy is used to deduce the short range order parameters, is also present on a similar scale in the pure metal where the impurities are said to be less than 0.1%. Cywinski and Hicks (1978) consider several explanations of this, and conclude the most likely to be the freezing in of vacancies and other defects due to strain, even though the sample was annealed at over 1000°C for 24 hours. In the opinion of the present author, a more likely explanation is the anisotropy of the multiple scattering, which was assumed by Cywinski and Hicks to be isotropic. Indeed, detailed calculation of the multiple scattering is prohibitively difficult, requiring a detailed knowledge of the entire first order scattering function $S(\underline{q},\omega)$. Burke, who used a smaller sample, with less multiple scattering, did not find the same anisotropy of the non-spin-flip cross-section.

Thus the assumptions of Friedel and Hedman's theory appear to be shaky, although the good agreement claimed with the susceptibility data

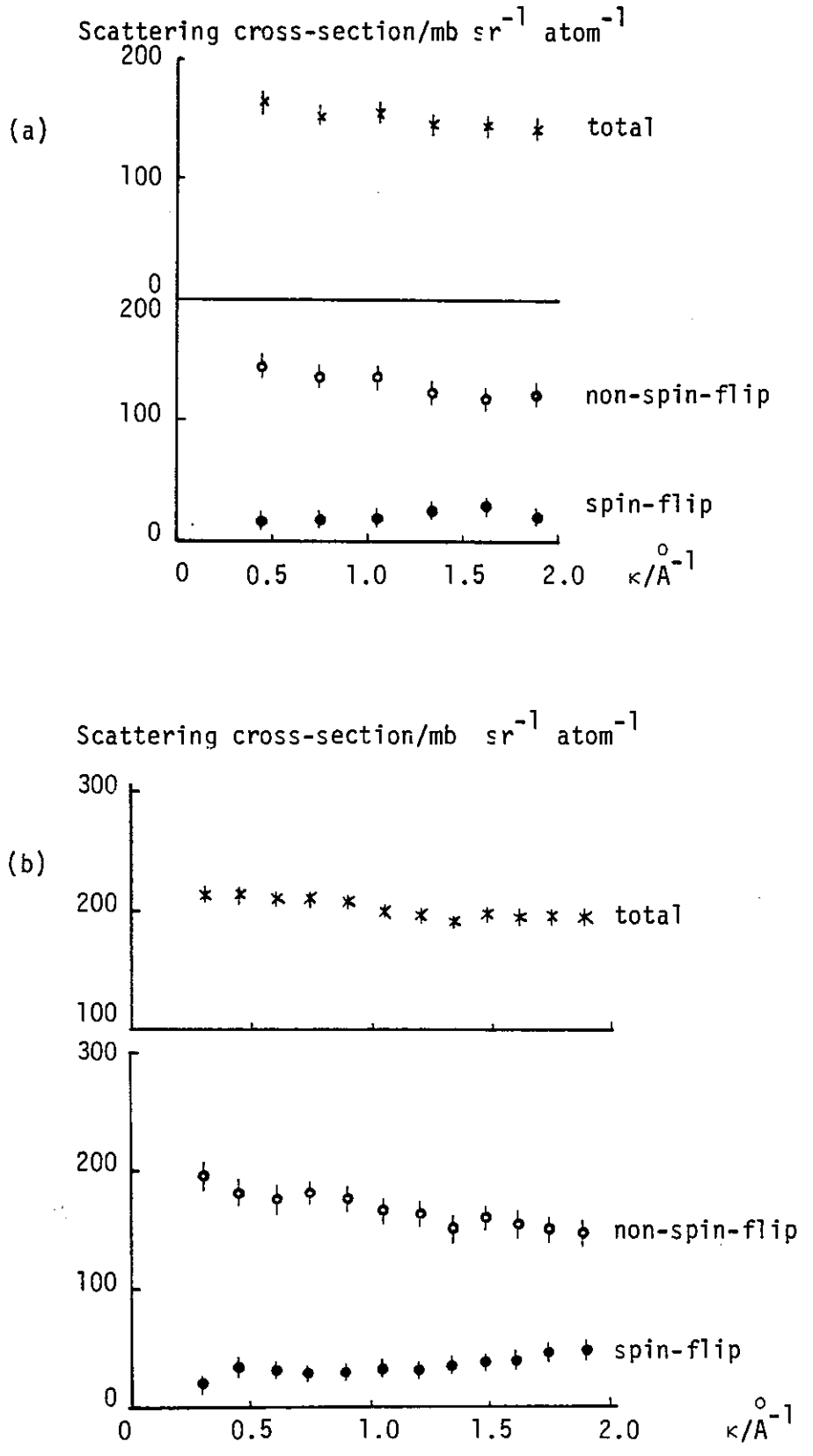

FIGURE 4.12 Diffuse neutron scattering cross-section, separated by polarisation analysis for
(a) pure chromium
(b) chromium 6.5% iron.
From Cywinski and Hicks (1978 and 1980).

means that the theory deserves closer scrutiny and experimental testing.

The strong coupling assumption limits the contribution to the susceptibility of isolated iron atoms in the commensurate phase to a constant, temperature independent, term. However, in the incommensurate phases, by assuming that the SDW may easily be distorted, the iron moments can contribute a Curie-like term to the susceptibility, with a Curie constant which depends on the structure, whether it be longitudinal or transverse SDW. (The destruction of the long range order by the distortions connected with the fluctuating iron moments does not, however, seem to be reflected in a broadening of the magnetic Bragg peaks.) The susceptibility is predicted to be highly anisotropic with respect to the SDW wave-vector.

The Mössbauer results are difficult to account for in this theory, in two main areas. Firstly, the observed distribution of hyperfine fields in the commensurate alloys would not appear if there were only single iron atoms, all experiencing the same exchange field of the host order, and nearest-neighbour coupled pairs, which behave superparamagnetically. Secondly, the results would not be so similar in the incommensurate and commensurate samples.

Indeed, the smooth transition of many properties between the incommensurate and commensurate phases, such as the low temperature Curie constant and Curie-Weiss temperature, also poses problems for any theory, such as this, which demands that one property (in this case the Curie constant) have different origins in the different phases.

Perhaps the most severe difficulty with the strong coupling theory is the lack of paramagnetic scattering in the neutron spin-flip cross-section of a 5% sample, corresponding to the superparamagnetic iron nearest neighbour pairs (Burke 1980), such as is seen in the equivalent cross-section for a 12% alloy (Costa et al. 1981).

Summary

There is no single explanation yet for all the observed properties of chromium-rich chromium-iron alloys, even on the ad hoc level.

There is no compelling evidence for any one picture of the iron site moment in these alloys. In principle, the most direct evidence is provided by the neutron scattering differential cross-section, which is related to the magnetic correlation function. The diffuse part of the magnetic cross-section relates directly to the disordered part of the correlation function, and so to the static disorder introduced by the iron (defect scattering) and also the fluctuating disorder (paramagnetic scattering). Any model of the iron site moment predicts both of these, so a direct measurement of these provides a means to distinguish between alternative models. The degree of chemical short range order, important in some models, may also be measured by the modulation of the nuclear cross-section.

The diffuse neutron polarisation analysis experiment of Burke (1980) was therefore repeated with a larger sample, and a better method of magnetic scattering separation. An attempt was also made to extend the measurement to smaller momentum transfers with a small-angle neutron scattering measurement.

Also, the model of Friedel and Hedman was further tested by measuring the anisotropy of the bulk susceptibility with respect to the SDW wave-vector.

Polarisation Analysis Neutron Diffuse Scattering Experiment

i. Theory

The diffuse neutron scattering from chromium is large mainly because of the large nuclear incoherent cross-section which arises because of the different nuclear scattering lengths of the different isotopes of natural chromium, ^{50}Cr, ^{52}Cr and ^{53}Cr. The last mentioned

isotope, which constitutes about 10% of natural chromium, also has a nuclear moment, and this gives rise, at temperatures above the millikelvin range at least, to yet more diffuse scattering known as nuclear spin incoherent scattering. These two mechanisms give rise to isotropic scattering of the order of 0.2 barns per steradian per atom (1 barn = 10^{-28} m^2). The magnetic diffuse cross-sections are not likely to exceed about 20 mb sr^{-1} at^{-1} (Holden and Fawcett 1978). It is necessary therefore to devise some means to separate the various contributions to the diffuse scattering, and one way is to make use of the different dependences on the spin of the scattered neutrons. This requires the use of a polarised incident neutron beam, and also the analysis of the scattered beam with respect to neutron polarisation. The details of the theory, and of the polarisation analysis instrument, D5, at the Institut Laue-Langevin in Grenoble used for the experiments, are given by Burke (1980). Only a brief summary will be given here.

Nuclear incoherent scattering leaves the spin of the scattered neutron unchanged. This is a non-spin-flip process. Nuclear spin incoherent scattering is divided between spin-flip and non-spin-flip in the ratio 2:1. Magnetic diffuse scattering is all spin-flip if the neutron guide field at the sample is parallel to the scattering vector, but if the field is perpendicular to the scattering vector, it is half spin-flip and half non-spin-flip. Nuclear coherent (Bragg) scattering is non-spin-flip, and magnetic Bragg scattering is spin-flip. In an alloy, some additional (Laue) scattering appears in the non-spin-flip channel if the scattering lengths of the alloy components are unequal. If, in addition, the alloy is not a random alloy, this scattering is modulated by a function which is essentially the spatial fourier transform of the chemical short range order.

Thus it is possible to identify unambiguously the magnetic diffuse scattering by taking the difference between the spin-flip cross-

sections when the guide field at the sample is first parallel, and then perpendicular, to the scattering vector. This is half of the magnetic diffuse cross-section.

The magnetic diffuse scattering may consist of two components. The first is strictly elastic and derives from the static magnetic disorder if the impurity carries a moment different from the ordered moment of the host, or if it disturbs the moments of the neighbouring host atoms. The second is quasi-elastic (that is, it is peaked at zero energy transfer, but has a finite energy width corresponding to some relaxation time) and derives from the magnetic fluctuations. This may be loosely termed "paramagnetic" scattering. Note that the energy resolution of D5 is only about 15 meV, and so most of the quasi-elastic scattering appears in the elastic window, except for scattering with exceptionally broad energy half-widths.

ii. Sample Preparation and Analysis

The need for a very large sample, to give sufficient scattering intensities for good statistics, meant the need for an alternative method of sample preparation, as the arc furnaces available were neither large enough nor powerful enough to contain or melt the sample.

Two samples were prepared (nominal 2.0% and 4.0% iron) from Johnson Matthey Specpure 99.999% pure chromium and iron. As noted in chapter 3, this material contains a certain amount of oxygen in the form of Cr_2O_3 inclusions, but unfortunately, there was not sufficient ex-iodide chromium available for this experiment. The elements were melted together in an R.F. induction furnace in the laboratoire Louis Néel, C.N.R.S., Grenoble, using a recrystallised alumina crucible to prevent discharge. One fifth of an atmosphere of high purity argon was admitted to the furnace to reduce the vaporisation of the chromium. The alloys, in cylindrical ingots, 45 mm in diameter, and more than 10 mm thick, were too large to homogenise in the conventional furnaces,

and so were subjected to a heat treatment of over half an hour at just over 1500°C in the furnace previously used to melt them. The temperature was measured with the aid of an optical disappearing filament pyrometer. They were not quenched, but allowed to cool as fast as possible in the furnace.

The nominal 2% sample was not used eventually, because of insufficient beam time. The 4% sample was cleaned of surface contamination firstly by turning in a lathe, and then with emery paper. Electron microprobe analysis of this sample gave a mean composition of 4.1% iron, with fluctuations corresponding to 4.1 ± 0.4% over a characteristic length of about 20 μm. X-ray diffraction Guinier photographs revealed only the lines corresponding to the b.c.c. structure for most of the sample, but a piece taken from one small volume of the ingot which looked badly contaminated revealed a small amount of f.c.c. impurity, with lattice constant 3.625 Å.

iii. Measurements

The polarisation analysis instrument D5 is described by Maier (1981). The neutrons from the beam tube H4, from the hot source, were polarised and monochromated by reflection from the (111) planes of a Heusler alloy crystal in a permanent magnetic field. A wavelength of 0.84 Å was used, in order to reduce the second order contamination using erbium filters, which have a resonant absorption at 0.42 Å. A guide field must be maintained over the entire flight path of the neutrons between the polariser and the analyser, and this is achieved using permanent magnet guide tubes. For this experiment, boron carbide apertures of 42 mm diameter were attached to the ends of the guide tubes for collimation purposes. The spin and energy of the scattered neutrons were analysed using a second Heusler crystal in the same configuration, and set for the same wavelength as the polariser (i.e. for elastic scattering). The counter is a single ^{3}He detector.

The guide field at the sample was supplied by an electromagnet, either vertical (perpendicular to the scattering vector) or horizontal (parallel), and was about 250 Oe. This is assumed not to disturb the sample's magnetic response significantly. The sample was masked with a sheet of cadmium with a 37 mm diameter aperture. This allowed rotation of the sample up to 20^{o} in either sense while maintaining the same volume of sample in the beam. The sample was mounted in a helium flow cryostat 63 IL HV 71 which allowed the temperature to be controlled within 0.1 K from 1.5 K to 300 K.

The polarisation of the incident beam can be inverted to measure the spin-flip cross-section using a tuned radio frequency flipper. This was used throughout with a duty cycle of three seconds on to one second off.

The instrument was used in the so-called "focussing-W" configuration to improve the resolution. The arrangement used is sketched in figure 4.13. Calibration of the cross-section was achieved by comparison with a standard vanadium sample, and corrections due to the "empty cell" (with no sample present), were also made. The attenuation by the sample of the straight-through beam was measured to enable sample absorption corrections to be made.

The spin-flip and non-spin-flip cross-sections were measured for the chromium 4% iron sample over a range of momentum transfer from 0.26 $\mathring{A}^{-1}$ to 3.2 $\mathring{A}^{-1}$, with the guide field at the sample both parallel and perpendicular to the scattering vector, at a temperature of 11.5 K. A similar, but less detailed, measurement was also performed at 287 K, well above the Néel temperature. The Néel temperature itself was measured by monitoring the peak height of the (100) magnetic Bragg peak as a function of temperature.

Subsequently, a small section of the sample was spark machined into a cylinder of suitable size (1.25 g) and the bulk magnetic

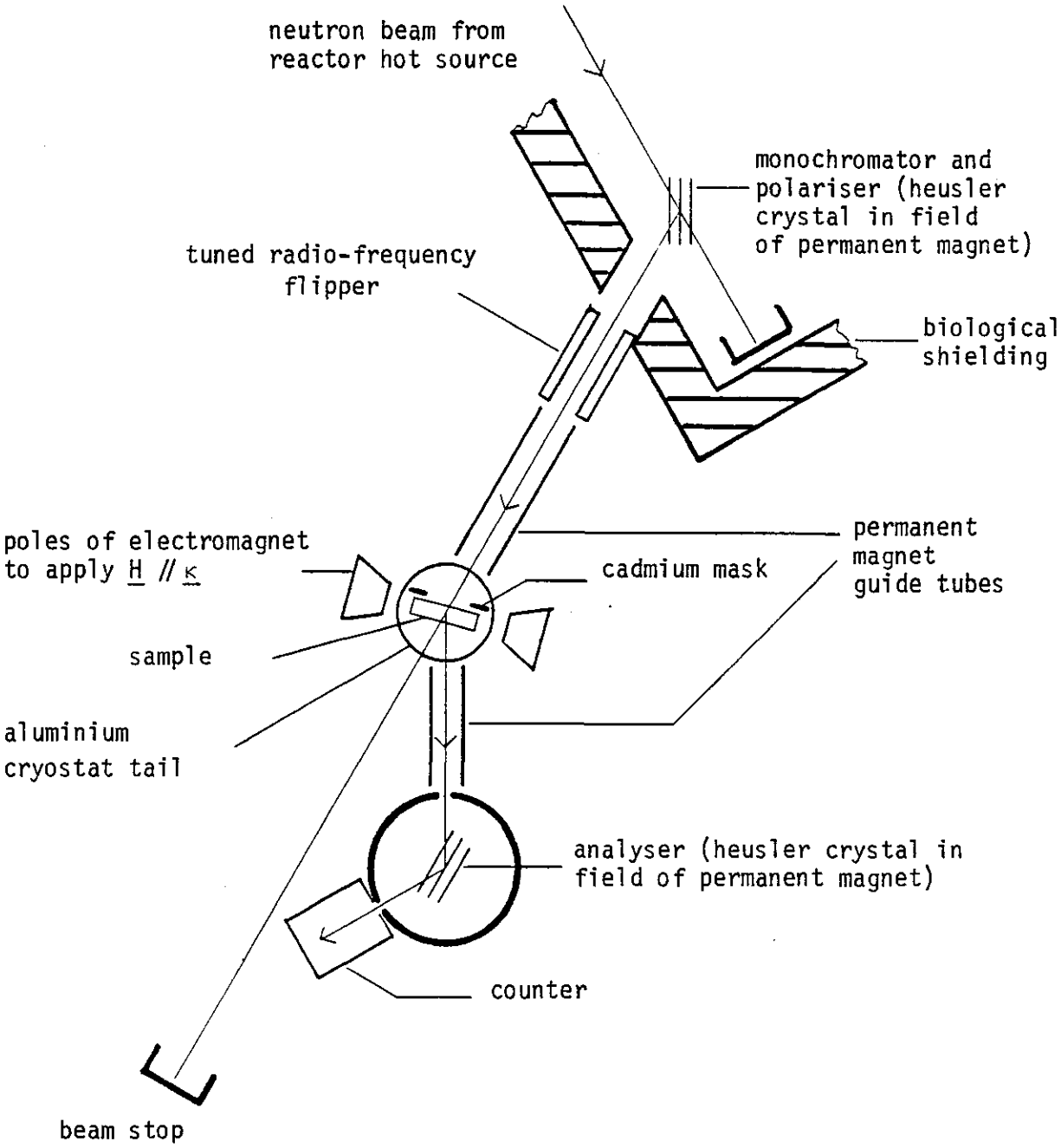

FIGURE 4.13 D5 polarisation analysis diffractometer. There is also a Helmholtz pair to provide a field at the sample perpendicular to the scattering vector $\underline{\kappa}$. The W-configuration improves the resolution by "focussing" neutrons of slightly different wavelengths.

susceptibility was measured using the low field vibrating sample magnetometer described in appendix B.

iv. Data Analysis and Results

The two quantities of greatest interest in this experiment are the (low temperature) difference in the spin-flip cross-section with the guide field parallel and perpendicular to the scattering vector, which is an unambiguous measure of the magnetic diffuse cross-section, and the non-spin-flip cross-section, with guide field parallel to scattering vector, which may yield information on the chemical short range order of the alloy.

Corrections were made to the data for the incomplete polarising efficiency of the polariser and analyser (each greater than 97%), for the background when the analyser was not set to scatter into the detector, for sample absorbtion, for empty cell scattering (mostly air scattering, strongly peaked in the forward direction), for the Debye-Waller factor (less than 1% in the range studied at 11.5 K) and for multiple scattering. This last correction is difficult, and was assumed to be isotropic. The semi-analytic method of Sears (1975) was adopted, with slight modifications to cope with the different effects on spin-flip and non-spin-flip cross-sections. The correction to the non-spin-flip cross-section is larger than that for the spin-flip, because multiple scattering from the latter may appear in the former, while the reverse is not true.

The multiple scattering turned out to be quite large, as was to be expected in such a large sample, and the ratio of multiple to single scattering processes in the non-spin-flip was 0.23, and in the spin-flip 0.13. This was checked, and found to be reasonable, by comparison with the total single process cross-section, found from the difference between the total cross-section as measured by the transmission, and the true absorbtion cross-section as measured by Koester, Knopf and

Waschkowski (1978) for pure chromium.

The results for the 11.5 K magnetic diffuse cross-section are shown in figure 4.14. It is apparent that the cross-section is barely different from zero over the complete range, although there is some small average cross-section greater than zero.

The peak at 1.8 $\mathring{A}^{-1}$ is not mirrored in the non-spin-flip cross-section, and is, therefore connected with an antiferromagnetic (or more complicated) ordered magnetic phase. This phase has not been identified, although the room temperature X-ray impurity-phase lines indicate an f.c.c. structure of lattice constant 3.625 $\mathring{A}$, and a magnetic (100) reflection from such a structure would appear where this peak is. It is therefore confidently attributed to some unknown antiferromagnetic impurity.

The dashed line drawn on figure 4.14 represents the quasi-elastic paramagnetic cross-section which would correspond to the Curie-law contribution to the magnetic susceptibility, if this were caused by single ion, free paramagnetic moments. This correspondence assumes that the susceptibility is related to the correlation function in the way outlined in chapter 1 above. That the system is in equilibrium is not doubted. The connection between the real and imaginary parts of the susceptibility is not so obvious, but is probably of the required form

$$\chi''(\omega) \propto \omega\chi'(\omega)$$

in the limit of small ω. In making this connection between the susceptibility and the paramagnetic scattering, we have also assumed the validity of the quasi-static approximation. The measured cross-section, with the relaxed energy resolution of about 15 meV (24 THz) is equivalent to the complete magnetic differential cross-section if the

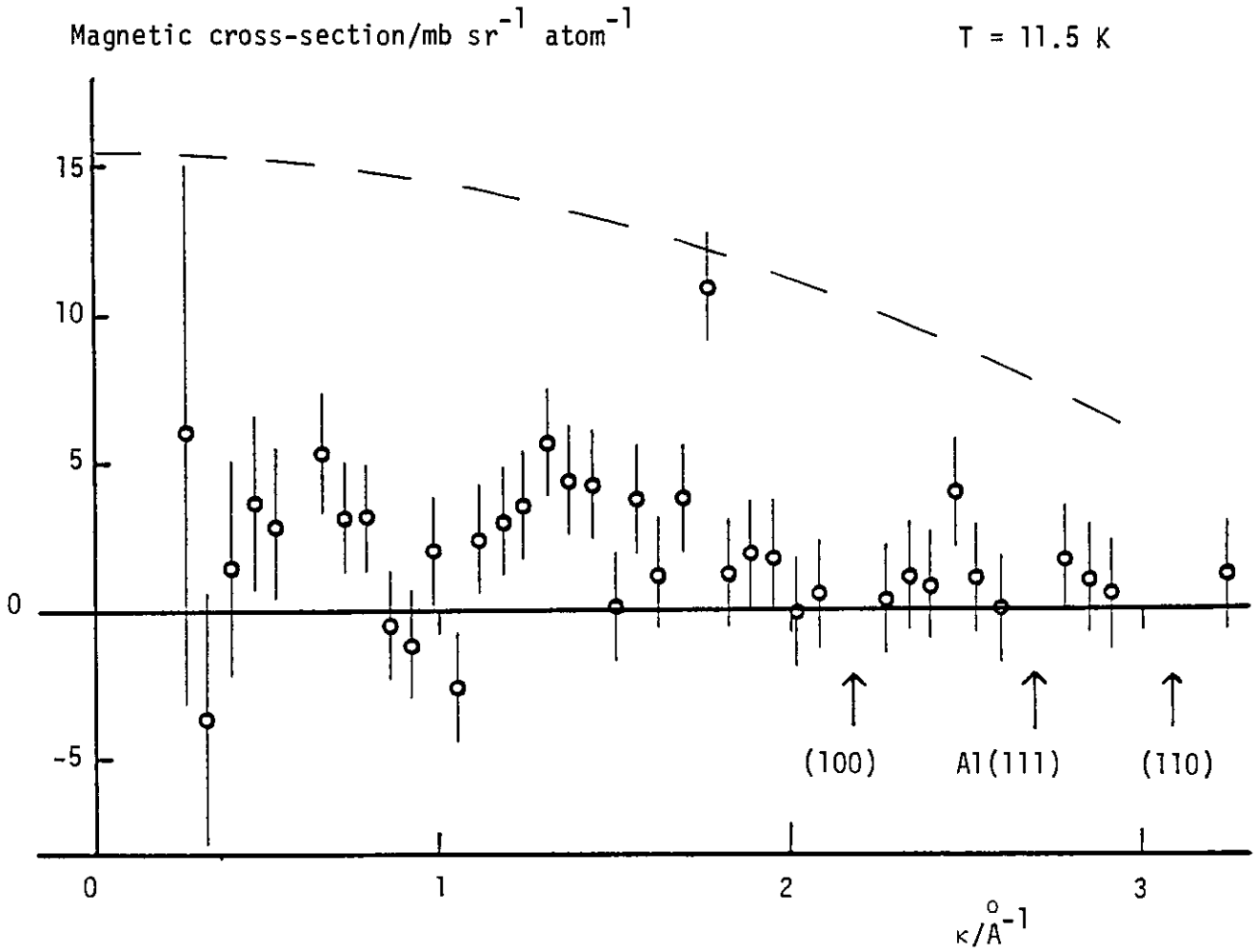

FIGURE 4.14 Magnetic diffuse cross-section of chromium 4% iron. The arrows indicate the positions of the (100) magnetic and (110) nuclear Bragg peaks from the sample, and the (111) nuclear Bragg peak from the aluminium of the cryostat tail. The dashed line has a dependence on κ of the square of a 3 d (iron) form factor, see the text.

energy width of the paramagnetic scattering is much less than the energy resolution. The quasi-static approximation involves assuming further that the energy dependent terms in the inelastic cross-section are constant over the range of the paramagnetic scattering.

$$\frac{d^2\sigma}{d\Omega dE'} \propto \frac{k'}{k} \cdot \frac{1}{1 - \exp\{-\hbar\omega\beta\}} \cdot \omega\chi'(\omega),$$

and so

$$\int_{\text{resolution}} \frac{d^2\sigma}{d\Omega dE'} \cdot dE' \propto \int_{-\infty}^{\infty} \chi'(\omega) d\omega$$

if, over the width of the scattering ω_o, the other two terms in the partial differential cross-section are constant.

$$\frac{k'}{k} \sim 1 \text{ if } \hbar\omega_o << \frac{\hbar k^2}{2m}.$$

$$\frac{1}{1 - \exp\{-\hbar\omega\beta\}} \simeq \frac{1}{1 - \{1 - \hbar\omega\beta + \hbar^2\omega^2\beta^2 - \ldots\}}$$

$$\therefore \quad \frac{\omega}{1 - \exp\{-\hbar\omega\beta\}} \simeq \frac{1}{\hbar\beta - \omega\hbar^2\beta^2}.$$

This term is constant if $\hbar\omega_o << \frac{1}{\beta}$.

The quasistatic approximation therefore involves three restrictions on the energy width of the scattering, $\hbar\omega_o$.

i. $\hbar\omega_o$ << instrumental resolution.

ii. $\hbar\omega_o$ << incident neutron energy, $\frac{\hbar k^2}{2m}$.

iii. $\hbar\omega_o$ << typical thermal energy, $\frac{1}{\beta}$.

Condition i. is more stringent than ii.. In this experiment, conditions i. and iii. are

$\hbar\omega_o$ << 15 meV

and $\hbar\omega_o$ << 1 meV

respectively.

It will be argued later that the energy width of the paramagnetic correlation function is much less than this latter condition, but some

doubt remains on this point. Direct tests, by inelastic scattering for example, are difficult because of the small signals to be expected in comparison with the large elastic cross-section.

The q-dependence of the dashed line in figure 4.14 is simply the 3 d (iron) magnetic form factor (Bacon 1975) squared, which appears as a factor in such scattering cross-sections. The zero-q value is calculated from the measured Curie constant in the bulk susceptibility, which is shown in figure 4.15, plotted as reciprocal susceptibility against temperature. If the susceptibility were due to nearest-neighbour coupled pairs of iron atoms, the forward cross-section would be the same, but the form factor squared would then fall off more sharply, falling to $\frac{1}{2}$ at about 1 $\mathring{A}^{-1}$. There is neither sort of response, from single ions or from pairs, in the measured cross-section. Similar scattering from larger superparamagnetic entities would appear, peaked even more sharply in the forward direction. However, the data at very small q become very uncertain because of a steeply rising air-scattering contribution to the cross-section.

Perhaps the most remarkable feature of this data is the unquestionably small cross-section which appears very close to the magnetic (100) reflection. This is in agreement with the results of Holden and Fawcett (1978), and Burke (1980), but in contrast to the results of Cywinski and Hicks (1980).

The remaining magnetic scattering may have a broad double-peaked structure, but the statistics are not good enough to be certain of this, nor is it smooth enough to warrant elaborate fitting attempts. For reasons which will be explained later (in the "Discussion and Conclusions" section), this data may be interpreted as diffuse elastic scattering with a form factor dependence on q, and within the framework of a certain model, some information may be extracted from this signal.

The non-spin-flip diffuse cross-section, with the guide field

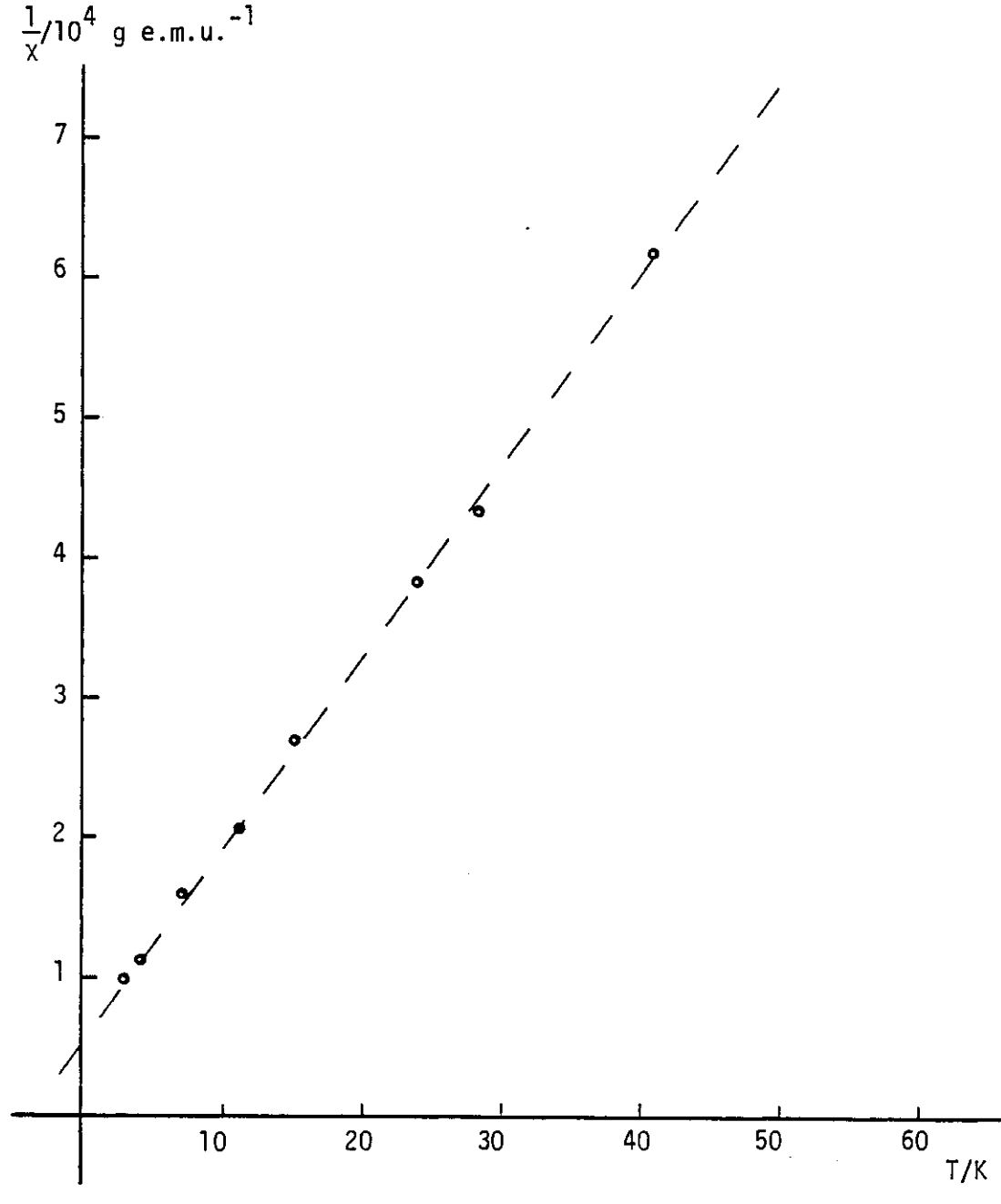

FIGURE 4.15 Inverse susceptibility of part of the chromium 4% iron sample used in the D5 experiment. The dashed line is a least squares fit to the data, for T < 100 K, of a Curie-Weiss law. The Curie constant is related to the neutron magnetic diffuse cross-section, see the text.

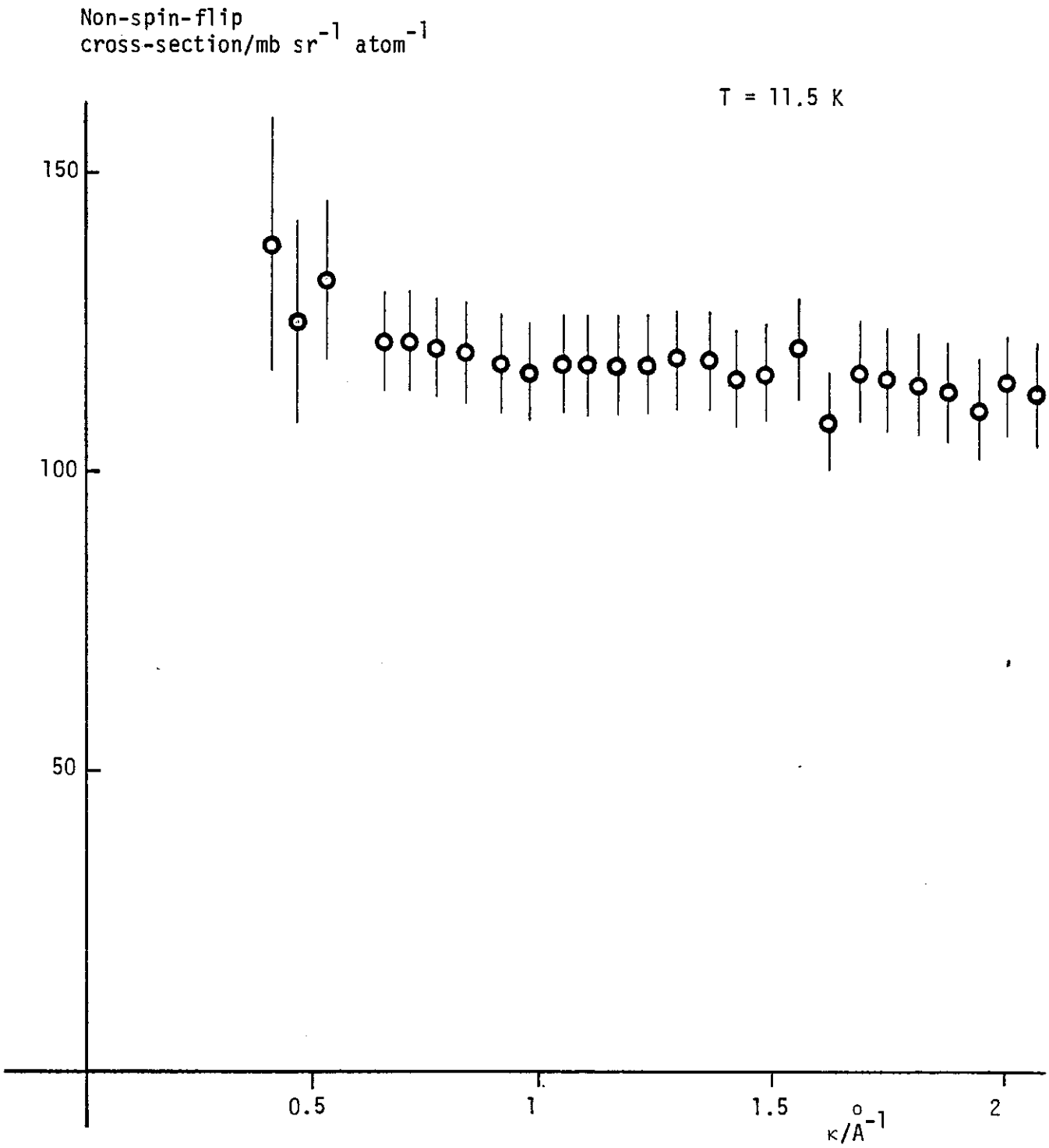

FIGURE 4.16 Non-spin-flip cross-section of chromium 4% iron with the guide field at the sample parallel to the scattering vector, κ.

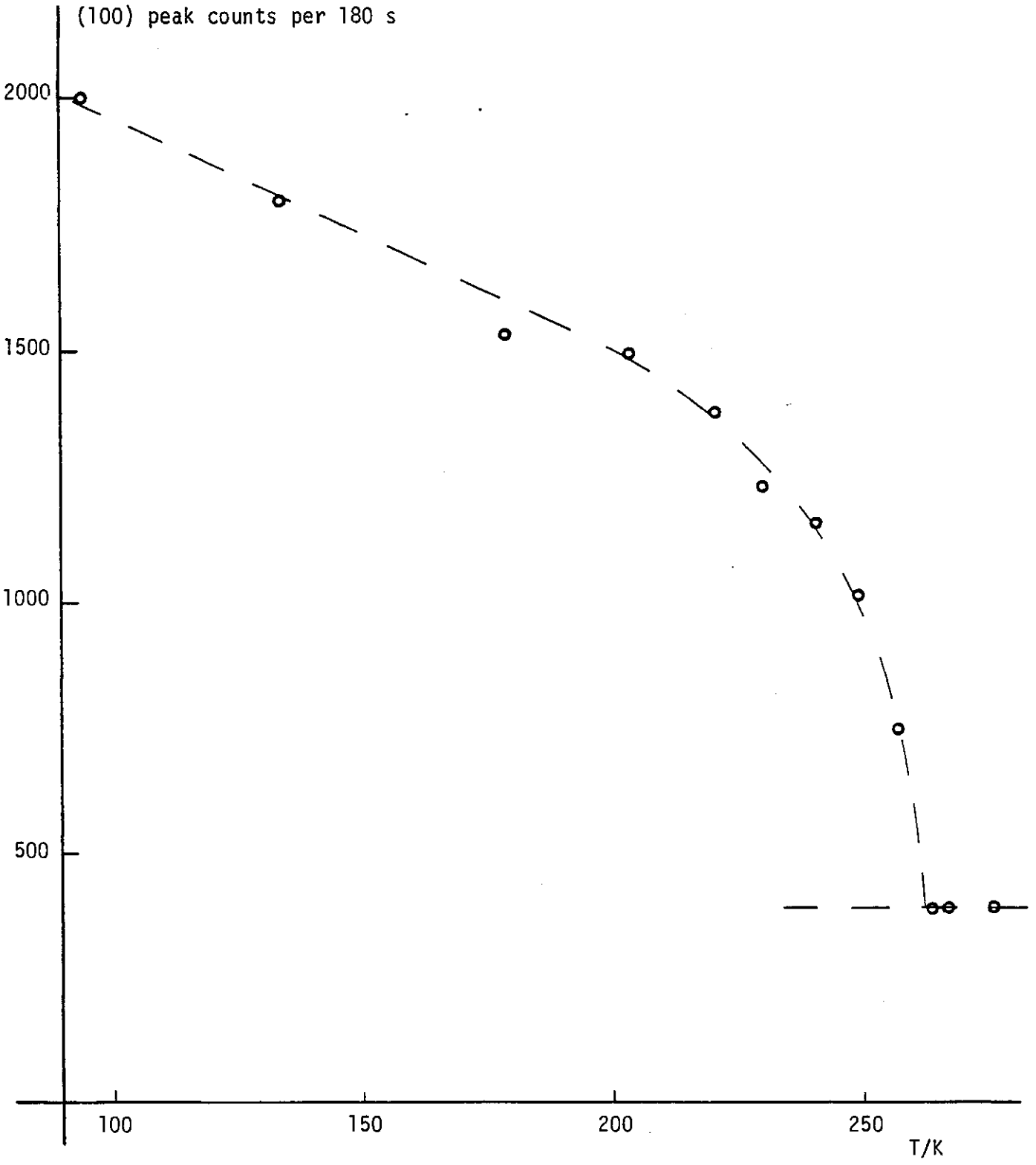

FIGURE 4.17 (100) magnetic Bragg peak counts at one fixed detector position as a function of temperature, T, for chromium 4% iron. The dashed lines are guides to the eye. The Néel temperature, T_N, is 263 ± 3 K.

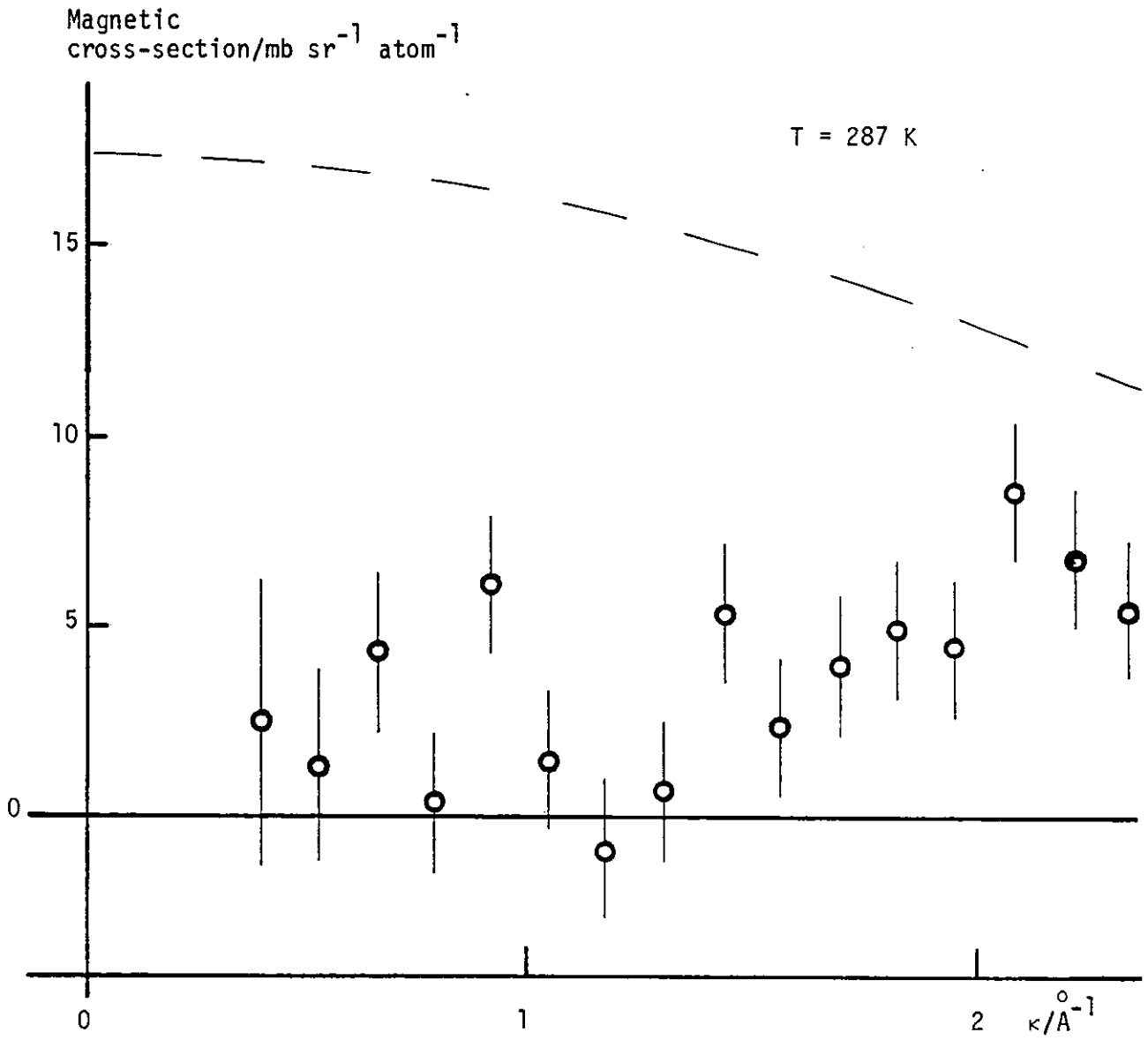

FIGURE 4.18 Magnetic diffuse cross-section of chromium 4% iron above the Néel temperature. For an explanation of the dashed line see the text.

parallel to the scattering vector, is shown in figure 4.16. A large proportion of this may confidently be attributed to the isotope disorder and nuclear spin disorder scattering as seen in pure chromium. There is an indication of some problem here in the magnitude of the isotropic incoherent cross-section, as compared with the expected value. The isotope and nuclear spin disorder scattering alone, are expected to be about 115 mb sr^{-1} at^{-1} (Cywinski and Hicks 1978). Then there is the Laue scattering, expected to be 13.8 mb sr^{-1} at^{-1}, with some modulation due to chemical short range order, if there is any. This discrepancy may be due to an overestimate of the multiple scattering, which is quite large. The q-dependence of the scattering, which also occurs in pure chromium, was discussed above, and is attributed to the q-dependence of the multiple scattering, rather than chemical short range order affecting the Laue scattering.

The results of measuring the peak height of the (100) reflection as a function of temperature are depicted in figure 4.17, and a well-defined Néel temperature of 263 ± 3 K is deduced, in reasonable agreement with previous measurements for this composition (see figure 3.1).

Finally, the spin-flip difference cross-section as measured at 287 K, well above the Néel temperature is presented in figure 4.18. The paramagnetic scattering expected on the basis of the local moment model, with values taken from the susceptibility data of Ishikawa et al. (1965) is marked as the dashed line. Clearly, the observed scattering does not correspond very well with this model.

Small Angle Scattering Experiment

The magnetic incoherent quasi-elastic cross-section in the forward direction is related directly to the product of the bulk magnetic susceptibility and the temperature (see chapter 1). However, the

scattering observed in the polarisation analysis experiment described above showed little sign of matching the measured bulk susceptibility down to 0.3 $\mathring{A}^{-1}$ in momentum transfer, where the magnetic diffuse cross-section is zero within statistics (figure 4.14). This suggests that the effective form factor of the magnetic entities giving rise to the susceptibility is sharply peaked in the forward direction, which in turn implies that the spatial extent of these entities is large. This could not be verified in the D5 measurement because of the large air-scattering of the straight-through beam, which gives rise to very large count rates, both spin-flip and non-spin-flip, close to the forward direction. This is an inevitable consequence of the long monochromator to detector neutron flight-path in air on D5. In order to avoid this problem, an instrument with an evacuated flight-path must be used.

To fill in the gap in the small-q cross-section, therefore, an experiment to measure the diffuse cross-sections was attempted using the small-angle neutron scattering instrument at the Pluto reactor at the Atomic Energy Research Establishment, Harwell. It was known that the attempt to measure such a small cross-section, on top of the large nuclear disorder and nuclear spin disorder cross-sections without the assistance of polarisation analysis would be difficult, but it was thought that if the magnetic diffuse cross-section were sharply peaked, as suggested by the argument above, it might be possible to separate it by assuming all the other contributions to be isotropic in reciprocal space.

A sample was cut from the ingot used in the polarisation analysis experiment to provide an area of 1 cm × 1 cm with a thickness of 1 cm, which gives a transmission factor of 1/e for a neutron wavelength of 6 $\mathring{A}$, which maximises the measured scattering by balancing the gain in scattering because of an increased number of scatterers, with the loss due to absorption of the beam by the sample. The multiple scattering

is negligible in this experiment using 6 Å neutrons, firstly because the absorption to scattering ratio is larger (the absorption cross-section is proportional to the wavelength) and secondly because there is no Bragg scattering. The Bragg equation

$$n\lambda = 2d\sin\theta$$

can not be satisfied for any non-zero integer n, and angle θ when

$$\lambda > 2d_{max}$$

where d_{max} is the largest inter-planar spacing in the structure, which in this case is 2.88 Å. The wavelength $\lambda_c = 2d_{max}$ is called the Bragg cut-off.

The sample was mounted in a CT14 helium flow cryostat, with no additional collimation or screens at the sample.

The Pluto S.A.S. instrument consists, quite simply, in a rotating drum velocity selector, a collimator, an evacuated cloche to house the sample, in this case in the cryostat, and a two dimensional multi-detector at a distance of 2.1 m from the sample, with a cadmium beam-stop to absorb the unscattered beam.

The experiment failed to give any significant results for two reasons. Firstly there was a significant, temperature independent signal peaked in the forward direction as the inverse of q^2. This may have been partly avoidable by more careful collimation at the sample position, although some of it may have been due to effects such as grain-boundary scattering. Secondly, and decisively, the intensity was too low to give results significant at the level of a few mb sr^{-1} at^{-1}. The isotropic scattering found at higher q-values (up to 0.17 $Å^{-1}$), which at a lower limit represents 120 mb sr^{-1} at^{-1} of incoherent scattering from the chromium, has an uncertainty of ±5 mb sr^{-1} at^{-1} after 24 hours of counting. This would mask completely the

anticipated magnetic cross-section. Increasing the counting time would increase background problems, the background accounting for about 30% of the signal.

The conclusion of this experiment was that a more subtle method would have to be employed to measure the magnetic diffuse elastic scattering at small values of momentum transfer. Polarisation analysis using long-wavelength incident neutrons would be ideal, but at the time of writing, no instrument exists for this. The installation of polarisation analysis using the highly efficient polarising super-mirrors on the cold-source diffuse scattering instrument D7 at I.L.L., Grenoble, might make this experiment possible. However, at present, this facility is under test and not yet available for experiments.

Single Crystal Single-$\underline{Q}$ Experiment

i. Introduction

As described above, the theory of Friedel and Hedman (1978) predicts a marked anisotropy in the susceptibility in the incommensurate SDW phases when iron moments contribute a temperature dependent susceptibility. This derives from the anisotropy in the environment in that theory, which gives two-dimensional freedom in the transverse phase, and one-dimensional in the longitudinal. In the transverse phase, there is a Curie-Weiss-like susceptibility normal to the SDW wave vector $\underline{Q}$, but not parallel to it, while in the longitudinal phase, the Curie-Weiss-like susceptibility appears only parallel to $\underline{Q}$. So, if a single-$\underline{Q}$ sample could be prepared of an incommensurate alloy, the theory predicts that the susceptibility would be highly anisotropic, in one sense in the transverse phase, where the direction of $\underline{Q}$ would correspond to a hard direction, and in the other sense in the longitudinal phase, where $\underline{Q}$ lies in an easy direction.

It emerged as a result of the neutron magnetic Bragg scattering

experiment described in chapter 3 above that some of the samples prepared had undergone considerable grain growth. This provided an opportunity to mine out some single crystal alloy samples, and one of these, a nominal 1.0% iron alloy, was prepared to test the anisotropy prediction of Friedel and Hedman's theory.

ii. Sample Preparation

The polycrystalline ingot prepared as described in chapter 3 above was etched in hydrochloric acid to reveal the crystallite structure, which was easily identified by the strong contrast in reflectivity between crystallites of different orientation. A crystallite of suitable size was cut from the ingot using the spark erosion technique. The faces were planed down using the spark planing device to enable X-ray Laue back reflection photographs to be taken. These were taken using a Phillips vertical tube X-ray generator and a specially built Laue camera. This camera is described in appendix C.

Laue pictures taken from many points on the surface confirmed that this was indeed a single crystal. A cylindrical sample was cut from the crystal with its axis in a [110] direction. The cylinder was trepanned from the crystal using a rotating tube as the spark cutting tool. Suitable drillings in the tube allowed the free flow of paraffin (dielectric) to ensure fast and even erosion. The tube was turned by the spark planing device, into which it was carefully wedged in order to turn without lateral movement (figure 4.19). The surface of the cylindrical crystal was cleaned and the orientation of the crystal directions determined with respect to a small flat face on the side of the cylinder (figure 4.20), again using an X-ray Laue photograph. The final size of the cylinder was about 2.5 mm long by 4 mm diameter, with a mass of nearly 200 mg.

iii. Experimental Details

The susceptibility was measured by a quasi-d.c. method in large

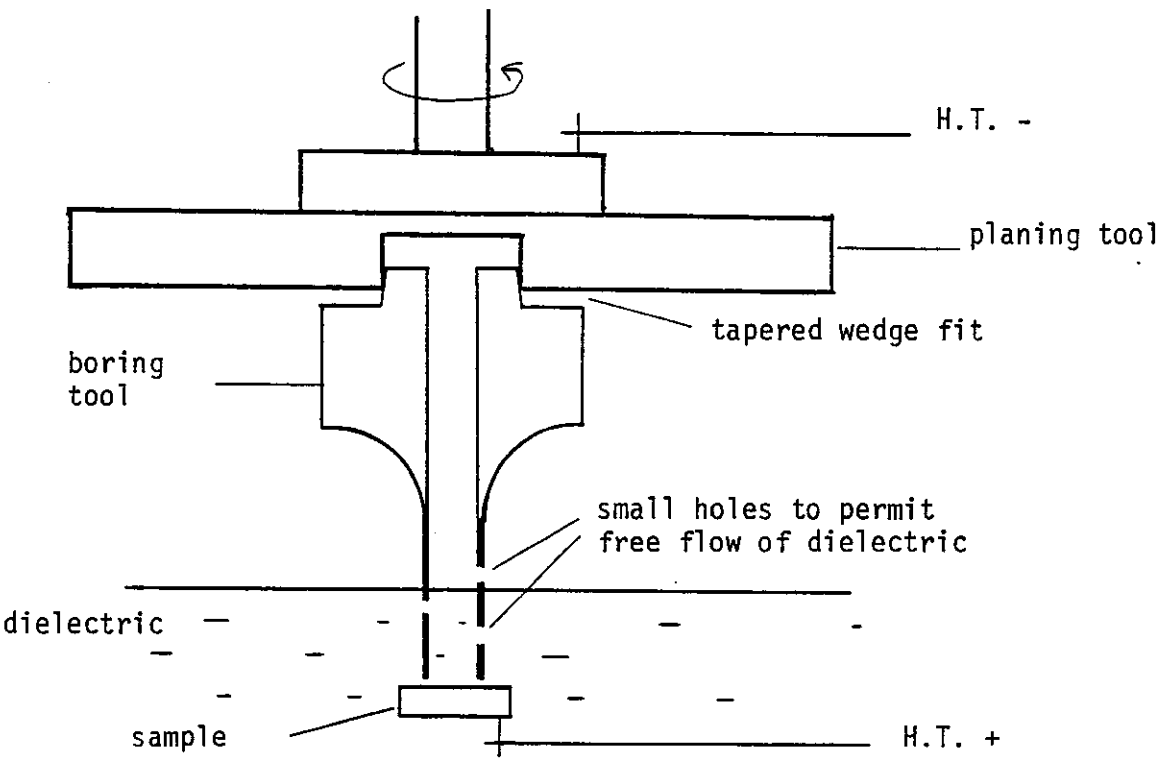

FIGURE 4.19 Spark boring tool.

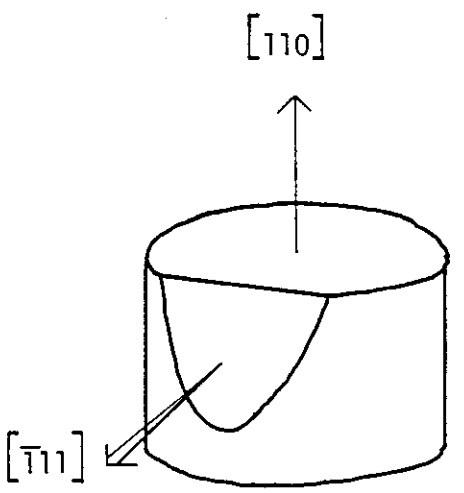

FIGURE 4.20 Crystal of chromium 1% iron, as orientated by X-ray Laue photographs.

magnetic fields (16 kOe) using the high field vibrating sample magnetometer described in appendix B.

In order to be able to rotate the crystal, a special sample holder was designed and built to allow any direction in the $[1\bar{1}0]$ zone to be brought to the vertical, parallel to the vibration direction and the applied magnetic field. This holder, illustrated in figure 4.21, is made from delrin and consists of a capstan with a space for the sample. The capstan is mounted by a lug on each end into the part which screws onto a copper stud, which in turn provides thermal contact with the thermometer and heater in the sample rod. The capstan is turned by a piece of nylon fishing line, one end of which is held under tension by a spring. The other end may be positioned at any position in a screw clamp mounted on the sample rod in a position which is accessible when the rod is in position for measurements to be made. Thus the sample may be turned continuously through the $[1\bar{1}0]$ zone, it is free to be vibrated, and its temperature may be controlled and monitored.

iv. Generating a Single-$\underline{Q}$ Domain

The least satisfactory aspect of this experiment is the absence of any means of testing, independently of the susceptibility, whether a single-$\underline{Q}$ domain state has been created. The most satisfactory method would be a 4-circle neutron diffractometer measurement of the intensities of the magnetic satellite reflections, which are zero when the scattering vector is perpendicular to the magnetic moments (i.e. when $\underline{q} \parallel \underline{Q}$ in the transverse SDW, and when $\underline{q} \perp \underline{Q}$ in the longitudinal SDW). However, this has not so far been possible.

Thus it is not known how successful the attempts to generate a single-$\underline{Q}$ domain were. Werner, Arrott and Kendrick (1966 and 1967) found that in pure chromium, a single-$\underline{Q}$ state could be generated by field-cooling through T_N in any field greater than about 24 kOe. Isothermal application of fields greater than 160 kOe also generated,

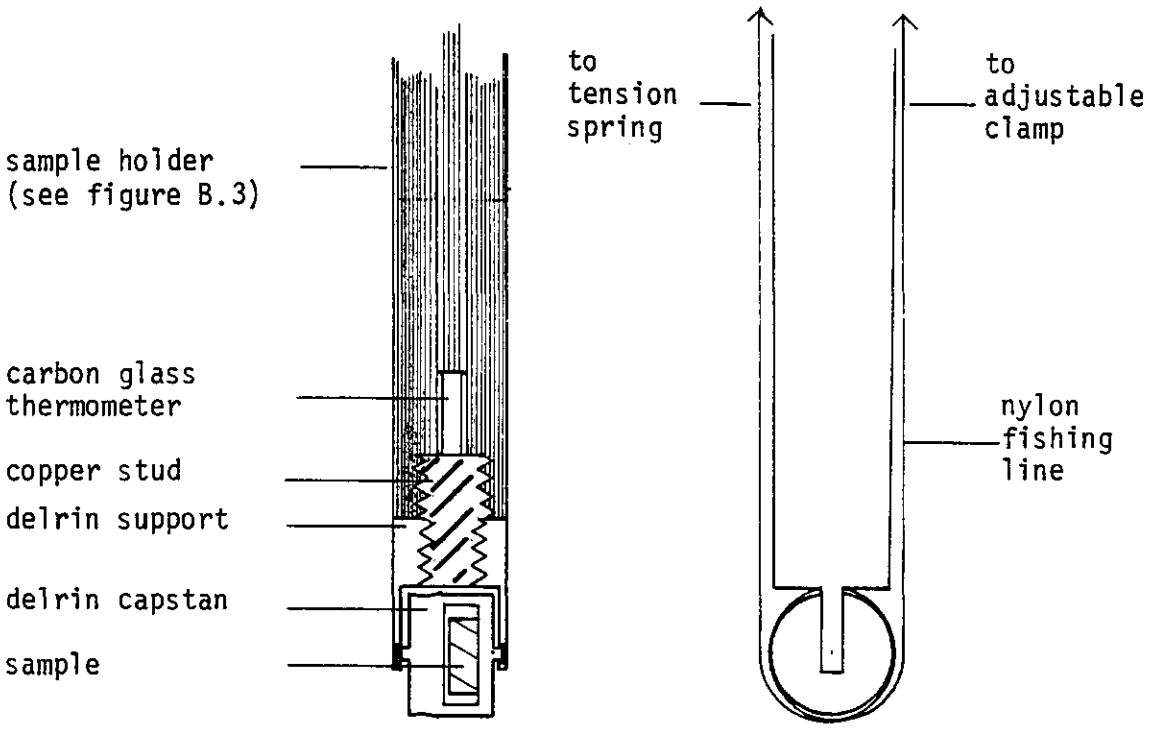

FIGURE 4.21 Rotating sample holder.

at low temperature, in the longitudinal phase, a two-$\underline{Q}$ state. Isothermal application of fields up to 12 kOe changed the proportion of the various domains, but in a reversible manner. The $\underline{Q}$-vectors did not rotate during this process. The torque magnetometer measurements of magnetocrystalline anisotropy by Montalvo and Marcus (1964) in pure chromium found that the susceptibility perpendicular to $\underline{Q}$ is about 6% greater than that parallel to $\underline{Q}$, so this provides an explanation of the coupling to the applied field.

Werner et al. (1967) concluded that strain in a crystal could stabilise a particular domain structure, and it may be that in our crystal, there is strain built in which is sufficient to prevent the single-$\underline{Q}$ state forming.

The method used to attempt to generate a single-$\underline{Q}$ state was to cool the sample through its Néel temperature in a magnetic field of 74 kOe, the maximum field available in this laboratory. Two attempts were made to do this, once before and once after annealing the sample at 1000^{o}C for 4 days. This annealing was followed by slow cooling in the furnace, and was intended to remove any significant strain from the crystal.

v. Results

Because of the unusual nature of this measurement, several problems arose which were not anticipated. Rotation of the sample also caused a slight translation, and this affected the magnitude of the signal. This gave rise to an angular dependence of the signal which had a period of one rotation of the sample. So it could be distinguished from any crystal anisotropy which must, by symmetry considerations, have a period of one half of one rotation of the crystal (or some submultiple).

After the first attempt to generate a single-$\underline{Q}$ state, the susceptibility was measured as a function of angle of sample rotation

in a field of 16 kOe both at low temperatures (2.0 K and 4.2 K) and at high temperature (250 K) and no anisotropy was found.

After annealing, and the second attempt to induce a single-$\underline{Q}$ state, the susceptibility was found to have increased at low temperature by about 15%, while remaining the same at high temperature ($T \sim T_N$). However, there was still no anisotropy detectable at 4.2 K, while the resolution would permit detection certainly of 5% anisotropy, and possibly less than that.

The magnetisation against field plots for this sample in all cases were straight lines passing through the origin, once corrections had been made for the background from the sample holder ($\sim$8% of the signal at T = 4.2 K). That is, there was no remanence, and no evidence of any field-induced transition (e.g. irreversible rotation of the $\underline{Q}$-vector).

vi. Discussion of the Single-$\underline{Q}$ Experiment

The results of this experiment are ambiguous. The lack of any observed anisotropy could be due to the failure of Friedel and Hedman's model, or else to the failure to produce in the sample a single-$\underline{Q}$ state.

It is possible that the conditions used would not induce a single-$\underline{Q}$ state, perhaps because of a vast increase in the "pinning" effect of the magnetic iron impurities, resisting the formation of such a state. However, this is considered unlikely to be the explanation, because even if this were so to some degree, there is likely to be some preferential $\underline{Q}$-alignment, and this would give a corresponding degree of anisotropy. However, there remains a degree of doubt until such time as a neutron diffraction measurement can be made on the sample.

There is also a slight possibility that the measuring fields used in this experiment (16 kOe) were sufficient to disturb the $\underline{Q}$-structure of the sample, though this is very unlikely in view of the difficulties in producing a single-$\underline{Q}$ state, and in the light of the linearity of the

magnetisation-field plots.

So the tentative conclusion that is drawn from this null result is that Friedel and Hedman's description, while largely accounting for the temperature dependence of the susceptibility, does not account for its observed isotropy.

Discussion and Conclusions

What can now be said about the magnetic correlations in dilute chromium-iron alloys below the Néel temperature? We consider the average fourier transformed correlation, as a function of wave-vector and frequency, $C(\underline{q},\omega)$

$$C^{\alpha\beta}(\underline{q},\omega) = \int d\underline{r}_1 \int \exp\{-i\underline{q}.(\underline{r}_1 - \underline{r}_2)\} d\underline{r}_2 \int_{-\infty}^{\infty} dt \exp\{-i\omega t\} C^{\alpha\beta}(\underline{r}_1,\underline{r}_2,t)$$

where

$$C^{\alpha\beta}(\underline{r}_1,\underline{r}_2,t) = \langle \hat{\zeta}^{\alpha}(\underline{r}_1,0)\hat{\zeta}^{\beta}(\underline{r}_2,t)\rangle$$

(see chapter 1 for a discussion of this function).

The bulk magnetic susceptibility is composed of a nearly-temperature-independent part very similar to that of pure chromium, and a part which, except below about 4 K, looks like a Curie-law susceptibility. This corresponds to a fluctuating spin-spin correlation whose transformed value at $\underline{q} = \underline{0}$, $\omega = 0$ is roughly constant as a function of temperature. What is the $\underline{q}$-dependence of this second part? The neutron diffuse scattering experiment described above shows, indirectly, that it must be sharply peaked near $\underline{q} = \underline{0}$. What of its energy dependence? The Mössbauer data give a rough estimate of the weight of $C^{\alpha\alpha}(0,\omega)$ up to $\omega = \omega_M$, the Mössbauer reciprocal lifetime ($\sim$10 MHz). This increases as the temperature decreases roughly as

$$\int_0^{\omega_M} d\omega C^{\alpha\alpha}(0,\omega) \propto \frac{1}{T + 60}$$

according to Herbert et al. (1972). Taken with the susceptibility data, this indicates that $C^{\alpha\alpha}(0,\omega)$ is narrower in energy at lower temperatures than it is at higher. This is to be expected. The width must be comparable to the Mössbauer reciprocal lifetime, which is extremely narrow on the scale of a neutron scattering experiment. A small energy width is consistent with the notion, derived from the very small Curie-Weiss temperature deduced from the bulk susceptibility, that whatever is causing the susceptibility is only weakly interacting. The small width in wave-vector suggests a long spatial range of the fluctuating magnetic correlations.

The time averaged part of the magnetic correlation function, or the contribution to $C^{\alpha\alpha}(\underline{q},0)$ which has zero width in energy, reflects the magnetic structure. In the commensurate alloys, there are antiferromagnetic Bragg peaks at the b.c.c. superlattice positions {100}, {111} and so on. The iron moments, if there are any, and if they contribute to the structure, should give rise to magnetic elastic diffuse scattering, within the linear superposition theory of Marshall (Marshall and Lovesey 1971),

$$X(\underline{q}) = c(1 - c)|F(\underline{q})|^2\{\mu_{Cr} - \mu_{Fe} + G(\underline{q} - \underline{\tau})\}^2$$

where

$$X(\underline{q}) \propto C^{zz}(\underline{q},0),$$

with z the local direction of spins. (Note that this direction may vary, and the neutron cross-section must take this into account with a suitable average.) $G(\underline{\kappa})$ represents the disturbance of the magnetic structure by an isolated iron atom in wave-vector space. According to the theory of Marshall, $G(\underline{\kappa} = \underline{0})$ may be related to the concentration dependence of the mean ordered moment, μ

$$\frac{\partial \mu}{\partial c} = \mu_{Cr} - \mu_{Fe} + G(\underline{\kappa} = \underline{0}).$$

There is a certain amount of disagreement about the detailed form of $\mu(c)$ for $c < 0.05$ (Arrott et al. 1967 and Ishikawa et al. 1967) and in any case, it seems that μ is far from a linear function of c, as assumed by Marshall's theory. Ishikawa et al. find that μ is more or less constant within the incommensurate phases, while Arrott et al. suggest that it increases with concentration. For $c > 0.05$, the mean ordered moment μ at low temperature follows the form of the Néel temperature as a function of c (Burke and Rainford 1978), decreasing almost linearly to zero as c increases to about 0.16. In this case, in the region of $c = 0.05$, it seems likely that the expression for $G(0)$ should include a term in the second derivative of μ with respect to c. Holden and Fawcett (1978) used a positive value for $\frac{\partial \mu}{\partial c}$ while Burke (1980) used a negative value, in their analyses for 2.8% and 5% samples respectively.

As noted above, the magnetic diffuse cross-section showed no clearly defined behaviour as a function of q, and certainly showed no tendency to peak at the magnetic reciprocal lattice vector, $\underline{\tau}$, <100> in our case. Now because our experiment was performed on a polycrystalline sample, it is by no means obvious what is the relationship between the observed cross-section and the cross-section predicted, which involves the term

$$|F(\underline{q})|^2\{\mu_{Cr} - \mu_{Fe} + G(\underline{q} - \underline{\tau})\}^2.$$

If G is a very long-ranged function in real space, or a very sharply peaked function in reciprocal space, then this term separates into two kinds of scattering. Some is nearly isotropic, modified only by the form factor, while the rest resembles Bragg peaks at the magnetic Bragg position, and the usual powder/polycrystalline resolution-dependent

terms (e.g. Bacon 1975) will enter the observed cross-section for the Bragg-like peaks. If G is very short ranged in real space, then it will be almost isotropic, and hardly dependent on q. This will then appear in full in the observed cross-section in the polycrystal as in the single crystal with only a form factor dependence on q. If G falls between these two extremes, the calculation of the true cross-section from a polycrystalline scattering function becomes very difficult. Cywinski and Hicks (1980) made an assumption of spherical symmetry, but this must be of doubtful value, especially if the scattering is peaked around the reciprocal lattice positions.

The conclusion from this data, however, is that any such scattering <u>is</u> sharply peaked at the Bragg position, and this is in agreement with the results of Holden and Fawcett in their single crystal experiment. This means that, for practical purposes, the defect scattering is inseparable from the Bragg scattering. In this case, the extended defect is absorbed into the measured values of the mean sublattice moment. In general we must allow the moments carried on the two types of atoms to be dependent on the concentration of iron, c. Then the mean sublattice moment, μ is

$$\mu = c\mu_{Fe}(c) + (1 - c)\mu_{Cr}(c).$$

We do not have sufficient data to establish $\mu_{Fe}(c)$ and $\mu_{Cr}(c)$. It may not be a bad approximation to suppose that μ_{Fe} is not a function of concentration. That is purely a guess. Then

$$\frac{\partial \mu}{\partial c} = (\mu_{Fe} - \mu_{Cr}(c)) + \frac{\partial \mu}{\partial c}Cr(c).$$

If we treat our diffuse scattering experiment as a measurement of the function

$$c(1 - c)|F(q)|^2\{\mu_{Fe} - \mu_{Cr}(c = 0.04)\}^2,$$

we can fit our data to this form. This returns a value of

$$\{\mu_{Fe} - \mu_{Cr}(0.04)\}^2 = 1.58(\mu_B)^2.$$

Let us assume further that the iron moment adopts the same sense as the chromium it replaces, and is larger, then

$$\mu_{Fe} - \mu_{Cr} = 1.26\ \mu_B.$$

The mean sublattice moment as deduced from Burke and Rainford (1978) for $c = 0.04$ is $\mu = 0.76\ \mu_B$. Then we may deduce that

$$\mu(c = 0.04) = 0.04(\mu_{Fe} - \mu_{Cr}) + \mu_{Cr}(0.04)$$

which implies that

$$\mu_{Cr}(0.04) = 0.76 - 0.04 \times 1.26$$
$$= 0.71\ \mu_B$$

and $\mu_{Fe} = 1.97\ \mu_B$.

If the iron moment adopts the opposite sense to the host moment it replaces, then

$$\mu_{Cr}(0.04) = 0.81\ \mu_B$$

$$\mu_{Fe} = -0.45\ \mu_B.$$

We can not, with the present data, distinguish between these two possibilities. The fit of the data is not impressive, and the whole model may be wrong. However, the first combination above has an appeal of simplicity.

We have assumed that the iron moment is not a function of concentration, and that value, if we assume the moment lines up in the obvious sense in the structure, is almost 2 μ_B, which is a very common value for iron atoms in many environments. Note that this is an

ordered moment. That is, it is not fluctuating, and therefore not contributing to the susceptibility. It would not be surprising to find that the chromium site moment did vary rapidly with composition, since the moment is known to be a sensitive function of temperature and environment, and the transition to paramagnetism at T_N destroys the moment in pure chromium. The lack of a short ranged defect is surprising, but quite consistent with the observed scattering. A long ranged defect is indistinguishable from the average chromium site moment.

This model for the order leaves no firm guide as to what to expect for the fluctuating correlations, or the susceptibility. We are certain that the observed diffuse scattering can not account for the observed susceptibility. We therefore attribute the observed scattering to elastic scattering, and find it to be reasonable if the iron moment of $\sim 2\ \mu_B$ is locked into the ordered structure. That leaves the conclusion that the fluctuating correlations are long ranged in real space, or sharply peaked in reciprocal space.

This contradicts the weak interaction picture unambiguously. It also contradicts the strong interaction picture of the susceptibility (Friedel and Hedman 1978), while endorsing the view of a strong interaction between impurity moment and host structure. The lack of anisotropy found in the single-$\underline{Q}$ experiment also indicates that Friedel and Hedman's picture of the susceptibility is incorrect.

The answer to the problem of the temperature dependent susceptibility may possibly be found in the consideration of the formation of antiferromagnetic micro-domains. In a hand-waving way, an antiferromagnetic domain wall may be considered to carry a moment, and to have degenerate states which are split by the application of a magnetic field, and hence a Curie-law susceptibility. If the phase of the antiferromagnetic order within a domain can be pinned by a cluster

of three nearest-neighbour iron atoms coupled together, which occur with a concentration proportional to the cube of the iron concentration, then the magnitude of the domain wall moment may increase linearly in the iron concentration. However, quantitative agreement of such a model with the observed parameters has not been found. Nor is it clear why the proposed pinning should occur. In support of the idea, we may quote the development of a Curie-law component in the susceptibility in many chromium alloys, notably ternary alloys with manganese and vanadium (Adachi and Maki 1977), and it is seen also in the purest chromium available (Sousa 1980). Perhaps it could arise from any pinning mechanism, mechanical or magnetic.

As a final speculation, the problem may be intimately bound up with the curious excitation spectrum of pure chromium (Burke, Ziebeck and Booth 1980) and the possibility that such domain walls could move with very low energies, once excited, in a way not dissimilar from a more conventional soliton, if such exist (Loveluck 1981).

In summary, we conclude that the simplest explanation of the observed magnetic correlations is that the iron sites sustain a moment of 2 μ_B, which is aligned with the ordered structure. The susceptibility originates from some low energy, but large spatial range, fluctuations, which may arise from the quasi-static, or dynamic, behaviour of antiferromagnetic domain walls.

CHAPTER 5

CHROMIUM-IRON ALLOYS - iii. FERROMAGNETS

Introduction

The destruction of long range ferromagnetic order in alloy systems by dilution of a ferromagnet with a non-magnetic solute is a subject of great interest, both from the point of view of the nature of the magnetic entities, their interactions and the consequent magnetic order, and also viewed more generally as an example of a phase transition in a random system. Many experiments have been performed on both gold-iron and chromium-iron alloys, and many diverse physical models and hypotheses have been used to explain the observed behaviour. The chromium-iron alloy system has the advantage that (more or less) random substitutional b.c.c. alloys may be prepared with any average composition through from pure chromium to pure iron. This is not so for (f.c.c.) gold-iron alloys, though the two systems exhibit many similarities, and we shall have occasion to compare the two systems.

Experimental Review

A review of the experimental work done on ferromagnetic chromium-iron alloys is given by Burke (1980), chapter 5. He also presents an account of a series of neutron small-angle scattering experiments performed on alloys from 16% iron to 25% iron both in zero applied field as a function of temperature, and at low temperature as a function of applied field. This has established by two conditions that the critical composition is 19% iron, and that alloys with more iron do undergo a transition to ferromagnetism, while those with less do not. The first condition is that alloys with 19.5% iron and more show characteristic critical scattering, while those with 18.5% iron and less do not (figure 5.1). The second is that the minimum value of the

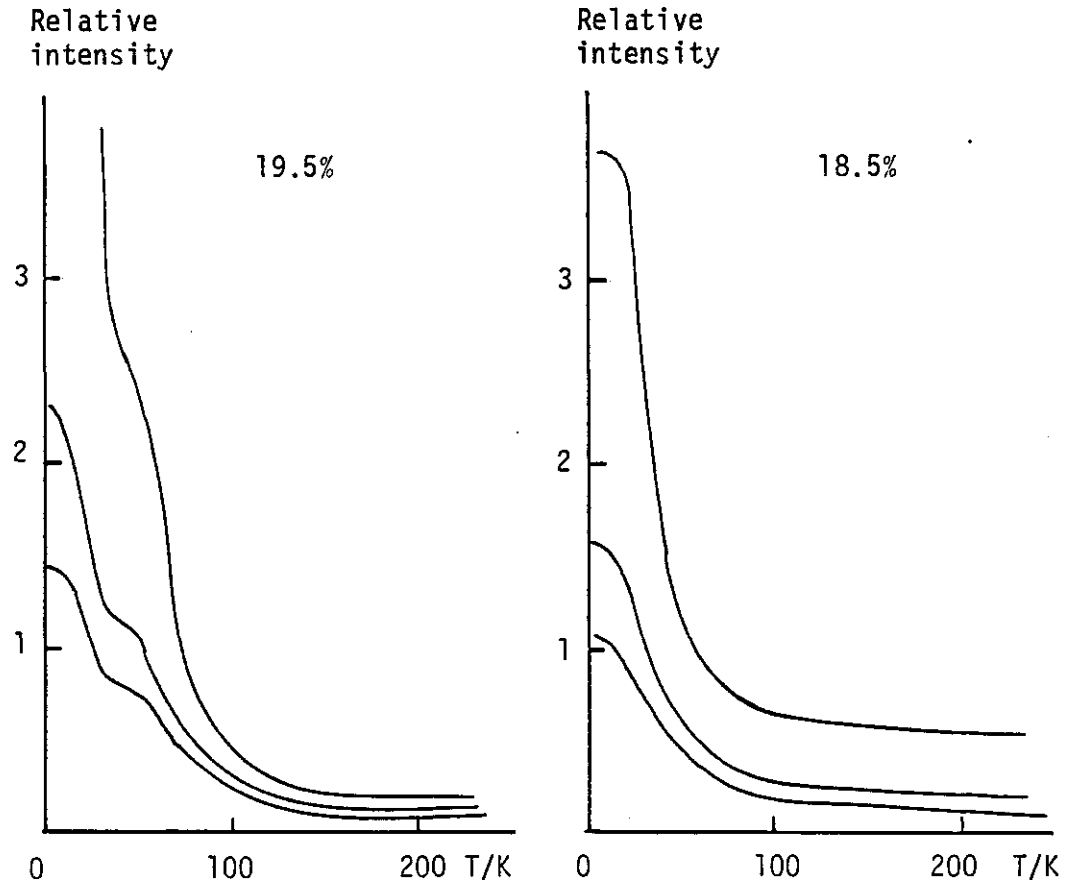

FIGURE 5.1 Temperature variation of small angle scattering for chromium 19.5% iron and chromium 18.5% iron. Radially averaged intensities are shown for constant κ values of 0.019 $\mathring{A}^{-1}$ (upper curve), 0.032 $\mathring{A}^{-1}$ (middle curve) and 0.040 $\mathring{A}^{-1}$ (lower curve).

From Burke (1980).

inverse correlation range of the magnetic fluctuations as a function of temperature is non-zero for alloys with 18.5% iron or less, but extrapolates to zero for 19.0% iron (figure 5.2).

There are some difficulties with this data. The first is connected with the form of the scattering law. It is assumed to be Lorentzian in q,

$$S(q) \propto \frac{A}{\kappa_1^2 + q^2}$$

where κ_1 is the inverse correlation range. There are, however, deviations at large q which are to be expected, as these reflect the details of the correlations, but also at very small q, which are more worrying, as the Lorentzian form should fit best here (figure 5.3). The second problem is to do with the large signal which appears at low temperatures, apparently independent of the critical scattering, loosely termed subcritical scattering. The amplitude of this scattering reaches a maximum at the critical concentration for the onset of ferromagnetism (figure 5.4). The third problem lies in the observed field-induced anisotropy of this subcritical scattering (figure 5.5). Qualitatively the effect is in agreement with the magnetic cluster model which Burke used to interpret it, but quantitatively, the agreement is poor.

Another very important contribution to the understanding of these alloys is the observation of pathological spin wave modes by Fincher, Shapiro, Palumbo and Parks (1980). They used polycrystalline samples, and so were not able to examine much of the zone. (This is because, away from the forward direction, all the crystallites contribute to the scattering from different directions in the zone, and the resultant smearing of the excitations makes detailed studies impossible.) At small momentum transfers, they observed normal ferromagnetic spin waves with a very small gap in a 34% iron alloy, while in a 26% iron alloy,

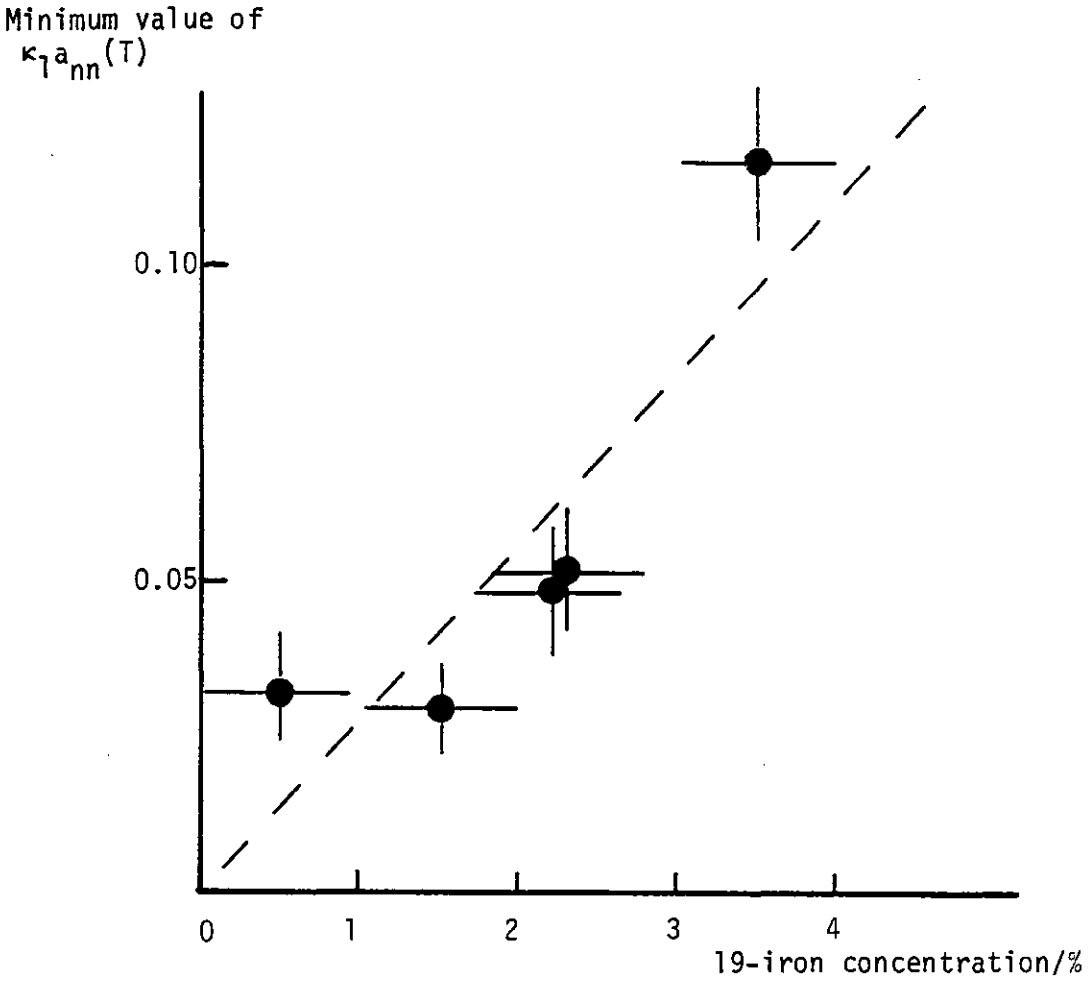

FIGURE 5.2 The concentration dependence of the minimum value of the inverse correlation range, κ_1, multiplied by the nearest neighbour distance a_{nn}. The dashed line is a guide to the eye.

From Burke (1980).

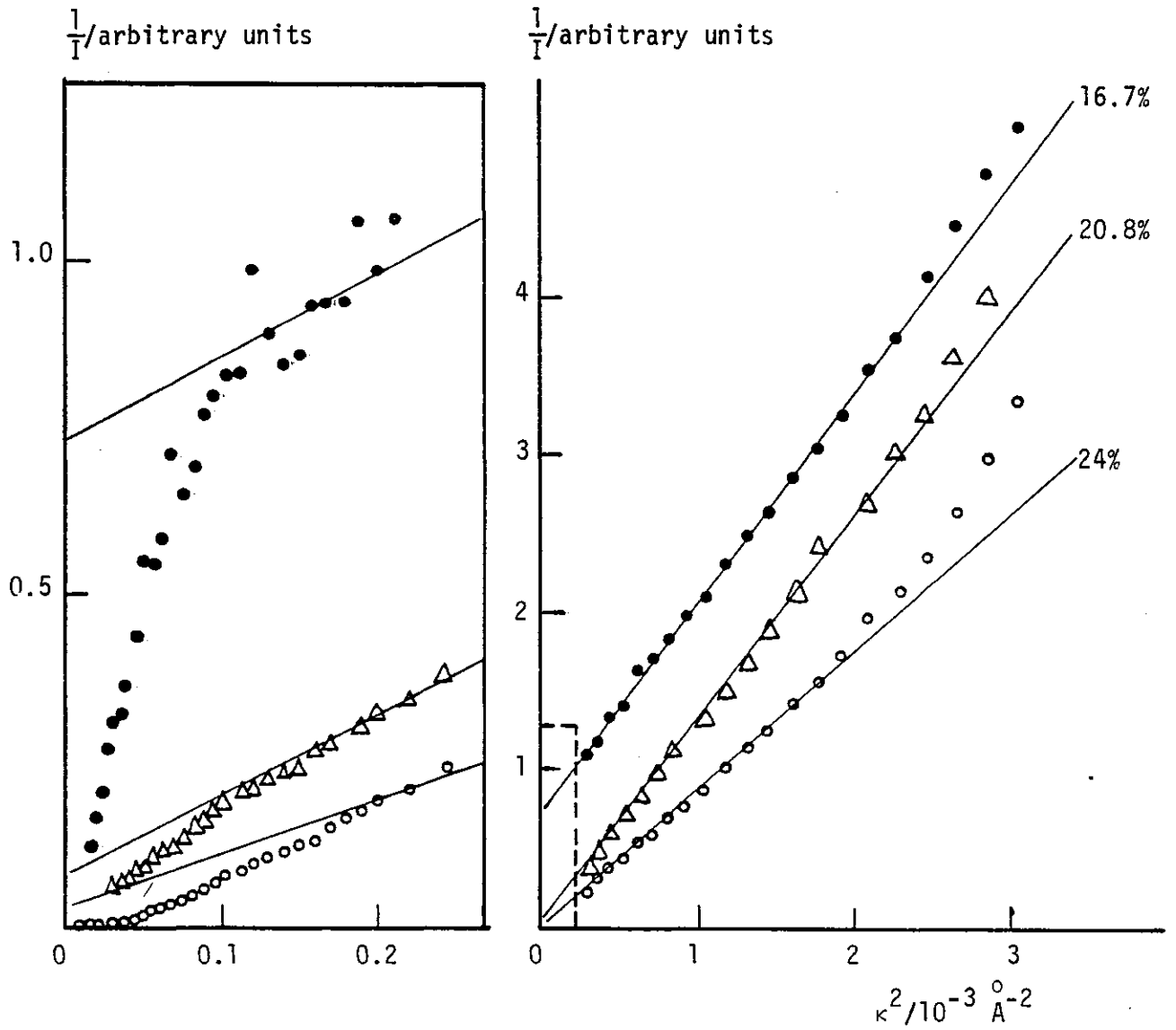

FIGURE 5.3 Debye plots ($1/I$ vs. κ^2) of magnetic small angle scattering at T = 4.2 K for alloys with compositions below, above and almost equal to the composition for the onset of ferromagnetism. Note the deviations in all three from Lorentzian (linear in this plot) at very small κ. From Burke (1980).

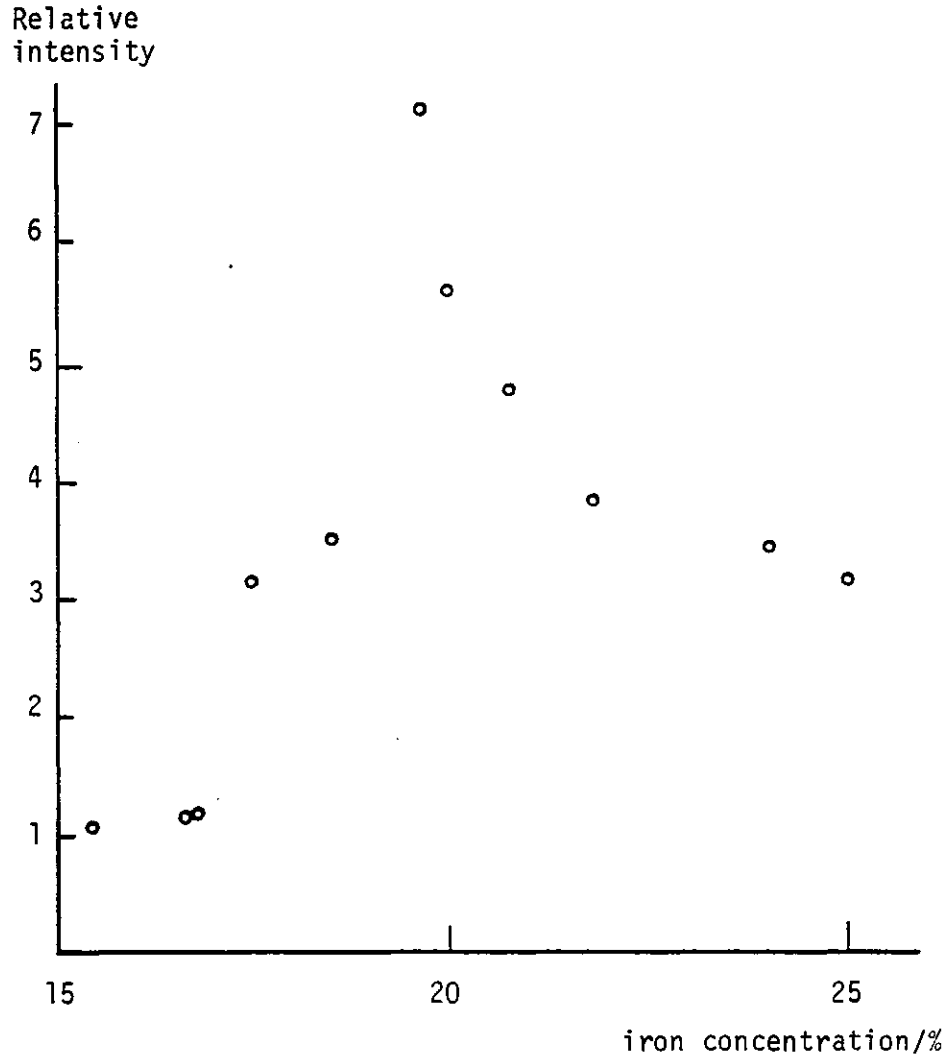

FIGURE 5.4 Amplitude of sub-critical scattering at 4.2 K for $\kappa = 0.019\ \mathring{A}^{-1}$, as a function of iron concentration. From Burke (1980).

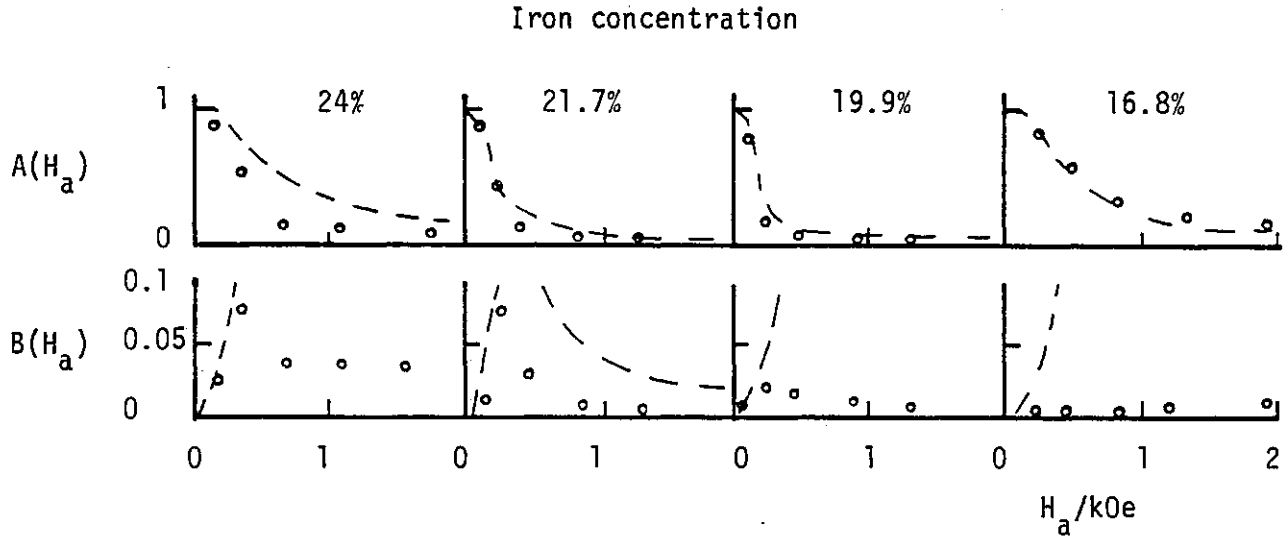

FIGURE 5.5 Extrapolated forward intensity of isotropic and anisotropic parts of small angle scattering as a function of applied field, H_a, $A(H_a)$ and $B(H_a)$ respectively. The dots are experimental points and the dashed lines represent the best fit of the magnetic cluster model. From Burke (1980).

the magnon mode appeared at the Curie temperature, and moved to higher energies, but at lower temperatures, the mode "collapsed" into a quasi-elastic peak. It is not clear whether the higher-q spin waves are affected, but it indicates that the magnetic state is not one of simple ferromagnetism at low temperature.

In the light of these neutron scattering experiments, the bulk magnetic properties are, to some extent, understandable. The low field susceptibility both of the ferromagnetic alloys and of the alloys with just a little less iron show a maximum which is not very sharp, as a function of temperature (Burke 1980, Larica 1981). The low temperature magnetisation as a function of field shows a gradual evolution with concentration from a typical, saturating, ferromagnetic curve, to a curve which saturates only in 120 kOe or so, and still has a large high field slope (Loegel 1975, Babic, Kajzar and Parette 1981). There is a little remanence in the ferromagnetic alloys, while more develops at temperatures lower than 4 K in the non-ferromagnetic, and even the antiferromagnetic alloys (Ishikawa, Tournier and Filippi 1965). This is consistent with the small anisotropy measured by David and Heath (1971) in a single crystal E.S.R. experiment in the ferromagnetic alloys, and the small anisotropy gap observed by Fincher et al. The magnetisation at low temperatures shows time dependent effects (Shull and Beck 1974).

Arrott plots of the magnetisation isotherms are curved when the magnetisation is large, and also in the critical region near the Curie temperature (figure 5.6) (Loegel 1975, Aldred and Kouvel 1977), and this has been said to be evidence for magnetic inhomogeneity (see chapter 1 for the reasoning behind this). However, comparison with similar data for many other ferromagnets, for example pure nickel (figure 5.7, taken from Kouvel and Comley 1968) indicates that this is not necessarily a valid conclusion.

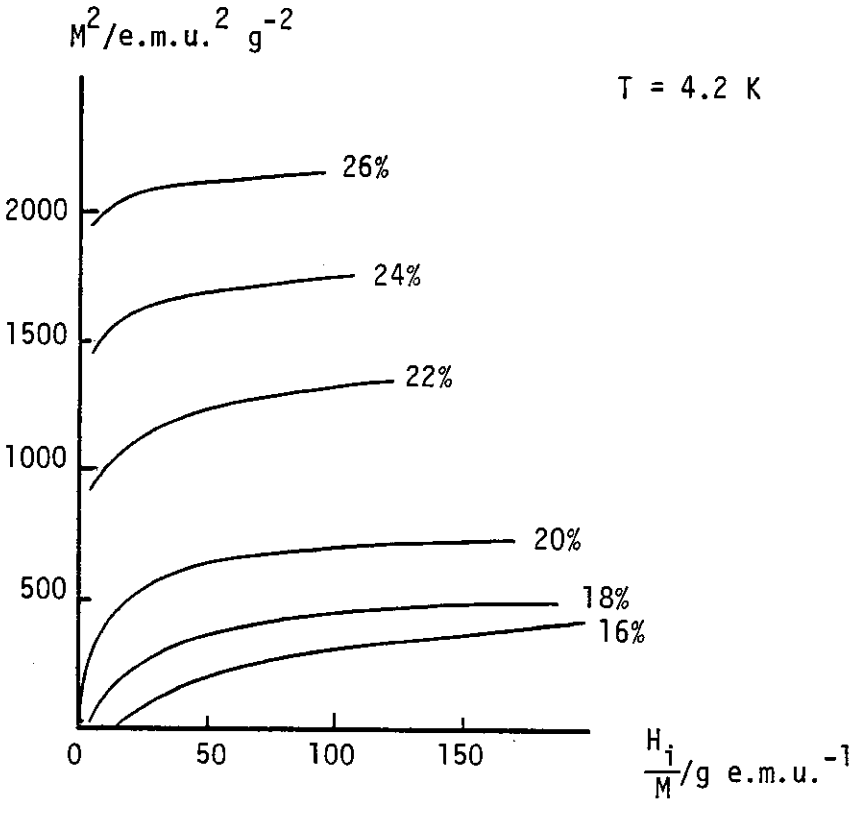

FIGURE 5.6 (a) Arrott plots for chromium-iron alloys at 4.2 K.
From Loegel (1975).

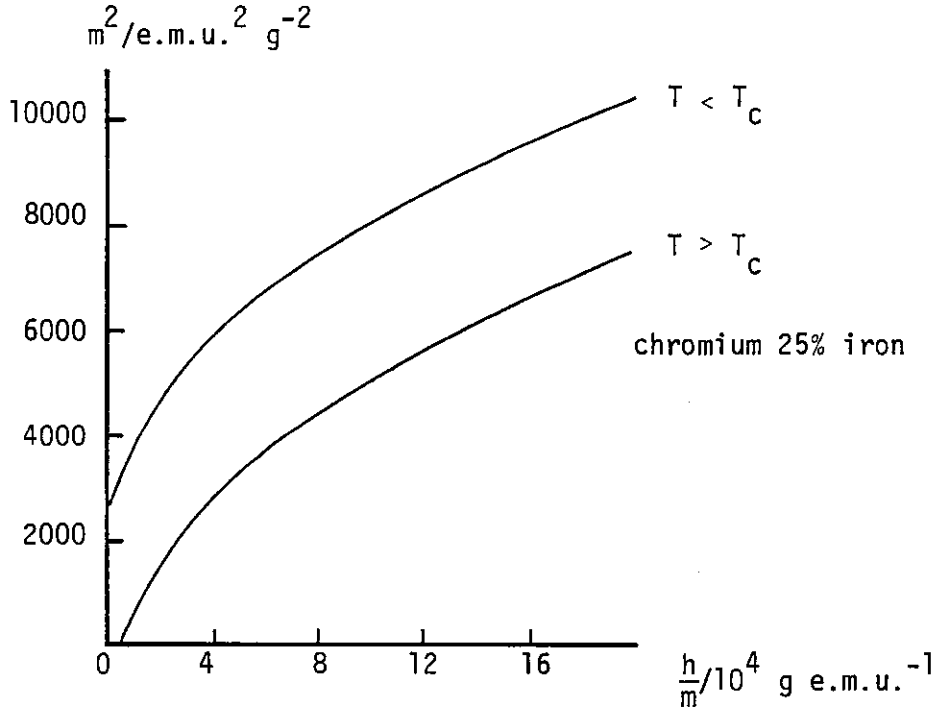

FIGURE 5.6 (b) Normalised Arrott plots for chromium 25% iron in the vicinity of the Curie temperature, T_c.
From Aldred and Kouvel (1977).

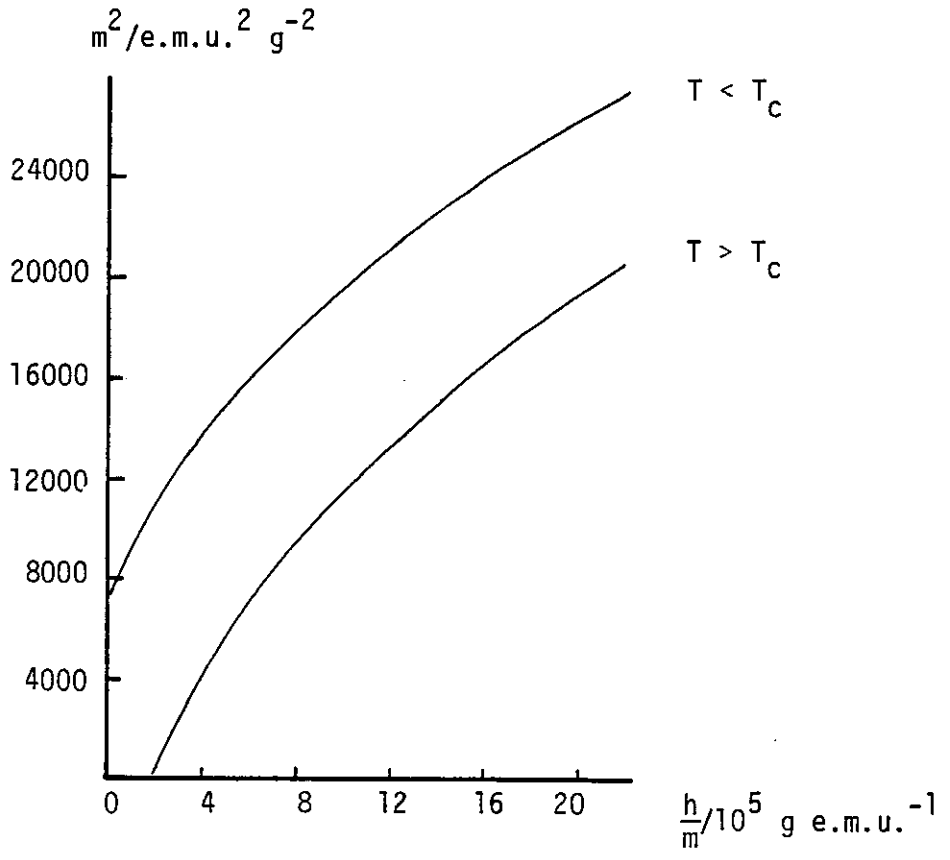

FIGURE 5.7 Normalised Arrott plots for pure nickel near T_c, the Curie temperature.

$$m = \frac{M}{|1 - T/T_c|^{\beta}}$$

$$h = \frac{H_i}{|1 - T/T_c|^{\beta + \gamma}}$$

Note the curvature of the isotherms.

From Kouvel and Comly (1968).

Aldred, Rainford, Kouvel and Hicks (1976), in a diffuse neutron scattering measurement found significant chemical short range order in alloys from iron-rich ones through to chromium 27% iron, but the range of the magnetic disturbance decreased as the chromium concentration increased, becoming predominantly a nearest neighbour disturbance in the chromium-rich alloys. The ordered moment on the chromium sites fell from -1.16 μ_B at the iron-rich end, in chromium 98% iron, to zero in the region of 30% iron.

A parallel study by Aldred (1976) of the magnetisation as a function of field and temperature yielded the average ordered moment at low temperatures as a function of composition, and the temperature dependence at each composition was analysed in terms of spin wave theory, and a value of spin wave stiffness extracted. This study covered alloys from pure iron to a composition of chromium 30% iron, and at the low iron end, severe discrepancies began to emerge from the theory, appearing as a large and negative coefficient D_1, where

$$D(T) = D_0 - D_1 T^2$$

and D_1 represents the renormalisation of the stiffness D, and is usually positive.

An electron spin resonance (E.S.R.) experiment in a sample of chromium 22.9% iron, reported by Larica (1981) showed a marked decrease in the resonance field at a temperature well below T_C. It is not clear how this ties in with the other strange properties of these alloys.

Analogy with Gold-Iron Alloys

A comparison of the magnetic properties of f.c.c. gold-iron alloys with b.c.c. chromium-iron alloys was given briefly in chapter 3 above, concerning the spin glass phase. The ferromagnetic phases are thought to be similar. In particular, it may be useful here to mention some

experiments performed on gold-iron alloys in the ferromagnetic composition range (>15% iron) which have a bearing on the question of the nature of the low temperature state of the ferromagnetic alloys.

Murani (1980), in a neutron diffraction measurement from a 19% alloy, measured the integrated intensity of the Bragg peak plus the associated small angle scattering using very relaxed collimation, and found an odd temperature dependence, with two low temperature step-like increases in intensity. Murani suggested that this was similar to experiments in other, non-metallic systems, where the intensity of the resolution-limited Bragg peak decreased, but where the integrated intensity of the associated scattering might be found to increase. Note that the loss of resolution-limited intensity implies a loss of the Bragg peak as such, and hence of the long range order. It is not entirely certain that the step-like increases in intensity were not artefacts, the experiment having been performed on the same instrument as that used for the experiment described in chapter 3 above, where effects due to the imperfectly-random polycrystalline nature of the sample were extremely large.

Hamzic and Campbell (1981), found low temperature negative magnetoresistance in samples up to gold 28% iron, and claimed that this is indicative of a spin system which, while retaining, and increasing, its degree of ferromagnetic order as the temperature is reduced, also introduces some random canting away from the axis of macroscopic magnetisation at low temperatures. The weakness of resistance as a probe of magnetic order was mentioned in chapter 1, namely, that the range of spin correlations investigated is only of the order of the electronic mean free path. This data can not therefore be used to support or oppose hypotheses about the long range correlations.

Sarkissian (1981) has observed a marked low temperature reduction in the a.c. magnetic susceptibility in ferromagnetic gold-iron alloys

from 15% to 24% iron. A similar effect in chromium 22.9% iron was reported by Larica (1981).

Brief Theoretical Review

The chromium-iron alloys near to 19% iron, the composition for the onset of ferromagnetism, are in some ways extremely complicated systems. Models of magnetic insulators are simpler to deal with than those of metals, and especially so when the magnetic electrons are conduction band electrons, as in this case. Random alloys do not have the same translational invariance properties as crystals of elements or ordered compounds, and these alloys are not even quite random, in that there is some chemical clustering of the magnetic atoms.

These alloys do have some encouraging features. The chromium atoms behave as non-magnetic sites, certainly for iron concentrations between 16% and 30%, and the iron site moment is thought to be roughly constant from 12% to 30% of iron ($\mu_{Fe} = 1.8\ \mu_B$, Aldred et al. 1976 and Babic et al. 1981).

There are several points to start from in dealing with a system like this. The first is pure b.c.c. iron. The ground state at least is well understood in terms of the theory of itinerant ferromagnetism in the Hartree-Fock approximation, although the thermal properties can not yet be described in detail within the framework of this theory. Various attempts to refine the itinerant model by recognising the importance of fluctuations are currently being pursued (e.g. Hubbard 1981, Hasegawa 1981), and the influence of many-body effects (Kim 1981) and of collective magnetic excitations (spin waves) should also be included in a complete description. The importance of the spin waves in determining the thermal properties, at least up to room temperature, has been demonstrated convincingly by Argyle, Charap and Pugh (1963) and Aldred and Froehle (1972).

Another starting point is the geometrical percolation picture of nearest-neighbour-interacting local magnetic moments, assumed to interact in a Heisenberg-like way. That is, the interaction energy between nearest-neighbour iron moments is simply

$$E_m = - J\underline{S}_i \cdot \underline{S}_j .$$

Such a theory, in the case of a system close to percolation (the establishing of an infinite cluster of nearest neighbour magnetic atoms) leads naturally to an intuitive idea of magnetic clusters of finite size. This approach has been used to describe the critical phenomena of chromium-iron alloys, in different ways by Aldred and Kouvel (1977) and by Burke (1980), with some degree of success, despite the inherent improbability of the model's applicability in this case, where the interactions between effective local moments are thought to be long ranged, and certainly not just with nearest neighbours.

The third idea which may be useful in this context is the randomness inherent in the system, which is pursued vigorously in various theories of spin glasses. A recent theory of the infinite-interaction-range local Heisenberg moment model, interacting with random interactions with a Gaussian distribution (Gabay and Toulouse 1981) predicts a ferromagnetic phase with an increase in disorder at temperatures below the Curie temperature, while retaining long range ferromagnetic order. These authors suggest an application of this theory to metallic alloy systems.

There is a long way to go before a complete theory is worked out for these alloy systems.

Purpose and Scope of the Present Investigation

In the light of the results noted above for the odd behaviour of the spin wave neutron scattering in chromium 26% iron (Fincher et al.

1980), and in view of the apparent success of spin wave theory in accounting for the low temperature ($T<T_c/2$) magnetisation in more concentrated alloys (Aldred 1976), it was decided to investigate the field and temperature dependence of the magnetisation of several alloys close to the critical composition.

Disagreement between the magnetisation change as a function of temperature and that predicted by simple spin wave theory arises in many materials, and probably for a variety of reasons. In itinerant systems, the single particle magnetic excitations (Stoner excitations) may contribute to the magnetisation (Stoner 1938). If the ground state of the ferromagnet involves a non-collinear arrangement of the moments, this may lead to a more complicated excitation spectrum, and it is not clear then that the simple spin wave theory holds because of a possible contribution to the magnetisation from diffusive excitation modes (Rivier and Continentino 1980).

These experiments were performed in order to establish whether the form of the magnetisation was correctly predicted by simple spin wave theory, and if so whether the spin wave stiffness agreed with the values determined from the neutron scattering results (a discrepancy was found, for example, in the amorphous ferromagnet $(Fe_{93}Mo_{07})_{80}B_{10}P_{10}$ by Axe, Shirane, Mizoguchi and Yamauchi (1977), although the form of the magnetisation dependence on temperature is in agreement with simple spin wave theory). The neutron measurements of Fincher et al. found very small, and strongly temperature dependent values of the spin wave stiffness at low temperatures, so the results could be quite unusual.

Sample Preparation and Analysis

Four small samples of chromium-iron alloys of nominal compositions 21, 25, 29 and 34% iron were prepared by argon arc melting Johnson Matthey Specpure 99.999% pure elements. From about 100 mg total

starting mass, a small piece, typically 25 mg, was broken off and re-melted to form a roughly spherical sample.

Each sample was then sealed under vacuum in a quartz capsule and annealed for 42 hours at 1050^{o}C to ensure macroscopic homogeneity. To preserve the high temperature disordered state, the samples were quenched into water at room temperature, breaking the capsules to ensure rapid cooling.

After the measurements, the samples were ground to expose a large surface, which was then examined by electron microprobe analysis. The compositions were found to be close to the nominal, except for the 21% sample (see table 5.1). The homogeneity on the scale of μm was found to be good, although there were some inclusions of oxide, probably Cr_2O_3 (Monk 1981 (b)). The extraordinary discrepancy between nominal and actual compositions for the 21% nominal sample is corroborated by the magnetisation results, which appear to be intermediate between those of Ishikawa et al. (1965) for 9% and 15% samples. This discrepancy may be attributed either to loss of some of the starting material before melting, or to gross inhomogeneity in the ingot before removing the small piece to make the magnetisation sample.

Experiments

The magnetisation isotherms were measured at various temperatures below half the Curie temperature using the high field vibrating sample magnetometer system described in appendix B. The field was swept up to its maximum value of 72 kOe with a full sweep time of five minutes. This was found to be a convenient rate which allowed the sample to remain in thermal equilibrium at the controlled temperature of the sample holder. A change in magnetic field ΔH changes the sample temperature by ΔT, where

TABLE 5.1

RESULTS OF ELECTRON MICROPROBE ANALYSIS (MONK 1981 (b))

NOMINAL IRON COMPOSITION/%	COMPOSITION AS MEASURED BY ELECTRON MICROPROBE/%
21.0	13.3
25.0	24.4
29.0	27.8
34.0	31.8

$$\Delta T = - \frac{T}{C_H}\left(\frac{\partial M(T)}{\partial T}\right)_H \Delta H$$

where C_H is the specific heat at constant field H (Kouvel and Brooks 1954, as quoted by Keffer 1966). Using a value of $C_H/T \simeq 10^{-2}$ cal. mol^{-1} K^{-2} interpolated from Cheng et al. (1960) and Schröder (1962) at T = 70 K, and M(T) for a 30% iron alloy of Aldred (1976),

$$\frac{\Delta T}{\Delta H} \simeq 0.026 \text{ K(kOe)}^{-1}.$$

A field of 70 kOe could cause a change in T of nearly 2 K if conditions were adiabatic.

The magnetic moment and applied field signals were recorded simultaneously throughout the upward sweep by means of the X-Y plotter, and the data were analysed by measuring values of the magnetisation on each isotherm.

Data Analysis

According to simple ferromagnetic spin wave theory,

$$M(H,T) = M(0,0) - g\mu_B \cdot \frac{1}{(2\pi)^3}\int \frac{dq}{\exp\{\beta\varepsilon(q)\} - 1}$$

where the integral is over the complete Brillouin zone, g is the Landé splitting factor, which is 2.07 (David and Heath 1971), μ_B is the Bohr magneton, β is the reciprocal temperature ($\beta = 1/k_BT$, where k_B is Boltzmann's constant) and $\varepsilon(q)$ is the energy of the spin waves as a function of the wave vector q.

The energy of the spin waves is assumed to be of the form (Herring and Kittel 1951)

$$\frac{\varepsilon^2(q)}{\hbar^2} = D^2q^4 + (2DH + 4\pi M_S D\sin^2\theta)q^2\mu_B + H^2\mu_B{}^2 + 4\pi HM_S\sin^2\theta\mu_B{}^2$$

where D is the spin wave stiffness,

H is the sum of the internal field (applied field, H_a, less the

demagnetising field, NM) and the anisotropy field, H_{an}

$$H = H_a - NM + H_{an},$$

M_S is the saturation magnetisation = M(0,0),

θ is the angle between the spin wave propagation vector $\underline{q}$ and the applied field, and

$\hbar$ is Planck's constant.

This expression for the energy is exact in a continuum model. In an atomic solid, it is a good approximation when q is very much smaller than the (average) zone boundary, q_{ZB}, but at higher values of q, contributions to the energy proportional to even powers of q greater than 2 become significant.

The expression for M(H,T) omits some terms which are often included for comparison with experimental data,

$$M(H,T) = M(0,0) - \Delta M(\text{spin wave}) - \frac{a}{H} - \frac{b}{H^2}$$

(Aldred 1976). The term in 1/H accounts for the influence of crystalline defects in the sample, and the $1/H^2$ term is included to deal with the effect of anisotropy in a polycrystalline sample. For applied fields greater than 10 kOe, both of these terms are expected to be negligible in these samples.

The anisotropy field, H_{an}, is neglected. It is thought to be very small in comparison with M_S (Aldred 1976).

The analysis is restricted to data taken at high fields, and this allows further approximations, but first, the average of the angular dependence is taken. When

$$T >> 4\pi M_S \frac{\mu_B}{k_B},$$

we may replace $\sin^2\theta$ in the expression for the energy by a population weighted average. This condition on the temperature is equivalent to

assuming an isotropic population of propagation directions, and the weighted average is

$$\langle \sin^2\theta \rangle = \frac{\int_0^{\pi} \sin^2\theta . \sin\theta d\theta}{\int_0^{\pi} \sin\theta d\theta} = \frac{2}{3}.$$

An approximate form is assumed for $\varepsilon(q)$,

$$\varepsilon(q) = D'q^2 + \varepsilon_g$$

which agrees with the first expression for $\varepsilon(q)$, when

$$D' = D$$

$$\varepsilon_g = g\mu_B(H + \frac{4\pi M_S}{3}),$$

to within 1%, when $H > 5M_S$.

Using this expression,

$$M(H,T) = M(0,0) - g\mu_B . \frac{1}{2\pi^2} \int_{q=0}^{q_{Z.B.}} \frac{q^2 dq}{\exp\{\beta(Dq^2 + \varepsilon_g)\} - 1},$$

and this may be reduced to an integral over the reduced energy, x, where

$$x = \beta D q^2,$$

$$M(H,T) = M(0,0) - \frac{g\mu_B}{2\pi^2} . \frac{1}{(\beta D)^{3/2}} \int_0^{\beta D q^2_{Z.B.}} \frac{x^{\frac{1}{2}} dx}{\exp\{x + \beta\varepsilon_g\} - 1},$$

which gives the well-known dependence of M on $T^{3/2}$ if the gap function integral is constant.

The upper limit of the integral is usually replaced by infinity, corresponding to the extremely small probability of thermal excitation of spin waves at the zone boundary. In this case, when D may become quite small, this approximation was not made, although it turned out to be an unnecessary measure, as the integral was always found to be insensitive to the upper limit. Note that this expression does not account for the downwards deviations from the quadratic dispersion encountered near the zone boundary, which may contribute to the

magnetisation even when this integral is insensitive to the upper limit.

To evaluate the integral for each data point, an approximate value of D was assumed for the upper limit, and the measured values of N, the demagnetising factor and M, the magnetisation were used. M_S, the saturation magnetisation, was taken as $M(H_a = 74$ kOe, $T = 4.2$ K). The integral was evaluated numerically by Simpson's rule.

The data were then plotted in the form of magnetisation against $T^{3/2}$ multiplied by the appropriate integral.

Results

The results for the ferromagnetic alloys are presented in figures 5.8 to 5.10. For each concentration, the data at 35 kOe and 70 kOe are shown as magnetisation against $T^{3/2}$ multiplied by the integral to account for the gap in the spin wave spectrum. The data for the 31.8% alloy represent a reasonable straight line up to 60 K or so, while the 27.8% alloy data show marked curvature at temperatures below 20 K, and the 24.4% alloy data are curved over the entire temperature range measured.

The data for the 13.3% alloy are not monotonic, showing an anomaly corresponding to the low field susceptibility maximum at about 10 K, and, as this alloy is a long way from ferromagnetism, showing no convincing saturation at all, the analysis in terms of spin wave theory was not attempted. The data for this alloy are shown simply as magnetisation against temperature in figure 5.11.

An alternative plot of the data for the 24.4% alloy is given in figure 5.12. The magnetisation is plotted against $T^{3/2}$, without the complication of the gap function integral. This is really rather a good straight line up to about 40 K.

These data are in agreement with the trend of the data of Aldred

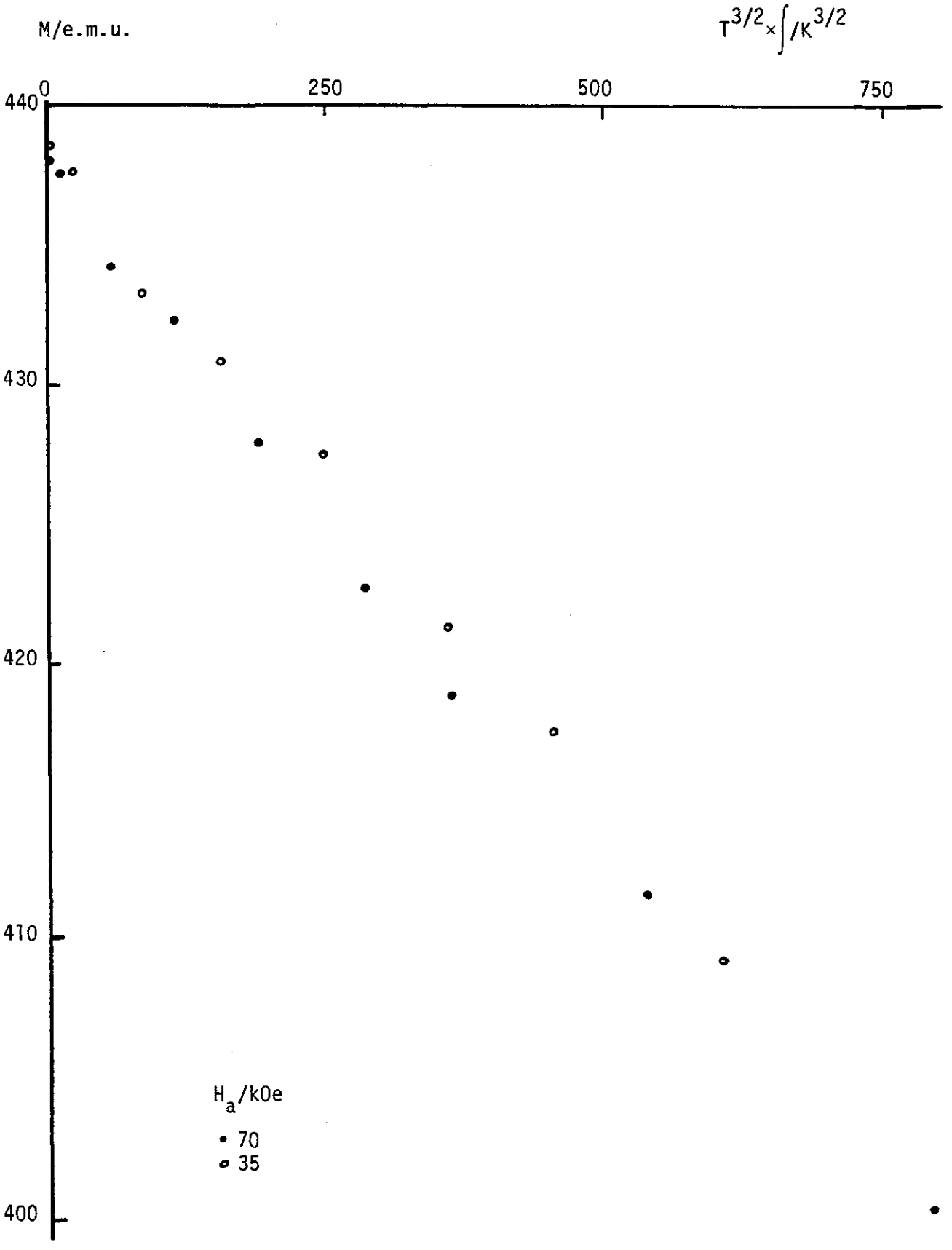

FIGURE 5.8 Magnetisation, M, of chromium 31.8% iron plotted against $T^{3/2}\times\int$, where $\int$ represents the gap integral correction. A straight line gives a temperature independent spin wave stiffness. Values of D = 37.5, 41.1 meV $\AA^2$ are deduced from the 70 kOe, 35 kOe data respectively.

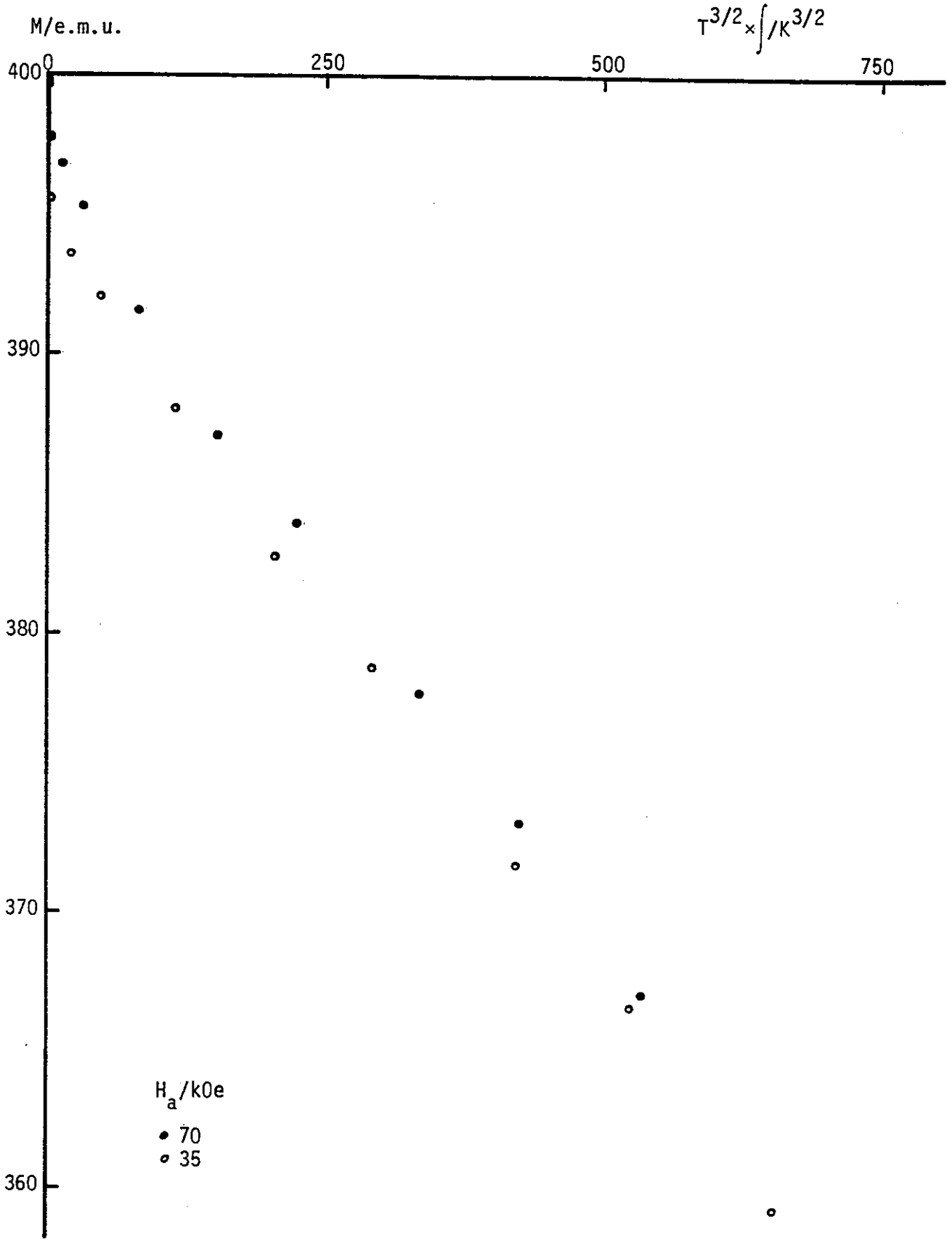

FIGURE 5.9 Magnetisation, M, of chromium 27.8% iron against $T^{3/2}\times\int$.

Note the curvature at low temperatures.

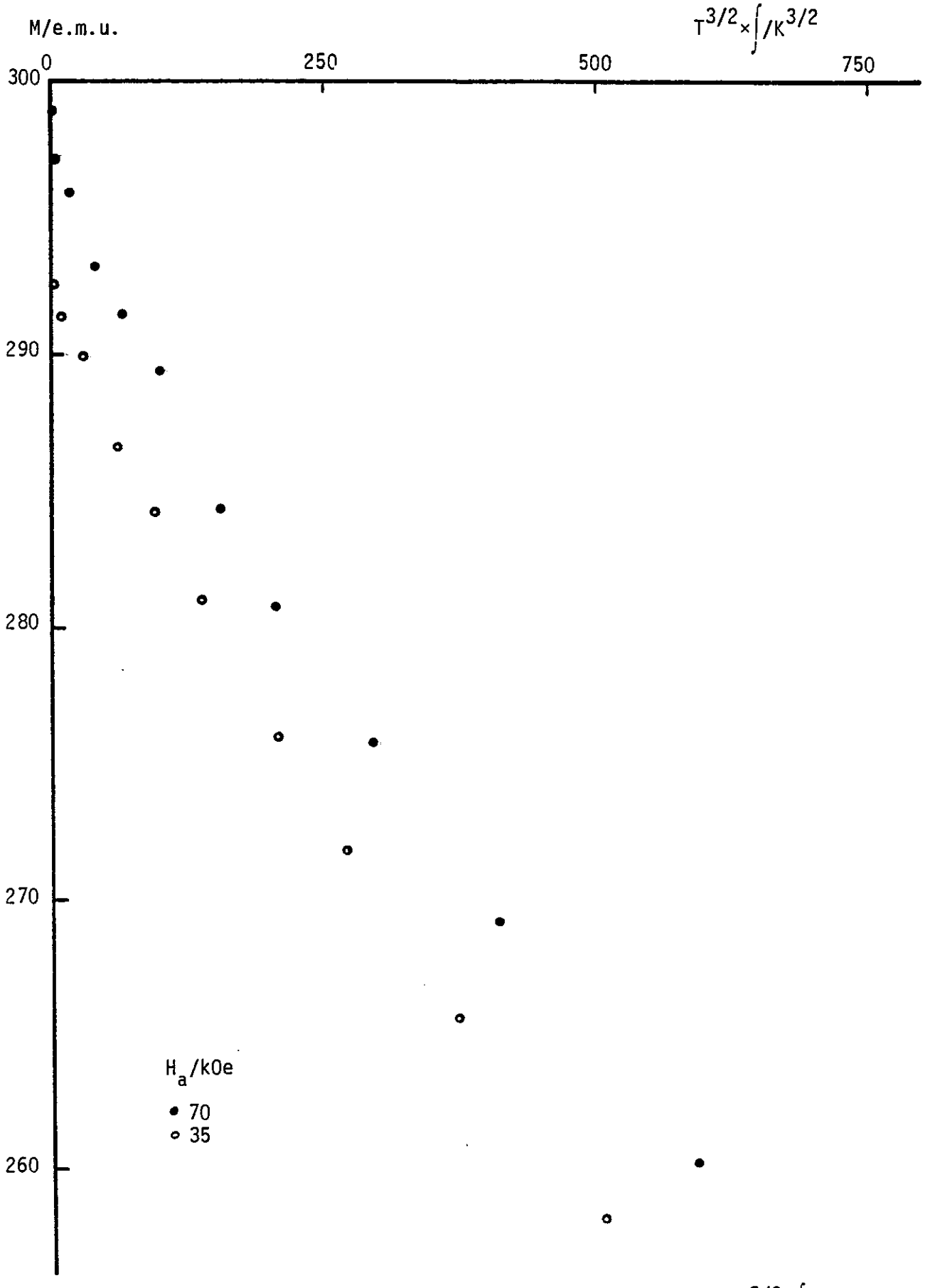

FIGURE 5.10 Magnetisation, M, of chromium 24.4% iron against $T^{3/2}\times\int$. There is significant curvature over the whole range illustrated.

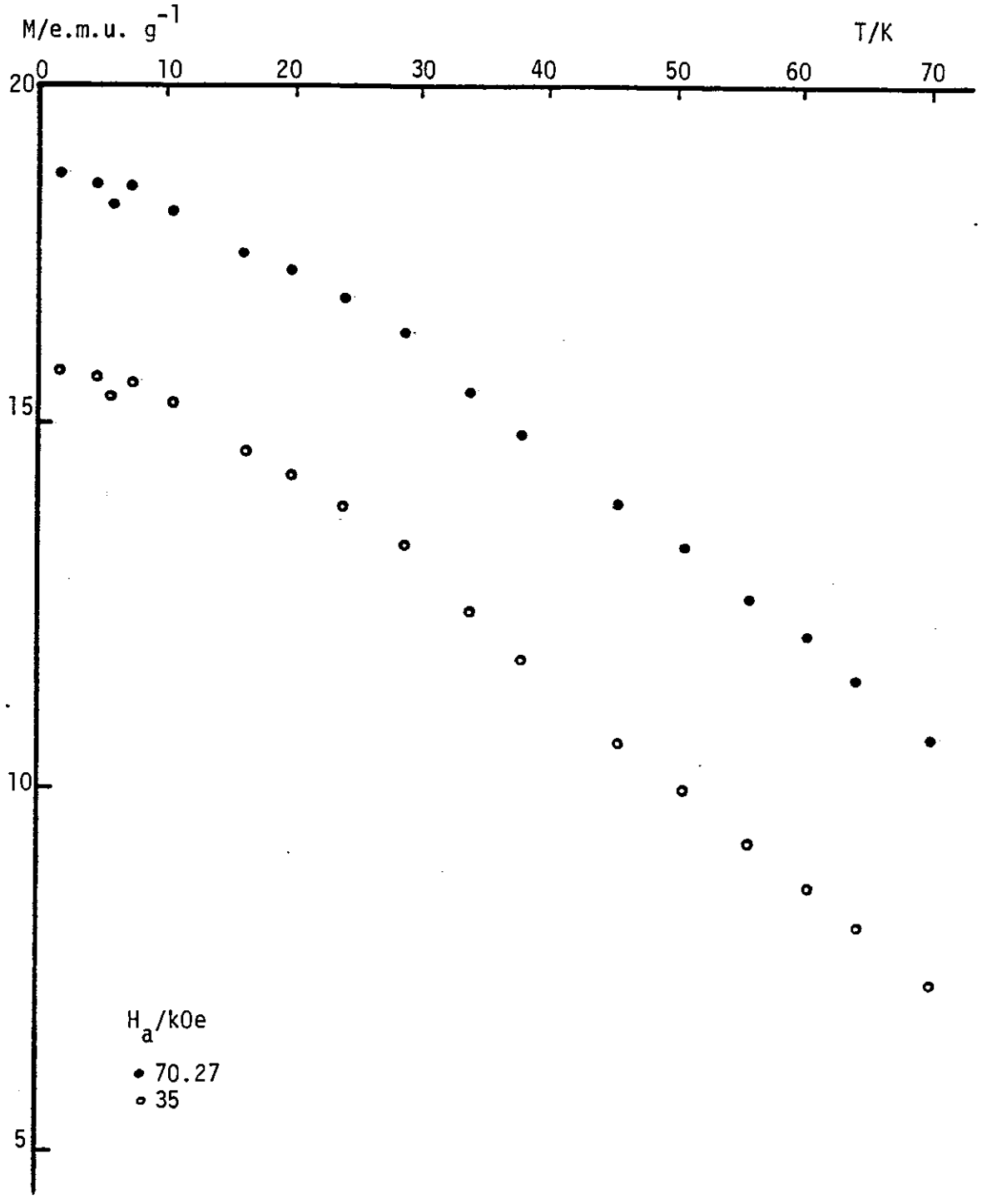

FIGURE 5.11 Magnetisation, M, of chromium 13.3% iron as a function of temperature, T.

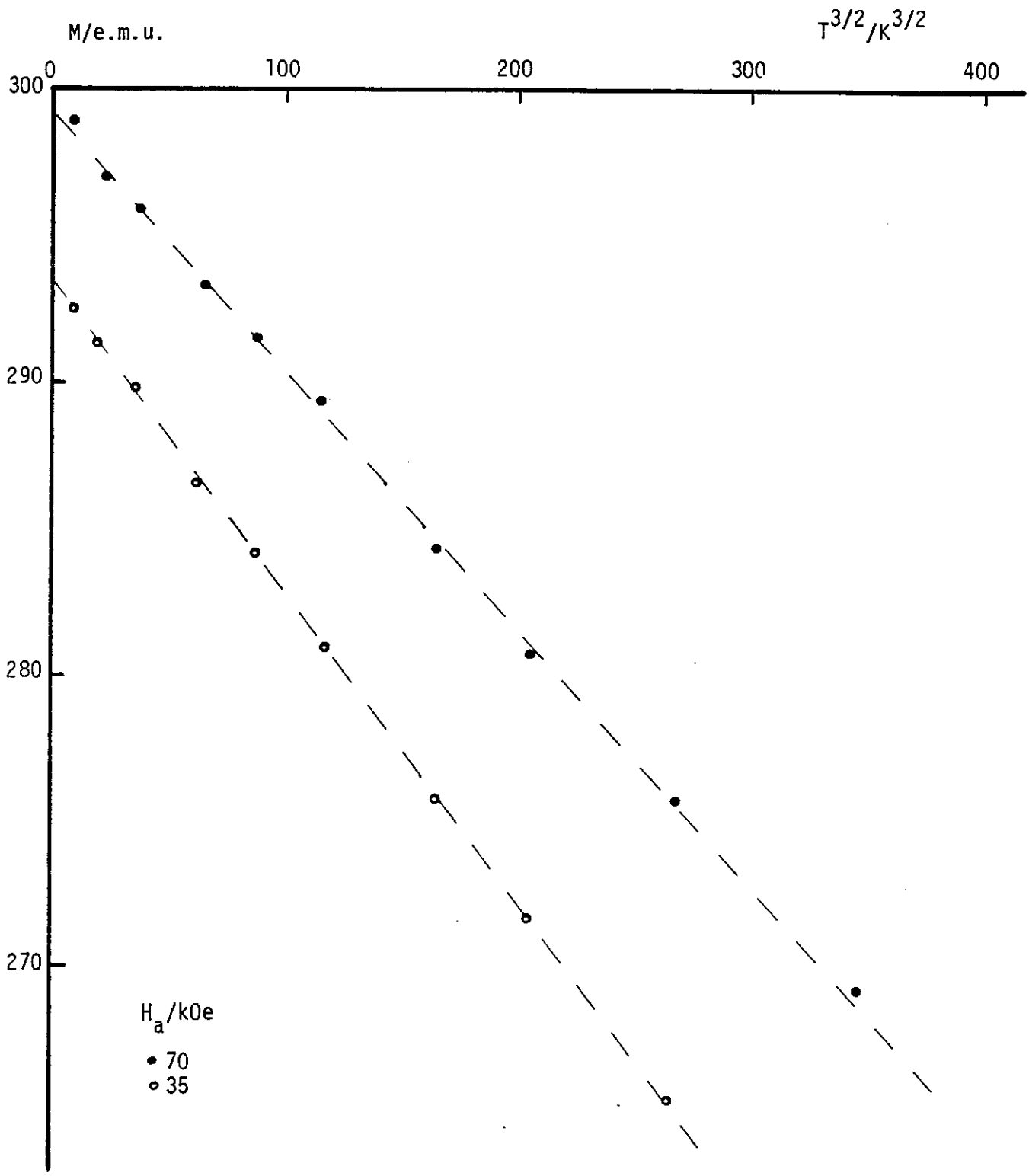

FIGURE 5.12 Magnetisation, M, of chromium 24.4% iron as a function of $T^{3/2}$. The dashed lines are guides to the eye.

c.f. figure 5.10.

(1976), who calculated the temperature dependent part of the stiffness in his fit, represented by the coefficient D_1, where $D(T) = D_0 - D_1 T^2$. He found that D_1 was small and positive in iron-rich alloys, and fell to zero for 50% iron, and then suddenly became negative as the concentration approached the critical composition.

Conclusions

If the neutron scattering experiment of Fincher et al. (1980) had not returned the peculiar result of a spin wave stiffness which became smaller at lower temperatures, the conclusion from this magnetisation experiment would be that the spin wave theory was breaking down as a description of the magnetisation at low temperatures. All kinds of reasons might be quoted as possible causes, (see the discussion above under "Purpose and Scope of the Present Investigation").

However, in the light of the neutron data, it is not unreasonable to interpret the magnetisation data as reflecting that same temperature dependence of the spin wave stiffness. This approach is followed in drawing figures 5.13 and 5.14, where the gradients obtained from adjacent points in figures 5.9 and 5.10 are converted to stiffnesses, as a function of the mean temperature. For comparison, the neutron data of Shapiro et al. (1981) is shown in the same type of plot in figure 5.15. The scatter of the data is amplified by this procedure, and while the initial measurements of magnetisation had an uncertainty of about 0.05%, this becomes 25%, in the worst case, in the spin wave stiffness value. With this in mind, the agreement on the form of D(T) between the bulk measurements and the neutron data is quite striking.

The magnitude of the spin wave stiffness, however, appears to be different, in that the value deduced from the magnetisation is about 60% larger than the neutron value. Discrepancies of a similar magnitude occur frequently in comparisons of the stiffness derived from

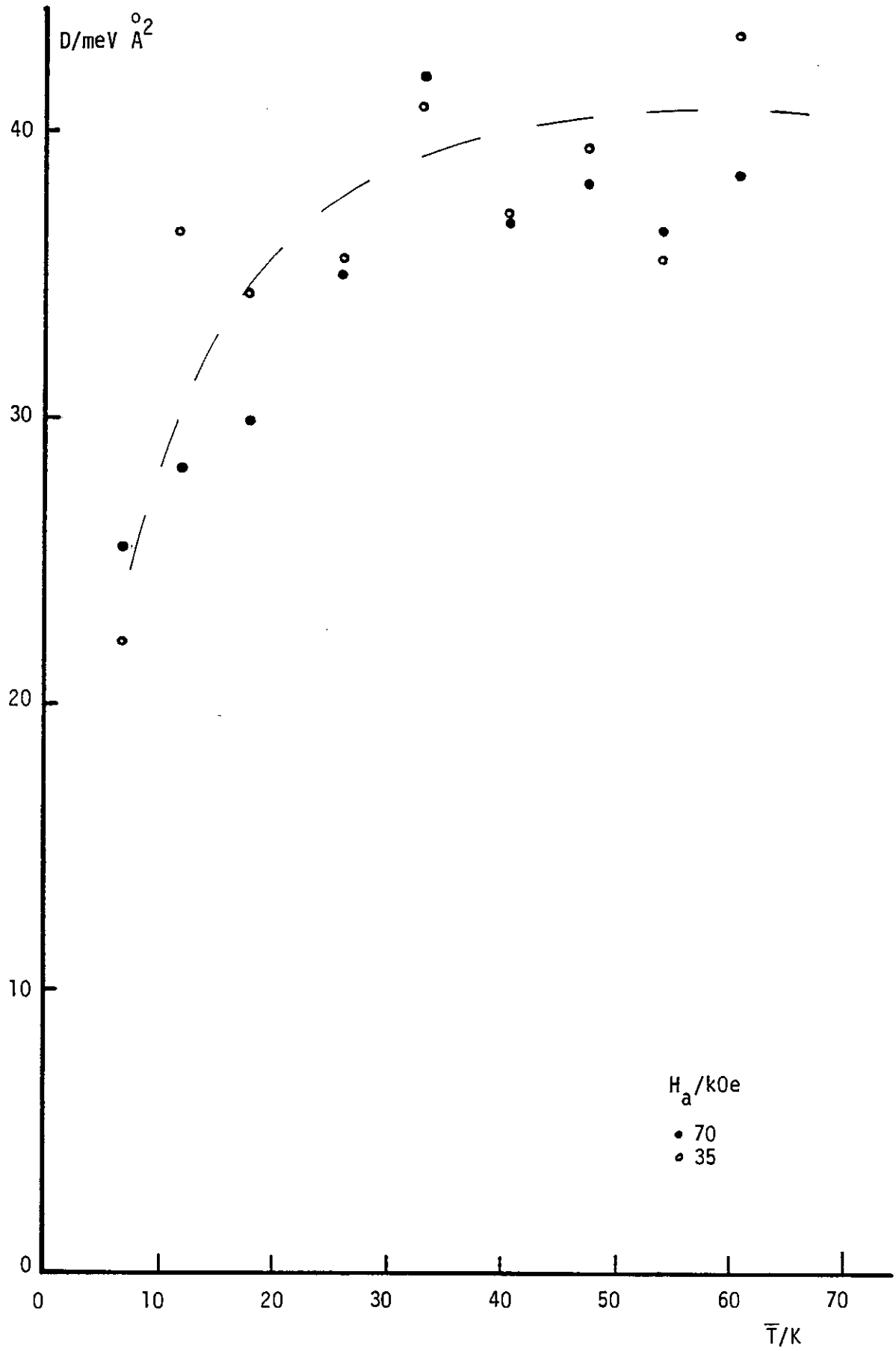

FIGURE 5.13 Spin wave stiffness, D, of chromium 27.8% iron as a function of mean temperature, $\bar{T}$. The D values are derived from adjacent points in figure 5.9.

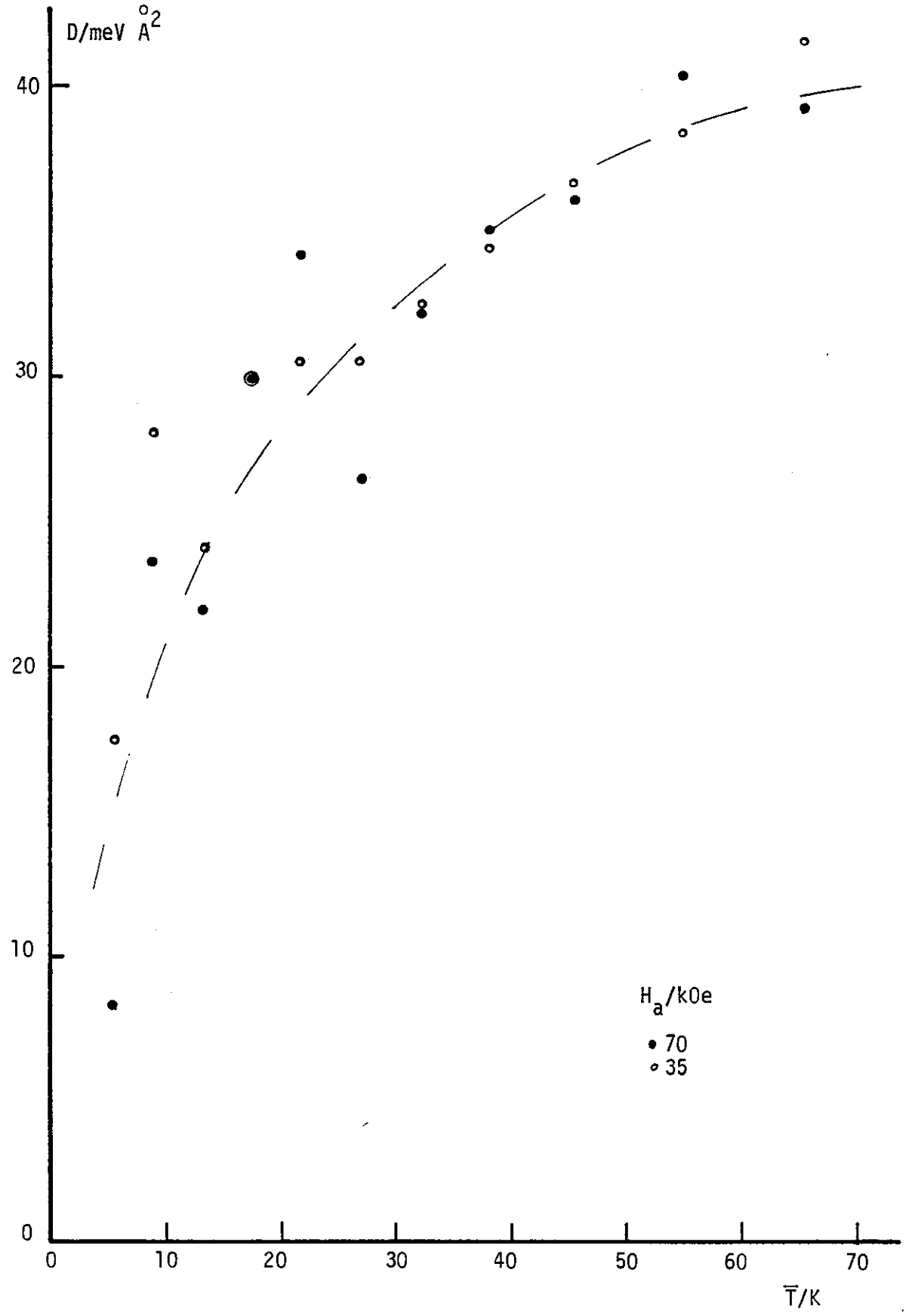

FIGURE 5.14 Spin wave stiffness, D, of chromium 24.4% iron as a function of mean temperature, $\overline{T}$. The D values are derived from adjacent points in figure 5.10.

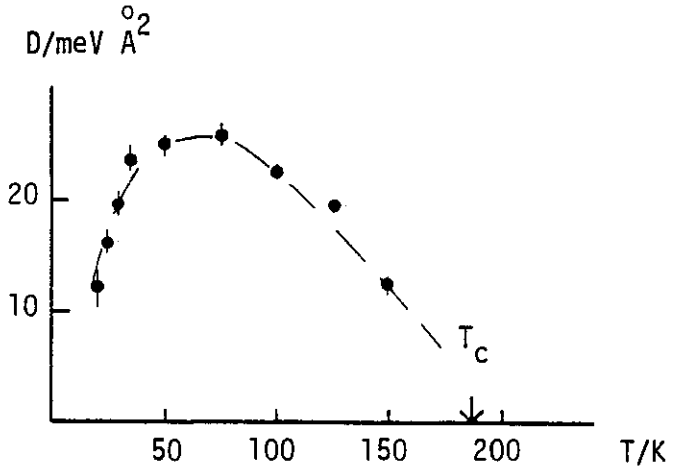

FIGURE 5.15 Temperature dependence of the spin wave stiffness, as measured by inelastic neutron scattering, in chromium 26% iron.

From Shapiro et al. (1981).

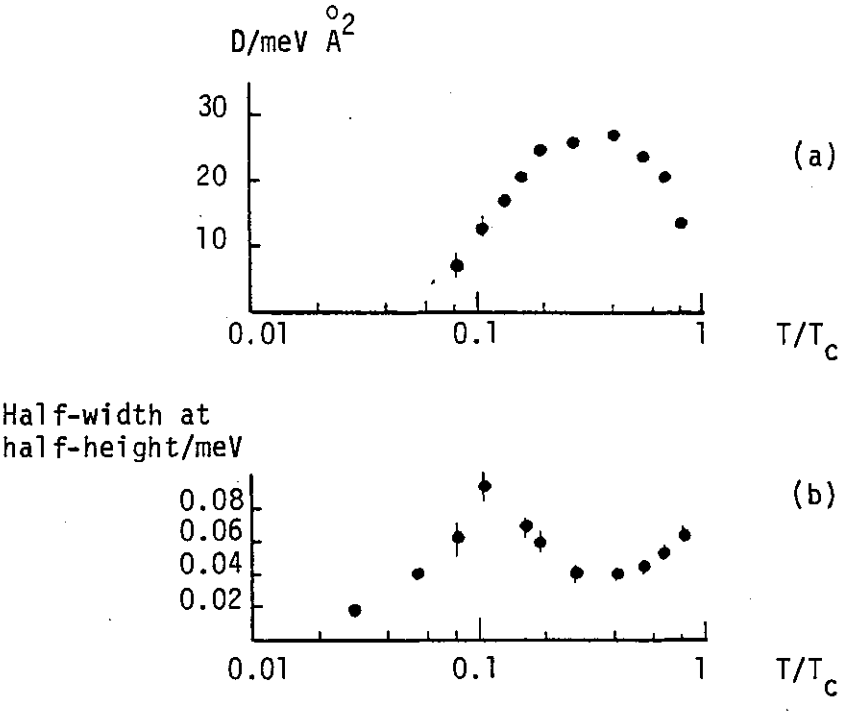

FIGURE 5.16 (a) As figure 5.15, but plotted against the logarithm of the reduced temperature.

(b) The Lorentzian half-width of the inelastic scattering.

From Fincher et al. (1980).

the magnetisation with that from the neutron scattering in many materials, and the various causes discussed above may contribute to this. However, it is significant that the form of the stiffness as a function of temperature agrees so well between the two techniques. It suggests that the whole spin wave spectrum, or at least that part of it which is sampled by the magnetisation measurement, which is the thermally occupied part, does all collapse in the same way as the small-q spin waves do.

A spin wave mode represents a resonance in the correlation function at finite q and ω. If the spin wave stiffness is reduced to zero, or if the spin wave damping becomes larger than critical damping, then the mode will have a maximum in the correlation function at zero frequency. If it is possible to distinguish between these two possibilities, the former is to be preferred because the Lorentzian line width observed by Fincher et al. never becomes large enough to constitute more than critical damping. Having said that, the line width undergoes a sharp change when the stiffness, as measured, becomes zero, so it is evident that the damping and the stiffness are related (figure 5.16).

What is clear is that the quasi-elastic scattering which remains at low temperatures is intimately related to the spin waves at higher temperatures. It represents collective magnetic excitations which are of near zero energy. They may be propagating or diffusive. This ties in well with the observed small-angle scattering, which represents an average of the transformed correlation function up to some small energy. The observed dependence of the small-angle scattering on applied field at low temperatures is also in qualitative agreement if the scattering is assumed to be caused by these quasi-spin-waves. The anisotropy is then due to the fact that a transverse spin wave propagating in a direction parallel to the applied field experiences no

coupling with the field, while one perpendicular to the field is raised in energy, and therefore the scattering is reduced. Quantitative comparison with the data of Burke (1980) has not proved tractable, because of the complicated effective resolution function of the small-angle scattering instrument.

If there are magnetic excitations with zero energy, then even at zero temperature, the magnetic structure is destroyed by them. It is difficult to distinguish between that and the disappearance of finite energy, small-q excitations being caused by the destruction of the long range order. The two things go together and both may be "caused" by some other factor.

How do the bulk susceptibility and magnetisation fit in with the picture outlined above of the transformed correlation function? As discussed in chapter 1, simple bulk susceptibility measurements include both the true dynamic response, and also part of the magnetisation, if there is any. Thus the usual Hopkinson effect seen in chromium-iron and gold-iron ferromagnetic alloys at low temperatures may be modified by the change to a structure with no long range order, which reduces the true magnetisation to zero. Measurements of the spontaneous magnetisation as such are impossible for the reasons outlined in chapter 1. When a magnetic field is applied, the energies of the excitations which destroy the order are raised, so that the order may be re-established. (Application of a field generates long range order in any system with a finite susceptibility.) The time dependence of the observed magnetisation is consistent with a frequency dependence of the bulk susceptibility, as discussed in chapter 2. This represents a very small width in frequency of the transformed correlation function at zero q.

Having established this curious form for the correlation function at low temperatures, the question remains as to why the ferromagnetism

is apparently established at higher temperatures, and why it disappears at lower temperatures. Bearing in mind the caveats of chapter 1, we may rephrase this as a question of why the domain size is large at higher temperatures, and becomes smaller at lower temperatures, perhaps even so low that the size of domain is no greater than the wall thickness.

One possible approach to this question is to consider the magnetic structure as being composed of two, almost non-interacting systems. The nearest neighbour percolation cluster forms one part, while clusters isolated from this infinite cluster (the "finite clusters") form the other. This approach has been discussed by Coles et al. (1978), Sarkissian (1981), Burke et al. (1978) and many others.

Another approach is based on the rather esoteric predictions of the infinite ranged random interactions model mentioned above. Gabay and Toulouse (1981), however, find that the ferromagnetic phase, once established, should persist to zero temperature, albeit with some additional disorder. There are indications that this persistence of the long range correlations is not found in these alloys.

A more phenomenological explanation will be briefly outlined here. The recently reported observation (Rode, Finkelberg, Wurl and Lyalin 1981) of an invar effect (negative coefficient of thermal expansion) in chromium 30% iron at low temperatures is suggestive. If we consider any ferromagnet, then we may, in principle, treat the macroscopic state in terms of the theory of micromagnetics (Shtrikman and Treves 1963), although this has not been achieved in quantitative detail here. The size of the domain walls is usually determined by the balance between exchange effects and the anisotropy. However, if the anisotropy is small enough, then the competing forces are the exchange forces and the magnetic dipolar forces. This would result in a state which, while appearing ferromagnetic on a small scale, loses its long range order by

(static) slow rotation in space of the magnetisation axis.

For most ferromagnetic materials, the first anisotropy constant, K_1, bears a relationship to the spontaneous magnetisation, σ

$$K_1(T) = K_1(0)\left(\frac{\sigma(T)}{\sigma(0)}\right)^n.$$

In the theory of Zener (1954), at low temperatures, n = 10. In fact, in real materials, we find that $n \neq 10$. For example, in iron, n = 4 at low temperatures. One of the causes for the discrepancy is the effect of thermal expansion, (Brenner 1957)

$$\Delta K_1 = b_3\left(\frac{\Delta V}{V_o}\right)$$

where b_3 is the third magnetoelastic constant, and may be of either sign. If in this instance b_3 is negative (it is positive in pure iron, but dilution with chromium improves the fit to n = 10 (David and Heath 1971), so it may become small, and even negative), a negative coefficient of thermal expansion will give rise to an increase in K_1 with temperature at low temperatures.

The magnetostatic effect will be proportional to the square of the "local magnetisation" and may be expected to increase monotonically to low temperatures. So we may expect a cross-over at low temperatures from exchange-anisotropy competition to exchange-dipolar competition, with a consequent change from a well-defined domain structure to a continuously varying magnetisation direction. The anisotropy is known to be very small in alloys in this composition region (David and Heath 1971, Aldred 1976).

The question as to whether the invar effect invoked in the above explanation is the cause, or an effect of the magnetic phenomena which we are trying to explain, is uncertain.

The other two models suggested above are rejected for the following reasons. The infinite range model predicts the maintenance

of long-range order to low temperatures, which probably does not occur. The infinite and finite clusters model is implausible on the grounds that, when long range order is established (in the infinite cluster) the long ranged R.K.K.Y. interactions would be expected to couple the remaining, finite clusters to the order at higher temperatures than those observed for the peculiar effects described above.

CHAPTER 6

CONCLUSIONS

Spin Glasses

Much effort has been expended on spin glass properties, without much reward in terms of physical understanding of the spin glass state. The somewhat arid debate about whether or not there is a phase transition, or equivalently, whether or not there is a "truly elastic" response, can not be answered. It must be recognised that any experiment has an associated time scale, and spin glasses appear to show evidence of relaxation at times as long as the measuring time of any experiment performed so far. Thus there is no d.c. measurement. There is evidence, however, for a dramatic change in the (frequency) spectrum of dynamic response at and below the freezing temperature. The conclusion of the experiments described in chapter 2 is that the low frequency magnetic excitations in a spin glass are essentially different from those in a freezing superparamagnet. The aim, then, should be to chart the response function in this frequency range, either by measuring the isothermal susceptibility, and establishing the connection with the adiabatic response, or by direct measurement of the fluctuating part of the correlation function. These experiments are not easy, but are probably the best way to make progress in these interesting materials.

Dilute Chromium-Iron Alloys

The essential problems in the understanding of dilute alloys of iron in chromium still remain after more than two decades of investigation. The minor contribution of this work has been to undercut the two proposed avenues of interpretation. Neither the weak coupling nor the strong coupling pictures explain the curious behaviour

of these alloys. This indicates that some other explanation is needed, possibly along the lines of the domain theory outlined in chapter 4, although at this stage, that is purely speculation. Progress is rendered difficult by the small signals and the large backgrounds. In neutron scattering, this is the result of a great deal of unkind nuclear scattering, while in bulk experiments, the susceptibility contribution of pure chromium becomes significant in very dilute alloys.

Two angles of pursuit are suggested. One, an examination of the dynamics of the observed magnetic neutron scattering, is to be attempted on currently available samples as soon as possible. The other is to make a (single crystal) sample of isotopically enriched ^{52}Cr (the most abundant isotope) doped with a little iron. This will cut down the elastic nuclear scattering by up to two orders of magnitude, and enable the experiment of chapter 4 to be repeated to much greater precision without the complications of a large background and large multiple scattering. The cost of such a crystal would be large, however.

Ferromagnetic Chromium-Iron Alloys

Ferromagnetic chromium-iron alloys, in the composition range around and above 19% iron, are only one example of a class of similar systems which form the focus of much current debate and investigation. Here, much as in the spin glass problem, there is much vociferous support for the views maintaining and denying the persistence of ferromagnetism to zero temperature.

Progress, I believe, is to be made by measuring the response function, and again it is the low energy excitations which must be the focus. Average methods, like specific heat and magnetisation, which are relatively simple to do, and reveal correspondingly little information,

must be supported by detailed investigation using low frequency susceptibility measurements and low energy inelastic neutron scattering. All of these methods have been employed in these alloys, but there is still a long way to go with all of them. The magnetisation results presented in chapter 5 above will be followed up soon, I hope, with single crystal neutron triple-axis spectrometry, to examine in detail, over a wide range in reciprocal space and frequency, the low energy magnetic excitations.

In the light of the discussion in chapter 5, an investigation of the magneto-volume effects in this and similar alloy systems might prove fruitful. Thermal expansion, magneto-striction and pressure dependence of magnetisation experiments might all be informative.

Concluding Remarks

"No man is an island", and no more is a thesis such as this. The experiments described herein do not stand alone, but as part of a much greater investigation which began centuries ago and is being pursued worldwide today.

A line of investigation has been pursued, and the presentation above mirrors the chronological development of the work. Some of the avenues followed have been fruitless, while others have produced more definite results. They are all alike described in the hope that the former will reduce unprofitable investigations in the future, and that the latter may contribute to the understanding of transition metal alloy magnetism and stimulate further exploration.

APPENDIX A

ESTABLISHING A TEMPERATURE SCALE

Introduction

For the laboratory experiments on the chromium-iron alloys, it was necessary to establish a temperature scale both for reliability in the measurements as functions of temperature (measuring Curie constants, Curie-Weiss temperatures and the like) and also for comparison with other measurements (including the neutron experiments). A scale which would be reliable to better than ±0.5 K from 1.5 K to 300 K was therefore established.

For this purpose, a germanium resistance thermometer, the "Texas", was obtained, which had previously been calibrated against another germanium resistance thermometer, CR 1000 4368, which was calibrated by the manufacturer, Lake Shore Cryotronics Ltd. (Guy 1976). This calibration was from 4.2 K to 20 K, and fitted smoothly onto a calibration against ^{4}He vapour pressure at 4.2 K.

To complement this, a platinum resistance thermometer was used for the range up to 300 K, and ^{4}He vapour pressure down to 1.5 K.

The thermometers were mounted in the d.c. resistivity apparatus described by Barber (1974), which has a suitable potentiometer for use with the platinum thermometer, and a demountable ^{4}He cryostat.

Germanium Resistance Thermometer

The Texas germanium resistance thermometer was mounted on the copper block and the four leads were thermally anchored to the block, since the germanium itself is not in very good thermal contact with the thermometer case.

The resistance was measured by a standard four terminal technique, using the circuit as described by Barber (1974).

Platinum Resistance Thermometer

Some platinum wire (Johnson Matthey, grade 4) of 0.15 mm diameter was available, but measurement of the residual resistance ratio by a simple four terminal method revealed a value of 18.6. Attempts to anneal the wire by passing a current to heat it to red heat in air, and by heating in a resistance furnace (also in air) to 500^{o}C for 76 hours, changed the resistance ratio to 33 and 36 respectively.

High quality platinum resistance thermometers have residual resistance ratios of the order of 2000 or more, but even in these, deviations from Mattiessen's rule (DMR) can be significant on a milli-Kelvin scale at temperatures about 20 K (Besley and Kemp 1978). It was therefore necessary to obtain some higher purity platinum wire.

A small platinum wire of room temperature resistance about 0.4 Ω, with a measured residual resistance ratio of 720 was kindly supplied by Dr. D. Caplin of this laboratory. It was wound into a shape suitable for mounting on the copper block, and annealed in air at 550^{o}C for 16 hours, both to oxidise impurities and to relieve the strain caused by winding. It was mounted on the block using GE varnish and cigarette paper as shown in figure A.1, to provide good thermal contact to the block. Four connections were made by spot welding short lengths of (low grade) platinum wire to the resistor, and these were then soldered into the connections which were provided for potentiometric resistance measurements. A measuring current of about 10 mA was used at all temperatures.

Two points were needed for the calibration, the liquid ^{4}He normal boiling point (4.22 K), and the ice point (273.15 K). The latter was achieved by immersing the block in a beaker full of partly frozen high purity (0.35 MΩ) single glass-distilled water. Conversion of resistance to temperature was performed using the tabulated values of the function Z(R(T)) given by

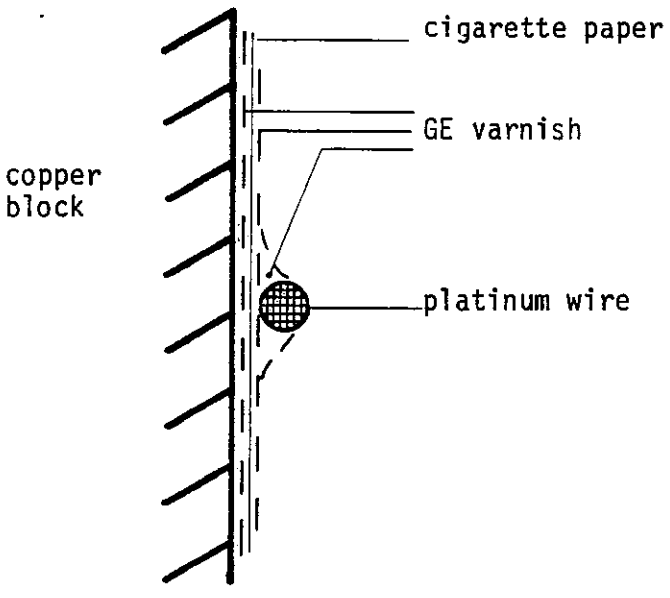

FIGURE A.1 Mounting of the platinum thermometer.

$$Z(T) = \frac{R(T) - R(4.22\ K)}{R(273.15\ K) - R(4.22\ K)},$$

which is simply a device to compare the values of different thermometers, assuming the validity of Mattiessen's rule. The tabulated values used were, for 18 K to 100 K, the values of CCT 64 (White 1968), and for 100 K to 273 K, the mean values given by Besley and Kemp, as quoted by White (1979). These values are summarised in table A.1. The smoothing error at 100 K is about 25 mK. For the accuracy required here, a linear interpolation between tabulated values proved sufficient.

Reasonable precision in measuring the platinum resistance could be achieved down to 16 K (corresponding to a precision of 10 mK), but because of the relatively small resistance ratio of this thermometer, DMR could be significant at the level of 0.1 K in this temperature range.

Besley and Kemp (1978) found deviations in the temperatures given by several high quality platinum resistance thermometers, ΔT, of the following form,

$$\Delta T_{T*} = \Delta T_{13.8}\left(1 - \left(\frac{T*}{40}\right)^{\frac{1}{2}}\right) \Big/ \left(1 - \left(\frac{13.8}{40}\right)^{\frac{1}{2}}\right),$$

where $\Delta T_{13.8}$ is the deviation from the mean temperature of all the thermometers at 13.8 K, and T* is the temperature as given by the thermometer concerned. Following a similar procedure, it was decided to correct the platinum temperature reading to the germanium temperature at 18 K, and apply a correction in the range 18 K to 40 K,

$$\Delta T_{T*} = \Delta T_{18}\left(1 - \left(\frac{T*}{40}\right)^{\frac{1}{2}}\right) \Big/ \left(1 - \left(\frac{18}{40}\right)^{\frac{1}{2}}\right)$$

where $\Delta T_{18} = T*_{Pt} - T_{Ge}\Big|_{T_{Ge} = 18\ K}$

and now $T_{Pt} = T*_{Pt} - \Delta T_{T*}$.

TABLE A.1

VALUES OF $Z(T) = \frac{R(T) - R(4.22\ K)}{R(273.15\ K) - R(4.22\ K)}$ USED TO DEFINE ICMPT 80

From T = 18 K to T = 100 K, these are CCT 64 (White 1968), and from T = 105 K to T = 273.15 K, these are averages computed by Besley and Kemp (White 1979).

T/K	$Z \times 10^6$	T/K	$Z \times 10^6$	T/K	$Z \times 10^6$
18	2 481	55	94 021	165	560 783
19	3 067	60	114 109	170	581 490
20	3 747	65	134 874	175	602 150
21	4 526	70	156 085	180	622 765
22	5 409	75	177 572	185	643 335
23	6 402	80	199 214	190	663 864
24	7 508	85	220 928	195	684 352
25	8 732	90	242 655	200	704 802
26	10 073	95	264 359	205	725 213
27	11 536	100	286 011	210	745 588
28	13 120			215	765 927
29	14 826	105	307 511	220	786 230
30	16 653	110	329 014	225	806 499
32	20 670	115	350 439	230	826 733
34	25 158	120	371 787	235	846 933
36	30 096	125	393 058	240	867 099
38	35 460	130	414 253	245	887 232
40	41 224	135	435 376	250	907 333
42	47 351	140	456 431	255	927 401
44	53 816	145	477 420	260	947 439
46	60 584	150	498 346	265	967 447
48	67 625	155	519 213	270	987 427
50	74 912	160	540 025	273.15	1 000 000

ΔT_{18} was measured several times, and was found to be +0.14 ± 0.03 K.

This difference is not large, given the criterion of ±0.5 K accuracy, but this correction provides a plausible smoothing procedure to match the readings of the two standard thermometers.

Definition of the ICMPT 80 Scale

The Imperial College Metal Physics Temperature scale 1980 is defined from 1.5 K to 300 K operationally as follows.

A. 1.5 K to 4.2 K

The vapour pressure of liquid ^{4}He, as measured by a Wallace and Tiernan aneroid manometer, is used with a standard tabulation (White 1968). Note that the precision obtained by this method is better than 0.01 K without undue difficulty. This also provides a smooth continuation of the germanium thermometer readings (Guy 1976).

B. 4.2 K to 18 K

The scale is defined by the calibration curve of the "Texas" germanium resistance thermometer shown in figure A.2 (Guy 1976).

C. 18 K to 40 K

The temperature T is given by

$$T = T^* - \Delta T_{T^*}$$

where T* is the temperature given by the platinum resistance thermometer in conjunction with the Z-values, table A.1, together with the calibration values

$$R_{4.22} = 0.000533\ \Omega$$

$$R_{273.15} = 0.368032\ \Omega$$

and $Z(T^*) = \dfrac{R_T - R_{4.22}}{R_{273.15} - R_{4.22}}$,

and finally,

$$\Delta T_{T^*} = \Delta T_{18} \times \frac{(1 - (T^*/40)^{\frac{1}{2}})}{(1 - (18/40)^{\frac{1}{2}})}$$

with $\Delta T_{18} = 0.14$ K.

D. 40 K to 273.15 K

The temperature is given by the platinum resistance thermometer and the Z-values of table A.1.

E. 273.15 K to 300 K

The temperature is given by the standard extrapolation formula

$$R(T) = R(273.15)(1 + A\theta + B\theta^2)$$

where $\theta = T - 273.15$ K

$A = 4.0496 \times 10^{-3}$ K^{-1}

$B = 5.9571 \times 10^{-7}$ K^{-2}

(values taken from White (1968)).

Note that this extrapolation formula may be used with confidence well beyond 300 K.

Check on New Scale

The normal boiling point of liquid nitrogen was measured using ICMPT 80, and found to be 77.34 K. There is some uncertainty associated with this point because of the strong possibility of dissolved oxygen in the nitrogen, but the nominal temperature for pure nitrogen is 77.36 K (White 1968).

The precision of this scale is much higher than the nominal ±0.5 K over all the range, and, especially at low temperatures, the accuracy is probably better than 0.1 K. This nitrogen point, and the agreement with partly calibrated thermometers described below, foster confidence in this belief.

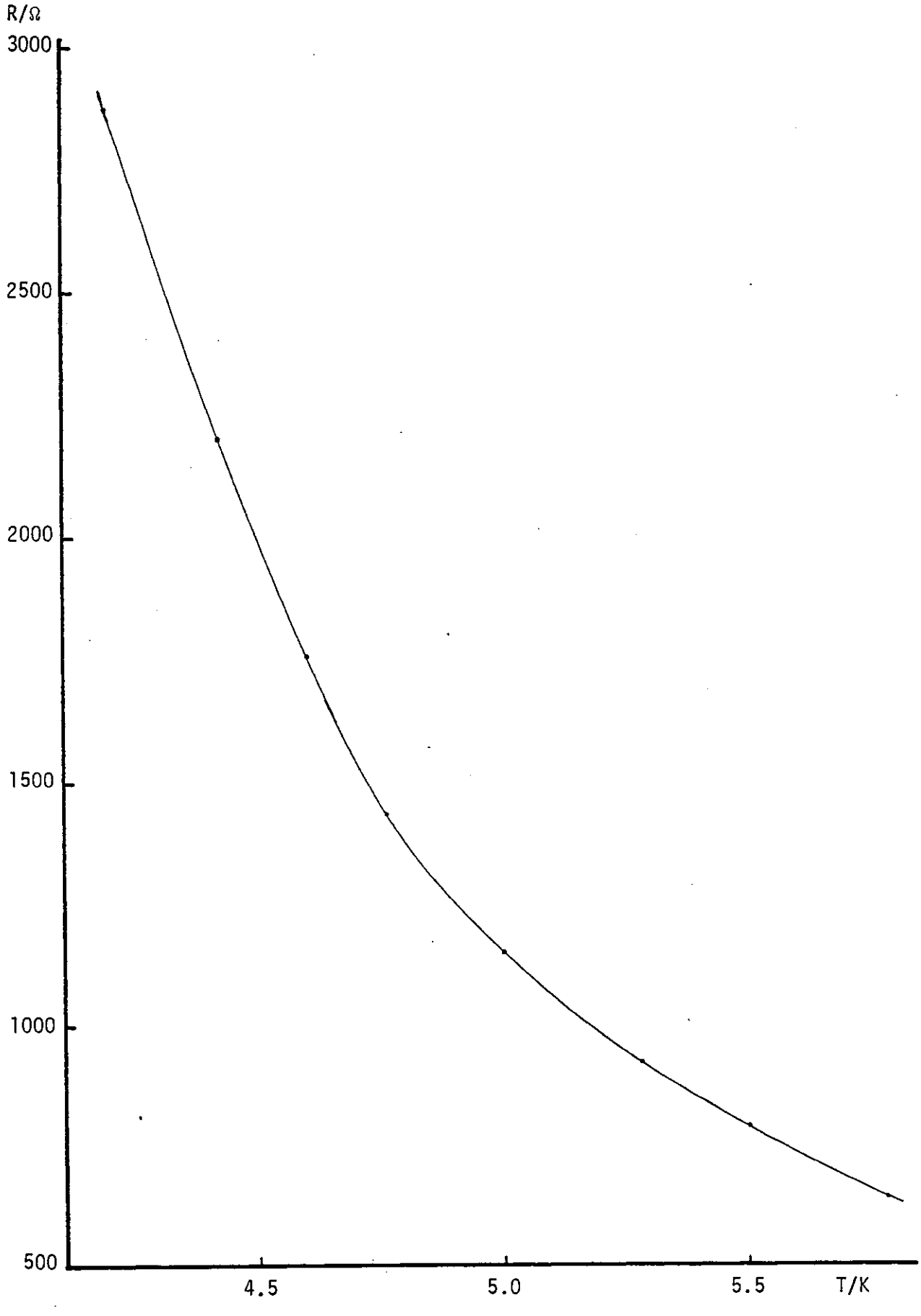

FIGURE A.2 (a) Texas germanium calibration. Resistance, R, as a function of temperature, T, from 4.2 K to 5.8 K. From Guy (1976).

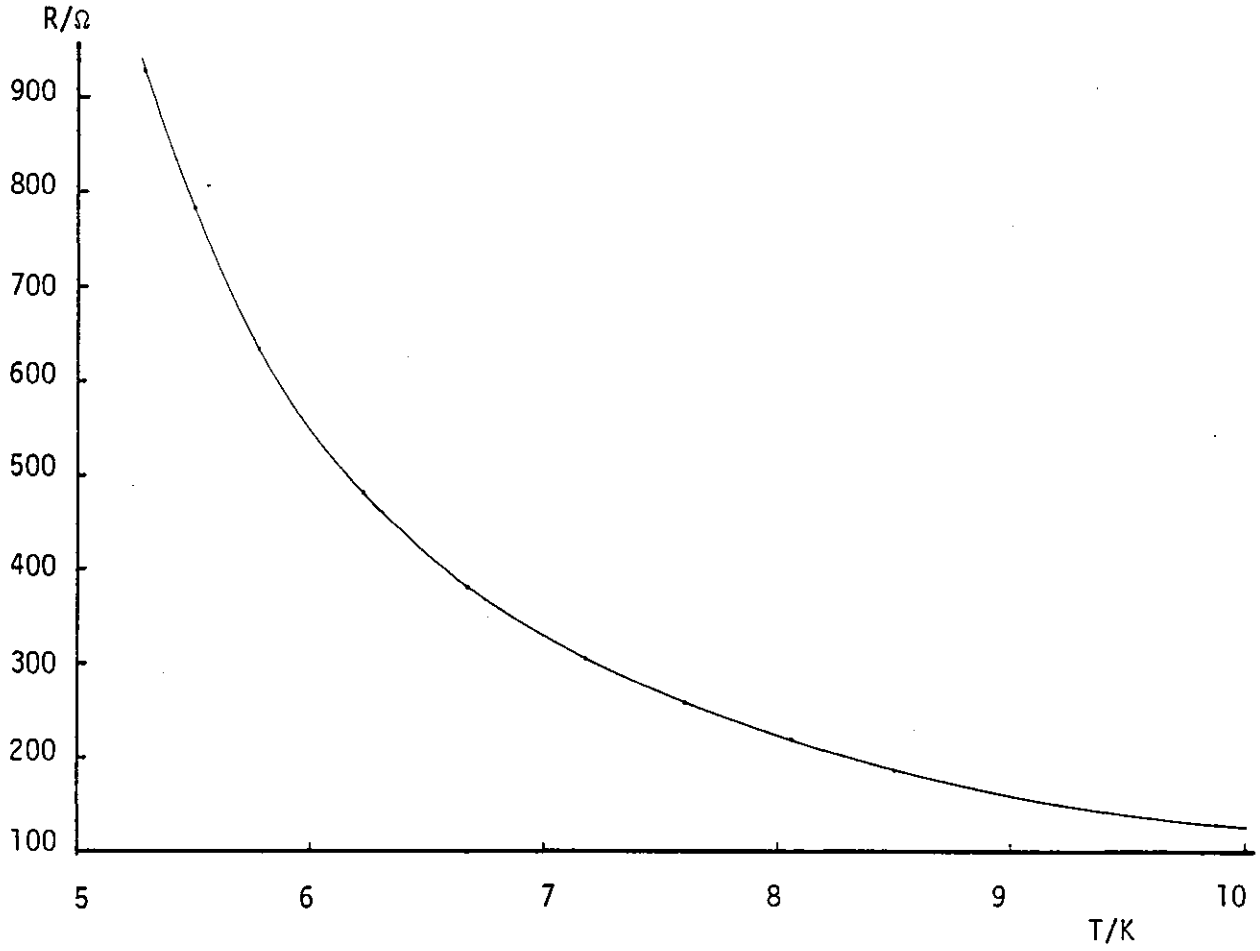

FIGURE A.2 (b) Texas germanium calibration. Resistance, R, as a function of temperature, T, from 5 K to 10 K. From Guy (1976).

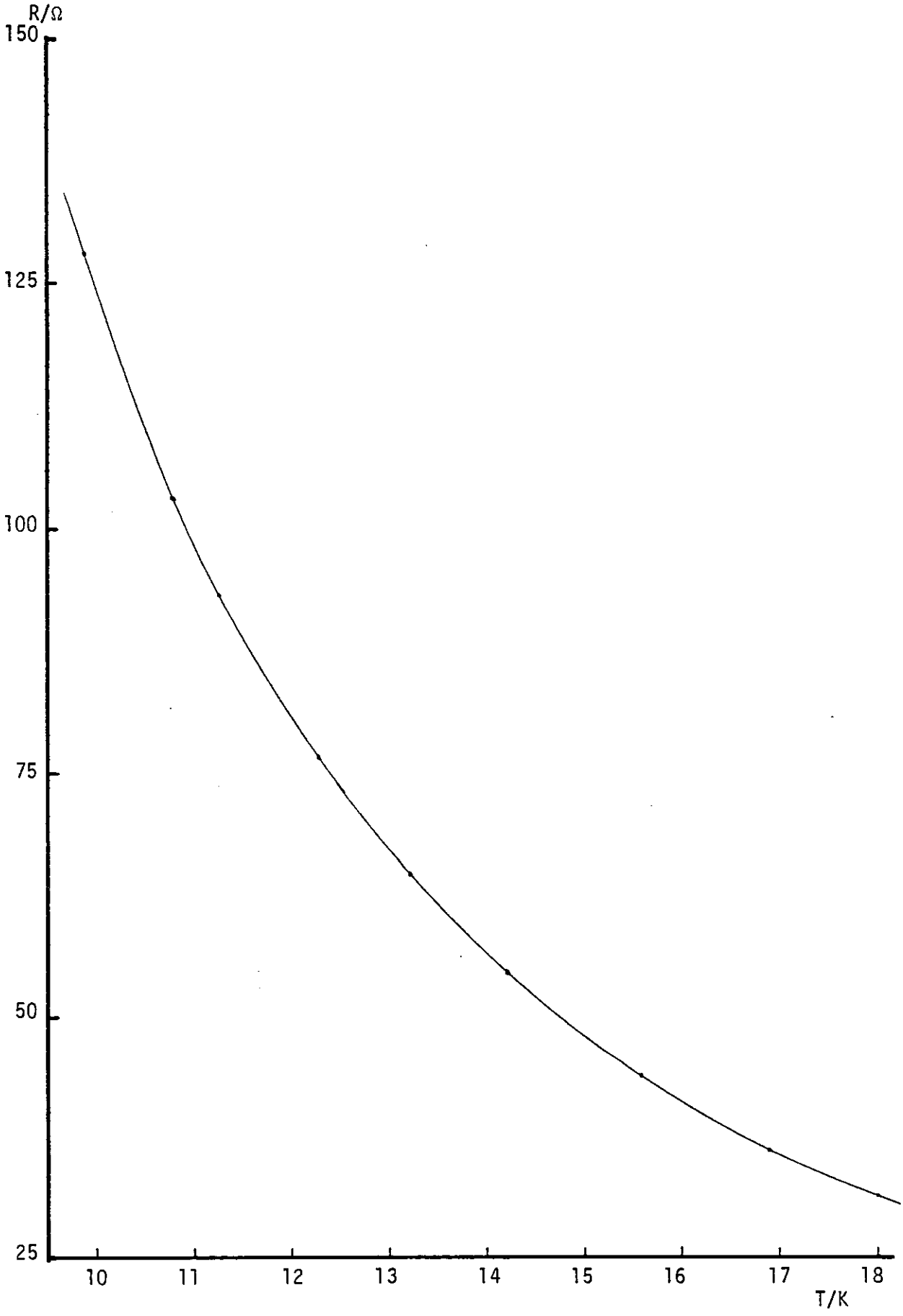

FIGURE A.2 (c) Texas germanium calibration. Resistance, R, as a function of temperature, T, from 9.5 K to 18 K. From Guy (1976).

Secondary Calibration of Other Thermometers

The secondary thermometers for use in the measurements in the vibrating sample magnetometers were of two types, namely carbon glass resistors, and silicon diodes.

The temperature was varied and controlled as described by Barber (1974). In the region from 18 K to 300 K, it was found desirable to monitor the temperature with the copper/constantan thermocouple as described by Barber. This thermocouple was calibrated on ICMPT 80. As noted by Barber, the tabulated e.m.f. values (White 1968) gave a systematic error which was largest at 20 K, when it read 2 K high. Above 50 K, the error was never more than 0.8 K, and was of fluctuating sign.

i. Carbon Glass Resistance Thermometers

Two carbon glass resistance thermometers (C2445, C2454) made by Lake Shore Cryotronics Ltd. were used. Details of the construction and characteristics are given by White (1979). The reasons for preferring them in the present work are their comparatively high sensitivity and monotonicity up to 300 K, their comparatively small magnetoresistance, their reproducibility under thermal cycling, and their magnetic response, which is small and not markedly temperature dependent. These properties, combined with their compact size (5 mm long, 2 mm diameter), make them the best choice for a thermometer that is to be mounted near to a sample in a vibrating sample magnetometer in the presence of large magnetic fields.

For the calibration, the thermometers were secured to the same copper block as the standard thermometers, using GE varnish to attach both the cases and about 3 to 4 cm of all of the leads, to ensure good thermal contact with the block at all temperatures.

The resistance was measured by a four terminal technique. The current was supplied by the potentiometer current supply which also fed

the platinum thermometer (10 mA). It was suitably divided to give the required measuring current recommended to avoid excessive Joule heating. The simple device of a constant resistance (1 Ω) shunt across the two carbon glass thermometers in series (figure A.3) was found to adjust the current automatically to an acceptable value at all temperatures from 4.2 K to 300 K.

About forty calibration points were recorded in the range 4.2 K to 300 K for both carbon glass thermometers. The calibration points supplied with the thermometers at 4.2 K, 77 K and 298 K were found to be consistent with the present calibration to within 0.05 K.

For practical purposes, two methods were used for presentation of the calibration. Firstly, a chart was drawn, in several sections, plotting the variation of resistance of each thermometer as a function of temperature. The calibration points were connected by a smooth line drawn in by eye. This enables rapid conversion of resistance to temperature, accurate to ±2 K, or better at low temperatures. The second method was to incorporate the calibration points as data values in a programme stored on a magnetic disc on a Commodore "Pet" computer. The programme first linearises the data points by converting them to the form $(T,(\ln R)^{-7})$, and then performing a cubic Lagrange interpolation on the four data points nearest to the resistance value fed in, thereby extracting a corresponding temperature, the precision and accuracy of which are almost equal to those of the calibrated values. Several attempts were made to fit all of the data points to some analytic form, but none was very satisfactory. The best relation that was tried was

$$T = a + b(\ln R)^{-7} + c(\ln R)^{-14} + d(\ln R)^{-21}.$$

The coefficients c and d were small.

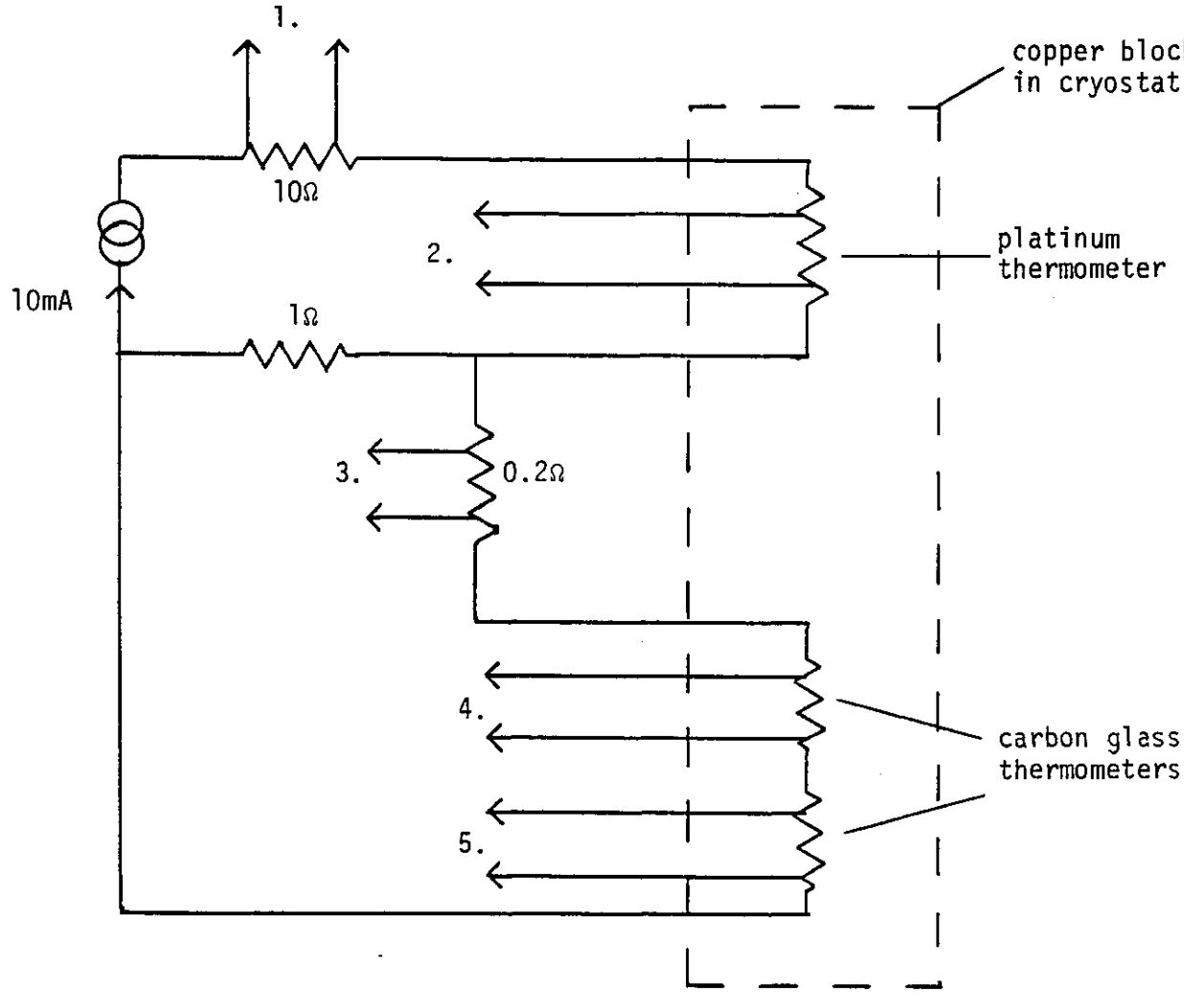

Each of the numbered leads is connected to the potentiometer via a multi-way switch.

1. Platinum current.
2. Platinum voltage.
3. Carbon glass current.
4. Carbon glass voltage (1).
5. Carbon glass voltage (2).

FIGURE A.3 Carbon glass measuring circuit.

ii. Silicon Diodes

A commercial signal silicon diode may be used as a cryogenic thermometer by measuring the potential difference needed to maintain some small, constant current flowing in the forward direction. The voltage required is typically 0.5 V at room temperature, rising to 2 V at liquid helium temperatures. These values are insensitive to the measuring current, which is typically 10 μA. This makes them attractive as "quick look" thermometers, as no special precautions are required, and a two-terminal measurement is adequate even for quite high precision.

However, they do suffer changes in calibration on thermal cycling, especially if they are heated much above room temperature. They are also very sensitive to magnetic fields and radio-frequency interference, and they usually come with ferromagnetic leads.

Two special diodes (with non-magnetic leads, DI6186 and DI6188) supplied by Lake Shore Cryotronics Ltd., and three "off-the-shelf" signal diodes (called HFVSM, LFVSM and SKB) were mounted on the copper block and calibrated against ICMPT 80.

The circuit used to supply the measuring current to all five diodes in series was a standard diode supply, with a higher voltage supply (±18 V) than usual (±9 V) to cope with the voltage drop across all five at low temperatures. Each voltage could be switched in turn to a digital voltmeter.

As with the carbon glass thermometers, about forty calibration points were taken for the diodes, but with a higher density around 20 K, where there is marked curvature in the V,T plots. Below 15 K and above 30 K, these plots are nearly linear.

The calibration was presented again in two forms, a graphical sketch interpolated by eye, to be used for quick conversion, and a simple two-point linear interpolation programme for use on an HP9820A

desk computer. The data and programme in the latter case were stored on magnetic cards. A linear interpolation is sufficient to give a conversion to temperature whose precision is equal to the inherent accuracy of the diodes.

APPENDIX B

VIBRATING SAMPLE MAGNETOMETERS

Low Field Vibrating Sample Magnetometer

The equipment was built by Dr. C. N. Guy, and is described in detail by Howarth (1978). The magnetometer and cryostat were used unmodified, but the circuitry was adapted to suit the alternating field measurements undertaken.

i. Modifications

The phase-shifter and phase sensitive detector (p.s.d.) described by Howarth were replaced by a Brookdeal Ortholoc SC 9505 two-phase lock-in analyser (= p.s.d.). The signal channel incorporated a 5011F notch filter set to attenuate the mains supply frequency, and a non-linear transient noise filter 5014 to decrease the time the system took to recover from the effects of the large amplitude, wide band interference caused intermittently by local embassy transmitters. The two phase channels (in-phase and quadrature) greatly facilitated the setting up and monitoring of the phase of the coherent signal.

The way in which the magnetisation signal was measured was changed radically. The potential divider used by Howarth was retained to provide a continuous range adjustment, but a simple control loop was used to supply the current to the reference coil to maintain the in-phase component of the p.s.d. output at zero. At the time these experiments were performed, this loop consisted of a simple d.c. amplifier with a voltage gain of 100 and a transistor output stage capable of supplying ±100 mA, whose input was the p.s.d. output and whose load was the reference coil and a standard resistor (Cropico 0.1% 10 Ω nominal) in series. The potential difference across this resistor is a measure of the reference current, which in turn is proportional to the magnetometer coil signal, and hence to the sample moment. This

enables the use of an X-Y or X-t chart recorder to take data continuously.

The output signal from this standard resistor was filtered using a variable time constant, first order, buffered, low-pass filter, with switched time constants between 5 s and 10 ms (three per decade), to reduce the output noise level. The time constant was selected to give an attenuation of between 0.1% and 1% at the frequency of the applied field, and resulted in a gain in signal to noise ratio by two orders of magnitude at the lowest frequency used. The filter attenuation was calculated for each measurement, and the data was corrected to zero attenuation.

This filter was necessary because the control loop used to supply the reference coil also effectively reduces the output time constant of the p.s.d. by a factor which is just the open loop gain of the loop, and which is large to ensure the equivalence of the reference and sample signals. In this way, using control loop and output filter, the sensitivity was maintained at approximately 5×10^{-7} e.m.u. (erg G^{-1}) at low frequencies (c.f. Howarth, who quoted a sensitivity of 10^{-6} e.m.u.).

In the final experiment of chapter 2, on the gold 4% iron sample, the noise of the input circuit was reduced by replacing the adding pre-amplifier and potentiometer with a transformer (figure B.1). This transformer was designed and built by Jarvis (1972) and has a turns ratio of 30, and a flat frequency response from 1 Hz up to 10 kHz, which characteristics made it suitable for the present application. Use of this transformer resulted in a gain in signal to noise ratio of a factor of three over the other method at low temperatures because of the improved impedance matching of the signal source and p.s.d. input. However, it would be unsuitable for variable temperature measurements because the phase of the input signal varies as the impedance of the

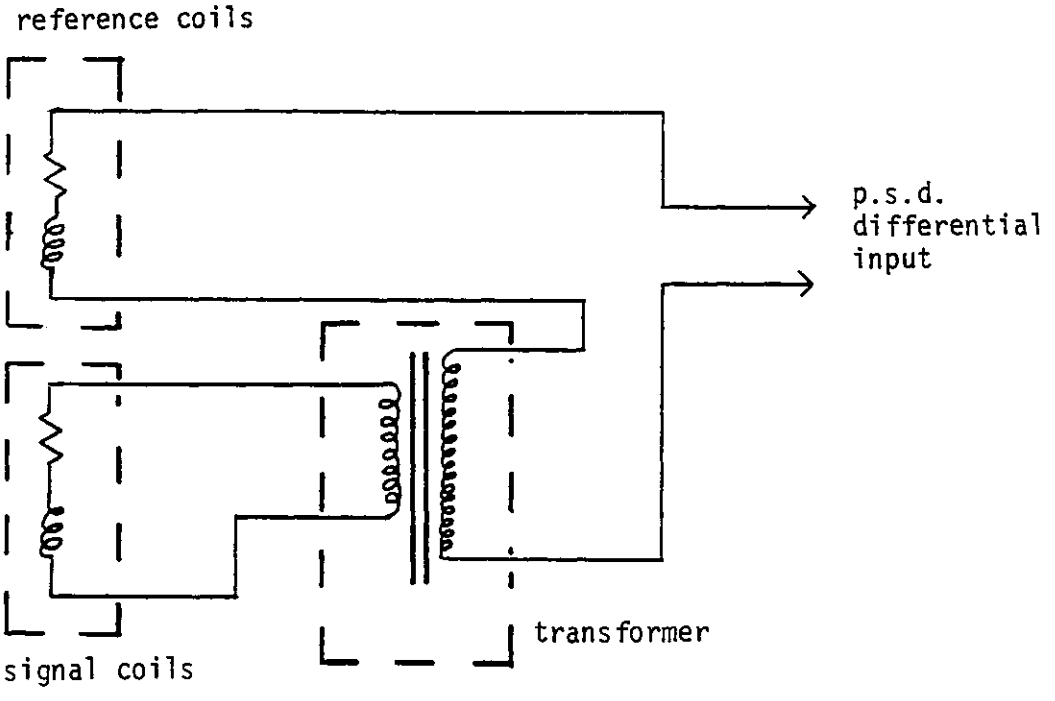

FIGURE B.1 Transformer input circuit.

signal coil varies with temperature.

The sine-wave signal for the alternating field was provided by a Brookdeal signal source type 471, and amplified using a Hewlett-Packard 6824A power supply/amplifier in constant voltage mode. A Cropico 10 Ω standard resistor in series with the Helmholtz pair allowed continuous reading of the applied field, so enabling magnetisation against field to be drawn out on an X-Y recorder.

ii. Calibration

The vibrator itself was removed for repair, and after re-assembly, the magnetometer was re-calibrated, as suggested by Howarth. The calibration used a small, spherical lead sample below its superconducting transition temperature (7 K), and the Meissner effect produces an effective diamagnetic moment. This calibration was checked using a small spherical nickel sample at room temperature, using both the demagnetising slope and the saturation moment. All three methods agreed to within about 3%, which is within the estimated reproducibility of the apparatus.

The current to field calibration for the Helmholtz pair was repeated using a Hall probe.

iii. Temperature Control

All of the experiments described in chapter 2 were performed at a fixed temperature, namely 4.22 K, the normal boiling point of ^{4}He. The stability was determined by the fluctuations in the helium return line pressure, which were generally such that the temperature was stable to within ±10 mK.

High Field Vibrating Sample Magnetometer

i. Description

This equipment was designed and built by Dr. C. N. Guy, with some modifications by the author. The principle of operation is the same as

for the low field magnetometer described by Howarth (1978) and above. A sketch of the apparatus is given in figure B.2. The electronics used to measure the signal are largely the same. The essential differences are as follows.

1. The sample and pick-up coils are contained within the bore of a superconducting solenoid magnet. Initially this was a 40 kOe magnet, but this was replaced in the autumn of 1980 by a 74 kOe magnet, with improved homogeneity. The direction of the field is parallel to the axis of the pick-up coils, which is parallel to the vibration direction.

2. The sample may be removed and replaced when the cryostat is cold. Top loading enables several samples to be run in a batch.

3. The sample stick is equipped with a carbon glass resistance thermometer (see appendix A), and a heater, which are both in good thermal contact with the sample via the holder, which is fashioned from a bundle of copper wires cast in an epoxy resin (figure B.3).

4. The input circuit, which combines the sample and reference signals, is replaced by an operational amplifier adding circuit which combines the signals in one of five different, switched, proportions, before feeding the sum to the "virtual zero" of the p.s.d. input.

5. The feedback amplifier is replaced by a more versatile unit. Two versions were built. The first incorporated a versatile lead/lag filter to improve the performance of the control loop (three-term control), and also the low-pass filter described above for use with the low field apparatus. The second version, which proved more robust and easier to use, also incorporated a switched, single parameter lead/lag circuit. Both versions used an integrated circuit output stage capable of supplying up to ±300 mA.

ii. Performance

Magnetisation may be measured as a function of applied field,

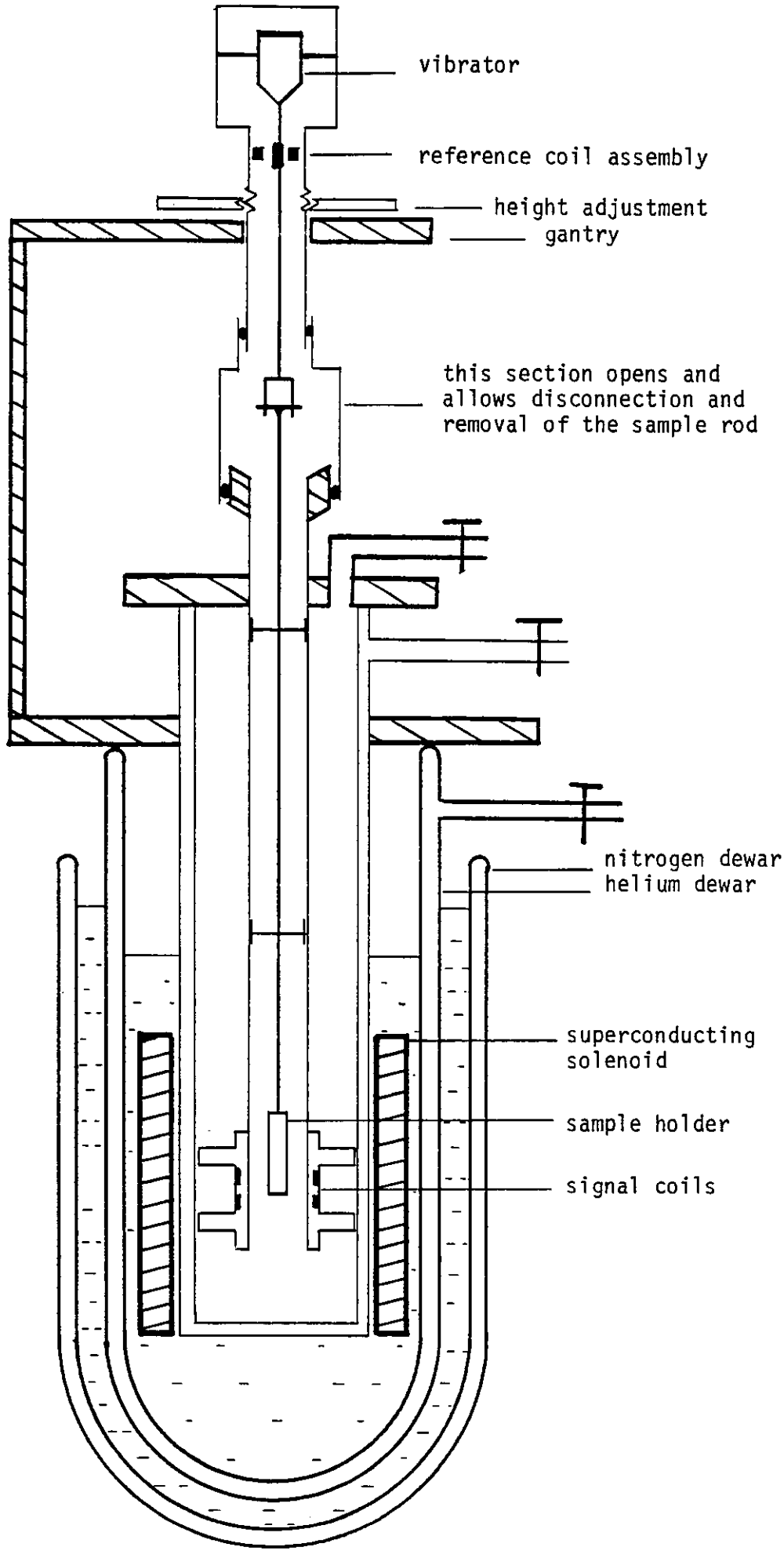

FIGURE B.2 High field vibrating sample magnetometer (schematic).

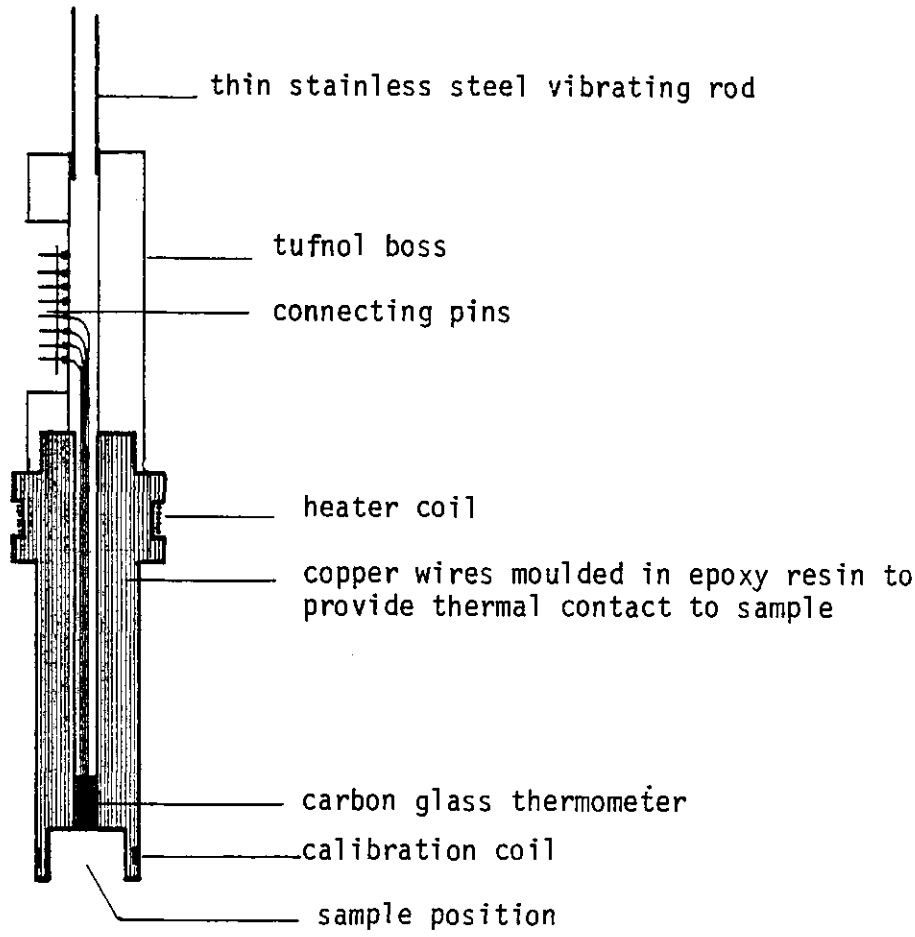

FIGURE B.3 Sample holder for high field vibrating sample magnetometer.

parallel to the field direction. The bore of the access tube and pick-up coil former is 14 mm, and this enables various ancillary devices to be used (e.g. pressure cell, rotating sample holder). Samples up to 2.5 g in weight have been measured successfully. The range of magnetisation to be measured can be switched in five ranges from 5 e.m.u. to 2×10^{-3} e.m.u. with a resolution between 0.01% and 0.3% of full scale, depending on the conditions.

The temperature may be varied continuously from 1.3 K to room temperature, although the heat transfer to the magnet helium bath becomes quite large for sample temperatures above about 100 K, and the power supplied to the heater needs to be large. If liquid helium is transferred to the sample space, the depth may be monitored by a ladder of three silicon signal diodes.

The mean sample position can be varied continuously from a few millimetres below the centre of the pick-up coils to a few centimetres above. This is a useful facility and greatly adds to the versatility of the device. However, it does render precise calibration somewhat difficult.

iii. Calibration

The calibration procedure involved three different methods, and they all agreed to within 5%. The relative calibration between measurements on the same sample in the same position (stability) is much more precise. The three calibration runs were on a small nickel sphere, a small lead sphere, and a small coil of known dimensions. The moment of a known d.c. current in the coil, the lower and upper critical fields of the lead at 4.2 K, the saturation magnetisation of the nickel at 4.2 K, and the demagnetising slopes of both lead and nickel spheres were all used to achieve consistent calibrations for the field and magnetisation. Most of the 5% discrepancy can probably be attributed to the imperfect sphericity of the samples, which affects

the demagnetising slopes.

APPENDIX C

X-RAY LAUE CAMERA

Background and Theory

A Phillips X-ray generator with a vertically mounted, copper target, 54 kV tube was available, with line or spot focussed beams. This was used with the Guinier camera to examine some of the samples, as described in chapter 4. However, a need arose to examine single crystal samples, to establish their orientation. It was decided, therefore, to build a back-reflection Laue camera for use with a spot focus beam which would allow orientation identification.

The theory of this type of X-ray diffraction is well-documented, for example by Cullity (1956). A useful tabulation of Laue patterns compiled by Preuss, Krahl-Urban and Butz (1974) was used to identify the high-symmetry directions observed in these b.c.c. alloys.

Camera Details

The camera is simple in conception, being simply a film holder with a de-mountable flange plate to hold a standard size of X-ray film, with a brass collimator protruding through the plate. Four interchangeable collimator pieces allow the use of a finer, less intense incident beam, or a coarser, more intense beam for preliminary photographs.

It was found necessary to include an aluminium filter 0.25 mm thick in front of the film to prevent excessive blackening of the film near the centre by the modified Compton scattering and fluorescence. This filter was found to increase the exposure times necessary by about 25%, while greatly increasing the ratio of the density of the Bragg reflections to the incoherent images on the film.

An exploded view of the camera is shown in figure C.1. Also shown

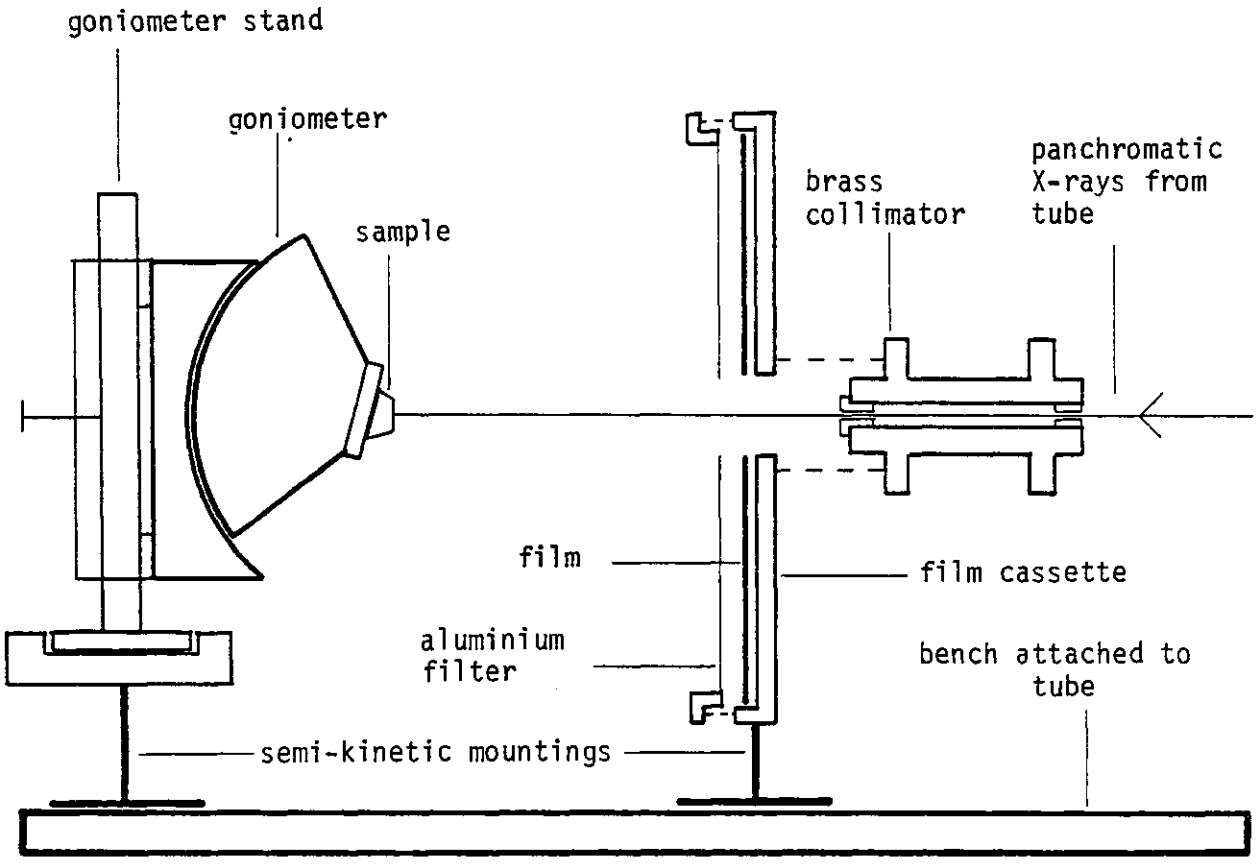

FIGURE C.1 Schematic, exploded view of Laue camera.

is the goniometer stand with lateral adjustment. This supports the goniometer, on which the crystal is mounted both for X-ray pictures and for spark machining.

REFERENCES

Adachi, K. and Maki, S. 1977.
Physica, 86-88B, p263.

Aldred, A.T. 1976.
Phys. Rev., B14, p219.

Aldred, A.T. and Froehle, P.H. 1972.
Intern. J. Magnetism, 2, p195.

Aldred, A.T. and Kouvel, J.S. 1977.
Physica, 86-88B, p329.

Aldred, A.T., Rainford, B.D., Kouvel, J.S. and Hicks, T.J. 1976.
Phys. Rev., B14, p228.

Arajs, S. and Dunmyre, G.R. 1966.
J. Appl. Phys., 37, p1017.

Argyle, B.E., Charap, S.H. and Pugh, E.W. 1963.
Phys. Rev., 132, p2051.

Arrott, A., Werner, S.A. and Kendrick, H. 1967.
Phys. Rev., 153, p624.

Ashcroft, N.W. and Mermin, N.D. 1976.
Solid State Physics. Holt, Rinehart and Winston.

Astrom, H.V., Benediktsson, G. and Rao, K.V. 1978.
J. Phys. (Paris) Colloq., 39, pC6-785.

Axe, J.D., Shirane, G., Mizoguchi, T. and Yamauchi, K. 1977.
Phys. Rev., B15, p2763.

Babic, B., Kajzar, F. and Parette, G. 1980.
J. Phys. Chem. Solids, 41, p1303.

Bacon, G.E. 1975.
Neutron Diffraction. 3rd edition. Clarendon Press.

Barber, A.J. 1974.
Ph.D. thesis, University of London.

Bennett, L.H., Page, C.H. and Swartzendruber, L.J. 1976.
A.I.P. Conf. Proc., 29 (MMM 1975), pxix/1-3.

Besley, L.M. and Kemp, R.C. 1978.
Cryogenics, August 1978, p497.

Blandin, A. 1973.
Rado and Suhl (1973) op. cit. chapter 2.

Blandin, A. 1978.
J. Phys. (Paris) Colloq., 39, pC6-1499.

Blum, N.A. and Grodzins, L. 1964.
Phys. Rev., 136A, p133.

Booth, J.G. 1966.
J. Phys. Chem. Solids, 27, p1639.

Booth, J.G. and Ziebeck, K.R.A. 1981.
To be published. Quoted by Costa et al. (1981).

Borg, R.J., Booth, R. and Violet, C.E. 1963.
Physical Review Letters, 11, p464.

Brenner, R. 1957.
Phys. Rev., 107, p1539.

Burke, S.K. 1980.
Ph.D. thesis, University of London.

Burke, S.K. and Rainford, B.D. 1978.
J. Phys. F: Metal Phys., 8, pL239.

Burke, S.K., Ziebeck, K.R.A. and Booth, J.G. 1980.
I.L.L. Annual Report. Exp. 04.03.149.

Cannella, V. and Mydosh, J.A. 1972.
Phys. Rev., B6, p4220.

Cheng, C.H., Wei, C.T. and Beck, P.A. 1960.
Phys. Rev., 120, p426.

Coles, B.R., Sarkissian, B.V.B. and Taylor, R.H. 1978.
Phil. Mag. B., 37, p489.

Costa, M.M.R., Booth, J.G., Ziebeck, K.R.A. and Brown, P.J. 1981.
J. Appl. Phys., 52, p1681.

Crangle, J. and Scott, W.R. 1964.
Phys. Rev. Lett., 12, p126.

Cullity, B.D. 1956.
Elements of X-Ray Diffraction. Addison-Wesley.

Cywinski, R. and Gray, E.M. 1980.
Physics Letters, 77A, p284.

Cywinski, R. and Hicks, T.J. 1978.
J. Phys. C: Solid State Phys., 11, pL899.

Cywinski, R. and Hicks, T.J. 1980.
J. Phys. F: Metal Phys., 10, p693.

Dahlberg, E.D., Hardiman, M., Orbach, R. and Souletie, J. 1979.
Phys. Rev. Lett., 42, p401.

David, P. and Heath, M. 1971.
J. Phys. (Paris) Colloq., 32, pC1-112.

Dolezal, N. and Guy, C.N. 1981.
Private communication.

Edwards, D.M., Mathon, J. and Wohlfarth, E.P. 1973.
J. Phys. F: Metal Phys., 3, p161.

Elliott, R.P. 1965.
Constitution of Binary Alloys, First Supplement. McGraw-Hill.

Fenton, E.W. and Leavens, C.R. 1980.
J. Phys. F: Metal Phys., 10, p1853.

Feynman, R.P. 1964.
The Feynman Lectures on Physics II. Addison-Wesley.

Fincher, C.R., Shapiro, S.M., Palumbo, A.H. and Parks, R.D. 1980.
Phys. Rev. Lett., 45, p474.

Friedel, J. 1969.
The d-band in transition metals. In "The Physics of Metals: I electrons", ed. J. M. Ziman. C.U.P.

Friedel, J. and Hedman, L.E. 1978.
J. Phys. (Paris), 39, p1225.

Gabay, M. and Toulouse, G. 1981.
Phys. Rev. Lett., 47, p201.

Gray, E.M. 1979 (a).
Private communication.

Gray, E.M. 1979 (b).
J. Phys. F: Metal Phys., 9, pL167.

Gray, E.M. and Cywinski, R. 1979.
Private communication.

Guy, C.N. 1976.
Private communication. "Texas Ge" calibration.

Guy, C.N. 1977.
J. Phys. F: Metal Phys., 7, p1505.

Guy, C.N. 1978.
J. Phys. F: Metal Phys., 8, p1309.

Guy, C.N. 1979.
J. Appl. Phys., 50, p7308.

Guy, C.N. 1981.
Private communication.

Hamann, D.R. and Schrieffer, J.R. 1973.
Rado and Suhl (1973) op. cit. chapter 8.

Hamzic, A. and Campbell, I.A. 1981.
J. Phys. Lettres, 42, pL309.

Hansen, M. 1958.
Constitution of Binary Alloys. McGraw-Hill.

Hasegawa, H. 1981.
Solid State Commun., 38, p401.

Hedgcock, F.T., Strom-Olsen, J.O. and Wilford, D.F. 1977.
J. Phys. F: Metal Phys., 7, p855.

Hedman, L.E., Rao, K.V. and Astrom, H.V. 1978.
J. Phys. (Paris), 39, pC6-788.

Herbert, I.R., Clark, P.E. and Wilson, G.V.H. 1972.
J. Phys. Chem. Solids, 33, p979.

Herring, C. and Kittel, C. 1951.
Phys. Rev., 81, p869.

Hirst, L.L. 1974.
J. Phys. (Paris) Colloq., 35, pC6-21.

Holden, T.M. and Fawcett, E. 1978.
J. Phys. F: Metal Phys., 8, p2609.

Holtzberg, F, Tholence, J.L., Godfrin, H. and Tournier, R. 1979.
J. Appl. Phys., 50, p1717.

Hopkinson, J. 1889.
Phil. Trans. Royal Soc., A180, p443.

Howarth, W. 1978.
Ph.D. thesis, University of London.

Hubbard, J. 1981.
J. Appl. Phys., 52, p1654.

Ishikawa, Y., Hoshino, S. and Endoh, Y. 1967.
J. Phys. Soc. Japan, 22, p1221.

Ishikawa, Y., Tournier, R. and Filippi, J. 1965.
J. Phys. Chem. Solids, 26, p1727.

Jarvis, P. 1972.
Ph.D. thesis, University of London.

Kajzar, F., Parette, G. and Babic, B. 1981.
J. Phys. Chem. Solids, 42, p501.

Katano, S. and Mori, N. 1979.
J. Phys. Soc. Japan, 46, p1265.

Katano, S. and Mori, N. 1980 (a).
J. Mag. Magn. Mat., 15-18, p73.

Katano, S. and Mori, N. 1980 (b).
J. Phys. Soc. Japan, 49, p1812.

Keffer, F. 1966.
Hand. der Phys., 18, p20 et seq.. Springer-Verlag.

Kim, D.J. 1981.
Solid State Commun., 38, p451.

Koester, L., Knopf, K. and Waschkowski, W. 1978.
Z. Physik A., 287, p61.

Kouvel, J.S. and Brooks, H. 1954.
Technical Report 198, Cruft Lab., Harvard.

Kouvel, J.S. and Comly, J.B. 1968.
Phys. Rev. Lett., 20, p1237.

Landau, L.D. 1957.
Sov. Phys. JETP, 3, p920.

Landau, L.D. and Lifshitz, E.M. 1969.
Course of Theoretical Physics, vol. V, Statistical Physics. 2nd edition. Pergamon Press.

Larica, C. 1981.
Ph.D. thesis, University of London.

Lingelbach, R. 1958.
Z. physik. Chem., Neue Folge 14, p1.

Loegel, B. 1975.
J. Phys. F: Metal Phys., 5, p497.

von Lohneysen, H., Tholence, J.L. and Tournier, R. 1978.
J. Phys. (Paris), 39, pC6-922.

Lonzarich, G.G. 1980.
Fermi surface studies in itinerant electron ferromagnets. In "Electrons at the Fermi Surface", ed. M. Springford. C.U.P.

Loveluck, J.M. 1981.
Institute of Physics, theoretical magnetism meeting. Unpublished.

Maier, B. (ed.) 1981.
I.L.L. Neutron Beam Facilities Available for Users.

Makarov, V.A., Tret'yakov, B.N., Puzei, I.M., Kalinin, G.P. and Tokmakova, V.A. 1979.
Sov. Phys. Solid State, 21, p527.

Marshall, W. and Lovesey, S.W. 1971.
Theory of Thermal Neutron Scattering. O.U.P.

Mezei, F. (ed.) 1980.
Lecture Notes in Physics, 128. Neutron Spin Echo. Springer-Verlag.

Mezei, F. and Murani, A.P. 1979.
J. Mag. Magn. Mat., 14, p211.

Mitchell, M.A. and Goff, J.F. 1972.
Phys. Rev., B5, p1163.

Monk, P.R. 1981 (a).
I.C.S.T. Dept. of Metallurgy and Materials Science Electron Microprobe Report MP294.

Monk, P.R. 1981 (b).
I.C.S.T. Dept. of Metallurgy and Materials Science Electron Microprobe Report MP305.

Monod, P., Préjean, J.J. and Tissier, B. 1979.
J. Appl. Phys., 50, p7324.

Montalvo, R.A. and Marcus, J.A. 1964.
Phys. Lett., 8, p151.

Mukhopadhyay, A.K., Shull, R.D. and Beck, P.A. 1975.
J. Less Common Met., 43, p69.

Mulder, C.A.M., van Duyneveldt, A.J. and Mydosh, J.A. 1981.
Phys. Rev., B23, p1384.

Murani, A.P. 1980.
Solid State Commun., 34, p705.

Mydosh, J.A. 1975.
A.I.P. Conf. Proc., 24 (MMM 1974), p131.

Mydosh, J.A. 1981.
Proceedings of the Scottish Universities Summer School in Physics, Dundee.

Néel, L. 1955.
Adv. Phys., 4, p191.

Newmann, M.M. and Stevens, K.W.H. 1959.
Proc. Phys. Soc. Lond., 74, p290.

Preuss, E., Krahl-Urban, B. and Butz, R. 1974.
Laue Atlas. Wiley.

Rado, G.T. and Suhl, H. 1973.
Magnetism V. Magnetic Properties of Metallic Alloys. Academic Press.

Rajan, N.S., Waterstrat, R.M. and Beck, P.A. 1960.
J. Appl. Phys., 31, p731.

Rice, T.M., Jayaraman, A. and McWhan, D.B. 1971.
J. Phys. (Paris) Colloq., 32, pC1-39.

Rivier, N. and Continentino, M.A. 1980.
J. Mag. Magn. Mat., 15-18, p1419.

Rode, V.E., Finkelberg, S.A., Wurl, B. and Lyalin, A.I. 1981.
Phys. Stat. Sol. (a), 64, p603.

Rowland, H.A. 1874.
Phil. Mag., 48, p321.

Salamon, M. and Feigl, F.J. 1968.
J. Phys. Chem. Solids, 29, p1443.

Sarkissian, B.V.B. 1978.
Inst. Phys. Conf. Ser., 37, ch8, p233.

Sarkissian, B.V.B. 1981.
J. Phys. F: Metal Phys., 10. To be published.

Schröder, K. 1962.
Phys. Rev., 125, p1209.

Schröder, K., Yessik, M.J. and Baum, N.P. 1966.
J. Appl. Phys., 37, p1019.

Sears, V.F. 1975.
Adv. Phys., 24, p1.

Shapiro, S.M., Fincher, C.R., Palumbo, A.C. and Parks, R.D. 1981.
J. Appl. Phys., 52, p1729.

Shtrikman, S. and Treves, D. 1963.
Magnetism III. Ed. Rado and Suhl. Academic Press.

Shull, R.D. and Beck, P.A. 1975.
A.I.P. Conf. Proc., 24 (MMM 1974), p95.

Sixtus, K.J. and Tonks, L. 1931.
Phys. Rev., 37, p930.

Smith, D.A. 1975.
J. Phys. F: Metal Phys., 5, p2148.

Sousa, J.B. 1980.
Private communication.

Stone, H.E.N. 1979.
J. Mater. Sci., 14, p2787.

Stoner, E.C. 1938.
Proc. Roy. Soc. (London), A165, p372.

Suzuki, T. 1966.
J. Phys. Soc. Japan, 21, p443.

Suzuki, T. 1976.
J. Phys. Soc. Japan, 41, p1187.

Syono, Y. and Ishikawa, Y. 1967.
Phys. Rev. Lett., 19, p747.

Teraoka, Y. and Kanamori, J. 1977.
Physica, 91B, p199.

Tholence, J.L. 1979.
J. Appl. Phys., 50, p7310.

Tholence, J.L. 1980.
Solid State Commun., 35, p113.

Tholence, J.L. and Tournier, R. 1974.
J. Phys. (Paris), 35, pC4-229.

Werner, S.A., Arrott, A. and Kendrick, H. 1966.
J. Appl. Phys., 37, p1260.

Werner, S.A., Arrott, A. and Kendrick, H. 1967.
Phys. Rev., 155, p528.

Wertheim, G.K. 1961.
J. Appl. Phys., 32, p1105.

White, G.K. 1968.
Experimental Techniques in Low-Temperature Physics. 2nd edition.
O.U.P.

White, G.K. 1979.
Experimental Techniques in Low-Temperature Physics. 3rd edition.
O.U.P.

Wohlfarth, E.P. 1977.
Physica, 86-88B, p852.

Wohlfarth, E.P. 1979.
Phys. Lett., 70A, p489.

Wohlleben, D.K. and Coles, B.R. 1973.
Rado and Suhl (1973) op. cit. chapter 1.

Zener, C. 1954.
Phys. Rev., 96, p1335.

Zibold, G. 1978.
J. Phys. F: Metal Phys., 8, pL229.